THE FETAL MEMBRANE MICROBIOTA IN HISTOLOGICALLY CONFIRMED CHORIOAMNIONITIS

ROCHELLE HOCKNEY

A thesis submitted in partial fulfilment of the requirements of Teesside University for the degree of Doctor of Philosophy (PhD).

This research was carried out in collaboration with Northumbria University, Newcastle and The Royal Victoria Infirmary, Newcastle.

April 2020

Abstract

Introduction

Histological chorioamnionitis (HCA) is inflammation of the fetal membranes. Understanding the fetal membrane microbiota linked to inflammation and bacterial infection is incomplete. This research aimed to increase current knowledge of the fetal membrane microbiota in HCA, including bacterial profile, bacterial load and correlation to inflammatory response. In addition, to investigate the application of Formalin-Fixed Paraffin-Embedded (FFPE) tissues to microbiota research. Finally, to optimise Raman spectroscopy on low biomass cultures for future application to HCA detection.

Methods

A retrospective cohort study was employed on fetal membranes from patients with preterm spontaneous labour and HCA (n=12), or preterm (n=6) and term labour without HCA (n=6), plus low risk term patients (n=58). To investigate bacterial profiles, 16S rRNA Illumina sequencing was performed. Bacterial loads were assessed by 16S rRNA BactQuant qPCR, with bacterial loads also correlated to inflammatory marker data. The spectral fingerprint and biochemical composition of three bacteria were analysed using Raman spectroscopy.

Results

Bacterial loads were significantly greater from HCA patients (5013.066 copies/µl) compared to preterm (288.873 copies/µl) and term without HCA (254.819 copies/µl). Increased bacterial load was positively correlated with maternal inflammatory staging, and the expression of five inflammatory markers. Non-HCA patients, low risk term patients and negative controls did not display distinct bacterial loads (200-300 copies/µl). A trend for increased *Prevotella* with increased inflammation was detected. Over half of sequences from FFPE fetal membranes were identified as contaminants. Bacteria were identified by one Raman spectral peak (1003 cm^{-1}).

Discussion

Inflammatory HCA involves bacterial infection and increased bacterial load in a dose response relationship, with an association to increased *Prevotella*. Bacteria is not acquired *in utero* on fetal membranes without an inflammatory condition. Frozen tissues remain the gold standard for microbiota research. Optimisation of Raman microspectroscopy for bacterial detection on clinical tissues is required to improve diagnosis.

Table of Contents

Abstract	**ii**
Table of contents	iii
List of figures	xii
List of tables	xiv
Acknowledgements	xvi
Declaration	xvii
List of abbreviations	xviii
Chapter One: Introduction.	**1**
1.1 The placenta and fetal environment	1
1.1.1 Fetal membrane morphology	2
1.1.1.1 Amnion	2
1.1.1.2 Chorion	3
1.1.2 Characteristics of the fetal membranes	4
1.1.3 Immunology of the fetal membranes	5
1.2 Preterm birth: Epidemiology, risk factors, complications and treatments	6
1.3 Chorioamnionitis	7
1.3.1 Clinical chorioamnionitis (CCA)	8
1.3.2 Histological chorioamnionitis (HCA)	8
1.3.3 Maternal risk factors for chorioamnionitis	10
1.3.4 Complications in chorioamnionitis	10
1.3.5 Diagnosis, prevention and treatment of HCA	11
1.4 Microbiology and the microbiota	12
1.4.1 Microbiology of the fetal environment and HCA	13
1.4.1.1 Sterile placenta theory	13

1.4.1.2 Sterile inflammation theory 14

1.4.1.3 Genuine microbiota theory 14

1.4.2 Placental and fetal membrane microbiota with chorioamnionitis 15

1.4.3 Pathway of initiation in chorioamnionitis 17

1.5 Microbiota research and evolving techniques 18

1.6 Thesis relevance 19

1.7 Overview of thesis aims 19

Chapter Two: Research methodology. **21**

2.1 Sample and tissue selection 21

2.2 Fetal membrane preparation 22

2.3 Sample selection demographics 22

2.4 Genomic DNA extraction 24

2.4.1 Genomic DNA extraction: Frozen membranes 25

2.4.2 Genomic DNA extraction: FFPE membranes 26

2.5 Theory of DNA quantification 27

2.5.1 NanoDrop spectrophotometer method 27

2.5.2 Agarose gel electrophoresis method 28

2.5.3 Bioanalyzer chip-based electrophoresis method 28

2.6 Theory of Illumina sequencing 29

2.6.1 Illumina sequencing method 32

2.6.2 Microbiota data processing 33

2.6.2.1 Sequencing data processing and statistical analysis methods 34

2.6.2.2 Decontam processing for FFPE samples 35

2.7 BactQuant quantitative PCR 36

2.7.1 Theory and review of qPCR 36

2.7.2 Absolute qPCR with standard curve 38

2.7.3 Primer design 38

2.7.4 SYBR or TaqMan fluorescently labelled probes 39

2.7.5 qPCR methodology limitations 40

2.7.6 BactQuant qPCR methods 42

2.7.6.1 Creating a plasmid for the standard curve 42

2.7.6.2 Creating a standard curve 44

2.7.6.3 PCR optimisation 45

2.7.6.4 BactQuant qPCR protocol 45

2.7.6.5 Statistical analysis of qPCR data 46

2.7.6.6 Relative qPCR for inflammatory gene fold change 46

Chapter Three: The microbiota of frozen fetal membranes with and without histological chorioamnionitis. 48

Abstract 48

3.1 Introduction 49

3.2 Microbiota method recap 49

3.3 Results 51

3.3.1 Patient characteristics 51

3.3.2 Quantification of extracted DNA 54

3.3.2.1 NanoDrop spectrophotometer results 54

3.3.3 Sequencing read counts 54

3.3.4 The microbiota of fetal membranes: Comparison between HCA and non-HCA tissues 55

3.3.4.1 Relative and percentage abundance 55

3.3.4.2 Bacterial diversity structure 57

3.3.5 Maternal stage and grade related to the microbiota in fetal membranes 59

3.3.5.1 Relative and percentage abundance for inflammatory stage 59

3.3.5.2 Relative and percentage abundance for inflammatory grade 62

3.3.5.3 Bacterial diversity structure across HCA inflammatory staging and grading 64

3.3.6 The microbiota of frozen fetal membrane tissues and negative controls 67

3.3.6.1 Relative and percentage abundance in samples and controls 67

3.3.6.2 Bacterial diversity structure in samples and controls 69

3.4 Discussion 71

3.4.1 Optimum DNA quantity from frozen fetal membranes 71

3.4.2 Sequencing read counts from frozen fetal membranes 71

3.4.3 HCA patients have distinctly different bacterial profiles compared to non-HCA patients 72

3.4.4 HCA inflammation levels are associated with bacterial profiles of the fetal membranes 75

3.4.5 Negative controls and samples have distinct bacterial profiles and differ by four specific genera 76

3.5 Conclusion 78

Chapter Four: The utilisation of Formalin-Fixed Paraffin-Embedded fetal membrane samples for microbiota research; FFPE and frozen comparison. 79

Abstract 79

4.1 Introduction 80

4.1.1 Application of FFPE samples 80

4.1.2 Placental and fetal membrane FFPE samples 81

4.1.3 Decontam applied to FFPE samples 81

4.2 Microbiota method recap 83

4.3 Results 84

4.3.1 Matched paired patient demographics 84

4.3.2 Results of matched paired fetal membranes 86

4.3.2.1 Sequencing read counts from matched paired patients 86

4.3.2.2 Relative and percentage abundance of matched paired patients 86

4.3.2.3 Bacterial diversity structure of matched paired patients 91

4.3.3 Quantification of extracted DNA from matched paired patients 92

4.3.3.1 NanoDrop spectrophotometer results from matched paired patients 92

4.3.3.2 Agarose gel electrophoresis results from matched paired patients 92

4.3.4 FFPE sample comparison to negative controls 94

4.3.4.1 Sequencing read count results from FFPE samples and negative controls 94

4.3.4.2 Relative and percentage abundance from FFPE samples and negative controls 94

4.3.4.3 Bacterial diversity structure from FFPE samples and negative controls 100

4.3.5 DNA extraction kit comparison 101

4.3.5.1 NanoDrop spectrophotometer results from kit comparison 101

4.3.5.2 Relative and percentage abundance from kit comparison 101

4.3.5.3 Bacterial diversity structure from kit comparison 104

4.3.6 Decontam results from FFPE samples 105

4.4 Discussion 108

4.4.1 FFPE samples have diminished DNA quantity and quality compared to frozen tissues 108

4.4.2 Decontam identifies over half of bacterial sequences from FFPE membranes as contaminants 109

4.4.3 Biological and methodological variation across FFPE and frozen tissues 111

4.4.4 Further considerations 112

4.5 Conclusion 114

Chapter Five: Bacterial load in fetal membranes with and without histological chorioamnionitis. 115

Abstract 115

5.1 Introduction 117

5.2 qPCR method recap 118

5.2.1 Sample processing 118

5.2.2 BactQuant qPCR method recap 119

5.3 Results 122

5.3.1 PCR optimisation 122

5.3.1.1 Temperature gradient 122

5.3.1.2 $MgCl_2$ concentration 122

5.3.1.3 Formamide concentration 122

5.3.1.4 Tissue sample inhibition results 124

5.3.2 Standard curve results 126

5.3.3 Low risk patient demographics 130

5.3.4 Low risk patient sample qPCR results 131

5.3.4.1 The majority of low risk fetal membranes were OOR for the assay 131

5.3.4.2 Mode of delivery does not impact bacterial load of low risk term fetal membranes 131

5.3.4.3 Low risk fetal membrane bacterial load is comparable to negative controls 132

5.3.5 HCA cohort sample demographics 134

5.3.5.1 Tissue sample qPCR results 134

5.3.5.2 The majority of fetal membrane samples had detectable bacterial loads 134

5.3.5.3 Bacterial load is increased with histological inflammation of the amnion and chorion 135

5.3.5.4 Non-HCA samples and negative controls have comparable bacterial loads 138

5.3.6 Increased bacterial load is positively correlated to increased inflammatory stage and grade 139

5.3.6.1 Increased bacterial load is positively correlated with inflammatory gene expression 141

5.4 Discussion 143

5.4.1 Bacterial load cannot always be detected in low risk term fetal membranes, but are increasingly detected in negative pregnancy outcomes 143

5.4.2 HCA fetal membranes have significantly greater bacterial load than PTB and term without HCA 145

5.4.3 Bacterial load is positively correlated to severity of inflammatory response in a dose dependent manner 145

5.4.4 Bacterial load correlates with five inflammatory factors across the amnion and chorion 146

5.4.5 Amnion and chorion display comparable bacterial loads irrespective of HCA 148

5.4.6 There is no difference in bacterial load between non-HCA fetal membranes irrespective of gestational age or mode of delivery 149

5.4.7 The bacterial load of non-HCA fetal membranes cannot be distinguished from negative controls 149

5.5 Conclusion 151

Chapter Six: Raman spectroscopy for the detection and distinction of bacteria in mono and polymicrobial culture conditions. 152

Abstract 152

6.1 Introduction 153

6.1.1 Clinical relevance of Raman spectroscopy 154

6.2 Theory and review of Raman spectroscopy 156

6.2.1 Theory of Raman spectroscopy 156

6.2.2 Raman spectroscopy instrumentation 156

6.2.3 Raman spectral processing 158

6.2.4 Sample processing for Raman spectroscopy 159

6.3 Raman spectroscopy methods 160

6.3.1 Bacterial culture 160

6.3.2 Bacterial preparation for Raman spectroscopy 160

6.3.3 Raman spectroscopy experimental set up 160

6.3.4 Instrument calibration 161

6.3.5 Bacterial spectral acquisition 161

6.3.6 Raman spectral processing method 161

6.3.7 Raman data analysis 162

6.4 Results 163

6.4.1 Calibration and background reference spectra 163

6.4.2 Example spectral processing results 165

6.4.3 Raman spectra from monomicrobial droplets 167

6.4.4 Raman spectra from polymicrobial droplets 172

6.4.5 Raman spectral intensity results 174

6.5 Discussion 176

6.5.1 Bacteria can be detected by a Raman peak at 1003 cm^{-1} 176

6.5.2 *E. coli, K. pneumoniae* and *S. aureus* have similar spectral fingerprints 177

6.5.3 Bacterial distinction in polymicrobial environments is inconclusive 178

6.5.4 Peak intensity was related to bacterial concentration in *E. coli* and *K. pneumoniae* 178

6.5.5 Strengths and limitations of Raman spectroscopy 179

6.5.6 Future research and applications of Raman spectroscopy 180

6.6 Conclusion 182

Chapter Seven: Discussion and concluding remarks. **183**

7.1 Research project aims 183

7.2 Summary of key findings 184

7.3 Strengths and limitations 185

7.4 Future research 188

7.5 Research implications and clinical relevance 190

7.6 Conclusion 191

References **192**

Appendices **227**

A.1. List of reagents, chemicals and commercial kits 227

A.2. List of equipment 229

A.3. Table of primers 230

A.4. Serial dilution calculations 230

A.5. Formalin-Fixed Paraffin-Embedded tissue block images 231

A.6. Additional results 234

A.6.1 NanoDrop spectrophotometer DNA extraction example 234

A.6.2 Bioanalyzer chip-based electrophoresis results 235

A.6.3 Additional qPCR sample results 237

Publications **244**

List of Figures

Figure 1.1 Schematic diagram of the fetal environment 2

Figure 1.2 Schematic diagram of the fetal membrane structure 3

Figure 1.3 Histological image of the of the fetal membrane structure 4

Figure 2.1 Paired end bridge amplification, with sequence by synthesis 31

Figure 2.2 Diagrammatic representation of quantitative polymerase chain reaction 37

Figure 2.3 TaqMan qPCR probe technology 41

Figure 3.1 Relative abundance of chorion and amnion fetal membranes 56

Figure 3.2 Diversity analysis of frozen fetal membranes 58

Figure 3.3 Relative abundance of inflammatory stage in the amnion and chorion 60

Figure 3.4 Relative abundance of inflammatory grade in the amnion and chorion 63

Figure 3.5 Diversity analysis of inflammatory grading and staging within the chorion 65

Figure 3.6 Diversity analysis of inflammatory grading and staging within the amnion 66

Figure 3.7 Relative abundance of frozen tissues and negative controls 68

Figure 3.8 Diversity analysis of frozen tissues and negative controls 70

Figure 4.1 Relative abundance of matched paired fetal membranes 87

Figure 4.2 Diversity analysis of matched paired fetal membranes 91

Figure 4.3 Agarose gel electrophoresis from matched paired fetal membranes 93

Figure 4.4 Relative abundance of FFPE membrane rolls and negative controls 95

Figure 4.5 Diversity analysis of FFPE tissues and negative controls 100

Figure 4.6 Relative abundance of DNA extraction kit controls 102

Figure 4.7 Diversity analysis of DNA extraction kit controls 104

Figure 5.1 PCR optimisation 123

Figure 5.2 qPCR standards amplification plot 127

Figure 5.3 qPCR standard curve example 129

Figure 5.4 qPCR analysis of bacterial load in low risk term fetal membranes by mode of delivery 132

Figure 5.5 qPCR analysis of bacterial loads from low risk term fetal membranes and negative controls 133

Figure 5.6 qPCR analysis of bacterial load by HCA status in the amnion and chorion 137

Figure 5.7 qPCR analysis of bacterial load from fetal membranes and negative controls 138

Figure 5.8 Amnion inflammatory stage and grade correlated to bacterial load 140

Figure 5.9 Chorion inflammatory stage and grade correlated to bacterial load 140

Figure 6.1 Typical Raman biological spectra 156

Figure 6.2 Internal view of inVia Raman enclosure 157

Figure 6.3 External view of inVia Raman enclosure 158

Figure 6.4 Reference calibration spectra of the internal silicon chip 163

Figure 6.5 Reference background spectra of a stainless steel microscope slide 164

Figure 6.6 Reference background spectra of culture media 164

Figure 6.7 Raman baseline subtraction example 165

Figure 6.8 Example of pick peak function and final processed spectra 166

Figure 6.9 Raman spectra from monomicrobial culture droplets 168

Figure 6.10 Raman spectra from polymicrobial culture droplets 173

Figure 6.11 Intensity of the 1003 cm^{-1} spectral peak from serial dilution curve 175

Figure A.1 Formalin-Fixed Paraffin-Embedded tissue block images 233

Figure A.2 Bioanalyzer chip-based gel electrophoresis example results 236

Figure A.3 qPCR samples and standards amplification plot 237

List of Tables

Table 1.1 Redline criteria for the detection of inflammatory response in the placenta and fetal membranes 9

Table 2.1 Maternal patient demographics 23

Table 2.2 Ligation reaction components 43

Table 3.1 Patient demographics of frozen fetal membranes 52

Table 3.2 Patient demographics from frozen fetal membranes of PTB patients only 53

Table 3.3 Ten most abundant ASVs in frozen fetal membranes 57

Table 3.4 Ten most abundant ASVs in fetal membranes across inflammatory staging 61

Table 3.5 Ten most abundant ASVs in fetal membranes across inflammatory grading 64

Table 3.6 Ten most abundant ASVs in frozen fetal membranes and negative controls 69

Table 4.1 Matched paired patient demographics 84

Table 4.2 Matched paired patient demographics from HCA and PTB only 85

Table 4.3 Univariate analysis of matched paired fetal membranes by genera 88

Table 4.4 Univariate analysis of matched paired fetal membranes by ASV 89

Table 4.5 Univariate analysis of FFPE samples compared to negative controls by genera 96

Table 4.6 Univariate analysis of FFPE samples compared to negative controls by ASV 98

Table 4.7 Univariate analysis of DNA extraction kit controls by ASV 103

Table 4.8 Genuine bacterial sequences in FFPE samples identified by decontam 106

Table 4.9 Contaminating bacterial sequences in FFPE samples identified by decontam 107

Table 5.1 qPCR tissue sample inhibition analysis 125

Table 5.2 qPCR standard curve copy number results 127

Table 5.3 Low risk term fetal membrane patient demographics 130

Table 5.4 Bacterial load correlated to inflammatory gene fold change in the amnion and chorion 142

Table 6.1 Cosmic ray removal table 166

Table 6.2 Raman spectral peak assignment for *Escherichia coli* 169

Table 6.3 Raman spectral peak assignment for *Klebsiella pneumoniae* 170

Table 6.4 Raman spectral peak assignment for *Staphylococcus aureus* 171

Table 6.5 Table of intensity for the 1003 cm^{-1} spectral peak from serial dilution curves 175

Table A.1 Primer sequences 230

Table A.2 Serial dilution calculations for qPCR standard curves 230

Table A.3 Example of NanoDrop spectrophotometer sample results following DNA extractions 234

Table A.4 qPCR fetal membrane sample copy number results 238

Table A.5 qPCR low risk fetal membrane sample copy number results 241

Acknowledgments

I cannot deny that I have dedicated unfathomable hours into the completion of this thesis, but I would not have made it through without a few amazing people.

My parents and partner have wholly supported my plans and helped me reach my dreams of conducting a PhD. They have put up with my 4am mornings, late night panics and general ‘head in the clouds’ nature because I am always reading, at my desk, or occupied with papers galore. You are angels!

The staff at Teesside University have inspired, supported and prepared me for the future. My supervisory team have always been there for unlimited questions. I would specifically like to thank Dr. Caroline Orr as my primary supervisor for transferring some of her amazing knowledge over to me, for the continual support and feedback on my ideas, weekly meetings (even skyping whilst in isolation) and providing guidance in work and life. Dr. Gillian Taylor as my second supervisor, for all of the encouragement and inspiration throughout my PhD. Plus, Dr. Andrew Nelson from Northumbria University who has gone above and beyond his external supervisory role. Also, Professor. Stephen Cummings, who without his initial project ideas and support throughout, this project would not have been possible. Thank you!

I would also like to thank the clinicians at the Royal Victoria Infirmary, Newcastle, and Newcastle University for providing external support. The main contributors including Dr. Gareth Waring, Dr. Judith Bulmer, Dr. Inge Christiaens and Professor. Stephen Robson for collection and approval of samples and methodological support.

Lastly, I would like to thank the PG.08 graduate tutors. Together we have been on a four year journey, jumping through hoops and over hurdles that we did not even know existed. I am proud of each and every one of you. My micro ladies, you are amazing, thank you for making me smile on a rainy day.

Declaration

I declare that the work presented in this thesis is my own work and has not been submitted for any other academic award or degree. I declare that any support conducting experiments within this thesis have been declared where relevant. The work was conducted in collaboration with Northumbria University, Newcastle and the Royal Victoria Infirmary, Newcastle.

List of abbreviations

%	Percentage
°C	Degrees centigrade
µl	Microlitre
µg	Microgram
6-FAM	6-Carboxyfluorescein
ANOVA	Analysis of variance
ASV	Amplicon sequence variant
BMI	Body mass index
bp	Base pair
bpm	Beats per minute
BSA	Bovine serum albumin
CaF2	Calcium fluoride
CCA	Clinical chorioamnionitis
CCD	Charge coupled device
CFU	Colony forming unit
cm	Centimetre
COX	Cyclooxygenase
CQ	Quantification cycle
CRP	C-reactive protein
DAMPs	Damage associated molecular patterns
dH_2O	Distilled water
DNA	Deoxyribonucleic acid
dNTP	Deoxyribonucleotide triphosphate
dsDNA	Double stranded DNA
E. coli	*Escherichia coli*

ELCS	Elective caesarean section
ELISA	Enzyme linked immunosorbent assay
FDR	False discovery rate
FFPE	Formalin-fixed paraffin-embedded
FRET	Fluorescence resonance energy transfer
FTIR	Fourier-transformed infrared
GUniFrac	Generalised UniFrac
H&E	Haematoxylin and eosin
HCA	Histological chorioamnionitis
HLA	Human leukocyte antigen
HMGB1	High mobility group box 1
IFN	Interferon
IHC	Immunohistochemistry
IL	Interleukin
IRAK	Interleukin-1 receptor associate kinase
K. pneumoniae	*Klebsiella pneumoniae*
LB	Luria-Bertani
LOD	Limit of detection
Log_{10}	Logarithm (base10)
LPS	Lipopolysaccharide
LY96	Lymphocyte antigen 96
MALDI	Matrix-assisted laser desorption/ionization
mg	Milligram
MGBNFQ	Minor groove binder non-fluorescent quencher
$MgCl_2$	Magnesium chloride
MIP-1β	Macrophage inflammatory protein-1β

ml	Millilitre
mm	Millimetre
mM	Millimolar
MMP	Matrix metallopeptidase
mW	Milliwatt
MyD88	Myeloid differentiation primary response 88
NF-κβ	Nuclear factor kappa beta
ng	Nanogram
NGS	Next generation sequencing
NICE	National institute for healthcare excellence
NK	Natural killer
nm	Nanometre
NTC	No template control
OD	Optical density
OOR	Out of range
OTU	Operational taxonomic unit
p	Probability value
PBS	Phosphate buffered saline
PCR	Polymerase chain reaction
PERMANOVA	Permutational analysis of variance
pg	Picogram
PMA	Propidium monoazide
PPROM	Preterm premature rupture of the membranes
PROM	Premature rupture of the membranes
PTB	Preterm birth
qPCR	Quantitative polymerase chain reaction

rRNA	Ribosomal ribonucleic acid
RT	Room temperature
S. aureus	*Staphylococcus aureus*
SARM1	Sterile alpha and TIR motif 1
SD	Standard deviation
SERS	Surface enhanced Raman spectroscopy
SIGIRR	Single immunoglobulin IL-1-related receptor
SOP	Standard operating procedure
sPTB	Spontaneous preterm birth
SQ	Starting quantity
ssDNA	Single stranded DNA
TIRAP	Toll-like receptor-1 associated protein
TLR	Toll-like receptor
TNF	Tumour necrosis factor
TRAM	TRIF-related adaptor molecule
TRIF	Toll/IL-1R domain containing adaptor inducing IFNβ
UNG	Uracil N-glycosylase
UV	Ultraviolet
V	Variable region
w/v	Weight per volume
WBC	White blood cell count
WHO	World Health Organisation

Chapter One: Introduction.

1.1 The placenta and fetal environment

The maternal-fetal interface composed of the maternal decidua and placental disk (Edmonds, 2008); plus the fetal components of the fetal membranes, amniotic fluid and umbilical cord, are essential for optimum fetal development (Edmonds, 2008)(Figure 1.1).

The placenta is a large transient organ acting as a key communicator between the maternal and fetal environment, which is vital for maintenance of pregnancy (Donnelly and Campling, 2019; Menon, Richardson and Lappas, 2018). Functions include gaseous exchange, vitamin and mineral transportation via a concentration gradient (Jones and Jansson, 2007), elimination of waste metabolites (Serrano *et al*, 2002) and secretion of human chorionic gonadotrophin (Donnelly and Campling, 2019). The maternal decidua which adheres to the fetal membranes contains differentiated stromal cells, maternal blood vessels and immune cells (Pansky, 1982)(Figure 1.1). Placental and chorionic villi act as an anchor for stability and to give increased maternal-fetal contact area (Pansky, 1982). The umbilical cord is also a maternal-fetal communication pathway (Di Naro *et al*, 2001)(Figure 1.1).

The fetal membranes overlay the placenta and decidua to create an internal capsule of the amniotic cavity (Pansky, 1982)(Figure 1.1). The contained amniotic fluid provides mechanical cushioning, plus growth factors and antimicrobial effectors to protect and aid development of the fetus (Underwood, Gilbert and Sherman, 2005). Amniotic fluid is also used as a diagnostic media during amniocentesis for prenatal assessment (Underwood, Gilbert and Sherman, 2005).

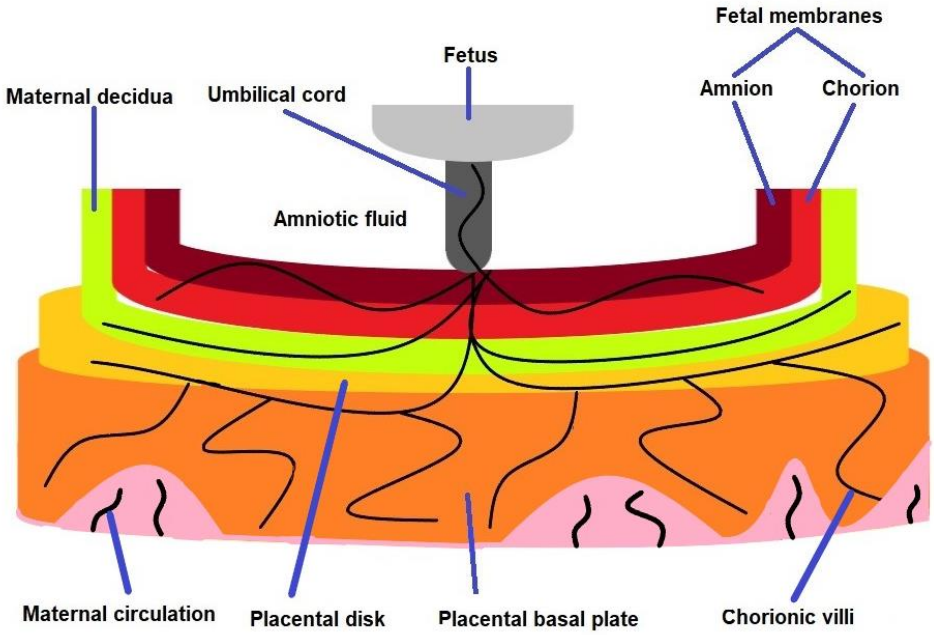

Figure 1.1 Schematic diagram of the fetal environment. A cross section of the fetal environment during gestation required for maintenance of pregnancy, displaying the fused amnion and chorion of the fetal membranes, in close contact with the maternal decidua. Invasion of the chorionic villi into the placenta creates maternal-fetal communication. Diagram not to scale.

1.1.1 Fetal membrane morphology

The fetal membranes which encapsulate the developing fetus are formed from the outer chorion and the deeper amnion, which overlay the placental disk (Sood *et al*, 2006)(Figure 1.2).

1.1.1.1 Amnion

The amnion is up to 500 µm thick and is composed of an epithelium layer, basement membrane, compact layer, avascular reticular tissue and sponge layer interconnecting to the chorion (Mamede *et al*, 2012)(Figure 1.2). The single cuboidal epithelial cell layer is the initial layer in contact with the amniotic cavity and amniotic fluid (Canzoneri *et al*, 2013). The basement membrane functions as a permeable barrier and aids with structural integrity (Mamede *et al*, 2012)(Figure 1.3). The dense outer collagen-rich layers have high tensile strength and flexibility to withstand movement and growth (Verbruggen *et al*, 2017).

1.1.1.2 Chorion

The outer chorion is formed from a fibrous reticular layer, basement membrane, and deeper trophoblast layer (Bourne, 1962)(Figure 1.2). The chorion acts as an immunological barrier of protection between the fetus and the maternal or external environment (Verbruggen *et al*, 2017). The chorionic villi interlock with the maternal decidua to allow nutrient transfer and stabilise the membranes (Sood *et al*, 2006)(Figure 1.3).

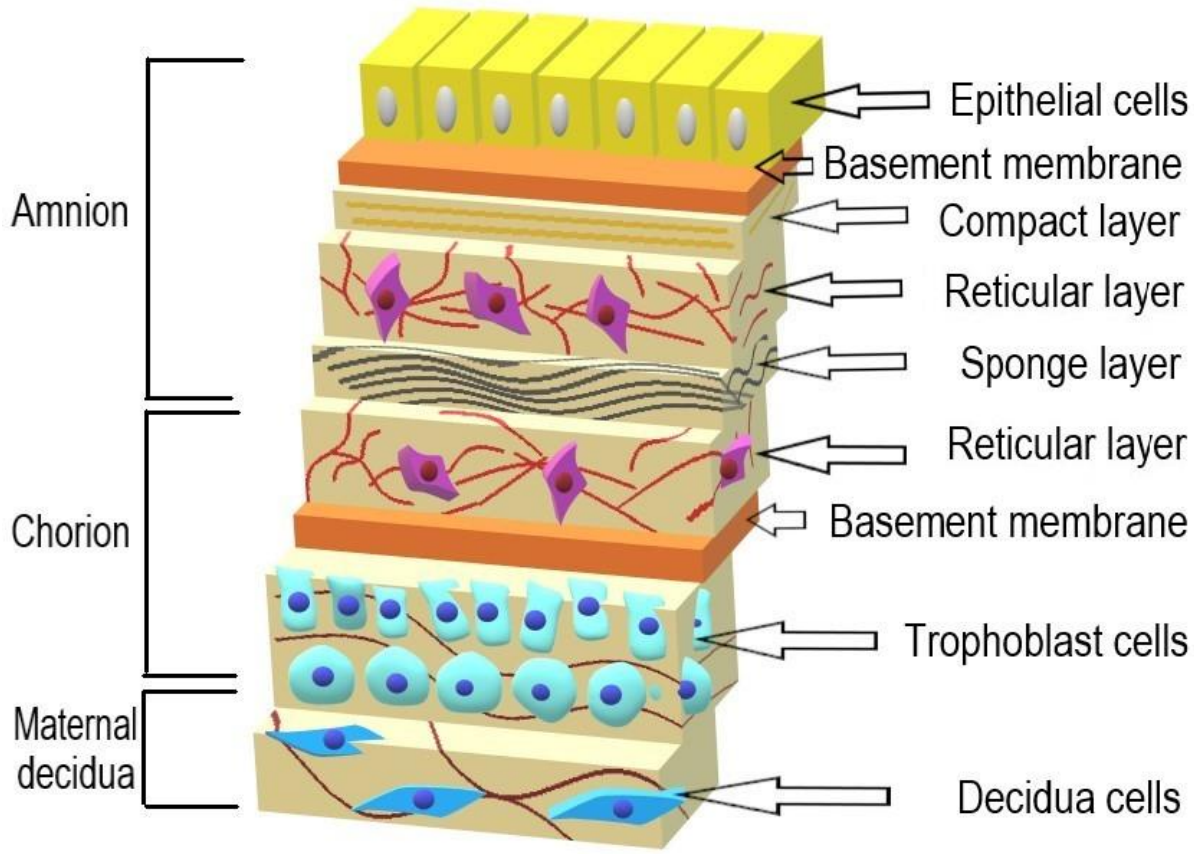

Figure 1.2 Schematic diagram of the fetal membrane structure. A schematic representation of a cross section of the multiple layered and multiple functioning fetal membranes, consisting of the amnion and chorion, plus the fused maternal decidua during gestation. For this diagram the uterine cavity would be superior to the fetal membranes, with the placental disk inferior to this diagram. Diagram not to scale.

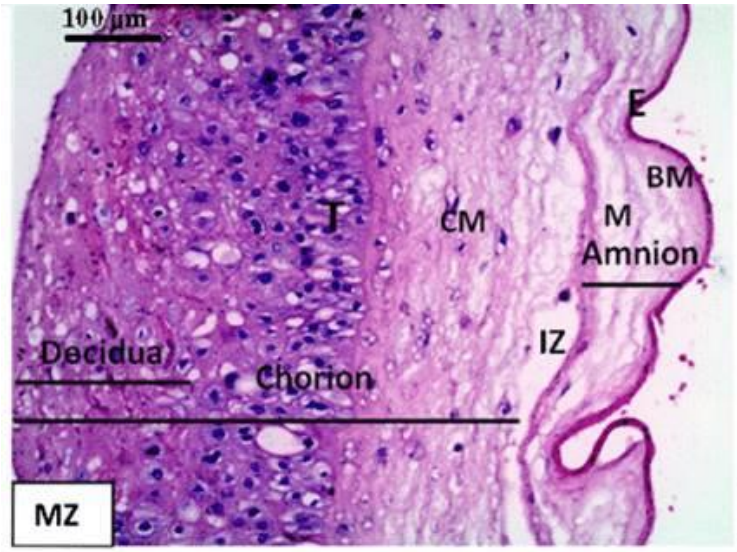

Figure 1.3 Histological image of the fetal membrane structure. A histological cross section of the fetal membranes and maternal decidua stained with haematoxylin and eosin. Image displays the amnion composed of the epithelial cells (E), basement membrane (BM), mesenchymal layer (M) and intermediate spongy layer (IZ). Chorion composed of the chorionic basement membrane (CM) and trophoblast cells (T). Prelabelled figure from Elfayomy and Almasry (2014).

1.1.2 Characteristics of the fetal membranes

The fetal membranes maintain structural integrity throughout gestation for continual survival of the fetus (Edmonds, 2008), with nutrients supplied via diffusion from amniotic fluid and the maternal decidua (Mamede *et al*, 2012). The fetal membranes express few class II HLAs to suppress immunological response and avoid immune rejection throughout gestation (Murphy *et al*, 2014). Alongside vital *in utero* functioning, fetal membranes possess anti-angiogenic and pro-apoptotic characteristics (Mamede *et al*, 2012), which have been exploited in regenerative medicine, superficial wounds and tissue engineering research (Lei *et al*, 2017; Mamede *et al*, 2012; Mi *et al*, 2012).

During development the amnion originates from the amniotic ectoderm, with the chorion from the somatic mesoderm (Edmonds, 2008). At 14-16 weeks gestation, the amnion and chorion fuse into an individual entity (Edmonds, 2008). At term, the morphology of the fetal membranes alter to create a specific zone of weakness, leading to membrane rupture and consequential parturition (Verbruggen *et al*, 2017). If the membranes are prematurely weakened, premature rupture of the membranes (PROM), preterm PROM (PPROM) and preterm birth (PTB) may occur

(Richardson *et al*, 2017; Verbruggen *et al*, 2017). PROM is defined as rupture of the fetal membranes prior to the onset of contractions and active labour (Goldenberg *et al*, 2008), with PPROM specific to occurrence at <37 weeks gestation (Fortner *et al*, 2014).

1.1.3 Immunology of the fetal membranes

The fetal membranes and placenta possess unique immunological characteristics, with versatile protective mechanisms and immune modulation to prevent invasion and allow fetal development.

Toll-like receptor (TLR) expression on the fetal membranes begins at 25 weeks gestation and matures throughout gestation (Mor, Aldo and Alvero, 2017). TLRs are the first line of immune defence to recognise pathogen associated molecular patterns, with TLR4 and TLR2 the greatest expressed (Mor, Aldo and Alvero, 2017; Waring *et al*, 2015). TLR4-MD2 complex recognises bacterial lipopolysaccharides (LPS) leading to TLR4 dimerisation and the recruitment of adaptor proteins, including MyD88 or TIRAP (Kawai and Akira, 2010). These factors recruit IRAK for rapid activation of the NF-κβ transcription factor and proinflammatory cytokine response (Kawai and Akira, 2010). Alternatively, internalisation of TLR4-MD2 leads to TRIF and TRAM activation to promote interferons (IFN) and further NF-κβ activation (Kawai and Akira, 2010). Alternatively, TLR2/TLR1 homo/heterodimers recognise Gram negative triacyl lipopeptides to activate TIRAP and MyD88 dependent pathway for NF-κβ expression (Kawai and Akira, 2010).

Further to this, the immunomodulated pregnancy state is characterised by suppression of type 1 T helper (Th1) proinflammatory cytokine and activation of type 2 T helper (Th2) anti-inflammatory profile at the maternal-fetal interface (Morelli *et al*, 2015). The amnion and decidua have a role in inhibiting Th1 activation due to the production of interleukin-13 (IL-13) and IL-4, with a reverse back to Th1 activity, including increased TNFα and IFNγ from the fetal membranes during active labour (Morelli *et al*, 2015). Negative regulation of T helper cells can lead to pregnancy related conditions including PTB and pre-eclampsia (Hsu and Nanan, 2014). In alternate body sites, a Th1/Th2 balance is optimum, with imbalance in the respiratory tract epithelia linked to allergies and asthma (Mazzarella *et al*, 2002).

The fetal membranes also possess atypical human leukocyte antigen (HLA) expression, with absence of HLA-A and HLA-B (Hori *et al*, 2006; Huddleston and Schust, 2004). This may increase vulnerability to natural killer (NK) cell mediated attack as HLAs are antigen presenting for NK cells, but chorionic extravillous cytotrophoblasts present HLA-C, HLA-G and HLA-E (Aagaard-Tillery, Silver and Dalton, 2006; Huddleston and Schust, 2004), leading to an immunosuppressive effect and preventing NK attack (Hsu and Nanan, 2014). The decidua constitutes mainly of NK cells, accounting for 50-90% of leukocytes (Aagaard-Tillery, Silver and Dalton, 2006; Mor, Aldo and Alvero, 2017). However, decidual NK cells differ to peripheral blood NK cells due to increased CD56 expression required for remodelling of spiral placental and decidual arteries (Hsu and Nanan, 2014; Mor, Aldo and Alvero, 2017), and lack of CD16 reducing cytotoxicity (Morelli *et al,* 2015). The characteristic HLA presentation is also seen in other immunomodulated locations including the retina, iris, and cornea (Aagaard-Tillery, Silver and Dalton, 2006; Hori *et al*, 2006; Hsu and Nanan, 2014).

1.2 Preterm birth: Epidemiology, risk factors, complications and treatments

Parturition (action of giving birth) is a physiological process controlled by endocrine, paracrine and autocrine mechanisms from placental, fetal and maternal components, including oxytocin and prostaglandin feedback loops (Kota *et al*, 2013). Term birth is defined as parturition at 37-42 weeks gestation and is the normal gestational length in human pregnancy (Pansky, 1982). PTB is classified as parturition <37 weeks, with this further categorised into late preterm (34-36 weeks; Shapiro-Mendoza and Lackritz, 2012), early preterm (28-34 weeks; Goldenberg *et al*, 2008; Tucker, 2004) and extreme preterm birth (<28 weeks; Morgan *et al*, 2016). PTB occurs in 15 million births worldwide per year (NICE, 2019; WHO, 2015). The global burden of PTB is 11%, varying from 5% occurrence and 90% survival rates in European countries, compared to 18% occurrence and 10% survival in African countries (Blencowe *et al*, 2012; Vogel *et al*, 2018).

The occurrence of PTB is spontaneous in 70% of cases (Goldenberg *et al*, 2008). In the remaining cases medical interventions and invasive procedures (Kemp, 2014), or maternal complication, including placenta previa or fetal distress may initiate PTB (Vogel *et al*, 2018). Regardless of spontaneity, PPROM is a significant risk factor, occurring prior to PTB in 30% of cases (Brown *et al*, 2018). PTB has

been associated with other risk factors, including maternal age (Londero *et al*, 2019), smoking (Varga *et al*, 2017), vaginal dysbiosis (Brown *et al*, 2018), multiple pregnancies, diabetes, high blood pressure (WHO, 2015) and infection, such as chorioamnionitis (Friese, 2003; Jones *et al*, 2009).

Preterm birth is a leading cause of mortality, accounting for 35% of mortality in newborns and 16% of mortality in children under five (UNIGME, 2017). Complications include necrotising enterocolitis (NEC), maternal and fetal sepsis, plus respiratory and neurological conditions (Tomlinson *et al,* 2019; Vogel *et al*, 2018).

The current World Health Organisation (WHO) and National Institute for Health and Care Excellence (NICE) guidelines for intervention of PTB include administering prophylactic corticosteroids and antibiotics to supress labour, plus supporting the neonate after birth with oxygen therapy, feeding support and thermal care (NICE, 2019; WHO, 2015).

1.3 Chorioamnionitis

Chorioamnionitis is an inflammatory condition of the fetal membranes, and is a causal factor of PTB (Redline *et al*, 2003). Two subcategories of chorioamnionitis exist (clinical and histological chorioamnionitis) and are defined by maternal and fetal clinical characteristics or morphological presentation of the placenta and fetal membranes.

Chorioamnionitis impacts 5% of pregnancies, with occurrence inversely related to gestational age as incident rates are greater in PTB, occurring at 11%, 35% and 40-94% in late, early and extreme PTB, respectively (Kim *et al*, 2015). Whilst occurrence is 2-4% at term (Kim *et al*, 2015). The prevalence of histological chorioamnionitis (HCA) varies worldwide due to environmental, maternal and healthcare factors (Chan *et al*, 2016; Malloy, 2014). The prevalence is higher in non-western countries, with 66% in Bangladesh (Chan *et al*, 2016), compared to 1-5% in developed countries, including the UK and USA (Malloy, 2014). This is due to increased occurrence of home births, absence of skilled midwives, plus reduced diagnostic and preventative care in non-western countries (Johnson, Adami and Farzin, 2017).

1.3.1 Clinical chorioamnionitis (CCA)

Clinical chorioamnionitis occurs in 10-30% of chorioamnionitis cases (Jessop and Sebire, 2011) and is diagnosed prior to and during parturition according to routinely monitored maternal and fetal clinical characteristics. Indicators include maternal fever (>38 °C), uterine tenderness, tachycardia (>100 bpm maternal, >160 bpm fetal), vaginal discharge and elevated maternal white blood cell count (WBC; Tita and Andrews, 2010). Maternal fever is the most sensitive method of diagnosis (95-100%; Tita and Andrews, 2010). But each characteristic is non-specific to chorioamnionitis when investigated individually (Tita and Andrews, 2010). Thus, maternal fever, plus two of the remaining characteristics are to be present for a definitive diagnosis (Sahni, Franco-Fuenmayor and Shattuck, 2019).

1.3.2 Histological chorioamnionitis (HCA)

Only one third of patients with chorioamnionitis present with clinical symptoms (CCA), with two thirds asymptomatic or subclinical (Redline *et al*, 2003; Smulian *et al*, 1999). HCA occurs more frequently in PTB (30-50%) than CCA (Jessop and Sebire, 2011). HCA is diagnosed following routine placental collection and assessment of tissue morphology for maternal and fetal inflammatory response factors (Redline *et al*, 2003). The placenta, fetal membranes and umbilical cord are collected following parturition and processed via fixative and embedding procedures to give Formalin-Fixed Paraffin-Embedded (FFPE) samples, before staining with haematoxylin and eosin (H&E; Holzman *et al*, 2007). Diagnosis is then performed by two independent clinicians, based on the abundance of macrophages and neutrophils within the fetal membranes, plus necrosis and thickening of the fetal membranes (Redline *et al*, 2003). The severity, progression and intensity of the condition is then categorised using Redline staging and grading criteria (Redline *et al*, 2003)(Table 1.1). Redline criteria is the combination of two historical diagnostic methods (Blanc, 1980; Salafia, Weigl and Silberman, 1989), and is the most universal method applied to current diagnostic research (Catano Sabogal, Fonseca and Garcia-Perdomo, 2018), due to the combination of staging and grading to increase specificity of detection (Redline *et al*, 2003). Inflammatory staging refers to the progression of the condition, whereas inflammatory grading measures intensity (Redline *et al*, 2003)(Table 1.1). Severity of HCA increases as more neutrophils

penetrate deeper across the membranes and into the amnion, eliciting a greater inflammatory response (Becroft, Thompson and Mitchell, 2012; Redline *et al*, 2003).

The inflammatory response in chorioamnionitis may not be isolated to the fetal membranes. Further inflammation involving the amniotic fluid or umbilical cord is defined as intra-amniotic infection (Han *et al*, 2009). Fetal involvement following inflammatory stimuli can lead to; fetal inflammatory response syndrome, with funisitis, involving outer umbilical cord neutrophil presence, plus umbilical artery and venous involvement (Redline *et al*, 2003; Redline, 2006); or fetal vasculitis, with neutrophil influx in the chorionic plate fetal vessels or umbilical cord (Hecht *et al*, 2009). Thus, specific identification and classification of each neonatal condition is important to tailor individual treatment.

The fixed and processed fetal membrane rolls used for HCA diagnosis are archived, but rarely utilised beyond immunological and pathological diagnosis. FFPE fetal membrane samples could be valuable when there is a shortage of biological sample, or biobank storage limitations (Janecka, Adamczyk and Gasinska, 2015). The beneficial application of FFPE fetal membranes to HCA microbiota research requires investigation.

Stage	**Characteristic**
One	<5 neutrophils within the chorionic plate or chorionic connective tissues
Two	>5 scattered neutrophils in the chorionic plate or amnion
Three	Degenerating neutrophils in the amniotic basement membrane
Grade	**Characteristic**
One	Small clusters of maternal neutrophils within the amnion or chorionic plate
Two	Multiple large clusters of neutrophils or leukocytes between the chorion and decidua or chorionic plate

Table 1.1 Redline criteria for the detection of inflammatory response in the placenta and fetal membranes. Histological chorioamnionitis is diagnosed by assessment of the placenta and fetal membranes postpartum following fixing and embedding the tissues and histological staining. Criteria displayed as stage or grade to detect inflammatory response on the fetal membranes, categorised by abundance of macrophages and neutrophils within the fetal membranes (Redline *et al*, 2003). Severity of inflammation increases numerically.

1.3.3 Maternal risk factors for chorioamnionitis

Multiple risk factors for developing chorioamnionitis have been suggested (Ategeka *et al*, 2019; Jung *et al*, 2010; Kim *et al*, 2015; Konwar *et al*, 2018). PPROM is a significant risk factor to chorioamnionitis, with 88% of PPROM also displaying chorioamnionitis (Steel *et al*, 2005), this is due to early rupture of membranes leading to extended time to labour, increasing the opportunity of ascending bacterial infection and early PTB (Czikk, McCarthy and Murphy, 2011; Jessop and Sebire, 2011; Jung *et al*, 2010). Further investigated risk factors for chorioamnionitis in PTB include large cervical dilation (Kim *et al*, 2015), multiple examinations, invasive fetal procedures (Czikk, McCarthy and Murphy, 2011) and short cervical length (Jung *et al*, 2010). These factors are also linked to increased opportunistic bacterial translocation. In term patients, ethnicity and extended delivery duration were risk factors for HCA (Becroft, Thompson and Mitchell, 2012). Maternal inflammation and infection are significantly associated with chorioamnionitis in term and PTB patients (Doyle *et al*, 2017; Sweeney *et al,* 2016) and will be discussed in detail in future sections.

1.3.4 Complications in chorioamnionitis

Chorioamnionitis is a leading cause of global PTB and the cases of PTB are rising (Tambor *et al*, 2015), thus research investigating HCA is increasingly important to understand development of the condition. Although incident rates vary across HCA and CCA, maternal and fetal complications are similar. If undiagnosed, chorioamnionitis may lead to further complication for the mother and neonate immediately and throughout life. In addition to PTB, HCA has been linked to adverse maternal and neonatal outcomes including, low birth weight (Ategeka *et al*, 2019), early onset sepsis (Sahni, Franco-Fuenmayor and Shattuck, 2019), cerebral palsy, structural brain lesions and developmental deficiency, due to persistent exposure to inflammation and immune activation (Becroft, Thompson and Mitchell, 2012; Galinsky *et al*, 2013). NEC, which is intestinal inflammation in the neonate, occurs more frequently in the presence of chorioamnionitis (Been *et al*, 2013; Taft *et al*, 2015), with NEC diagnosed in 10% of chorioamnionitis cases (Lu and Claud, 2018).

Improving current knowledge and diagnosis aims to reduce negative outcomes associated with chorioamnionitis. Along with affecting the individual, treatment, management and neonatal intensive care costs create collateral impact to the

economy and health care services (Kim *et al*, 2015). To improve the diagnosis and treatment of chorioamnionitis, first a greater understanding of the condition, including bacterial presence and inflammatory biomarkers is required.

1.3.5 Diagnosis, prevention and treatment of HCA

Early diagnosis and intervention of HCA is difficult due to the absence of clinical signs (Redline *et al*, 2003), thus it is increasingly important to continue research into diagnostic biomarkers. Although retrospective histological analysis is beneficial for management of the condition, informing of antibiotic treatment targeting potential causative microorganisms (Johnson, Adami and Farzin, 2017), alternate ways to diagnose HCA earlier are being studied (Catano Sabogal, Fonseca and Garcia-Perdomo, 2018; Jung *et al*, 2010). The inflammatory response to microorganisms within placental membranes creates a biomarker for predicting chorioamnionitis. Chemokines and cytokines, including interleukin-6 (IL-6) and IL-8 are routinely used for CCA severity diagnosis (Jung *et al*, 2010; Tita and Andrews, 2010), but are yet to be applied to asymptomatic HCA. Multiple biochemical markers have been suggested for maternal inflammatory detection; including IL-6, IL-8 and MMP-9 (Musilova *et al*, 2015; Roberts *et al*, 2012), with these increased in umbilical cord (Roberts *et al*, 2012) or amniotic fluid with inflammation and chorioamnionitis (Musilova *et al*, 2015). Current research relates a specific IL-6 gene allele characteristic to HCA (Konwar *et al*, 2019), yet this was limited to East Asian populations and not related to European, African or South Asian populations. A recent Cochrane systematic review and meta-analysis observed that inflammatory marker C-reactive protein (CRP) in maternal serum was the most beneficial measurement for HCA detection; with 69% sensitivity and 77% specificity to HCA (Catano Sabogal, Fonseca and Garcia-Perdomo, 2018). NICE also recommends further research into CRP for the prediction of HCA following PPROM (NICE, 2019). CRP is suggested to be lower in healthy preterm compared to healthy term (Tita and Andrews, 2010) indicating levels are gestational age dependent, limiting specificity to HCA. Alternatively, monitoring WBCs provided 67% sensitivity and 72% specificity to HCA (Jung *et al*, 2010).

Many biochemical diagnostic methods aim to detect maternal inflammation or infection rather than chorioamnionitis specifically. This can lead to false positive results and decrease the specificity of diagnosis to HCA as it is impacted by

inflammation elsewhere in the body (Cobo, Kacerovsky and Jacobsson, 2017). The inflammatory profile of maternal blood or plasma may not be reflective of the fetal membranes (Seong *et al*, 2014), with amniotic fluid samples a better predictor of infection and inflammation (Park *et al*, 2018). The combination of multiple biochemical and morphological diagnostic tests may be required to definitively diagnose the condition.

The absence of symptoms and delayed diagnosis creates difficulties for treatment interventions. Currently, there are no clear NICE guidelines for the treatment of chorioamnionitis (NICE, 2019). The main priority is to reduce time from membrane rupture until delivery, preventing exposure to external microorganisms (Doyle *et al*, 2014; Doyle *et al*, 2017). Treating the potential causative bacteria, including *Ureaplasma* and *Mycoplasma* by aminopenicillin and gentamicin is beneficial to reduce infection (Johnson, Adami and Farzin, 2017). Yet, antibiotic treatment should only be administered if chorioamnionitis is confirmed histologically (Higgins *et al*, 2016).

1.4 Microbiology and the microbiota

The microbiome is all of the genetic material of all the microorganisms in one environment or location at one specific time (Proctor, 2011), with the microbiota focussing specifically on bacterial gene elements (Proctor, 2011). Microbiomes are detected in diverse locations, from the human gut (Stewart *et al*, 2016; Young *et al*, 2017), lungs and sputum (Purcell *et al*, 2014), oral cavity (Fardini *et al*, 2010) and vaginal mucosal surface (Romero *et al*, 2014a), to environmental locations including hospital wards (Shin *et al*, 2015) and ultrapure water (Kulakov *et al*, 2002). The microbiota for each location varies in type, abundance and diversity of bacteria. The microbiota is the unique fingerprint of a sample, providing distinct characteristics and functions (Lloyd-Price, Abu-Ali and Huttenhower, 2016). The microbiota is also temporally dynamic, for example, *Lactobacillus* within the vaginal microbiota increases throughout gestation, decreasing again postpartum (MacIntyre *et al*, 2015).

1.4.1 Microbiology of the fetal environment and HCA

The microbiota of the placenta and fetal membranes is inconclusive (Aagaard *et al*, 2014; Jones *et al*, 2009; Leiby *et al*, 2018). The assumption that the placenta, fetal membranes and developing fetus remain sterile throughout a healthy pregnancy were originally accepted. However, in the 1980s bacteria were detected for the first time by culture methods from 16% of healthy chorion tissues (Kovalovski *et al*, 1982). This pioneering study questioned previously assumed theories and led to ongoing placental microbiota research and debates (Aagaard *et al*, 2014; Jones *et al*, 2009; Leiby *et al*, 2018). The three debated theories of the placental and fetal membrane microbiota are; the sterile placenta theory, sterile inflammation theory and the theory of a genuine placental microbiota.

1.4.1.1 Sterile placenta theory

The constant sterile placenta theory suggests that the placenta and fetal membranes are sterile and do not contain a genuine and unique microbiota (de Goffau *et al*, 2019; Kuperman *et al*, 2020; Perez-Munoz *et al,* 2017; Theis *et al*, 2019). Multiple microbiological and molecular methods (bacterial culture, Gram staining, immunohistochemistry (IHC), electron microscopy, quantitative polymerase chain reaction (qPCR) and next generation sequencing (NGS)) failed to detect any bacteria on healthy or pre-eclampsia placental tissues (Kuperman *et al*, 2020). With all samples and negative controls beyond the quantification and limit of detection in the qPCR methodology. Any bacterial detection in these tissues is attributed to exposure to the external maternal environment of the skin and vaginal cavity (Jones *et al*, 2009), linked to mode of delivery. This confirmed by vaginal originating bacteria including *Lactobacillus* present in vaginal births, and caesarean section births containing skin surface bacteria such as *Staphylococcus* (Dominguez-Bello *et al*, 2010). Contrasting evidence suggests low contribution from bacteria of vaginal origin, as Onderdonk *et al* (2008a; 2008b) discovered only 12% of placental membranes from vaginal delivery included vaginal originating *Lactobacillus*, with *Staphylococcus* and *Corynebacterium* detected in 42%, possibly originating from the maternal skin microbiota (Onderdonk *et al*, 2008a). Detection may be attributed to gestational age rather than mode of delivery, with diverse polymicrobial detection in PTB, including *Ureaplasma*, *Fusobacterium*, *Streptococcus* and *Mycoplasma* compared to a dominance of *Lactobacillus* at term (Jones *et al*, 2009; Onderdonk *et*

al, 2008b). Alternatively, bacteria detected in these tissues may arise from environmental contamination. Lauder *et al* (2016) and Shin *et al* (2015) suggested that fetal membrane bacteria originated from environmental sources, with sequencing methods unable to differentiate between negative technical controls of hospital environment, biological safety cabinets or DNA extraction kit negatives and healthy placenta (Theis *et al*, 2019), suggesting contribution during sample processing (Weiss *et al*, 2014).

1.4.1.2 Sterile inflammation theory

A second theory is the sterile inflammation theory, suggesting that the placenta is sterile without complication and bacteria are only detected if an infection, disease or pregnancy related condition is present (Fichorova *et al*, 2011; McCuaig *et al*, 2018; Seferovic *et al*, 2016). Sterile inflammation has been related to tissue trauma, hypoxic stress and danger signalling of damage associated molecular patterns (DAMPs; Rock *et al*, 2010). Bacterial detection has been correlated to the location of initial infection or inflammation, as oral pathogens, mainly *Fusobacterium* have been detected in the placenta following periodontal disease (McCuaig *et al*, 2018; Seferovic *et al*, 2016). This suggests haematogenous transfer of bacteria to the fetal membranes, with translocation from the oral environment explored in other conditions including, chronic kidney disease (Hickey *et al*, 2020). This supported by bacteria characteristic to bacterial vaginosis (*Gardnerella vaginalis* and *Prevotella*) detected only when bacterial vaginosis was confirmed (Fichorova *et al*, 2011).

1.4.1.3 Genuine microbiota theory

A third theory suggests that a constant, non-pathogenic, low abundance placental microbiota exists, consisting of *Escherichia, Proteobacteria* and *Tenericutes* (Aagaard *et al*, 2014). This profile was detected across 320 placentas compared to five alternate body sites taken from non-pregnant patients via whole genome sequencing. This study was one of the first to raise such controversial aspects, generating response from the scientific community and raising questions on the lack of contamination controls from identical patients and external environments (Kilman, 2014). Due to the low biomass of the placenta and fetal membranes, increased contamination from DNA extraction kits and laboratory reagents is apparent (Salter

et al, 2014). *Escherichia* is the suggested main component of the placental microbiota, y*et al*so the primary bacterium identified as a contaminant in low biomass microbiota research (Eisenhofer *et al*, 2019; Glassing *et al*, 2016; Salter *et al*, 2014; Stinson, Keelan and Payne, 2018b). Previous studies have detected genera in fetal membranes that originate from kit negative controls, including *Dorea* and *Pseudomonas* (Glassing *et al*, 2016; Salter *et al*, 2014). Careful consideration is required when interpreting findings and elucidating the microbiota of fetal membranes, with requirements to include negative controls, to detect and investigate the potential contaminating kit reagent microbiota or 'kitome' within each study.

1.4.2 Placental and fetal membrane microbiota with chorioamnionitis

Although the existence of a unique healthy fetal membrane microbiota remains debated (Aagaard *et al*, 2014; Jones *et al*, 2009; Leiby *et al*, 2018), research has expanded into investigating the placental and fetal membrane microbiota when a maternal condition is present, relating to the sterile inflammation theory. Findings suggest differences in bacterial profiles and diversity in patients diagnosed with chorioamnionitis, compared to patients without chorioamnionitis (Prince *et al*, 2016; Sweeney *et al*, 2016). The bacterial profile in PTB patients with HCA has shown to contain greater urogenital and oral bacteria (Prince *et al*, 2016), including greater *Fusobacterium* and *Ureaplasma* in HCA, yet increased *Lactobacillus* in term placenta, independent of HCA status (Prince *et al*, 2016). Yet, fetal membrane swabs were utilised rather than extracted tissue samples, with all patient demographics displaying consistently high levels of *Escherichia* (Prince *et al*, 2016).

Ureaplasma is the most frequently isolated bacteria from patients with HCA, occurring in 59% and 60% of preterm and term membranes with chorioamnionitis, respectively (Sweeney *et al*, 2016), proposing involvement in chorioamnionitis regardless of gestational age. However, only late preterm births were included in the cohort limiting generalisation to this research focussing on early preterm, which display the greatest risk of chorioamnionitis (Decembrino *et al*, 2014). This Gram-negative commensal vaginal bacterium was the only bacteria significantly correlated to chorioamnionitis in placental samples via species-specific multiplex qPCR, detected in 33% compared to 9% without chorioamnionitis (Cox *et al*, 2016). Other bacteria measured but not linked were *Mycoplasma*, *Gardnerella* and *Streptococcus*

(Cox *et al*, 2016). *Prevotella* is a Gram-negative commensal oral bacteria, which has been detected in 47% of HCA placenta with bacterial vaginosis via culture techniques (Fichorova *et al*, 2011). *Prevotella* has been strongly linked to vaginal pathologies and dysbiosis including bacterial vaginosis (Aroutcheva, Ling and Faro, 2008; Si *et al*, 2017), also to additional negative neonatal outcomes of spontaneous PTB (sPTB; Kim *et al*, 2015) and small gestational size (Doyle *et al*, 2017).

It may not be the type of bacteria or bacterial profile in the fetal membranes that impact chorioamnionitis, but the abundance of bacteria. Previous research has linked bacterial load to HCA (Doyle *et al*, 2017; Jones *et al*, 2009; Kim *et al*, 2009). Bacterial loads of up to 5.2 $\log_{10}$ copies/µl have been detected in fetal membranes with HCA (Doyle *et al*, 2017). Studies have linked bacterial loads and specific genera as combined factors in HCA, including a two-fold increase in *Prevotella* from cultured membranes (Hecht *et al*, 2009).

The inflammatory response in HCA displays high variation which may be bacterium dependent. Fetal membranes react to bacterial presence by increasing IL-1β, TNF-α and IL-6 cytokines (Maddipati *et al*, 2016), creating an inflammatory cascade to increase neutrophil influx and host defence response (Kim *et al*, 2015). Fichorova *et al* (2011) suggested bacterial dependent levels, with *Ureaplasma* generating an increase in MIP-1β and ITAC, yet *Mycoplasma* creating an increase in MMP-9.

Novel biomarkers have been studied to improve HCA detection and diagnosis, plus understand the inflammatory pathway response in HCA. The study initiating this research project investigated the gene expression of TLR signalling pathways in HCA via qPCR (Waring *et al*, 2015). Findings displayed increased TLR1, TLR2 and LY96 in HCA chorion, or increased IL-8 and IRAK2 within HCA amnion, with correlation between increased gene expression of these inflammatory factors and maternal inflammatory stage and grade (Waring *et al*, 2015). This suggests the involvement of bacteria as inflammatory agents, activating inflammation via the common IRAK and NF-$_{K}$β pathway (Waring *et al*, 2015). Yet further investigation into the amount and type of bacteria required to activate the inflammatory response in HCA is required.

1.4.3 Pathway of initiation in chorioamnionitis

To support the detection of bacterial communities in the placenta and fetal membranes, investigating the route of transportation and pathway of initiation is important. One theory states that bacteria ascend from the lower female reproductive tract (Park *et al*, 2009), with bacteria detected in the placenta from vaginal or lower reproductive tract origin, such as *Mycoplasma* and *Ureaplasma* supporting the theory (Prince *et al*, 2016). Contrasting research highlights that ascending bacteria are detected in a minority of chorioamnionitis cases, with active uterine contractions during parturition the initiating factor rather than a passive process occurring prior to, and therefore causing preterm labour (Jones *et al,* 2009). This route would require bacteria to possess the characteristics to transverse and survive through multiple immunologically active tissues and diverse environments within the reproductive system (Hyde and Schust, 2016), including the mucosal interface serving as an additional immunological and physical barrier to colonisation (Hyde and Schust, 2016). *In vitro* studies have demonstrated this capability, with *Prevotella* able to invade human cervical endothelial cells (Strombeck *et al*, 2007). A further theory generating increased support is the haematogenous and systemic transport of bacteria. Animal studies support this pathway, as oral or intravenous inoculation with the intestinal originating *Lactobacillus reuteri* led to detection of this bacterium in 20% of placentas, where it would not otherwise naturally reside (Seferovic *et al*, 2016). As one of the most diverse body sites, the likelihood of isolating comparable bacteria from oral origin is high (Gomez-Arango *et al*, 2017), yet human studies reveal conflicting research, suggesting no bacterial correlation exists between amnion and oral samples (Bearfield *et al*, 2002). Bacteria may also reach the fetal membranes following invasive procedures during gestation, including amniocentesis (Jackel and Lai, 2013; Rode *et al*, 2000). By disrupting the protective multiple membrane barrier and exposing the fetal environment to external sources, pathogenic bacterium may be introduced to the fetal membranes (Jackel and Lai, 2013). The collection of multiple body site and environmental samples would support research to determine the origin of bacteria in the fetal membranes.

1.5 Microbiota research and evolving techniques

Originally the universal method for bacterial detection was microbiological culturing, as this is a low cost, low time commitment technique, which remains useful for medical microbiological diagnostics (Bilen *et al*, 2018). Yet, methodological detection limits prevent the investigation of uncultivable and low-density bacterium (Han *et al*, 2009; Prosser *et al*, 2007). The 16S rRNA gene now used in qPCR allows sensitive and reliable detection of uncultivable bacterium, including *Fusobacterium* (Han *et al*, 2009; Nadkarni *et al*, 2002). The universal 16S rRNA gene is ubiquitous to all bacteria, with specific variable regions allowing detection and differentiation across bacterial genera and species (Fuks *et al*, 2018). Molecular and microbiological techniques are highly beneficial for quantitative research of the microbiota, with focus on abundance and bacterial loads or quantitative changes in biomarkers. However, minimal qualitative information can be derived from these methods. The requirement for high sample processing within sequencing and qPCR increases the occurrence of contamination, especially in low biomass samples (de Goffau *et al*, 2018; de Goffau *et al*, 2019; Eisenhofer *et al*, 2019).

Microbiological sequencing of the fetal membranes will improve current knowledge, but spatial location and visual identification of bacteria would be beneficial to confirm bacterial presence. Integration of analytical methods is increasing, with various spectroscopy techniques used in reproductive related research studying cervical remodelling (O'Brien *et al*, 2014) and pre-eclampsia (Chen *et al*, 2014). However, is yet to be used for investigating biochemical profiles in fetal membranes with chorioamnionitis or combined with sequencing technologies. Novel techniques, including Raman spectroscopy monitor independent biochemical properties of bacteria or tissues to differentiate between conditions (Chen *et al*, 2014). Detection of a spectral fingerprint specific to HCA by a timely, non-destructive and label free method would improve point of care diagnosis, plus confirm bacterial location in a biochemical context. Raman spectroscopy is beneficial to HCA and fetal membrane analysis due to a reduction in sample processing, plus decreased impact of external bacterial contribution and contamination of these low biomass tissues (Pahlow *et al*, 2015). Current placental research has focussed on biochemical structures, including detection of differentiated α-helix and β-pleated sheet structure in pre-eclampsia patients (Chen *et al*, 2014). Intrauterine growth restriction has been linked to Raman shifts in amide functional groups (I, II and III; Pielesz *et al,* 2019), plus differential haemoglobin Raman shifts in hypoxic placental samples (Schlabritz-Loutsevitch *et*

al, 2017). Previous research highlights the potential beneficial application to HCA, but due to the low biomass characteristics of the fetal membranes, the ability for Raman spectroscopy to accurately detect low concentrations of bacteria must initially be determined prior to clinical application.

1.6 Thesis relevance

Knowledge of the fetal membrane microbiota with HCA is incomplete. Further research is required to identify associated microorganisms and inflammatory biomarkers of HCA in fetal membranes. Initial experiments aim to inform subsequent studies, enhance current knowledge on the pathological process behind HCA, plus aid in future development of novel diagnostic targets. With a combined aim to detect HCA, plus reduce associated negative maternal and neonatal outcomes, including PTB. Current literature highlights the difficulty of achieving a firm explanation of the fetal membrane microbiota in HCA, with involvement of a complex interactive polymicrobial pathway.

1.7 Overview of thesis aims

The overarching theme of this thesis was to increase current knowledge and understanding of the fetal membrane microbiota in HCA.

- The first results chapter aims to investigate the microbiota of frozen fetal membranes with HCA and compare this to non-HCA fetal membranes from preterm and term patients via Illumina sequencing (Chapter three). This also investigates the relationship between the microbiota, abundance, bacterial profile and individual bacteria to HCA inflammation levels.
- Chapter four aims to compare matched paired FFPE and frozen fetal membranes to determine if routinely collected and analysed FFPE samples could be utilised in microbiota research.
- Chapter five aims to determine if bacterial loads can be detected on low risk term fetal membranes, plus to further clarify and confirm bacterial load levels on fetal membranes with HCA compared to preterm and term patients via 16S rRNA gene qPCR. In addition to investigate the link between bacterial load and HCA inflammation levels or inflammatory marker expression.

- Chapter six aims to investigate if the novel non-invasive, non-destructive Raman spectroscopy method can identify and differentiate bacteria in low biomass cultures. This aims to understand the potential application to bacterial detection on fetal membranes.

Chapter Two: Research methodology.

To investigate the fetal membrane microbiota multiple methodologies were explored. Firstly, fetal membrane tissues were collected, DNA was extracted with commercial DNA extraction kits, then quantified via NanoDrop spectrophotometer, agarose gel electrophoresis and Bioanalyzer chip-based electrophoresis. Illumina sequencing was performed for microbiota analysis and 16S rRNA gene qPCR for bacterial load investigations. The theory of each method is explained followed by specific methodological processes.

A list of reagents, chemicals, commercial kits and equipment used throughout this research can be found in the appendix (A.1).

2.1 Sample and tissue selection

Fetal membrane samples utilised for this retrospective cohort study are a subset of samples included in a previous study investigating inflammatory signalling of the Toll-like receptor (TLR) pathway in chorioamnionitis (Waring *et al*, 2015). This research project expands on previous findings by focussing on the bacterial involvement of the inflammatory response in HCA. Samples were utilised for current research via a transfer agreement, with prior approval from Newcastle and North Tyneside 1 Research Ethics Committee (10/H0906/71).

Women were recruited for the original prospective study following admission to Newcastle Upon Tyne NHS Foundation Trust Hospitals with spontaneous labour. Over 12-months, 24 women gave written consent to collect and store their placental and fetal membrane samples and use outcome data for research purposes. Samples were categorised into three groups; preterm spontaneous labour with histological chorioamnionitis (HCA; n=12), preterm spontaneous labour without HCA (PTB; n=6) and term spontaneous labour without HCA (Term; n=6). Spontaneous labour was defined as the presence of regular spontaneous uterine contractions with progressive cervical dilation leading to delivery. Inclusion criteria for preterm patients were; singleton pregnancy, spontaneous labour, and gestational age <34 weeks covering early PTB. Alternatively for the term cohort; singleton pregnancy, spontaneous labour, and ≥37 weeks gestation. Term patients were excluded if displaying histologically confirmed chorioamnionitis.

2.2 Fetal membrane preparation

Placental tissue and amniochorionic membranes were collected immediately following delivery. Amniochorionic membranes were sterile dissected from the placental edge and stored in sterile ice cold phosphate buffered saline (1X PBS), before being washed thoroughly in 1X PBS to remove blood and debris. The amnion and chorion were separated, with the maternal decidua scraped from the chorion. Individual membranes were then divided into 4-5 cm segments and stored at -80 °C, until required. These samples form the fresh-frozen fetal membrane subset used in this study.

To detect and diagnose HCA, two amniochorionic membrane rolls were assessed. Combined unseparated membranes were fixed in 10% neutral buffered formalin, embedded in paraffin wax, sectioned to 3 µm slices, stained with haematoxylin and eosin (H&E) and histologically examined. Maternal and fetal inflammatory response was assessed by a consultant gynaecologist and histopathologist (Dr Judith Bulmer). HCA was defined by standardised Redline criteria at maternal inflammatory response stage two or above, with subchorionitis classified as stage one maternal inflammatory response (Redline *et al*, 2003). Amniochorionic membrane rolls were stored within a sealed cassette case at room temperature (RT), creating the Formalin-Fixed Paraffin-Embedded (FFPE) fetal membrane subset analysed in this study.

2.3 Sample selection demographics

Samples available for analysis included 24 FFPE and frozen fetal membranes (Table 2.1). Frozen samples consisted of HCA (n=12), PTB (n=6) and Term (n=6). With both amnion and chorion processed (HCA=8, PTB=5, Term=0), amnion only (HCA=1, PTB=0, Term=0), or chorion only (HCA=3, PTB=1, Term=6). FFPE fetal membrane rolls consisted of HCA (n=12), PTB (n=6) and Term (n=6). Multiple locations on the fetal membranes were processed for chorioamnionitis and PTB samples giving biological replicates from frozen (n=78) and FFPE tissues (n=111).

		HCA (n=12)	PTB (n=6)	Term (n=6)
Maternal age (mean (SD))		29.3 (8.0)	27.0 (5.5)	32.2 (6.0)
Maternal BMI (mean (SD))		22.0 (9.2)	22.5 (4.5)	22.3 (2.1)
Smoker	Yes	4.0 (33.3)	2.0 (33.3)	0.0 (0.0)
	No	6.0 (50.0)	4.0 (66.7)	6.0 (100.0)
	NA	2.0 (16.7)	0.0 (0.0)	0.0 (0.0)
Parity (mean (SD))		1.6 (2.2)	1.5 (1.8)	0.7 (1.2)
Antibiotics	Yes	7.0 (58.3)	4.0 (66.6)	-
	No	5.0 (41.7)	1.0 (16.7)	-
	NA	0.0 (0.0)	1.0 (16.7)	-
Antenatal corticosteroids	Yes	11.0 (91.7)	5.0 (83.3)	-
	No	1.0 (8.3)	1.0 (16.7)	-
Maternal stage (mean (SD))		2.2 (0.4)	1.0 (0.0)	-
Maternal grade (mean (SD))		1.6 (0.5)	1.0 (0.0)	-
Number of clinical CA signs (mean (SD))		0.9 (1.2)	0.2 (0.4)	-
C-reactive protein (mean (SD))		55.6 (54.9)	6.4 (2.6)	-
White blood cell count (mean (SD))		19.1 (6.9)	12.9 (5.2)	-
Previous PTB	Yes	5.0 (41.7)	1.0 (16.7)	-
	No	7.0 (58.3)	5.0 (83.3)	-
Previous early PTB	Yes	2.0 (16.7)	1.0 (16.7)	-
	No	10.0 (83.3)	5.0 (83.3)	-

Table 2.1 Maternal patient demographics. Maternal characteristics from all patients providing fetal membrane samples for the study, including preterm birth with histological chorioamnionitis (HCA), plus preterm (PTB) and term without HCA (Term). Values displayed as n (%) unless stated.

2.4 Genomic DNA extraction

Commercially available DNA extraction kits have improved the speed, cost and efficiency of extracting DNA from complex sources (Demeka and Jenkins, 2009), but have received criticism due to increased contamination (de Goffau *et al*, 2019; Laurence, Hatzis and Brash, 2014; Salter *et al*, 2014). Commercial kits aim to extract DNA via chemical, enzymatic, mechanical and thermal methods, plus selective binding of silica-based membranes (Lauder *et al*, 2016). The alternative to commercial DNA extraction kits is phenol-chloroform isolation (Senguven *et al*, 2014). However, optimised commercial kits increase DNA concentration, improving PCR amplification and sequencing (Senguven *et al*, 2014). The lowest contamination levels in kit comparison research was from MoBio (Salter *et al*, 2014), with Qiagen also recommended due to high quality and quantity DNA extracts (Janecka, Adamczyk and Gasinska, 2015).

Throughout the study, methodology and reagents were kept consistent wherever possible. However, FFPE and frozen samples were extracted using different commercial kits, due to independent tissue characteristics and preparation methods. Kit negative controls were included and analysed from both extraction kits to monitor variability. Fixative methods increase the complexity of DNA retrieval from FFPE tissues. FFPE tissues were fixed in paraffin, thus they require additional processing steps. A commercially available FFPE specific DNA extraction kit has improved the yield and purity of DNA extracts, plus decreased inhibition in downstream analysis (Dietrich *et al*, 2013). This is due to the deparaffinisation steps involving combined use of specific chaotropic salt-based lysis and enzymatic buffers, plus high temperature incubations to melt the paraffin wax and reverse crosslinkages (Al-Attas *et al*, 2016; Senguven *et al*, 2014). These intense processing steps decrease the ability to transfer this method to frozen samples. These kits also utilise silica membrane columns or magnetic beads to reverse DNA binding from fixative processes (Arreaza *et al*, 2016; Senguven *et al*, 2014). Although fragmentation is universal in FFPE samples, the silica membranes in commercial kits will bind only DNA fragments ≥100 bp, improving DNA quality (Dietrich *et al*, 2013). Comparison between commercially available kits has suggested optimum use of the Qiagen or MoBio FFPE specific kit (Biesbroek *et al*, 2012), with these generating the highest yield, concentration and purity (Huijsmans *et al*, 2010; Janecka, Adamczyk and Gasinska, 2015; Patel *et al*, 2017; Senguven *et al*, 2014). The MoBio BiOstic FFPE tissue DNA isolation kit was utilised in this

research, with previous positive application to placental, umbilical and uterine samples (Ernst *et al*, 2015; Zhao *et al*, 2016). Whereas the QIAamp Fast DNA tissue kit (Qiagen) was selected for frozen tissue DNA extraction due to optimum outcomes from kit comparison studies, plus use in current placental and reproductive tract microbiota research (Jones *et al*, 2009; Stewart *et al*, 2019; Sweeney *et al*, 2016; Weiss *et al*, 2014).

2.4.1 Genomic DNA extraction: Frozen membranes

Total genomic DNA was extracted from 25 mg frozen membranes on ice under sterile conditions via QIAamp Fast DNA tissue kit (Qiagen). Sectioned and weighed fetal membrane tissues were added into individual QIAamp tissue disruption tubes containing a metal bead for mechanical lysis, alongside enzymatic and chemical lysis provided by the reagents. 265 µl of freshly prepared mastermix was added to all tubes, consisting of 200 µl AVE (0.04% NoN_3 sodium azide), 40 µL VXL (guanidinium chloride and Triton X-100), 1 µl DX reagent (antifoaming buffer), 20 µl Proteinase K and 4 µl RNase A (100 mg/ml). Tubes were vortexed for five minutes in a Vortex-Genie (Scientific Industries) before transferring to a thermal mixer (ThermoMixer, Eppendorf) for ten minutes at 56 °C and 1000 rpm to homogenise samples. To all tubes, 265 µl MVL (guanidine and isopropanol) was added and vortexed for ten seconds, before transferring the solution to QIAamp mini spin columns, with a silica membrane to isolate DNA. Tubes were centrifuged at 13,000 xg for one minute (Microfuge, Sigma), before transferring the spin column into a sterile tube. AW1 buffer (500 µl) was added to all tubes and centrifuged as previous, before transferring the spin column into a sterile tube and repeating with 500 µl AW2 buffer. AW buffers are wash buffers to improve the purity of the eluted DNA without affecting DNA quantity. Once transferred to sterile collection tubes, 50 µl elution buffer (ATE) was added to the membranes to elute nucleic acids. Tubes were incubated for two minutes at RT before centrifuging at 13,000 xg for one minute. Silica membranes were discarded, and the eluted nucleic acids were stored at -20 °C until required for analysis (maximum duration: 18 months). Genomic DNA was extracted from all amnion and chorion tissues (n=78). Kit negative controls were also processed identical to samples, with dH_2O replacing tissue samples (n=9).

2.4.2 Genomic DNA extraction: FFPE membranes

Nucleic acid extraction from FFPE samples were performed via BiOstic FFPE Tissue DNA isolation kit (MoBio) at RT under sterile conditions. Samples were sectioned to 10 µm in triplicate using a manual rotary microtome (Leica, RM2125). External slices were discarded to minimise the impact of environmental contamination. Processed slices were weighed and trimmed to 15 mg and added to collection tubes. 180 µl FP1 and 20 µl FP2 deparaffinisation solutions were immediately added to each tube to chemically and enzymatically dissolve the wax. Tubes were vortexed on a Vortex-Genie for 20 seconds and centrifuged (Microfuge, Sigma) at 13,000 xg for 30 seconds to bring the wax into contact with the buffers. 20 µl FP3 was added to the solution and vortexed for ten seconds before incubating in a heat block at 55 °C for two-hours. This was followed by a one-hour incubation at 90 °C. FP3 contains Proteinase K which enhances the breakdown of DNA-protein crosslinkage, with optimum performance at 55 °C. Following incubation, tubes were centrifuged at 13,000 xg for one minute and the digested solutions were transferred to new collection tubes, avoiding the transfer of remaining wax segments. 200 µl of FP4 was added to tubes and vortexed for ten seconds. This chaotropic salt buffer aids DNA binding to silica membranes. 200 µl 100% ethanol (FP5) was added to the tubes and vortexed for ten seconds to improve binding conditions. Extracts (650 µl) were transferred onto silica membrane spin columns used to purify and isolate DNA. Spin columns were centrifuged at 10,000 xg for one minute and excess solution discarded. 500 µl wash buffer (FP6) was added directly onto the membrane and centrifuged at 10,000 xg for one minute to remove excess proteins and contaminants. The filter column was transferred to a new sterile tube before adding 500 µl of ethanol wash solution (FP7) and centrifuging as previously. Excess solution was discarded, and tubes were centrifuged at 13,000 xg for two minutes before transferring the silica membrane to a new sterile tube. To the dried filter membrane, 50 µl elution buffer (FP8) was added and incubated at RT for five minutes. Tubes were centrifuged at 10,000 xg for one minute. The spin column was discarded, and eluted DNA stored at -20 °C until required for downstream processing (maximum duration: three months). Wax negative controls formed of excess paraffin wax which surround corresponding FFPE fetal membrane tissues (n=37) were analysed alongside samples (n=111) to identify the contribution of microorganisms within the wax. DNA extraction kit negative controls (n=18) were processed alongside with identical techniques**.**

Extracted DNA from FFPE and frozen tissues, plus wax and kit negative controls were loaded onto 96-well plates for use during sequencing.

2.5 Theory of DNA quantification

Analysing DNA extract quality and quantity is important prior to downstream processing. Determining DNA fragment size is especially crucial for FFPE samples, as fixing and embedding processes creates shorter targets for primer annealing in sequencing and qPCR (Nagahashi *et al*, 2017; Patel *et al*, 2017). NanoDrop spectrophotometer is an ultraviolet light absorption spectroscopy method (Ivarsson and Carlson, 2010), which determines the quantity (ng/µl) and quality of DNA extracts (purity ratios). Purity ratios of A260:A280 compare DNA purity to protein contamination, including residual phenol, with A260:A230 detecting organic molecules and contamination originating from guanidine, phenol and chaotropic salts (Desjardins and Conklin, 2010). Optimum ratios are ~1.8 and >2.0 for A260:280 and A260:230, respectively (Desjardins and Conklin, 2010). Values below the optimum indicate low DNA purity, issues with extraction methodology or contamination, which may impact downstream applications (Desjardins and Conklin, 2010). The NanoDrop is rapid and relies on small micro-volumes of liquid (1 µl), preventing sample wastage (Ivarsson and Carlson, 2010). However, has been criticised as overestimating sample DNA quantity, with low reproducibility between replicates (Simbolo *et al*, 2013).

Additionally, agarose gel electrophoresis analyses the size and molecular weight of DNA fragments when comparing to a reference HyperLadder. Analysis is based on separation via molecular size and structural conformation by use of an electric charge (Lee *et al*, 2012). Understanding DNA fragment size is crucial to determine if the assigned target sequence will amplify. However, reliance on reference HyperLadder quality and visual analysis from the investigator limits specificity (Lee *et al*, 2012). The Qubit has been suggested as an alternate measurement tool, with increased application for low biomass samples, accurately detecting DNA yield at 0.5 ng/µl (Seiler *et al*, 2016; Simbolo *et al*, 2013).

2.5.1 NanoDrop spectrophotometer method

To confirm successful DNA extraction and monitor yield and purity of DNA, NanoDrop spectrophotometer (1000, V3.8.1; Thermo Fisher) was performed on

extracted DNA from FFPE and frozen fetal membrane tissues, plus wax and kit negative controls. The system was cleaned using1 µl dH_2O and calibrated using 1 µl of respective elution buffer which the DNA is stored in, before measuring samples (1 µl) in triplicate. DNA concentration (ng/µl), and purity (A260:280 and A260:230) were assessed. Average concentration values were calculated and used for sequencing preparation. Low yield samples (<50 ng/µl for frozen and <20 ng/µl for FFPE) were concentrated using a vacuum centrifuge concentrator (Christ RVC2-18, Vacubrand) at 60 °C to evaporate and decrease the solvent and increase solute concentration. Samples were then reassessed via NanoDrop spectrophotometer, with all samples then displaying optimum concentrations.

2.5.2 Agarose gel electrophoresis method

A 1% (w/v) agarose gel electrophoresis was performed to further assess DNA quality. Agarose was dissolved in 1X TBE with 0.1 µl/ml SYBR Safe DNA gel stain (Invitrogen) and set in agarose gel tanks. 10 µl of DNA product of interest was combined with 4 µl DNA loading dye (Bioline, 5X) and 6 µl of this loaded into corresponding wells of the agarose gel. 5 µl HyperLadder 1KB (Bioline) was loaded into the first and last lanes of the gel to determine DNA molecular weight. Agarose gel electrophoresis conditions were 150 v for a maximum of one hour, before imaging on a Bio-Rad Gel Doc EZ Gel Imager (Image Lab 3.0).

2.5.3 Bioanalyzer chip-based electrophoresis method

Chip-based electrophoresis (Bioanalyzer) was applied to FFPE samples due to difficult detection from agarose gel electrophoresis, plus the inability to accurately detect fragmentation and molecular damage (Sah *et al*, 2013). NanoDrop may overestimate DNA concentration in FFPE samples by 17 fold (Heydt *et al*, 2014), possibly due to the combined detection of both single and double stranded DNA (Heydt *et al*, 2014). Overestimating DNA concentration can lead to underestimating the volume required in downstream analysis, plus utilising highly fragmented and degraded DNA (Heydt *et al*, 2014). The highly sensitive DNA chip system is optimum for the analysis of fragmented DNA from FFPE samples, due to a low detection limit (Wimmer *et al*, 2018). Chip-based gel electrophoresis aimed to further investigate the quality and quantity of extracted DNA and increase reliability of

findings, as this method measures DNA molecular weight and fragmentation. This method applies a similar theory to the classical agarose gel; however, samples travel through a charged capillary network before analysing via a detector. Numerical values are automatically applied to DNA fragment sizes alongside digital gel images for visual analysis (Agilent Technologies, 2014). This method improves the accuracy and precision of low abundant DNA detection, removes observer variation and requires low sample volumes (Agilent Technologies, 2014).

Firstly, the Bioanalyzer (Agilent 2100) was cleaned with 350 µl dH_2O using an electrode cleaner. The DNA chip was added to the chip priming station and 9 µl of gel dye mix (DNA dye concentrate and DNA gel matrix) was dispensed into wells. 1 µl sample or reference ladder was pipetted into respective wells. DNA marker (5 µl) was also added into all sample wells, plus one ladder only well as a reference. The loaded DNA chip was vortexed (IKA Vortex mixer) at 2400 rpm for one minute and loaded into the Bioanalyzer receptacle for 40 minutes. Sample concentrations (pg/µl) and molecular size (bp) were analysed by peak tables and electropherogram gel images (2100 Expert).

2.6 Theory of Illumina sequencing

Illumina sequencing is a paired-end bridge amplification technology, utilising sequencing by synthesis methods (Figure 2.1). Initially, denatured single stranded DNA with adapter sequences ligated onto the 5' and 3' blunt ends anneal onto complementary oligonucleotides on the surface of the flow cell (Buermans and den Dunnen, 2014). A new complementary strand of the sequence is created during extension. The original library sequence is then cleaved generating a reverse strand sequence template copy. An adapter on the newly synthesised complementary strand forms a bridge by annealing to another complementary oligonucleotide on the flow cell, to create a second synthesis site (Bentley *et al*, 2008). The sequence is resynthesised during extension to create a complementary DNA sequence, which matches the original library sequence. Two complementary DNA sequence strands are now annealed onto the flow cell surface generating templates for sequencing by synthesis (Bentley *et al*, 2008). Multiple rounds of annealing, extension and denaturing creates 1 µm sequence clusters (Bentley *et al*, 2008).

Sequencing by synthesis functions by per base nucleotide incorporation or base calling, where each base is labelled with a different fluorophore allowing simultaneous sequencing, base incorporation and fluorophore measurement after each cycle (Ledergerber and Dessimoz, 2011). Between each cycle a reversible terminator prevents multiple extensions (Buermans and den Dunnen, 2014), with labels and terminators then removed in preparation for synthesis of the next nucleotide (Ledergerber and Dessimoz, 2011). Errors in base incorporation leads to lagging (phasing) or addition of multiple bases per cycle (pre-phasing; Ledergerber and Dessimoz, 2011). Cycle performance is monitored by Phred score analysis, which detects the probability of these base call errors (Bokulich *et al*, 2013).

Illumina sequencing is a sensitive, specific, low-cost methodology (Caporaso *et al,* 2012), with MiSeq creating high quality data compared to other available methods, including Ion Torrent or Roche 454 technologies (Pollock *et al*, 2018). Sequencing short read lengths of 250 bp (V4) is shorter than the 1000 bp required by Sanger sequencing (Ledergerber and Dessimoz, 2011), but this limits coverage depth which may increase basecall errors (Bustin *et al*, 2009). A further limitation of sequencing is the multiple preparation and processing steps, increasing the impact of externally contributing contamination (Salter *et al*, 2014). The high sensitivity of this method can increase the amplification and detection of these low abundant contaminants (Laurence, Hatzis and Brash, 2014), with this impact greater in low biomass samples (Strong *et al*, 2014). Preventing contamination is difficult, so research focuses on post-processing reduction of contamination via data analysis algorithms (Davis *et al*, 2018; Karstens *et al*, 2019).

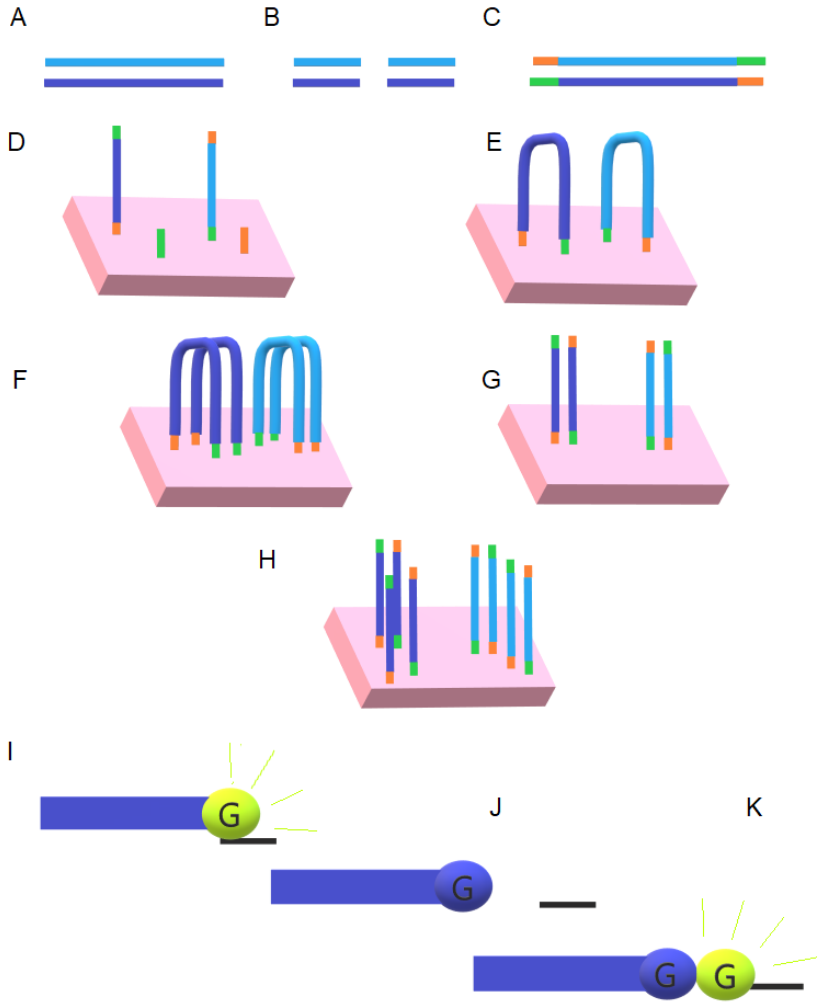

Figure 2.1 Paired end bridge amplification, with sequencing by synthesis. Template DNA (A) are prepared for sequencing by fragmenting the DNA (B) and annealing adaptors to the 3' and 5' end of the DNA sequence (C). The DNA is then denatured into single strands, each strand will then bind to complementary oligonucleotides primed onto the flow cell (D). A bridge will be formed as the opposite end of the DNA sequence hybridises to another complementary oligonucleotide on the flow cell (E). Polymerase then extends the complete sequence of DNA to recreate the double stranded DNA bridge (F). One end of the DNA is cleaved from the flow cell and now two strands of complementary DNA are present (G). This is then repeated for the reverse strand, with the original strand washed away to generate clusters of identical DNA strands (H). Sequencing by synthesis is performed via the addition of one base per cycle. The base will bind to the end of the DNA strand and fluoresce, allowing specific detection of that base (I). Each base has a unique wavelength and fluorescent colour, thus allowing detection on a base-by-base and cycle-by-cycle bases. Once bound and detected by the optical scanner, the terminator is cleaved, and fluorescence stops (J). Another base is now able to bind onto the sequence (K) and this continues for the number of programmed cycles.

The main target for sequencing and identification of microbial communities is the 16S rRNA gene phylogenetic marker. Sequencing the entire gene allows detection of conserved gene regions. In addition, variable gene regions allow specific and sensitive amplification and detection of bacterial genera and species (Wang and Qian, 2009). Primers can bridge the nine hypervariable and conserved regions for detection between phylogenetic groups and improve sequencing quality (Wang and Qian, 2009). Amplification bias, primer mismatch and sensitivity differences with each variable region is present, due to different evolutionary rates and coverage (O'Callaghan *et al*, 2019). The V4 variable region, used in this research is stated to be the most reliable region, along with the V5 region when compared across multiple sequencing platforms (Clooney *et al*, 2016), plus the most optimum for short reads and high coverage (Ghyselinck *et al*, 2013). Bias to specific taxa within each variable region has been observed, with an underestimation of *Proteobacteria*, but overestimation of *Firmicutes* from V3 and V4 regions detected using Ion Torrent sequencing (Laursen, Dalgaard and Bahl, 2017) or by computational construction (Wang and Qian, 2009). Benefits and limitations are present for all variable regions, thus matching the primer sequence to application is optimum.

2.6.1 Illumina sequencing method

To investigate the microbiota of the fetal membranes with and without HCA, Illumina amplicon sequencing was performed by Northumbria University (Newcastle) as described previously (Kozich *et al,* 2013), with the universal 16S rRNA gene primer specific to the V4 region (V4F: 5'-GTGCCAGCMGCCGCGGTAA-3', V4R: 5'-GGACTACHVGGGTWTCTAAT-3'; Biesbroek *et al*, 2012). Firstly, 17 µl AccuPrime PFX SuperMix was added to each well of a 96-well plate, as were 2 µl of each paired set of index primers (10 µm). 1 µl of sample, wax or kit negative control was transferred into corresponding wells. Each plate also contained one well of negative control (dH_2O) and one positive control well of PhiX mock microbial community (1 in 10, 2000 ng; ZymoBIOMICS). Plates were briefly vortexed before DNA was amplified in a thermal cycler (Applied Biosystem, 2720) according to PCR cycling conditions of: initial denaturation at 95 °C for two minutes, followed by 30 cycles of denaturation at 95 °C for 20 seconds, annealing at 55 °C for 15 seconds and extension at 72 °C for five minutes, plus a final extension step at 72 °C for ten minutes. A 1% agarose gel was prepared to confirm successful amplification. The product was normalised by loading 18 µl of PCR product and 18 µl binding buffer to

corresponding wells of the normalisation plate (Invitrogen SequalPrep) and incubating overnight at RT. Following incubation, the solution was removed from the wells, leaving only bound DNA on the plate. Wash buffer (50 µl) was added to wells and mixed by pipetting, before removing and repeating. 20 µl elution buffer was added, mixed by vortexing and incubated at RT for five minutes. 5 µl of eluted DNA from half of the wells were pooled and repeated for the other half of the plate.

Library quality and optimum dilutions were assessed by chip-based gel electrophoresis following dilution of pooled libraries to 1:10, 1:100, 1:1000, 1:2000 and 1:4000 in PCR grade H_2O. Results were used to calculate library concentration, with an optimum dilution selected as 1:2000. Libraries were quantified by qPCR with 6 µl KAPA SYBR Fast qPCR mastermix, plus 4 µl sample dilutions or standards in triplicate. Plates were vortexed before amplifying in a thermal cycler (C100; Bio-Rad) with the conditions of 95 °C for five minutes for initial activation, followed by 35 cycles of denaturation at 95 °C for 30 seconds and annealing at 60 °C for 45 seconds.

Positive sequencing controls were prepared, including a bacteriophage PhiX genome at 500 bp used as an in-run control for quality sequencing (2 µl PhiX, 3 µl nuclease free H_2O, 5 µl 0.2 NaOH), and 10 µl 0.2 NaOH was added to pre-prepared libraries. All were incubated for five minutes to denature the DNA, before library preparations and 15% PhiX were mixed and loaded onto the flow cell (600 µl). Forward and reverse sequence primers (3 µl), plus index primers (3 µl) were added to three independent wells. The flow cell was washed with dH_2O and blotted dry, before adding the reagent cartridge and flow cell to the MiSeq.

2.6.2 Microbiota data processing

Sequencing is high throughput, which results in increased data output available for analysis. FastQ files of forward (read 1) and reverse (read 2) sequences require post-processing to align, trim and filter via DADA2 (Callahan *et al*, 2016b), Bioconductor (Version 2; Callahan *et al*, 2016a) and Phyloseq (McMurdie and Holmes, 2013) pipelines and packages in R (R Core Team, 2017). Sequences are initially trimmed and filtered to remove low quality reads (quality score <30) and ensure consistent sequence lengths, this determined by forward and reverse error profiles (Callahan *et al*, 2016b).

Traditional methods clusters sequences into Operational Taxonomic Units (OTUs) at 97% similarity but may overestimate evolutionary similarity between sequences (Nguyen *et al*, 2016). In OTU analysis the inability to replicate or compare findings due to the arbitrary clustering percentage is a limitation (Callahan, McMurdie and Holmes, 2017). DADA2 clusters sequences into amplicon sequence variants (ASVs), with clusters differentiated by only one nucleotide alteration. This improves specificity, accuracy and resolution of bacterial detection (Callahan, McMurdie and Holmes, 2017). ASV analysis allows for improved comparison across studies, due to clustering via the specific DNA sequence (Callahan, McMurdie and Holmes, 2017). Low read counts are likely due to sequencing errors or contamination, with removal beneficial for downstream analysis (Dhariwal *et al*, 2017; Jervis-Bardy *et al*, 2015).

2.6.2.1 Sequencing data processing and statistical analysis methods

Sequencing data FastQ files were processed by Bioconductor workflow (Version 2; Callahan *et al*, 2016a) in R (R Core Team, 2017). Sequencing results were trimmed and filtered with a Q score of <30. Using DADA2 1.4 (Callahan *et al*, 2016b) sequence data was demultiplexed and dereplicated, with errors detected and removed. Forward and reverse paired sequences were merged, clustered into ASVs and chimeras removed. Low read count features with <2 for 20% ASVs were removed before assigning taxonomy via GreenGenes training set (Callahan, 2016). DECIPHER and phangorn packages were used to construct the phylogenetic tree. A Phyloseq object including sequencing table, taxonomy table and metadata was then created for further downstream analysis.

Filtered samples were analysed in the remaining analysis methods, this included removing <2 read counts in 20% of ASVs and ASVs with <10 counts merged. The filtered sample sets were processed through Phyloseq (McMurdie and Holmes, 2013) and Microbiome Analyst (Dhariwal *et al*, 2017) for abundance (relative and absolute), alpha diversity (Shannon), beta diversity (GUniFrac, PERMANOVA) and univariate analysis (nonparametric Man-Whitney or nonparametric Kruskal-Wallis). Results were then further analysed in R by nonparametric Kruskal-Wallis and nonparametric Pairwise Wilcoxon Rank-Sum (R Core Team, 2017).

Statistical analysis of sequencing data involves applying relative abundance measurements. This method analyses percentage composition of a genus in relative

comparison to total genera, at an overall abundance of 100% (Badri *et al*, 2018). This avoids bias and allows visualisation and comparison between subgroups independent of given bacterial abundance, which may not capture all DNA within a sample (Badri *et al*, 2018).

Diversity analyses includes Shannon alpha diversity indices and PERMANOVA for beta diversity. Alpha diversity assesses local bacterial sample composition, determining variety and number of bacterial genera (Shannon, 1958). Shannon diversity indices is the sum of a proportion of species relative to total number or species in community, accounting for species richness, abundance and evenness (Jovel *et al*, 2016; Schloss *et al*, 2016). This method is beneficial for low read counts and low biomass samples as it accounts for the impact of rare taxa (Schloss *et al*, 2016). Beta diversity investigates community level similarities (Jovel *et al*, 2016; Knight *et al*, 2018; McMurdie and Holmes, 2014). PERMONOVA investigates diversity clustering between groups and pairwise distances, with GUniFrac alpha 0.5 aiming to avoid dominance of highly abundant ASVs (Knight *et al*, 2018).

Initial analysis included all samples and negative controls. Following this, negative controls were removed, including wax controls from the FFPE subset. Samples were reprocessed through Phyloseq and Microbiome Analyst in an identical manner.

2.6.2.2 Decontam processing for FFPE samples

Alongside preventing contamination during pre-processing, post-processing filtering methods to detect and report contaminating sequences has been established (Davis *et al*, 2018; Oh *et al*, 2015). Some filtering methods may lead to the removal of genuine sequences alongside contaminants, as they remove any sequence detected in negative controls. But genuine sample originating sequences may be in low abundance within controls due to cross contamination (Davis *et al*, 2018). The R based decontam method has been utilised to detect contaminants, but avoid the removal of genuine sequence (Davis *et al*, 2018). The prevalence filtering method detects the presence/absence of genuine or contaminating ASVs from Phyloseq objects, determined by abundance of the ASV sequences in samples compared to a set of negative controls. This method works under the assumption that sequences present in higher abundance in negative controls are contaminants and those present in higher abundance in samples are genuine bacterial signals. However,

this does not account for DNA concentration (Davis *et al*, 2018). Alongside packages used previously, this post-processing method was applied to FFPE fetal membranes. The R code below was used to detect genuine sequences from FFPE samples. This method is preferable when samples are of low abundance with the possibility that contamination is dominant over genuine bacterium (Davis *et al*, 2018).

>isNotContaminant(physeq,neg="is.neg",method="prevalence",threshold=0.5,normalize=TRUE,detailed=TRUE)

Once detected ASVs were then separated into two independent Phyloseq objects; one containing only genuine sequences and the second only sequences identified as contaminants.

2.7 BactQuant quantitative PCR

qPCR is currently used for diagnosis of bacterial infection and clinical pathologies (Bustin, 2010; Kasper *et al*, 2010; Patel, Harris and Fitzgerald, 2017) for improved accuracy of bacterial load investigation and can be combined with culture and sequencing results to validate findings (Kralik and Ricchi, 2017; Parnell *et al*, 2017). To detect the bacterial load in fetal membranes with and without HCA, qPCR was performed using BactQuant 16S rRNA gene primers (Liu *et al*, 2012) on previously extracted DNA.

2.7.1 Theory and review of qPCR

qPCR is a molecular biology method used to amplify target sections of DNA, detecting and monitoring amplification in real-time using fluorescent primers and probes (Bustin, 2010). qPCR functions similarly to conventional PCR; with cycles containing a denaturation, annealing and extension step. However, rather than requiring external quantification of PCR product (e.g. agarose gel electrophoresis), a quantifiable output is generated following each qPCR cycle, which increases precision and decreases post-processing requirements (Bustin *et al*, 2009; Lind *et al*, 2006; Schrader *et al*, 2012).

Initial denaturation at high temperatures (95 °C) disrupts hydrogen bonds to separate double stranded DNA (dsDNA) and loosen the secondary structure in the

newly created single stranded DNA (ssDNA; Figure 2.2A). Complementary template DNA sequences are then hybridised by the primer of choice during annealing at a primer dependent melting temperature (Thermo Fisher Scientific Inc, 2014)(Figure 2.2B). *Taq* (*Thermus aquaticus*) DNA polymerase extends the DNA sequence (Figure 2.2C), to generate dsDNA of the target sequence (Thermo Fisher Scientific Inc, 2014)(Figure 2.2D). Conditions are then repeated for an optimum number of cycles to increase PCR target product (Figure 2.2E). An additional incubation step may be required prior to denaturation if uracil N-glycosylase (UNG) is incorporated into the assay. This enzyme degrades remnant contaminating products including residual uracil, to avoid non-specific amplification (Pruvost, Grange and Geigl, 2018).

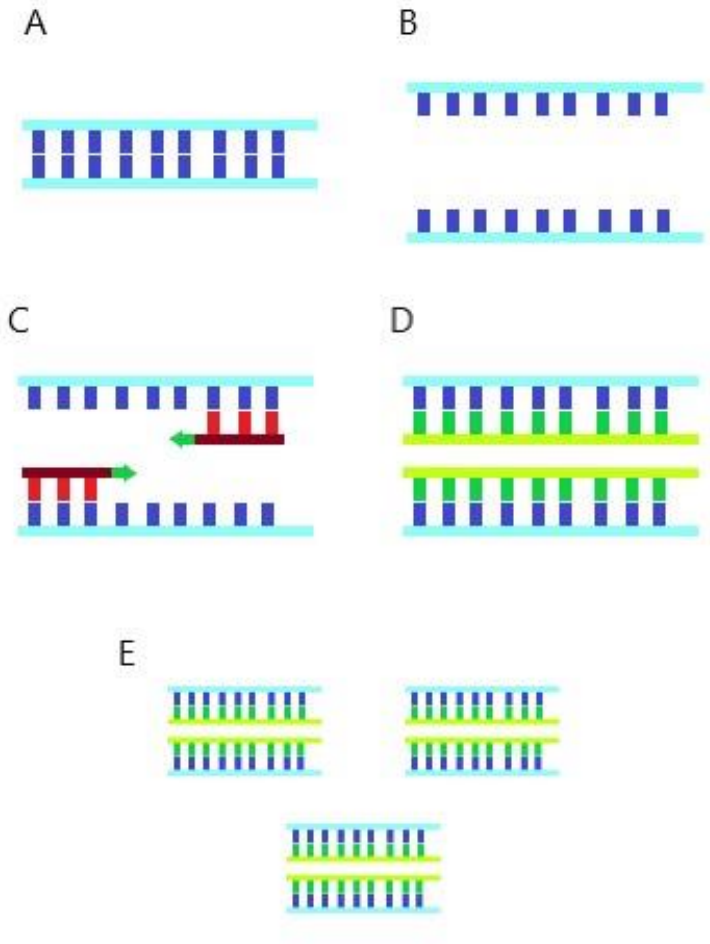

Figure 2.2 Diagrammatic representation of quantitative polymerase chain reaction. qPCR cycling methodology including input double stranded DNA (A), denaturation to create single stranded DNA (B), annealing of primers (C) and extension to create double stranded DNA of the target sequence (D). This process is repeated over multiple cycles to amplify the target DNA fragment product (E).

2.7.2 Absolute qPCR with standard curve

Absolute qPCR detects absolute copy number of a DNA target sequence within an input sample by comparing to a standard curve of known copy number (e.g. 16S rRNA gene; Ruijter *et al*, 2012). To determine sample copy numbers a ten-fold dilution of standards with a known starting quantity (SQ) is used to generate a reference standard curve for comparison. From this, the unknown SQ from a sample can be determined, with quantification cycle (CQ) inversely related to the SQ of target DNA (Forootan *et al*, 2017; Thermo Fisher Scientific Inc, 2014). CQ is the qPCR cycle number which the fluorescent signal of the amplified product crosses the cycle threshold representing background signal (Yuan *et al*, 2006). Using the standard curve as a reference CQ values are converted to SQ and can be calculated relative to sample requirements e.g. /µl or /mg of tissue, plus $\log_{10}$ transformed for visual analysis.

Standard curves are created mostly via a purified plasmid serial dilution, due to ease of use and stability (Kuperman *et al*, 2020; Theis *et al*, 2019). Standard curve dilutions should aim to cover the expected range of the assay (Bustin *et al*, 2009), pus 20% either side (Svec *et al*, 2015). Standard curves are especially important with expected low copy number samples, to ensure confidence in negative findings (Bustin *et al*, 2009).

qPCR is a highly sensitive method, with the theoretical ability to detect low amounts of DNA ($<10^1$; Bustin *et al*, 2009). However, a limit of detection (LOD) must be determined for each assay. LOD is the minimum concentration detected as significant from the control, with reasonable certainty across replicates within the experiment (Bustin, 2010; Bustin *et al*, 2009; Forootan *et al*, 2017; Kralik and Ricchi, 2017). The theoretical LOD is rarely met (10^1) due to experimental variation, background noise from samples and DNA carryover (Bustin *et al*, 2009).

2.7.3 Primer design

Primer choice for qPCR is dependent on the target of interest. For bacterial targets the broad range 16S rRNA gene covering the whole sequence has been applied (Nadkarni *et al*, 2002). Alongside specific variable regions of the 16S rRNA gene (Klindworth *et al*, 2013; Lauder *et al*, 2016; Liu *et al*, 2012; Theis *et al*, 2019). Recently, multiple studies have aimed to develop the most efficient primers for

variable region 16S rRNA gene targets, aiming to cover the broadest range of genera and species (Brukner *et al*, 2015; Lind *et al*, 2006; Liu *et al*, 2012).

The BactQuant primer and probe set is one of the developed methods which targets the V3-V4 region of the 16S rRNA gene (341-805 *E. coli* region) giving a 466 bp target (Liu *et al*, 2012). This primer covers 96.3% at the genus level, with a dynamic range of 10^2-10^8 copies at 95% efficiency (Liu *et al*, 2012). BactQuant presented with the least biased result (Hugerth *et al*, 2014), and covered the broadest phylum spectra in primer comparison research (Klindworth *et al*, 2013). This method has been beneficially applied to low biomass samples including reproductive tissues of vaginal (Brown *et al*, 2018), cervicovaginal (Shannon *et al*, 2017), and fetal tissues (Vitrenko *et al*, 2017); plus recently placenta and fetal membranes (Kuperman *et al*, 2020).

2.7.4 SYBR or TaqMan fluorescently labelled probes

Classic fluorescent probes for example SYBR, bind to all newly synthesised dsDNA. This creates non-specific binding, amplification and detection of high fluorescent signals (Lind *et al*, 2006). Target specific probes aim to increase specificity of the assay. Unlike SYBR probes, TaqMan probes are sequence specific, thus only fluoresce when bound to a targeted sequence, rather than all dsDNA contributing to fluorescence (Nagy *et al*, 2017). This reduces non-specific amplification and minimises the impact of primer dimers, which is a recognised issue with SYBR probes (Lind *et al*, 2006).

TaqMan hydrolysis probes utilise Fluorescence Resonance Energy Transfer (FRET). A fluorescent signal is only detected when a specific hybridisation event occurs (Dietrich *et al*, 2013). The short, sequence specific oligonucleotides have a reporter fluorescence dye at the 5’ and a quencher at the 3’ end, to form a donor and acceptor FRET pair (Ruijter *et al*, 2012). Multiple donor and acceptor pairs are available including molecular beacons and light up probes (Lind *et al*, 2006). However, focus here will be on 6-FAM and MGBNFQ. 6-Carboxyfluorescein (6-FAM) is the fluorescent donor of the pair (Lind *et al*, 2006), with minor groove binder non-fluorescent quencher (MGBNFQ) as the acceptor (Thermo Fisher Scientific Inc, 2014). Prior to amplification the fluorescent 6-FAM is quenched by close proximity to the second quencher probe (MGBNFQ; Nadkarni *et al*, 2002), As the donor/fluorophore transfers its high emission energy to the low emission

quencher/acceptor. The fluorophore is supressed, and no fluorescence is detected (Thermo Fisher Scientific Inc, 2014)(Figure 2.3A). During amplification the TaqMan probe hybridises only to the target sequence downstream of the primer and extends by DNA polymerase mediated activity in the 5'-3' direction (Trombley Hall *et al*, 2013)(Figure 2.3B). When MGBNFQ binds to target DNA it creates a minor groove within the DNA to strengthen probe binding, plus increase specificity and accuracy (Thermo Fisher Scientific Inc, 2014). Hydrolysis of the probe disrupts the FRET pair and displaces the fluorophore from the probe (Gallup and Ackermann, 2008; Nagy *et al*, 2017; Trombley Hall *et al*, 2013). Fluorescence is then released from the fluorophore as this is no longer in close proximity to the quencher, causing florescence at the dye specific wavelength to be detected (Gallup and Ackermann, 2008)(Figure 2.3C). The fluorescent signal released is proportional to the amount of starting template (Nagy *et al*, 2017)(Figure 2.3D).

2.7.5 qPCR methodology limitations

Inhibition in qPCR can lead to incorrect reporting of results. This occurs due to non-specific binding, DNA degradation or crosslinkage (Schrader *et al*, 2012). Inhibition can derive from sample matrices (Pennington, 2014; Schrader *et al*, 2012), sample storage buffers, sample handling or environmental plasticware (Gallup and Ackermann, 2008; Schrader *et al*, 2012). Inhibition can prevent amplification or lead to an inverse in expected CQ values (Pennington, 2014; Trombley Hall *et al*, 2013). Diluted samples are expected to contain lower target DNA, thus a higher CQ. However, inhibition may lead to a reverse in detection, with a diluted sample presenting with a lower CQ value falsely indicating increased SQ.

Although individual qPCR optimisation is beneficial, non-standardised protocols create inconsistency and reduce comparison across research. The MIQE qPCR guidelines (Bustin *et al*, 2009) have assisted with replication by encouraging researchers to supply maximum information on methodology within publications (Bustin, 2010).

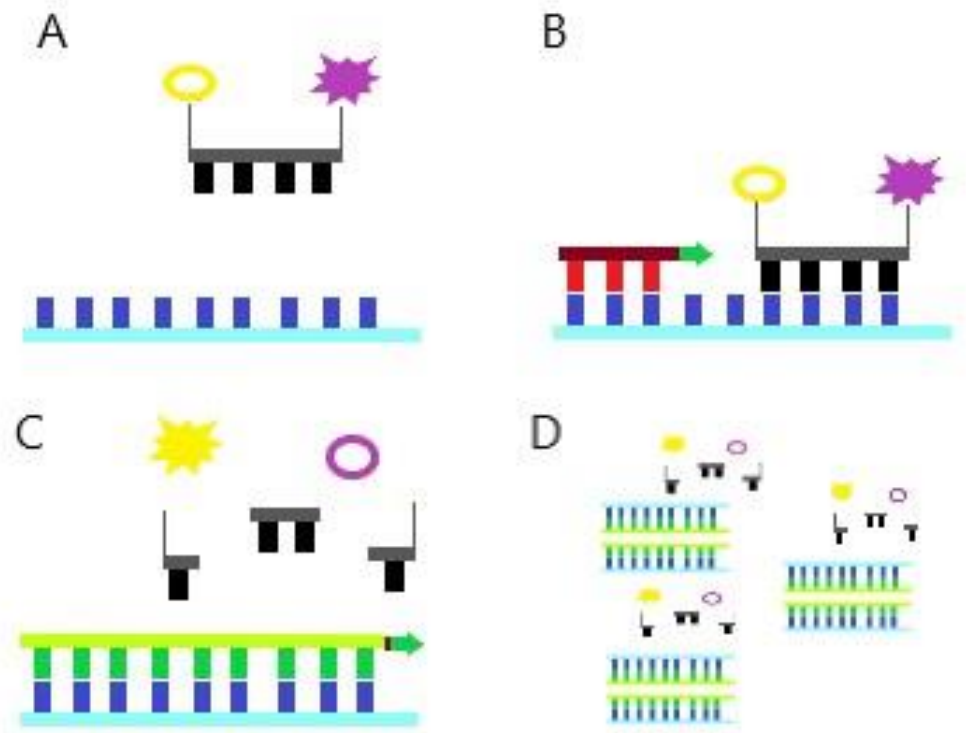

Figure 2.3 TaqMan qPCR probe technology. Diagrammatic representation of probe-based fluorescence activation utilised in qPCR methodology for improved sensitivity and specificity of target amplification and detection. When unbound, Florescence Resonance Energy Transfer (FRET) supresses fluorescence of the fluorophore (A). The sequence specific probe binds to target DNA (B). Hydrolysis during qPCR extension creates target specific fluorescence due to displacement of the fluorophore from the probe (C). Fluorescence is detected each cycle relative to the amount of specific target sequence amplified (D).

2.7.6 BactQuant qPCR methods

2.7.6.1 Creating a plasmid for the standard curve

Comparison of sample results to a reference of known quantity via standard curve is required to quantify bacterial load in absolute qPCR. Plasmid standards (16S rRNA gene) were created using *Escherichia coli* genomic DNA from Luria-Bertani (LB) agar streak plates prepared following overnight incubation in LB media. 16S rRNA gene end point colony PCR was performed to amplify *E. coli* bacterium. The PCR reaction was set up as follows: 2X PCR mastermix (Promega), 0.2 µm 27F primer (5'-AGAGTTTGATCMTGGCTCAG-3'), 0.2 µm 1492R primer (5'-TACGGYTACCTTGTTACGACTT-3', Eurofins), 2 µl template DNA, 1.25 µl Bovine Serum Albumin (BSA, New England BioLabs) and nuclease free H_2O to a total of 25 µl. PCR was performed in a thermal cycler (C100, Bio-Rad) with the conditions of initial denaturation at 95 °C for two minutes, followed by 35 cycles of denaturation at 95 °C for one minute, annealing at 54 °C for one minute and extension at 72 °C for 1.5 minutes, followed by a final extension at 72 °C for 15 minutes. Amplification of the 1465 bp product was confirmed via agarose gel electrophoresis.

PCR amplicons were purified by combining 4 µl ExoSap-IT reagent (ExoSap-IT PCR clean up Kit; Applied Biosystems) with 10 µl PCR product and incubated at 37 °C for 15 minutes to degrade remaining primers. Active enzymes were then deactivated by a 15 minute incubation at 80 °C.

Purified PCR products were cloned into TOP10 competent *E. coli* cells (Invitrogen) via PGEM-T Easy Vector System (Promega). Firstly, insert:vector was calculated:

ng of insert = ng of vector x kb size of insert ÷ kb size of vector x insert:vector ratio

10 ng = 50 ng/µl x 0.2 ng ÷ 3.015 kb x 3:1

Ligation reactions were then prepared to a total volume of 10 µl as per Table 2.2, including PCR product, positive controls of PCR and cloning kit positives, plus negative controls of PCR and cloning kit negative controls.

Component	PCR ligation product (µl)	PCR positive control (µl)	Cloning kit positive control (µl)	PCR negative control (µl)	Cloning kit negative control (µl)
2X rapid ligation buffer	5	5	5	5	5
PGEM-T vector (50 ng)	1	1	1	1	1
PCR product	2.5	2.5	-	1	-
Control insert DNA	-	-	2	-	-
T4 DNA ligase (3 Weiss)	1	1	1	-	-
Nuclease free H_2O	0.5	0.5	1	3	4
Total	10	10	10	10	10

Table 2.2 Ligation reaction components. Volume of components for cloning PCR product to prepare plasmids for standard curve analysis in qPCR. Reactions included PCR product, or positive controls of PCR and cloning positives, plus negative controls of PCR and cloning kit negative controls to a total volume of 10 µl.

Once prepared, ligation reactions were mixed by pipetting and incubated overnight at 4 °C to provide maximum number of transformants. Plasmids were transformed via the addition of 2 µl ligation reaction to 50 µl One Shot TOP10 competent *E. coli* cells and flicked to mix. Tubes were incubated on ice for 20 minutes, then added to a water bath to heat shock at 42 °C for 50 seconds, before returning immediately to ice. Cells were transferred to sterile tubes, combined with 950 µl RT SOC medium (Invitrogen), and incubated at 37 °C with shaking for 90 minutes. Tubes were centrifuged at 1000 xg for ten minutes and resuspended in 200 µl SOC. The above method was also performed with 10 µl pUC-19 DNA (Invitrogen) to determine transformation efficiency. 100 µl of each reaction was spread onto duplicate pre-prepared LB agar plates containing 10 mg/ml ampicillin (AMP, Gibco) and 50 mg/ml X-GAL (Invitrogen). Plates were incubated at 37 °C for 18 hours and blue:white transformation efficiency percentage was calculated. Positive methodology was accepted if the kit positive showed >60% white colonies and if kit negatives had no white colonies.

One white colony from one plate showing positive transformation was cultured overnight in LB/AMP broth and re-plated on LB/AMP agar plates. Following overnight incubations, the 16S rRNA plasmids were isolated as described below (PureYield Plasmid MiniPrep; Promega). Optical densities (OD_{600}) were measured via a UV spectrophotometer (Jenway 7305), with biomass of >1.4 processed (OD_{600} x µl of culture). A 1 ml overnight culture was centrifuged at 13,000 xg for 30 seconds, supernatant was discarded, and this step was repeated. Pellets were resuspended in 600 µl molecular grade H_2O. The suspension was combined with 100 µl cell lysis buffer and inverted to lyse cells. Within three minutes, 350 µl neutralisation solution was added to tubes to prevent further lysis, inverted and centrifuged at 13,000 xg for three minutes. Supernatant (950 µl) was transferred to PureYield minicolumns and centrifuged at 13,000 xg for 15 seconds. Contents were discarded and 200 µl endotoxin removal was added to the minicolumns and centrifuged as previously. Column wash solution (400 µl) was introduced and tubes were centrifuged at 13,000 xg for 30 seconds. Minicolumns were transferred to sterile tubes and 30 µl elution buffer was added. Tubes were incubated at RT for seven minutes and centrifuged at 13,000 xg for 15 seconds to elute all DNA. To confirm successful extraction, a 0.8% agarose gel electrophoresis was performed, and vector size was confirmed via restriction enzyme digest. *Eco*RI reaction buffer (2 µl, New England BioLabs) and nuclease free H_2O (7 µl) were combined in sterile tubes, along with extracted plasmid DNA (10 µl) and *Eco*RI enzyme (1 µl, New England BioLabs). Reactions were mixed gently before incubating at 37 °C for 3.5 hours. The enzyme was then inactivated by incubating at 70 °C for 20 minutes in a thermal cycler (C100, Bio-Rad). A 0.8% agarose gel was performed to check restriction enzyme digest product. Plasmid DNA was replaced by nuclease free H_2O (10 µl) for negative controls. Eluted plasmids were pooled, and concentration measured via NanoDrop spectrophotometer (NanoDrop One V1.4, Thermo Fisher).

2.7.6.2 Creating a standard curve

Firstly, the plasmid size was calculated by combining the size of plasmid used (3015 bp) and size of gene insert (1465 bp). The mass of a single plasmid molecule was calculated by combining calculated plasmid size (4465 bp) and average weight of one base pair (1.096×10^{-21}; Avogadro's constant). The mass of plasmid DNA required to contain the copy number of interest was calculated by multiplying the

copy number of interest (30-300,000) by mass of a single plasmid (4.894 x 10^{-18}). The mass of final plasmid DNA required per reaction was calculated by dividing the mass of plasmid DNA by volume of plasmid per reaction (1 µl), thus final plasmid DNA remained at 1.468 x 10^{-12}-10^{-16}. Working volumes were then calculated to generate a serial dilution for standard curves. The required volume of plasmid was determined via rearranging C1V1=C2V2 to C2xV2÷C1=V1. Where C1 was the pooled plasmid concentration determined by NanoDrop spectrophotometer. V1 and V2 are the respective volumes required for dilution four in the series, and C2 is the desired concentration (Table A.2). For example:

(1.468 x 10^{-12} x 100) ÷ 2.68 x 10^{-11} = 5.48 µl.

2.7.6.3 PCR optimisation

To ensure positive methodology, PCR reagents, primers and conditions were optimised. Firstly, a temperature gradient PCR was performed to optimise primer annealing temperature. PCR reactions contained 2X PCR master mix (Promega), 1 µl plasmid standard, 1.8 µm BactQuant forward and reverse primers (F=5'-CCTACGGGDGGCWGCA-3' *E. coli* 341-356, R=5'-GGACTACHVGGGTMTCTAATC-3' *E. coli* 786-806, Liu *et al*, 2012), 0.05 µg/ml BSA and nuclease free H_2O to a total of 10 µl. PCR conditions were; initial denaturation at 95 °C for two minutes, followed by 40 cycles of denaturation at 95 °C for one minute, annealing at 45-65 °C temperature gradient for one minute, extension at 72 °C for one minute, and a final extension at 72 °C for 15 minutes.

Further optimisation was performed for $MgCl_2$ concentration (3-7 mM, Promega) and formamide levels (0-10%, Sigma-Aldrich). PCR conditions were as above with the annealing temperature selected at 55 °C due to optimum amplification in previous steps. Following each protocol, an agarose gel electrophoresis was performed to detect optimum conditions for sample analysis.

2.7.6.4 BactQuant qPCR protocol

Absolute qPCR aimed to determine 16S rRNA gene bacterial load within fetal membranes. Reactions contained 1.8 µm BactQuant primers (F=5'-CCTACGGGDGGCWGCA-3'; R=5'-GGACTACHVGGGTMTCTAATC-3'), 225 nM

probe ((6FAM) 5'-CAGCAGCCGCGGTA-3' (MGBNFQ) *E. coli* 518-532; Eurofins, Liu *et al,* 2012), 0.05 µg/µl BSA 4 mM $MgCl_2$, 1% formamide, 1X Taqman Fast Advanced Master Mix (Applied Biosystems) and 1 µl fetal membrane DNA, plasmid standard for reference, or nuclease free H_2O for the no template control (NTC), to a total of 10 µl. CFX Connect Real Time System (Bio-Rad) was used to perform amplification as per BactQuant protocol (Liu *et al*, 2012), with additional UNG activation beneficial to degrade non-specific amplification products. Conditions were initial UNG activation at 50 °C for three minutes, *Taq* polymerase activation at 95 °C for ten minutes, followed by 40 cycles of denaturation at 95 °C for 15 seconds, annealing at 55 °C for one minute and extension at 60 °C for one minute. Extracted DNA from frozen amnion and chorion samples, DNA extraction kit negative controls, plus standard curve and NTCs were assayed in triplicate.

2.7.6.5 Statistical analysis of qPCR data

Analysis included collecting the CQ and SQ per sample and control and calculating 16S rRNA gene copy number/µl by comparison to in-run standard curves. Copy number/µl were converted to copy number/mg of tissue or log_{10} transformed. Replicates with a standard deviation >0.4 were removed, optimum R^2 standard curve was >0.98. The same pool of prepared standards were used in each run, however preparation was repeated if cycle numbers varied between consecutive assays. Inhibition was assessed via sample dilutions of neat, 1 in 2, 1 in 10 and 1 in 20.

Results were assessed by individual sample, per patient, per condition (HCA, PTB, term and low risk term), tissue type (amnion or chorion) and sample type (sample and negative controls). Investigations were conducted via nonparametric Kruskal-Wallis followed by nonparametric Pairwise Wilcoxon Rank-Sum and visual results created by ggplot2 in R (R Core Team, 2017). Histological inflammatory staging and grading were correlated to 16S rRNA gene copy number via nonparametric Spearman's Rho Bonferroni adjustment.

2.7.6.6 Relative qPCR for inflammatory gene fold change

Analysis of TLR signalling pathway gene expression was undertaken previously by relative qPCR (Waring *et al*, 2015). Briefly, genes showing significant change in

expression on signalling arrays were individually validated using relative qPCR compared to GAPDH as the endogenous control, due to consistent results as a house keeping gene in the signalling array study. Marker genes investigated were TLR1, TLR2, TLR4, TLR6, SARM1, MyD88, LY96, IL-8, IRAK2, HMGB1, SIGIRR and TIRAP. Each assay was performed in triplicate. Further methodological information can be found in Waring *et al* (2015). Inflammatory marker data from the previous study were correlated to bacterial loads from this research via nonparametric Spearman's Rho Bonferroni adjustment.

Chapter Three: The microbiota of frozen fetal membranes with and without histological chorioamnionitis.

Abstract

Aim

The aim of this chapter was to investigate the microbiota of frozen fetal membranes with histological chorioamnionitis (HCA) and compare this to fetal membranes from preterm and term birth without HCA. This aims to explore the relationship between the microbiota, bacterial profile and individual bacterial abundance to inflammation.

Methods

Amnion and chorion membrane from patients with preterm birth and HCA (n=12), preterm without HCA (n=6) and term birth without HCA (n=6) underwent sequencing via the V4 region of the 16S rRNA gene primer using Illumina MiSeq technology.

Results

Beta diversity differences were present between HCA, preterm and term amnion and chorion. A trend for increased *Prevotella* was detected at the genus level with HCA and increasing inflammation, with a significant increase in one *Prevotella* at the ASV level, with the same sequence significantly increased with higher level inflammation. Beta diversity differed between HCA inflammatory stage and grade in the chorion. A single *Lactobacillus* ASV was increased in samples with lower inflammation. Samples and negative controls have distinct bacterial profiles, with a significant increase of *Escherichia/Shigella*, *Pseudomonas, Blautia* and *Lactobacillus* in negative controls, at both the genus and ASV level.

Conclusion

Overall, chapter three highlights that HCA samples have a distinct bacterial profile, with a possible association to increased *Prevotella* in HCA. The microbiota may also be influenced by the severity of HCA, yet specific ASVs are only linked to inflammatory grading, and not staging. Amnion and chorion have different profiles for HCA inflammatory staging and grading, thus require individual analysis. Frozen samples and negative controls are distinct in bacterial profiles and four specific genera, questioning the origin of these bacteria.

3.1 Introduction

The detection of a genuine, consistent placental and fetal membrane microbiota remains widely debated (Aagaard *et al*, 2014; Jones *et al*, 2009; Leiby *et al*, 2018). Conflicting studies have suggested that the placenta and fetal membranes may be; sterile (Theis *et al*, 2019), typically sterile, unless a maternal condition is present (Bassols *et al*, 2016; Fichorova *et al*, 2011), or universally colonised with low abundant, non-pathogenic bacteria (Aagaard *et al*, 2014). These theories were discussed in detail within the first chapter. Agreement on the microbiota in fetal membranes with chorioamnionitis is yet to be reached (Bassols *et al*, 2016; Fichorova *et al*, 2011). Specific properties have been linked to HCA, with monomicrobial characteristics in 83% of HCA cases (Sweeney *et al*, 2016), supported by findings of low species richness in placenta and fetal membranes from HCA patients (Doyle *et al*, 2017). Multiple bacterial genera have been associated to the condition, with *Ureaplasma* the main genus detected in HCA, within 59% and 60% of preterm and term membranes, respectively (Sweeney *et al*, 2016). Alternatively, a polymicrobial distinct cluster of highly abundant urogenital and oral bacteria, including *Streptococcus* and *Fusobacterium* has been suggested (Prince *et al*, 2016). Similarly, in fetal membranes with HCA 14/20 operational taxonomic units (OTUs) were linked to vaginal and 2/20 OTUs were linked to bacteria of oral origin (Doyle *et al*, 2017). In contrast, 16S rRNA gene sequencing studies have reported no distinct bacterial communities in HCA membranes compared to environmental controls (Leiby *et al*, 2018).

The microbiota of the amnion and chorion fetal membranes individually is yet to be studied in HCA research. Thus, the aim of this section was to investigate the microbiota of individual fetal membranes with and without HCA via Illumina sequencing. In addition to determine the relationship between microbial profiles and HCA inflammation.

3.2 Microbiota method recap

To study the microbiota of fetal membranes with HCA, genomic DNA was extracted from 24 patients, including; preterm with HCA (n=12), plus preterm (PTB; n=6) and term birth without HCA (n=6), giving 78 samples. Nine DNA extraction kit negatives (Qiagen) were also processed alongside samples according to identical protocols. Sequencing of extracted DNA samples and negative controls were performed using

MiSeq (Illumina) wet lab standard operating procedure (SOP), with the universal 16S rRNA gene primer specific to V4 region (Callahan *et al*, 2016a; Callahan *et al*, 2016b; Kozich *et al*, 2013) by Northumbria University (Newcastle), as described previously. Data analysis of FastQ files were processed using R (R Core Team, 2017), package DADA2 1.4 (Callahan *et al*, 2016b), Bioconductor (Version 2; Callahan *et al*, 2016a), Phyloseq (McMurdie and Holmes, 2013) and Microbiome Analyst (Dhariwal *et al*, 2017) as previously described.

3.3 Results

3.3.1 Patient characteristics

Characteristics from patients, neonates and samples are listed in Table 3.1. Significance was detected between all HCA, PTB and term patients for gestational age and birthweight (p=0.001). This was expected due to increased gestational period in term cohorts, compared with PTB (p=<0.001), and HCA (p=<0.001). However, there was no difference in gestational age (p=0.799), or birthweight (p=0.160) between PTB and HCA only.

Significant differences were detected across tissue type, as only chorion samples were available from term patients (p=0.004). Significantly more males were delivered following PTB and more females from HCA and term (p=0.013). Apgar scores were greater in term compared to HCA and PTB (p=0.033). Apgar scores represent neonatal response and physical condition shortly after delivery (Apgar, 1953). Higher scores represent good to excellent health (7-10) and lower scores represent negative neonatal outcomes, possibly requiring medical interventions (<7; Apgar, 1953; Casey, McIntire and Leveno, 2001).

Characteristics only available from preterm patients were compared, including HCA and non-HCA PTB patients (Table 3.2). Maternal inflammatory stage (p=<0.001) and grade (p=0.036) were significantly greater from HCA compared to PTB without HCA. C-reactive protein (CRP) levels were also significantly increased in HCA (p=0.006). CRP is an innate immune system reactant protein investigated as an inflammatory marker (Catano Sabogal, Fonseca and Garcia-Perdomo, 2018). No other characteristic diverged significantly between groups.

		HCA (n=12)	PTB (n=6)	Term (n=6)	*p.value HCA PTB Term*	*p.value HCA PTB*
Chorion	Yes	11.0 (91.7)	6.0 (100.0)	6.0 (100.0)	1.000	1.000
	No	1.0 (8.3)	0.0 (0.0)	0.0 (0.0)		
Amnion	Yes	9.0 (75.0)	5.0 (83.3)	0.0 (0.0)	***0.004****	1.000
	No	3.0 (25.0)	1.0 (13.7)	6.0 (100.0)		
Gestational age (mean (SD))		29.6 (2.9)	29.9 (4.0)	40.4 (0.6)	***0.001****	0.779
Birthweight (mean (SD))		1387.0 (504.4)	1736.7 (402.3)	3250.0 (495.6)	***0.001****	0.291
Maternal age (mean (SD))		29.3 (8.0)	27.0 (5.5)	32.2 (6.0)	0.411	0.511
Maternal BMI (mean (SD))		22.0 (9.2)	22.5 (4.5)	22.3 (2.1)	0.515	0.580
Smoker	Yes	4.0 (33.3)	2.0 (33.3)	0.0 (0.0)	0.329	0.806
	No	6.0 (50.0)	4.0 (66.7)	6.0 (100.0)		
	NA	2.0 (16.7)	0.0 (0.0)	0.0 (0.0)		
Parity (mean (SD))		1.6 (2.2)	1.5 (1.8)	0.7 (1.2)	0.660	1.000
Fetal sex	Male	5.0 (41.7)	6.0 (100.0)	1.0 (16.7)	***0.013****	0.232
	Female	7.0 (58.3)	0.0 (0.0)	5.0 (83.3)		
Apgar (mean (SD))		6.3 (2.8)	6.5 (3.6)	8.9 (0.2)	***0.033****	0.885

Table 3.1 Patient demographics of frozen fetal membranes. Patient characteristic data from all patients providing fetal membrane samples for the study. Characteristics were assessed between conditions of preterm with chorioamnionitis (HCA), plus preterm (PTB), and term birth without chorioamnionitis (Term). Comparison between all three groups was performed via nonparametric Kruskal-Wallis and characteristics monitored in HCA and PTB groups only via nonparametric Wilcoxon Rank-Sum. Categorical data was assessed using nonparametric Pearson's chi-squared and Fisher's exact test. Significance threshold for comparisons was p=≤0.05. Unless stated results are displayed as n (%).

		HCA (n=12)	PTB (n=6)	*p.value*
Mode of delivery	Vaginal	8.0 (66.7)	5.0 (83.3)	1.000
	Caesarean section	4.0 (33.3)	1.0 (16.7)	
Type of labour	Spontaneous	3.0 (25.0)	2.0 (33.3)	0.600
	PPROM	9.0 (75.0)	3.0 (50.0)	
	NA	0.0 (0.0)	1.0 (16.6)	
Days to birth (following PPROM) (mean (SD))		7.0 (3.2)	1.7 (0.6)	0.051
Antibiotics	Yes	7.0 (58.3)	4.0 (66.6)	0.604
	No	5.0 (41.7)	1.0 (16.7)	
	NA	0.0 (0.0)	1.0 (16.7)	
Antenatal corticosteroids	Yes	11.0 (91.7)	5.0 (83.3)	1.000
	No	1.0 (8.3)	1.0 (16.7)	
Maternal inflammatory stage (mean (SD))		2.2 (0.4)	1.0 (0.0)	***<0.001****
Maternal inflammatory grade (mean (SD))		1.6 (0.5)	1.0 (0.0)	***0.036****
Number of clinical CA signs (mean (SD))		0.9 (1.2)	0.2 (0.4)	0.163
C-reactive protein (mean (SD))		55.6 (54.9)	6.4 (2.6)	***0.006****
White blood cell count (mean (SD))		19.1 (6.9)	12.9 (5.2)	0.069
Previous PTB	Yes	5.0 (41.7)	1.0 (16.7)	0.600
	No	7.0 (58.3)	5.0 (83.3)	
Previous early PTB	Yes	2.0 (16.7)	1.0 (16.7)	1.000
	No	10.0 (83.3)	5.0 (83.3)	

Table 3.2 Patient demographics from frozen fetal membranes of PTB patients only. Patient characteristic data from all preterm patients providing fetal membrane samples for the study. Characteristics were assessed between conditions of preterm birth with chorioamnionitis (HCA) and preterm without chorioamnionitis (PTB). Comparison between groups was performed via nonparametric Wilcoxon Rank-Sum. Categorical data was assessed using nonparametric Fisher's exact test. Significance threshold for comparisons was p=≤0.05. Unless stated results are displayed as n (%).

3.3.2 Quantification of extracted DNA

3.3.2.1 NanoDrop spectrophotometer results

NanoDrop results indicated that significantly greater yields of DNA were extracted from frozen chorion (310.7 ng/µl) compared to a lower mean yield from frozen amnion (164.3 ng/µl, p=0.018). Qiagen kit negative controls used for the extraction of DNA from frozen samples yielded low, but detectable amounts of DNA (1.1 ng/µl) significantly lower than frozen samples (p=0.001). There was no difference in the concentration of extracted DNA between the two Qiagen extraction kits used (kit 1= 202.1 ng/µl, kit 2= 296.2 ng/µl; p=0.951).

HCA samples had the greatest mean quantity of DNA (368.0 ng/µl), with PTB (148.1 ng/µl) and term (175.0 ng/µl) displaying lower comparable means, with no significance detected between HCA and non-HCA samples (p=0.219). A subset of NanoDrop result can be found in the appendix (Table A.3).

3.3.3 Sequencing read counts

Fetal membranes had detectable read counts within all sample replicates, with 2862 individual amplicon sequence variants (ASVs) within frozen samples. Read counts varied from 2 to 64,439, with a mean read count of 3758.4. All DNA kit negatives also yielded read counts, with 1767 individual ASVs, an average read count of 9895.3, ranging from 2 to 64,799. Samples with <2 read counts in 20% of ASVs were removed from downstream analysis, due to this being the minimum threshold of the negative controls, with limited reliability below this (Dhariwal *et al*, 2017; Jervis-Bardy *et al*, 2015).

3.3.4 The microbiota of fetal membranes: Comparison between HCA and non-HCA tissues

3.3.4.1 Relative and percentage abundance

Within samples, 2862 individual ASVs were detected. From this, 2401 were detected in HCA, 1120 detected in PTB and 353 in term samples.

Escherichia/Shigella was the most abundant genus across the majority of groups including PTB amnion (47%), HCA chorion (34%), PTB chorion (46%) and term chorion (52%; Figure 3.1). HCA amnion was the only patient cohort where *Escherichia/Shigella* was not the most abundant (27%), with increased relative abundance from *Prevotella* (32%; Figure 3.1). *Prevotella* was the second greatest genus in HCA chorion (23%), but contributed 10%, 5% and <1% to term chorion, PTB amnion and PTB chorion, respectively. HCA patients had the greatest levels of *Ureaplasma* in the amnion (16%) and chorion (11%), but PTB chorion also displayed 11% from *Ureaplasma*, with this reduced to 5% from PTB amnion and <1% from term chorion. Term chorion had the greatest relative abundance for *Lactobacillus* (18%), with preterm chorion and amnion presenting with 17% and 12% respectively, and this decreased in HCA chorion (4%) and HCA amnion (2%).

None of the genera displayed significant differences in relative abundance between HCA and PTB in the amnion or HCA, PTB and term in the chorion. In the amnion a trend for increased relative abundance of *Prevotella* in HCA was detected, but not significant following false discovery rate (FDR) correction (p=0.029, FDR=0.413). This trend was not reflected in the chorion (p=0.104, FDR=0.619).

At the ASV level, only one ASV was significantly greater in HCA amnion compared to PTB amnion (p=0.002, FDR=0.048). This ASV was assigned to *Prevotella*, and was the second highest abundant ASV in HCA patients (Table 3.3). A trend for greater *Lactobacillus* was observed in PTB amnion, but not significantly different following FDR correction (p=0.034, FDR=0.364). In the chorion, none of the ASVs were significantly different across HCA, PTB and term. A trend for increased *Lactobacillus* in term chorion was observed, from two individual ASVs assigned to this genus. Yet these were not significantly different between HCA, PTB and term following FDR corrections (p=0.007, FDR=0.110 and p=0.012, FDR=0.110).

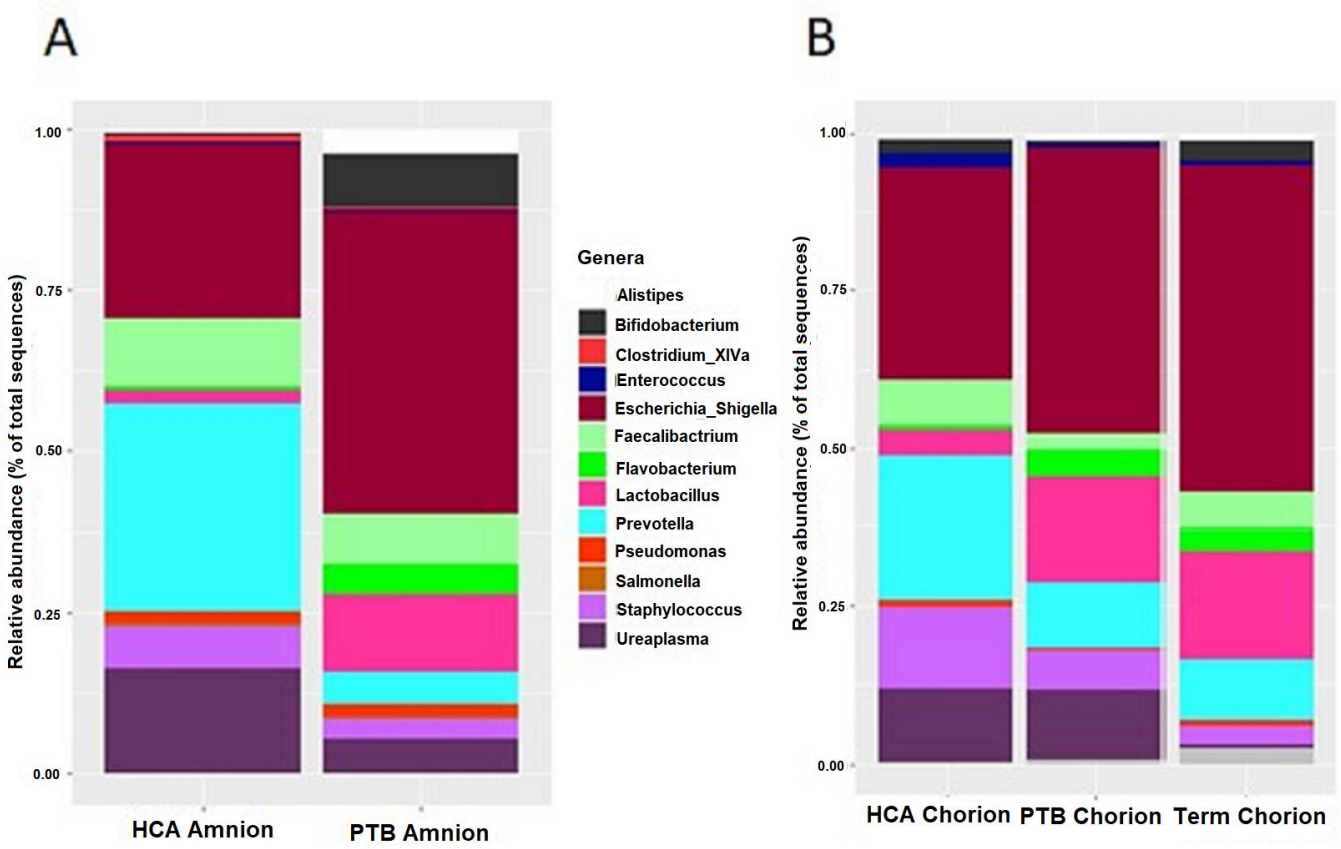

Figure 3.1 Relative abundance of amnion and chorion fetal membranes. Relative abundance plots from V4 16S rRNA amplicon sequencing of extracted DNA from frozen fetal membranes. ASVs were clustered into genera for visual analysis plots created using ggplot2 (R Core Teams, 2017). Samples were divided by tissue type of amnion (A) and chorion (B). Samples were then further divided by condition of chorioamnionitis (HCA), preterm without chorioamnionitis (PTB) and term without chorioamnionitis (Term).

	All samples	HCA	PTB	Term
1	*Escherichia/Shigella*	*Ureaplasma*	*Escherichia/Shigella*	*Escherichia/Shigella*
2	*Ureaplasma*	*Prevotella*	***Alpha-proteobacteria****	*Lactobacillus*
3	*Prevotella*	*Escherichia/Shigella*	*Prevotella*	***Campylobacter***
4	*Prevotella*	*Prevotella*	*Prevotella*	***Fusobacterium***
5	*Prevotella*	*Prevotella*	***Staphylococcus***	***Paraprevotella***
6	*Faecalibacterium*	*Faecalibacterium*	*Ureaplasma*	*Faecalibacterium*
7	*Prevotella*	*Prevotella*	***Acinetobacter***	*Prevotella*
8	*Streptococcus*	*Streptococcus*	*Streptococcus*	*Prevotella*
9	*Streptococcus*	*Streptococcus*	*Lactobacillus*	*Streptococcus*
10	*Faecalibacterium*	*Faecalibacterium*	***Acidobacteria****	*Faecalibacterium*

Table 3.3 Ten most abundant ASVs in frozen fetal membranes. Top ten most abundant amplicon sequence variants (ASVs) present in frozen fetal membrane samples and broken down into sample subtype of chorioamnionitis (HCA), plus preterm (PTB) and term without chorioamnionitis (Term). All bacterium displayed are classification genera, if this information was not available the next highest order is displayed (*). Bacteria presented in bold were only present in the respective group.

3.3.4.2 Bacterial diversity structure

Diversity analysis was performed by Shannon diversity, GUniFrac distance and PERMANOVA analysis.

HCA amnion had a lower mean diversity compared with PTB amnion, yet not significant (0.743 vs 1.047, p=0.110; Figure 3.2A). Across chorion tissues, HCA displayed the lowest mean diversity (0.796), compared to PTB (1.207) and term (1.104), though none were significant (HCA vs PTB p=0.480, HCA vs Term p=0.170, PTB vs Term p=0.170; Figure 3.2C).

For beta diversity analysis, significantly different distinct clusters were also displayed between HCA, PTB and term chorion (R^2=0.227, p=0.010; Figure 3.2B). Significant differences between HCA and PTB were detected in the amnion, with a distinct cluster for PTB observed yet greater beta diversity distances between HCA patients (R^2=0.162, p=0.015; Figure 3.2D).

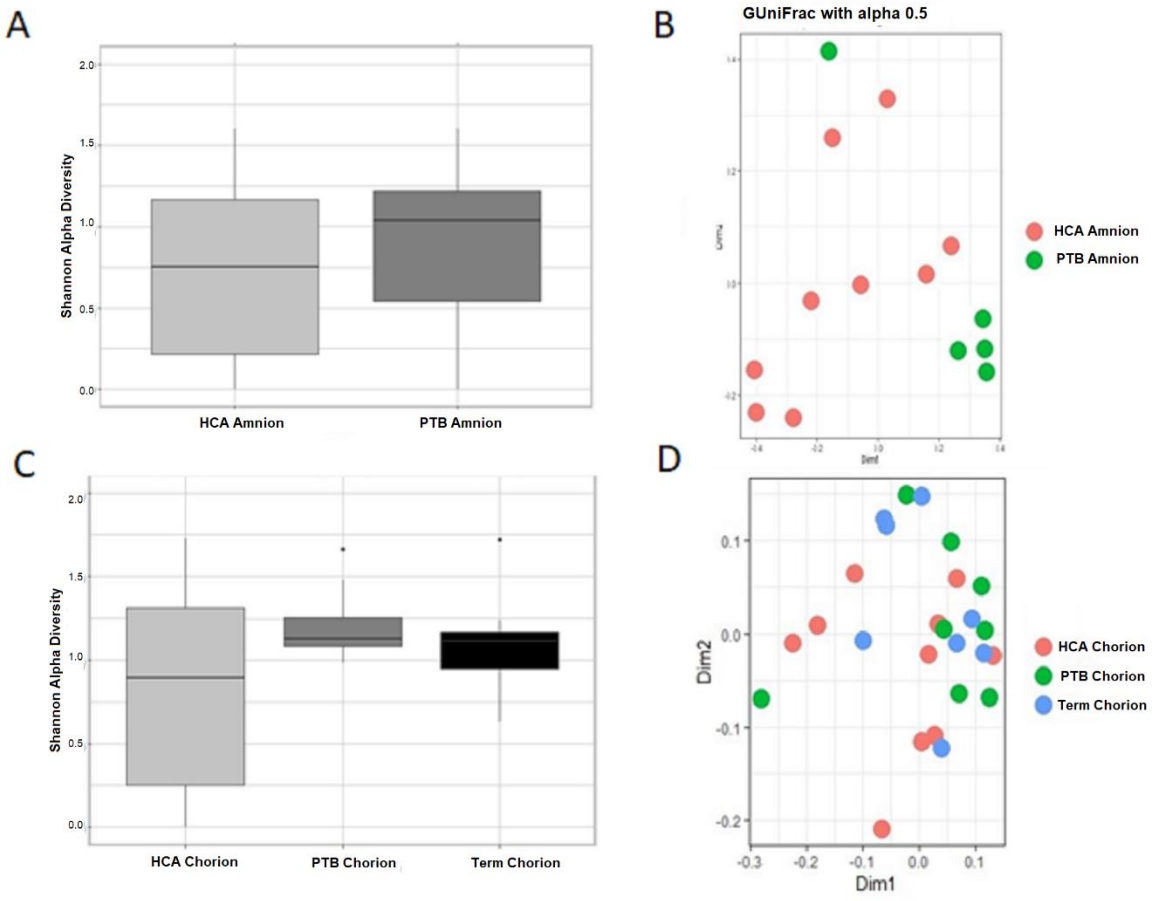

Figure 3.2 Diversity analysis of frozen fetal membranes. Alpha and beta diversity analysis of ASV data from V4 16S rRNA amplicon sequencing of frozen fetal membranes. Samples were divided into amnion (A+B) or chorion only (C+D), plus groups of chorioamnionitis (HCA), preterm without chorioamnionitis (PTB) and term without chorioamnionitis (Term). Diversity analysis was performed by Shannon alpha diversity (A+C) or GUniFrac PERMANOVA for beta diversity (B+D). Significance was analysed via nonparametric Kruskal-Wallis and nonparametric Pairwise Wilcoxon Rank-Sum to a threshold of p=≤0.05.

3.3.5 Maternal stage and grade related to the microbiota in fetal membranes

3.3.5.1 Relative and percentage abundance for inflammatory stage

Prominent bacterial relative abundance differs across inflammatory staging.

In the amnion, *Escherichia/Shigella* was the most abundant genus across all inflammatory staging, apart from the highest inflammatory stage. *Escherichia/Shigella* relative abundance decreased as stage increased as this was 65% from stage zero, 41% from stage one and 30% from stage two, but <1% from stage three (Figure 3.3A). The genus contributing the greatest to stage three was *Prevotella* (97%). This was detected at 25% in stage two, 5% stage one and 9% stage zero. *Ureaplasma* was higher in stage two (18%) compared to stage one (7%), zero (1%) and three (<1%). *Lactobacillus* was the greatest in stage one (14%), contributing 7%, 2% and <1% to stage zero, two and three, respectively.

At the genus level, no significant difference in abundance between inflammatory staging on the amnion was present. A trend for increased *Prevotella* in high stage inflammation (stage three) was detected, but not significantly increased following FDR correction (p=0.028, FDR=0.395).

Similar results were found in the chorion, with the greatest relative abundance of *Escherichia/Shigella* from the lowest inflammatory stage, decreasing as inflammatory staging increased (Figure 3.3B), as *Escherichia/Shigella* contributed 60% at stage zero, 40% at stage one, 28% at stage two and 11% at stage three. Once again, the genus contributing the greatest to stage three in the chorion was *Prevotella* (50%), with this reducing throughout inflammatory stages of stage two (17%), stage one (11%) and stage zero (10%). *Ureaplasma* was highest from stage two (14%) followed by stage one (13%), but reduced in stages zero and three (<1%). *Lactobacillus* was the greatest in stage one (19%), reducing in stage zero (15%), two (4%) and three (1%). At the genus level no significant differences in abundance between inflammatory staging on the chorion was detected.

At the ASV level, no ASVs were significantly different across inflammatory stages in the amnion or chorion. In the amnion one *Prevotella* ASV showed a trend for increased abundance in stage three inflammation, but was not significant following FDR correction (p=0.004, p=0.084; Table 3.4). In the chorion, two ASVs showed a trend for increased levels in stage one, but were not significant. Both ASVs were assigned to the *Lactobacillus* genera (p=0.029, FDR=0.282; p=0.031, FDR=0.282).

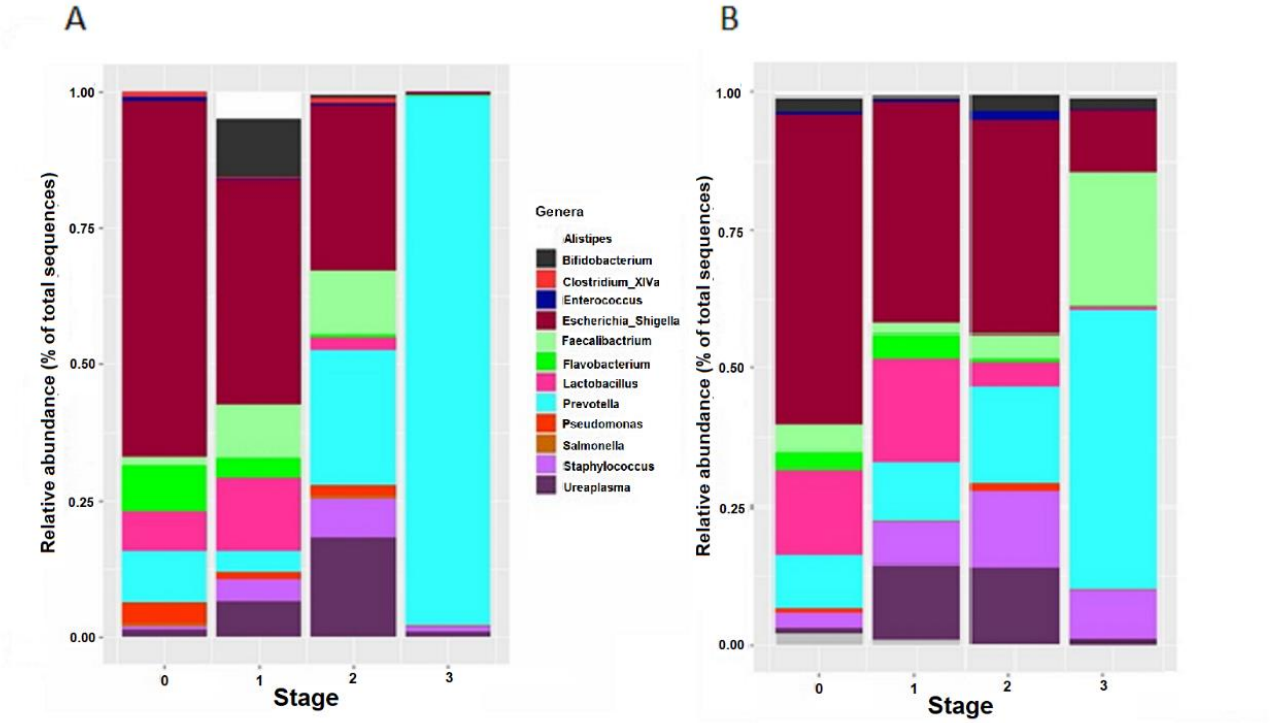

Figure 3.3 Relative abundance of inflammatory stage in the amnion and chorion. Relative abundance plots from V4 16S rRNA amplicon sequencing of extracted DNA from frozen fetal membranes. ASVs were clustered into genera for visual analysis plots created using ggplot2 (R Core Teams, 2017). Samples were divided by tissue type of amnion (A) or chorion (B) for relative abundance analysis of inflammatory stage, which is a histological diagnostic criteria for chorioamnionitis severity.

	Stage zero	Stage one	Stage two	Stage three
1	*Escherichia /Shigella*	*Escherichia /Shigella*	*Escherichia /Shigella*	*Prevotella*
2	***Acinetobacter***	***Alphaproteo-bacteria****	*Ureaplasma*	*Faecalibacterium*
3	***Campylobacter***	*Prevotella*	*Prevotella*	*Faecalibacterium*
4	*Lactobacillus*	*Prevotella*	*Prevotella*	***Clostridium_IV***
5	***Acidobacteria_ Gp4****	*Ureaplasma*	***Bacillus***	*Lactobacillus*
6	***Spartobacteria****	*Staphylococcus*	*Streptococcus*	*Faecalibacterium*
7	***Unclassified bacteria****	*Streptococcus*	***Bulleidia***	***Ruminococcaceae****
8	*Streptococcus*	*Lactobacillus*	***Haemophilus***	***Clostridium_XIVa***
9	*Faecalibacterium*	***Cloacibacterium***	*Faecalibacterium*	***Bifidobacterium***
10	***Fusobacterium***	***Enterococcus***	*Prevotella*	*Lactobacillus*

Table 3.4 Ten most abundant ASVs in fetal membranes across inflammatory staging. Top ten most abundant amplicon sequence variants (ASVs) displayed by inflammatory stage of zero, one, two or three. Inflammatory staging is a histological diagnostic criteria for chorioamnionitis severity. All bacterium displayed are classification genera, if this was not available bacteria is displayed as the next highest order (*). Bacteria in bold were detected for that group only.

3.3.5.2 Relative and percentage abundance for inflammatory grade

In the amnion, *Escherichia/Shigella* was the most abundant genus from the lowest grade inflammation (zero, 95%), followed by grade one (34%) and grade two (30%; Figure 3.4). *Prevotella* contributed the greatest relative abundance in grade two (41%), with this decreased in grade one (5%) and grade zero (9%). *Ureaplasma* was the greatest in grade one (16%), compared to grade two (10%), and not detected in grade zero. *Lactobacillus* was the greatest from grade one (10%), reduced in grade zero (7%) and grade two (2%). No significant differences were detected across relative abundance of genera and inflammatory grading in the amnion. A trend for increased *Prevotella* with greater inflammatory grading was detected, but not significant following FDR correction (p=0.015, FDR=0.208).

In the chorion, *Escherichia/Shigella* was the most abundant genera across all inflammatory grades, including zero (56%), one (33%), and two (37%). At inflammatory grade two, *Prevotella* was the second greatest contributor to relative abundance at 27%, with this decreased in grade one (13%) and zero (10%). *Ureaplasma* was the greatest at grade one (23%), with this <1% from both grade zero and two. *Lactobacillus* contributed 15% and 14% to grade zero and one, respectively, but only 1% in grade two. No genera were significantly different across inflammatory grading in the chorion. *Lactobacillus* showed a trend for increased abundance in lower inflammatory grading levels, yet not significant after FDR correction (p=0.012, FDR=0.411).

At the ASV level, one ASV was significantly increased as inflammatory grading increased in the amnion. This ASV was assigned to *Prevotella* and was the most abundant ASV from grade two compared to grade one and zero (p=0.002, FDR=0.039; Table 3.5). In the chorion, one ASV representing *Lactobacillus* was related to inflammatory grading, as this was significantly decreased as inflammatory grading increased in the chorion (p=<0.001, FDR=0.004).

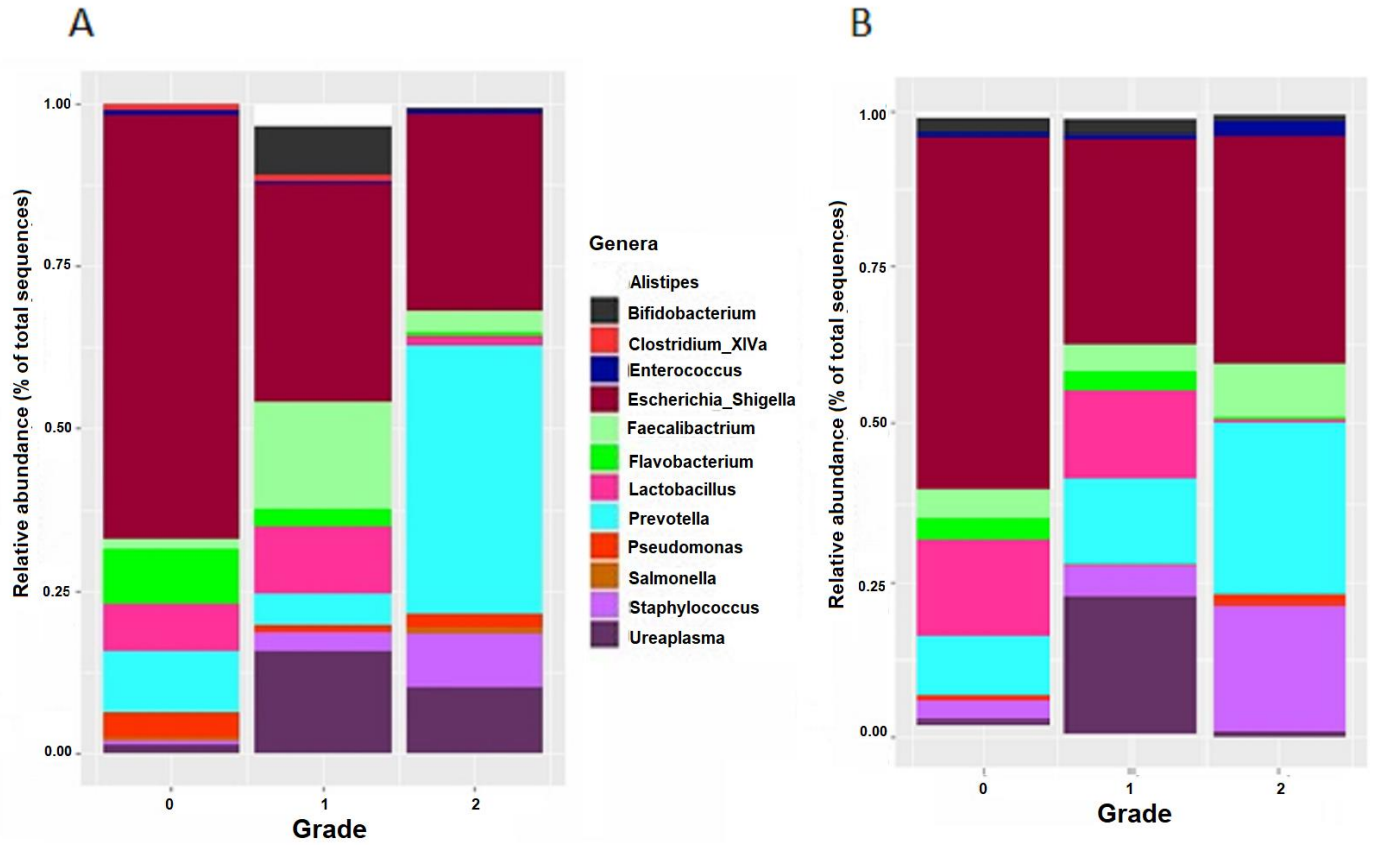

Figure 3.4 Relative abundance of inflammatory grade in the amnion and chorion. Relative abundance plots from V4 16S rRNA amplicon sequencing of extracted DNA from frozen fetal membranes. ASVs were clustered into genera for visual analysis plots created using ggplot2 (R Core Teams, 2017). Samples were divided by tissue type of amnion (A) or chorion (B) for relative abundance analysis of maternal inflammatory grade, which is a histological diagnostic criteria for chorioamnionitis severity.

	Grade zero	Grade one	Grade two
1	*Escherichia/Shigella*	*Escherichia/Shigella*	*Prevotella*
2	***Acinetobacter***	*Ureaplasma*	*Escherichia/Shigella*
3	***Campylobacter***	*Prevotella*	*Faecalibacterium*
4	*Lactobacillus*	*Prevotella*	*Ureaplasma*
5	***Acidobacteria_Gp4****	*Streptococcus*	***Bulleidia***
6	***Spartobacteria****	***Haemophilus***	*Faecalibacterium*
7	***Unclassified bacteria****	*Prevotella*	***Staphylococcus***
8	*Streptococcus*	*Faecalibacterium*	*Streptococcus*
9	*Faecalibacterium*	*Streptococcus*	***Clostridium_IV***
10	***Fusobacterium***	*Faecalibacterium*	*Lactobacillus*

Table 3.5 Ten most abundant ASVs in fetal membranes across inflammatory grading. Top ten most abundant amplicon sequence variants (ASVs) displayed by inflammatory grade of zero, one and two. Inflammatory grading is a histological diagnostic criteria for chorioamnionitis severity. All bacterium displayed are classification genera, if this was not available bacteria is displayed as the next highest order (*). Bacteria in bold were detected for that group only.

3.3.5.3 Bacterial diversity structure across HCA inflammatory staging and grading

No significant differences in alpha diversity were detected for HCA severity on amnion and chorion tissues. Greater alpha diversity was detected with lower stage inflammation in the chorion, at stage zero and one (1.133 and 1.130), compared to stage two (0.824) and stage three (0.747), yet not significant (p=0.472, Figure 3.5A). For inflammatory grading, grade zero (1.133) and grade one (1.107) displayed the greatest alpha diversity, compared to grade two (0.695) yet not significant (p=0.472; Figure 3.5B). Within the amnion, the greatest alpha diversity was from stage zero (1.064), compared to stage one (0.899), two (0.827) and three (0.177), yet not significant (p=0.467; Figure 3.6A). Inflammatory grading followed a similar trend, with lower grading displaying greater diversity. Comparison yielded no significance between grade zero (1.040), one (0.852) and two (0.762, p=0.467; Figure 3.6B).

Beta diversity differed between HCA staging and grading of inflammatory factors in chorion (Figure 3.5) and amnion tissues (Figure 3.6). Inflammatory level two and zero display distinct clusters for both stage and grade, with wider diversity at level one and three overlapping other inflammatory levels. PERMANOVA analysis highlighted differences in bacterial diversity within chorion tissues for staging (R^2=0.271, p=0.001; Figure 3.5C) and grading of inflammatory factors (R^2=0.190, p=0.003; Figure 3.5D). Similar beta diversity was detected within amnion tissues for staging (R^2=0.271, p=0.084; Figure 3.6C) and grading of inflammatory factors, with no distinct clusters detected (R^2=0.184, p=0.138; Figure 3.6D).

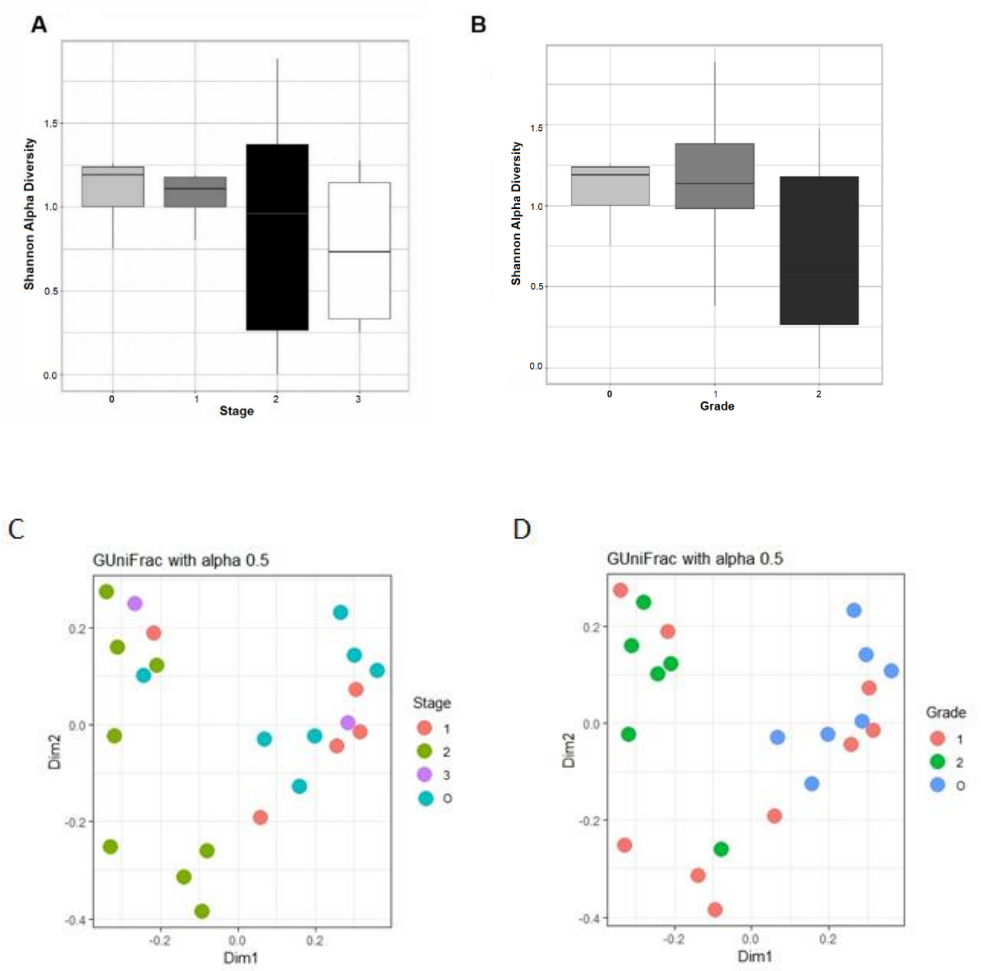

Figure 3.5 Diversity analysis of inflammatory grading and staging within the chorion. Alpha and beta diversity analysis of ASV data from V4 16S rRNA amplicon sequencing from frozen chorion samples categorised by staging and grading of the fetal membranes, which are histological diagnostic criteria for chorioamnionitis severity. Samples were divided into inflammatory stage (A+C) and grade (B+D) in chorion samples. Alpha diversity was measured using Shannon diversity indices for stage (A) and grade (B) and beta diversity was analysed via GUniFrac PEMANOVA for stage (C) and grade (D) to a significance of p=≤0.05 via nonparametric Kruskal-Wallis test.

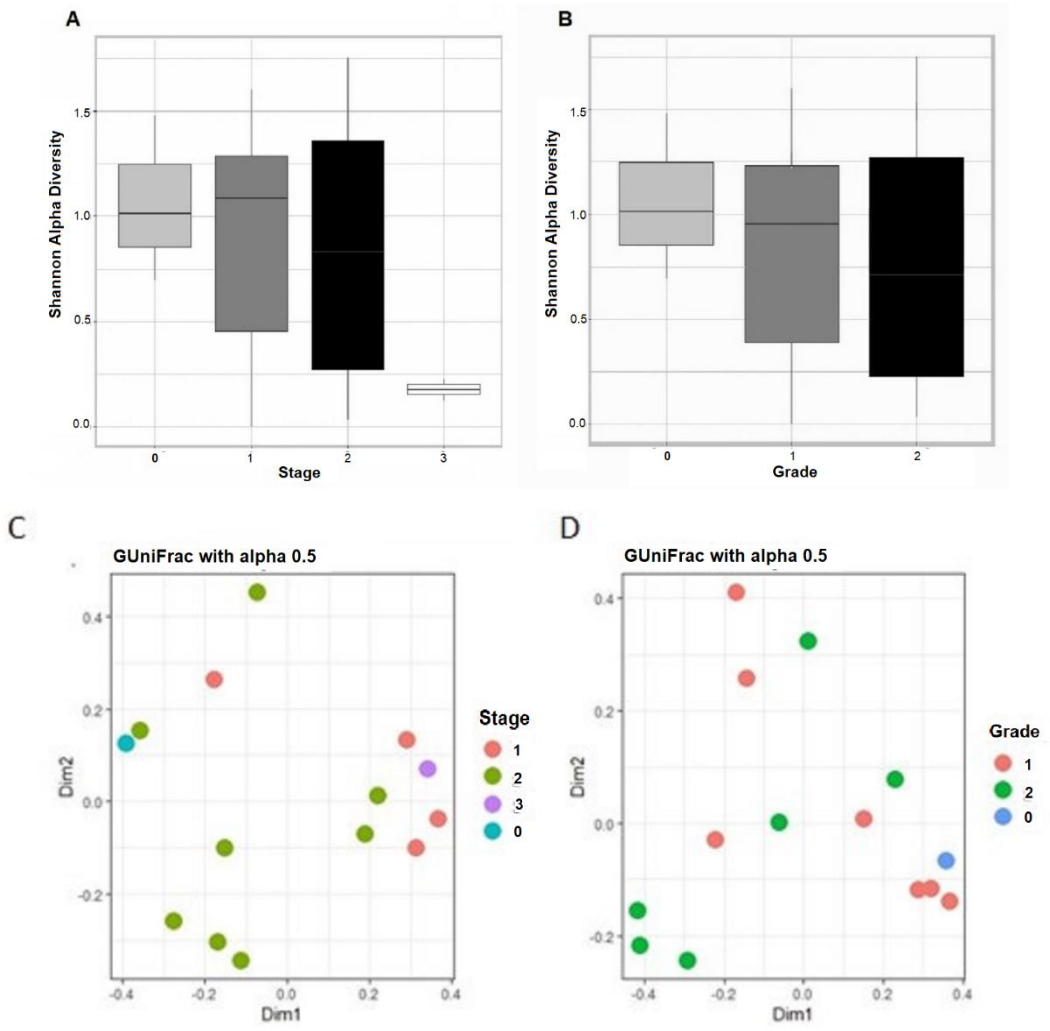

Figure 3.6 Diversity analysis of inflammatory grading and staging within the amnion. Alpha and beta diversity analysis of ASV data from V4 16S rRNA amplicon sequencing from frozen amnion samples categorised by staging and grading of the fetal membranes, which are histological diagnostic criteria for chorioamnionitis severity. Samples were divided into inflammatory stage (A+C) and grade (B+D) in amnion samples. Alpha diversity was measured using Shannon diversity indices for stage (A) and grade (B) and beta diversity was analysed via GUniFrac PEMANOVA for stage (C) and grade (D) to a significance of p=≤0.05 via nonparametric Kruskal-Wallis tests.

3.3.6 The microbiota of frozen fetal membrane tissues and negative controls

As the detection of a genuine bacterial profile in fetal membranes is questioned, sample results were compared to DNA kit negative controls.

3.3.6.1 Relative and percentage abundance in samples and controls

Escherichia/Shigella had the highest relative abundance in both samples and controls, contributing 41% to samples and 55% to negative controls (Figure 3.7A). When segmenting samples by membrane, the majority of *Escherichia/Shigella* originated from the amnion (74%), with less from the chorion (11%; Figure 3.7B). *Prevotella* was the second most abundant genera from samples (25%) and decreased in negative controls (6%). This mainly originated from the chorion (36%), with less from the amnion (16%). *Ureaplasma* was greater in samples (17%), compared to negative controls (<1%), with this mainly originating from the chorion (28%), and less from the amnion (4%).

At the genera level, four genera were significantly increased in negative controls compared to samples. These were *Escherichia/Shigella* (p=<0.001, FDR=<0.001), *Pseudomonas* (p=<0.001, FDR=0.003), *Blautia* (p=0.006, FDR=0.028) and *Lactobacillus* (p=0.011, FDR=0.037).

Within samples and negative controls, 2862 and 1767 individual ASVs were detected within each respective subset. At the ASV level, seven ASVs were significantly greater in negative controls compared to samples. These include one ASV assigned to *Escherichia/Shigella* (p=<0.001, FDR=<0.001; Table 3.6), one *Lactobacillus* (p=0.003, FDR=0.018), one *Blautia* (p=0.006, FDR=0.029), plus two *Faecalibacterium* (p=<0.001, FDR=0.003; p=0.008, FDR=0.032) and two *Pseudomonas* (p=0.001, FDR=0.008; p=0.014, FDR=0.049).

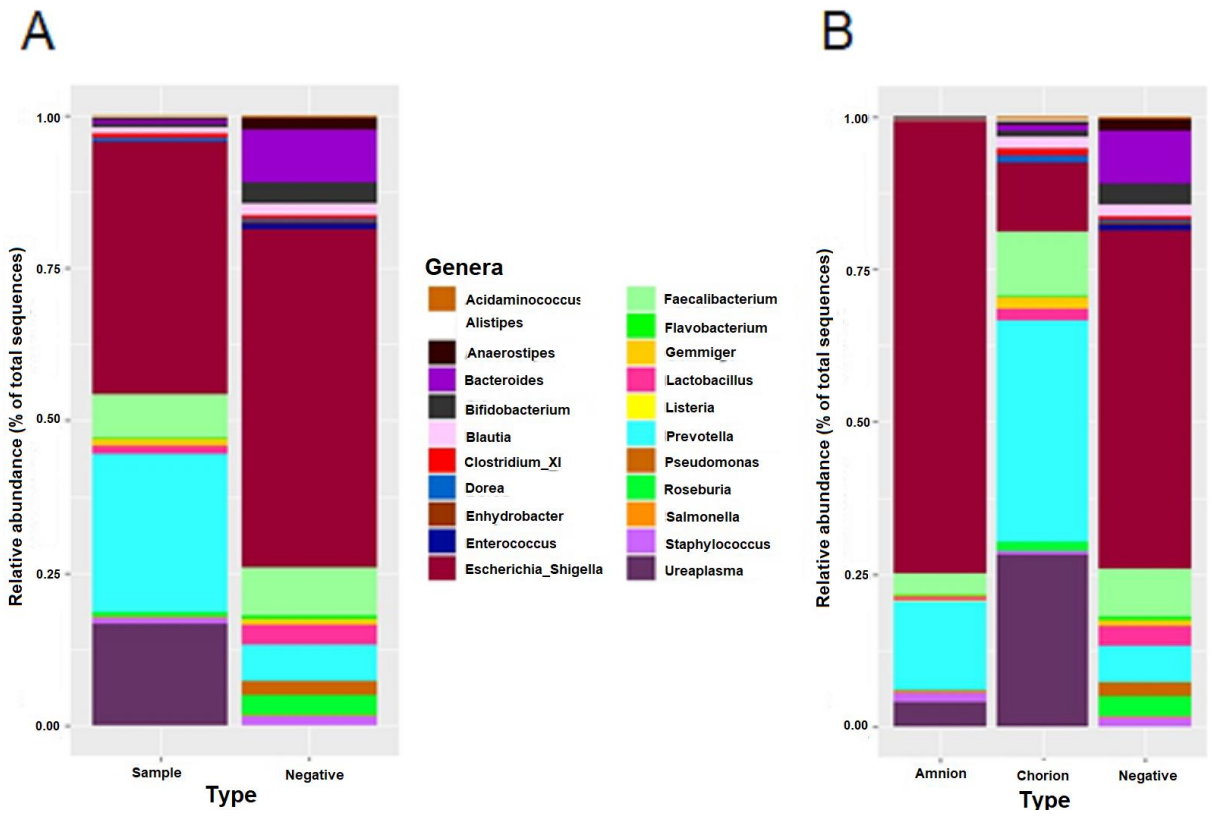

Figure 3.7 Relative abundance of frozen tissues and negative controls. Relative abundance plots from V4 16S rRNA amplicon sequencing of extracted DNA from frozen fetal membranes and DNA extraction kit negative controls to investigate kit contamination. ASVs were clustered into genera for visual analysis plots created in ggplot2 (R Core Teams, 2017). Samples were divided by fetal membrane samples and kit negative controls (A), with samples further subdivided by tissue type of amnion or chorion (B).

	Fetal membranes	Negative controls
1	*Escherichia/Shigella*	*Escherichia/Shigella*
2	*Ureaplasma*	***Bacteroides***
3	*Prevotella*	***Bacillus***
4	*Prevotella*	*Faecalibacterium*
5	*Prevotella*	***Roseburia***
6	*Faecalibacterium*	***Bacteroides***
7	*Prevotella*	*Prevotella*
8	*Streptococcus*	*Acinetobacter*
9	*Streptococcus*	*Prevotella*
10	*Faecalibacterium*	*Faecalibacterium*

Table 3.6 Ten most abundant ASVs in frozen fetal membranes and negative controls. Top ten most abundant amplicon sequence variants (ASVs) displayed by frozen fetal membranes or DNA extraction kit negative control. Bacteria in bold were detected for that group only.

3.3.6.2 Bacterial diversity structure in samples and controls

Samples displayed a higher mean alpha diversity (1.620) than negative controls (1.584), yet not significant (p=0.909; Figure 3.8A). When comparing across tissue type to negative controls, the chorion yielded the greatest mean alpha diversity (2.037), followed by amnion (1.620) and the lowest from negative controls (1.333), yet no significance was detected (p=0.393; Figure 3.8B).

A significant difference in beta diversity between fetal membrane samples and negative controls were present (R^2=0.042, p=0.001; Figure 3.8C). Diversity was also significantly different between tissue type of amnion and chorion, compared to negative controls, yet no distinct clusters were observed (R^2=0.060, p=0.004; Figure 3.8D).

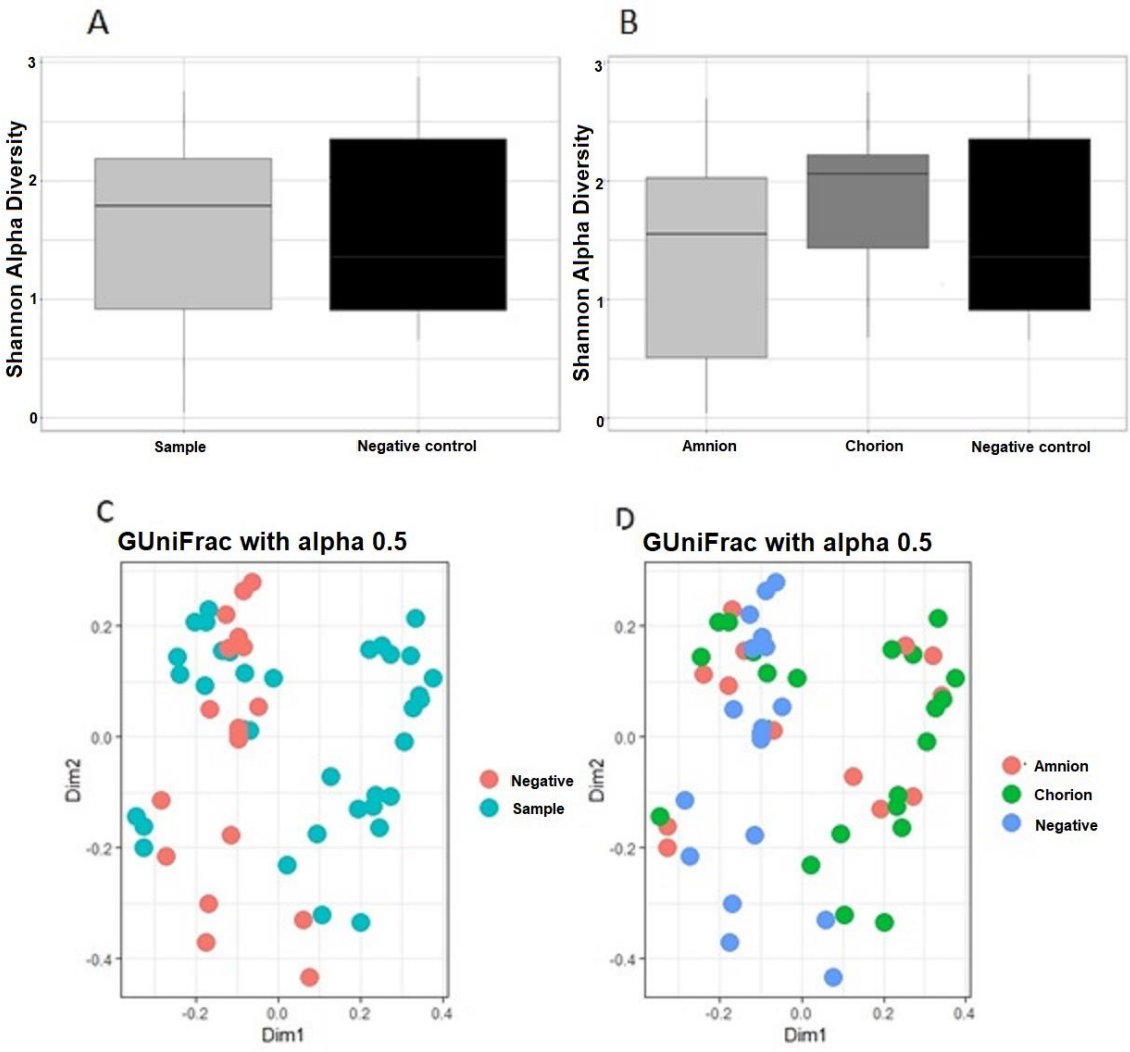

Figure 3.8 Diversity analysis of frozen tissues and negative controls. Alpha and beta diversity analysis of ASV data from V4 16S RRNA amplicon sequencing from fetal membrane samples and DNA extraction kit negative controls. Diversity values presented as samples and negative controls (A), then samples further divided by tissue type of amnion and chorion compared to negative controls (B), plus GUniFrac PERMANOVA beta diversity analysis from samples and negative controls (C) and subdivided by tissue types (D). Significance was analysed via nonparametric Kruskal-Wallis and nonparametric Pairwise Wilcoxon Rank-Sum to a threshold of p=≤0.05.

3.4 Discussion

The aim of this chapter was to investigate the microbiota in fetal membranes with and without HCA by Illumina amplicon sequencing. Also, to explore the microbiota in HCA related to maternal inflammatory staging and grading.

Overall, chapter three highlights that bacterial profiles differ between HCA and non-HCA fetal membranes, with a trend for increased *Prevotella* in HCA and higher inflammatory levels. Inflammatory staging and grading have distinct bacterial profiles, but specific bacteria are only linked to inflammatory grading and not staging, with increased *Prevotella* and decreased *Lactobacillus* as inflammatory grading increases in severity. Frozen tissues and negative controls are distinct in bacterial profile structure and four specific genera.

3.4.1 Optimum DNA quantity from frozen fetal membranes. NanoDrop and agarose gel electrophoresis results confirmed that optimum quality and quantity of DNA was extracted from all frozen fetal membranes, this was required to be >1 pg/µl for successful sequencing (Biesbroek *et al*, 2012). HCA yielded a greater DNA quantity compared to non-HCA patients, which is also reflected in sequencing read count values. However, during library preparation all samples were diluted to equal concentrations. Post-process rarefying of data has also been suggested as a method to normalise read counts. However, this can lead to discarding important samples in low library sizes and errors when differential abundance is displayed (McMurdie and Holmes, 2014), thus was not applied here.

3.4.2 Sequencing read counts from frozen fetal membranes. All frozen fetal membranes had detectable read counts from sequencing methodology, including non-HCA preterm and term membranes. Although the greatest read count was from HCA samples from both the amnion and chorion. Previous research has detected read counts in 68.1% of fetal membranes and 46.8% of placental samples from sequencing (Doyle *et al*, 2017), with mean read counts lower than detected here at 11,803. Leiby *et al* (2018) also detected read counts in 61.3% of placentas, with detection only confirmed if samples contained >100 reads. Utilising the 100 read count threshold would have led to the removal of 2869 ASVs in this research, which could have included rare sequences important to HCA (McMurdie and Holmes, 2014). Low biomass samples, such as placenta are expected to generate low read counts, so the threshold value was selected as <2 counts in 20% of features to

prevent the removal of important information (McMurdie and Holmes, 2014), this led to the removal of 1429 low abundant features. Read counts are arbitrary and do not represent abundance due to inconsistent 16S rRNA gene copy numbers across taxa and samples, plus differences in variable regions (Noecker *et al*, 2017). Greater read counts with the V1/V2 compared to the V3/V4 region were detected within a sequencing protocol comparison study, albeit using stool samples (Clooney *et al*, 2016). The use of qPCR to investigate bacterial load (Chapter five) improves upon abundance analysis and can be combined with sequencing to clarify findings and create a broad view of the microbiota.

3.4.3 HCA patients have distinctly different bacterial profiles compared to non-HCA patients in both amnion and chorion tissues when measured by beta diversity. A trend for increased *Prevotella* (38%) and *Ureaplasma* (24%) at genus level was detected in HCA patients compared to non-HCA patients (<10%), and one ASV assigned to *Prevotella* was significantly increased in HCA patients. Prince *et al* (2016) supported different diversity profiles in placental membranes with and without HCA (Prince *et al*, 2016). The research included comparable categories to this research project (HCA, PTB and Term), but also included term patients with chorioamnionitis. Research showed that bacterial communities at term with HCA were most like preterm without HCA (Prince *et al*, 2016). The inclusion of term patients with chorioamnionitis would have been beneficial within this study, however the occurrence of this condition in term patients is low, at 2-4% (Kim *et al*, 2015), and none were available at the time of collection for this research.

Although overall bacterial profiles differed between HCA, PTB and term patients, no significant differences in the presence or amount of any specific genus was detected. Trends for increased *Ureaplasma* and *Prevotella* were identified in HCA samples, with a trend for greater *Lactobacillus* in non-HCA fetal membranes. The detection of these opportunistic pathogens including *Ureaplasma* and *Prevotella* were detected in chorioamnionitis fetal membranes and placenta previously (Cox *et al*, 2016; Hecht *et al*, 2009; Sweeney *et al*, 2016).

Prevotella was the most abundant genus in HCA patients, but was also observed in PTB and term without HCA. Although insignificant at genus level, one *Prevotella* ASV was significantly greater in the amnion of HCA patients. Previous research relates *Prevotella* to placental inflammation (Hecht *et al*, 2009), whilst others

suggest high colonisation in the placenta but a low ability to elicit an inflammatory response, when measured by enzyme linked immunosorbent assay (ELISA; Fichorova *et al*, 2011). Detection in PTB (Han *et al*, 2009), preterm premature rupture of the membranes (PPROM; Brown *et al*, 2018) and microbial infection in amniotic fluid (DiGiulio *et al*, 2008) via PCR and sequencing highlights its involvement in fetal and maternal immune response, but suggests a non-specific target for HCA detection. *Prevotella* has also been observed in healthy placenta (Aagaard *et al*, 2014; Doyle *et al*, 2017; Leiby *et al*, 2018), but also as a component of the natural vaginal community (MacIntyre *et al*, 2015; Romero *et al*, 2014a; Satorki *et al*, 2010), linking it to a possible ascending pathway of initiation. No differences were found at the genus level, suggesting that a range of *Prevotella* ASVs were detected across the entire cohort. Seven different ASVs were in high abundance from *Prevotella*. However, a single *Prevotella* ASV was more abundant in HCA samples, suggesting it may illicit an inflammatory response. Within current literature, one *Prevotella* species has been the focus of reproductive health and placental research. *Prevotella bivia*, a common vaginal isolate, has been linked to bacterial vaginosis and PTB (Gilbert *et al*, 2019). Hecht *et al* (2009) found a two-fold increase in *P. bivia* from higher maternal inflammation (stage three, grade two) compared to stage and grade one, from chorion explant cultures (Hecht *et al*, 2009). This species has shown the *in vitro* capacity to invade human cervical endothelial cells to induce an inflammatory response (Strombeck *et al*, 2007). Species-specific qPCR could differentiate and confirm the bacterial load and importance of associated ASVs, which may be clinically beneficial for detection of the condition.

Ureaplasma was the second most abundant genus in HCA, but also present in PTB, yet not detected in term patients. Research has detected *Ureaplasma* as the most prevalent genus in chorioamnionitis placenta and fetal membranes, yet the majority of research focuses specifically on species of *Ureaplasma urealyticum* and *Ureaplasma parvum* (Sweeney *et al*, 2016). Sweeney *et al* (2016) found that 60% of HCA placenta were positive for *U. parvum*, and 13% for *U. urealyticum*, with mean bacterial loads of 10^8. Cox *et al* (2016) identified significantly greater *U. parvum* from chorioamnionitis chorion (33.3%), compared to without chorioamnionitis (9.1%); yet comparable levels of *U. urealyticum* from both groups (3-4%), suggesting species-specific variation. Thus, it may be important to determine if either of these species correlated to ASVs detected in HCA fetal membranes here. Contrastingly, *Ureaplasma* has been implicated in both spontaneous PTB (sPTB) and PPROM

(Witt *et al*, 2005), and is therefore not specific to HCA. *Ureaplasma* are present in the respiratory, urinary and reproductive tract (Urszula *et al*, 2014). But small amounts of this low virulence pathogen may be unable to elicit an inflammatory response (Aaltonen *et al*, 2007). It may be a greater overall bacterial load rather than presence required to initiate an inflammatory response, which will be explored in chapter five by 16S rRNA gene qPCR methodology. Further research may wish to use *in vitro* fetal membrane explants spiked at varied bacterial loads and for varied time points to investigate the impact of *Prevotella* and *Ureaplasma* on placental inflammation.

Further genera and ASVs detected in greater abundance with HCA, but not significantly so were contained within the phylum *Firmicutes*. This phylum is suggested as a primary contributor to the intestinal microbiota (Kim *et al*, 2015), plus highly abundant in the healthy vaginal, placental (Aagaard *et al*, 2014) and fetal membrane microbiota (Huang *et al*, 2014). Amplification bias towards *Firmicutes* from the V4 primer may increase the abundance in this study (Wang *et al*, 2009). However, this bias would then be expected in comparable amounts across all samples. Alternatively, *Firmicutes* have been linked to contamination due to detection in low relative abundance within commercial DNA extraction kit negative controls of MoBio PowerMax (Glassing *et al*, 2016).

The most abundant bacterium across non-HCA patients was *Escherichia/Shigella*, also the third most abundant in HCA patients. Support that *Escherichia* is the main bacteria detected in normal preterm and term placenta and fetal membranes is supported by Aagaard *et al* (2014) and Lee *et al* (2018). Aagaard *et al* (2014) stated *Escherichia*, specifically *E. coli* as the unique signature of a placental microbiota when compared to other body sites, including oral and vaginal (Aagaard *et al*, 2014). Prince *et al* (2016) also found consistent detection of *Escherichia* across preterm and term with and without chorioamnionitis via whole genome sequencing. Thus not relating detection to gestational age or inflammation. However, kit negative controls were not stated for either study, bringing into question the origin of bacteria (Kilman, 2014). Alternatively, Hecht *et al* (2009) detected *Escherichia* in double the amounts from higher grade HCA than mild HCA, relating abundance to severity of the condition. Despite analysing 1292 placentas, only patients with HCA delivering by caesarean section were included, without a healthy control group or patients

delivering vaginally used as a baseline. Thus, methodological limitations could possibly skew results. *In vivo* research corroborates findings as stimulation with *Escherichia* endotoxin increased HCA and inflammation in ovine fetal membranes (Kallapur *et al*, 2001). Lipopolysaccharides are not highly specific, and a number of Gram-negative bacteria could initiate the response, for example *Prevotella* rather than *Escherichia* specifically (Aroutcheva, Ling and Faro, 2008). The genuine detection of *Escherichia* from fetal membranes has been questioned and is the focus of many debates due to contamination from methodological processes (Kilman, 2014). *Escherichia* has been stated as a universal contaminant across low biomass microbiota research (Theis *et al*, 2019), as discussed throughout this thesis.

3.4.4 HCA inflammation levels are associated with bacterial profiles of the fetal membranes. Although no specific genera were significantly linked to HCA inflammatory stage or grade in amnion or chorion, there was a trend for increased *Prevotella* and decreased *Lactobacillus* with increasing histologically confirmed inflammation. The negative correlation between *Prevotella* and *Lactobacillus* has previously been observed in bacterial vaginosis (Si *et al*, 2010), suggesting that dysbiosis of the two bacteria may be linked to pathology. At the ASV level one *Prevotella* sequence was significantly greater in grade two amnion and one *Lactobacillus* ASV was significantly increased in grade one chorion. This highlights that individual fetal membranes have distinct influential bacteria across inflammatory response levels. It is beneficial to investigate each membrane individually prior to clinical diagnosis, as performed here. This is due to different structural properties and inflammatory responses to bacterial presence (Waring *et al*, 2015). Also as involvement of the amnion in chorioamnionitis is the most advanced stage of the condition (Park *et al*, 2009), which may explain why only increased *Prevotella* in higher inflammatory response was detected in amnion but not the chorion. This indicates that individual fetal membrane analysis is important for bacterial progression across the membranes and categorising HCA severity. Variation across membranes is also present from inflammatory gene expression research, with increased TLR1, TLR2 and LY96 in the chorion, but IL-8 and IRAK2 in the amnion (Waring *et al*, 2015). In PPROM, weakening of the chorion may compromise protection of the amnion, leading to membrane microbiota changes following PPROM (Canzoneri *et al*, 2013). PPROM was the most prevalent cause

of PTB here, occurring in 75% of HCA and 50% of PTB patients, thus it may be of interest to investigate HCA microbiota characteristics from PPROM and sPTB individually.

3.4.5 Negative controls and samples have distinct bacterial profiles and differ by four specific genera. Careful consideration is required when elucidating the microbiota of fetal membranes, with the need to investigate the contribution from the specific DNA extraction kit reagent microbiota within each study, and to investigate the impact of external contamination to avoid false positive conclusions. The use of commercial kits and reagents has increased external bacterial contribution (Biesbroek *et al*, 2012; Jervis-Bardy *et al*, 2015; Laurence, Hatzis and Brash, 2014; Salter *et al*, 2014), especially in low biomass samples, including placental and fetal membranes (Eisenhofer *et al*, 2019; Lauder *et al*, 2016).

Escherichia/Shigella, *Pseudomonas*, *Lactobacillus* and *Blautia* were observed in significantly greater abundance from DNA extraction kit negative controls compared to samples at both the genus and ASV level here, which suggests that these genera originated from the extraction process and contributed to sample contamination. *Escherichia/Shigella* and *Pseudomonas* have previously been detected in sequencing blanks and ultrapure water (Grahn *et al*, 2003; Laurence, Hatzis and Brash, 2014). Whilst, Theis *et al* (2019) detected *Escherichia/Shigella* as the most abundant in both placental samples and negative controls, as was presented here. Although findings suggest significant differences in relative abundance bacterial profiles between samples and negative controls, we must consider the impact if these bacteria are contaminants and question the relevance of highlighted genera. DADA2 does not distinguish between *Escherichia* and *Shigella* when clustering into ASVs, with amplicon sequencing of the V4 region unable to resolve bacteria to the species level. To generate a stable conclusion it would be beneficial to perform species-specific qPCR to detect the bacterial load of the primary *Escherichia/Shigella* on the tissues and negative controls.

Lactobacillus was detected in significantly greater amounts from negative controls at genus and ASV levels. These vaginal commensal bacteria have a beneficial role in vaginal health by maintaining a low pH (Ling *et al*, 2010). *Lactobacillus* was previously linked to decreased inflammatory grading in HCA chorion from this research project. Increased abundance in negative controls questions these findings as *Lactobacillus* has been identified as a contaminant from MoBio

PowerMax DNA extraction kit reagents when applied to low biomass samples (Glassing *et al*, 2016). Likewise, the origin of *Pseudomonas* from negative environmental controls of air swab (Leiby *et al,* 2018) and ultrapure water used in sample processing has been noted (Muhl *et al*, 2010; Salter *et al*, 2014). Further bacteria greater in negative controls were *Blautia, Dorea* and *Faecalibacterium*. These genera are core bacteria of the adult gut and faecal matter (Gomez-Arango *et al*, 2017). However, have also been detected in negative controls, originating from storage buffers (Sinha *et al*, 2015). Furthermore, half of the most abundant ASVs identified within negative controls were previously detected as the main contaminants from Qiagen DNeasy tissue extraction kits, including *Escherichia*, *Acinetobacter* and *Staphylococcus* (Leon *et al*, 2018), also *Bacteroides*, *Faecalibacterium* and *Roseburia* (Karstens *et al*, 2019). Post-processing methods can remove all bacterial sequences found in negative controls (Jervis-Bardy *et al*, 2015), but within this research project specific bacteria detected in greater amounts from negative controls were also observed in samples, thus may still belong to the fetal membrane microbiota.

Contamination biases can be introduced by variation in methodology including DNA extraction kit manufacturer, 16S rRNA gene variable region and reference database (Laurence, Hatzis and Brash, 2014; O'Callaghan *et al*, 2019; Salter *et al*, 2014). Sources of contamination include PCR and sequencing reagents or molecular biology grade water (Grahn *et al*, 2003; Jervis-Bardy *et al*, 2015; Laurence, Hatzis and Brash, 2014; Leiby *et al*, 2018). NanoDrop and agarose gel analysis prior to sequencing detected low quantity DNA from negative controls, thus sequencing reagents used after this may be the main source of contamination. Monitoring DNA quantity via NanoDrop or Qubit periodically throughout sample preparation and sequencing may be beneficial to determine the primary source of bacterial contamination.

Methodology without the need for DNA extraction kit processing and sequencing reagents would be beneficial to reduce contamination in low biomass samples. Application of Raman spectroscopy (Chapter six) aims to reduce the possibility of environmental and reagent contamination, remove the impact of DNA extraction reagents and detect genuine bacterial signals, due to this being a non-destructive technique (Pahlow *et al*, 2015). Raman microspectroscopy would allow visual location analysis of specific targeted species to confirm the location and presence of the debated bacteria on the fetal membranes.

3.5 Conclusion

Understanding the microbiota of the fetal membranes with HCA remains debated. Findings here suggest that a specific bacterial profile is present from fetal membranes with HCA, with links to increased *Prevotella* in higher inflammatory grade HCA. Amnion and chorion may react and respond to HCA differently, with different bacterial profiles and specific ASVs across membranes. Fetal membrane samples are distinct from negative controls in bacterial profiles and four specific genera.

Chapter Four: The utilisation of Formalin-Fixed Paraffin-Embedded fetal membrane samples for microbiota research; FFPE and frozen comparison.

Abstract

Aim

The aim of this chapter was to determine if Formalin-Fixed Paraffin-Embedded (FFPE) fetal membrane tissues yield comparable DNA quantity and bacterial profile to frozen samples, to determine if these routinely collected and archived samples could be used in histological chorioamnionitis (HCA) microbiota research. This to reduce preparation, storage and costs associated with frozen fetal membrane processing and biobanking.

Methods

Matched paired analysis (n=21) was performed by comparing FFPE and frozen microbiota data. Respective DNA extraction kit negative controls from two different manufacturers were also compared. Decontam was integrated into computational analysis to identify contaminating sequences in FFPE samples.

Results

Frozen fetal membranes yielded greater quality and quantity of extracted DNA compared to highly fragmented FFPE DNA. Different bacterial genera were observed between sample preparation methods and kit manufacturer. Over half of sequences from FFPE samples (52%, 1690), were identified as contaminants via decontam, with 318 of the genuine bacteria significantly different between samples and controls. The most abundant bacteria across tissues and negative controls (*Escherichia/Shigella*) was detected as a genuine signal.

Conclusion

FFPE fetal membranes are not comparable to frozen samples, with reduced DNA quality and quantity, plus high levels of contamination. It is not recommended to replace frozen tissues with FFPE samples for fetal membrane microbiota research.

4.1 Introduction

The current gold standard tissue preparation method for microbiota research is fresh or flash frozen samples (Arreaza *et al*, 2016; Roberts *et al*, 2019). However, the routine collection, preservation and availability, plus ease of retrospective and repeat analysis make Formalin-Fixed Paraffin-Embedded (FFPE) samples a potential candidate where frozen samples are not available (Arreaza *et al*, 2016; Roberts *et al*, 2019).

FFPE samples are routinely collected, processed, stored and archived for the preservation of clinical specimens. They are highly beneficial in tissue comparison research, due to structural integrity and morphological retention (Al-Attas *et al*, 2016). The procedure consists of collecting the tissue of interest, fixing in neutral buffered formalin, dehydrating with ethanol and clearing the sample with xylene before embedding in paraffin wax (Nagahashi *et al*, 2017). The use of formalin creates crosslinkage between molecules to stabilise protein composition (Berg *et al*, 2011). Dehydration then displaces water in the sample and replaces this with paraffin wax to preserve tissue structure (Belloni *et al*, 2013; Pikor *et al,* 2011). Initial analysis routinely includes sectioning the wax block and staining with haematoxylin and eosin (H&E) for microscopic analysis of internal structures (Stout *et al*, 2013).

4.1.1 Application of FFPE samples

FFPE sample processing is beneficial for immunohistochemistry and pathological diagnosis. Fixing tissues preserves the structural characteristics of the membranes, for long term storage at room temperature (RT), allowing retrospective analysis (Dietrich *et al*, 2013; Nagahashi *et al*, 2017). FFPE samples are a valuable resource when there is a shortage of biological samples, or biobank storage limitations (Janecka, Adamczyk and Gasinska, 2015). However, the beneficial application to microbiota research is yet to be confirmed.

Utilising one tissue type for both pathological diagnosis and microbiota research would be preferable to avoid duplication, plus reduce processing requirements and storage costs (Linder *et al*, 2018). With the ability to then accurately link molecular findings to pathological and clinical diagnosis. Thus, utilising remnant FFPE material from clinical assessment could be beneficial to advanced clinical research (Wimmer *et al*, 2018).

FFPE samples have been successfully utilised in sequencing and qPCR research applied to heart valve samples (Imrit *et al*, 2006), plus single nucleotide

polymorphism arrays in umbilical cord samples (Ernst *et al*, 2015). Successful application varies by processing and storage duration. The harsh fixative process creates a tough physical barrier, as the formalin reacts with amino groups and adds a methylol group, which increases crosslinkage between amino acids leading to DNA degradation and fragmentation, which may negatively impact downstream methodology (Bennike *et al*, 2016; Huijsmans *et al*, 2010). Archived ovarian FFPE samples display an 89.9% success rate in whole exome sequencing, however, fragment size reduced with increasing storage time of 32 years (Carrick *et al*, 2015). Conversely, archived FFPE samples stored for >100 years produced minimal difference in DNA damage throughout storage duration when analysed by Illumina HiSeq (Ruane and Austin, 2017). Seven years has been suggested as the maximum storage duration to ensure optimum results (Nagahashi *et al*, 2017). Alongside storage conditions, different protocols across medical research centres also impacts results (Burton *et al*, 2014).

4.1.2 Placental and fetal membrane FFPE samples

Placental morphology and characteristics are routinely investigated in a clinical setting using FFPE preparations. One application of FFPE fetal membranes is the diagnosis of HCA via morphological analysis of maternal inflammatory factors using Redline staging and grading criteria (Redline *et al*, 2003). Following diagnosis, these samples are stored but infrequently reused. Recently, IHC has been performed on FFPE fetal membranes for microbiological analysis (Kuperman *et al*, 2020). The application of FFPE fetal membranes to HCA microbiota sequencing analysis would be beneficial, yet positive usage is yet to be confirmed.

4.1.3 Decontam applied to FFPE samples

Due to the complex processing steps in FFPE sample preparation, it is important to detect external contaminating bacteria during microbiota analysis. Decontam open-source R package has been created for post-process sequencing analysis (Davis *et al*, 2018). This method uses prevalence or frequency filtering to detect contaminating or genuine amplicon sequence variants (ASVs) from sequencing outputs (Davis *et al*, 2018).

Low abundance and low biomass samples have been criticised for accuracy in microbiota research (Laurence, Hatzis and Brash, 2014), including FFPE samples (Arreaza *et al*, 2016), as genuine signals are more susceptible to being concealed

by contaminating sequences, thus masking the true microbiota (Glassing *et al*, 2016). The use of decontam on low biomass samples has received praise for the ability to identify the unique microbiota of the tissue of interest (Callahan *et al*, 2016b; Lauder *et al*, 2016; O'Callaghan *et al*, 2019; Salter *et al*, 2014). Decontam previously detected <1% bacteria as genuine when applied to healthy term placental sequencing research (Davis *et al*, 2018; Lauder *et al*, 2016). However, this has not yet been investigated in fetal membranes with a negative maternal condition, including HCA.

The comparative analysis of FFPE and frozen tissues has been performed previously from healthy (Bennike *et al*, 2016) or cancerous tissues (Coudry *et al*, 2007; Mittempergher *et al*, 2011; Wimmer *et al*, 2018). But, comparison of DNA quality and sequencing output is limited. One study using qPCR analysis highlighted high variability in fragmentation and amplification efficiency between FFPE and frozen placental tissues, with modified protocols required to achieve successful amplification (Dietrich *et al*, 2013). Alternatively, similar gene expression profiles from FFPE and frozen breast tissue have been observed, with the ability to correctly identify changes in tumour grades from FFPE samples with comparable accuracy to frozen tissues (Mittempergher *et al*, 2011).

Although project PLACENTA aims to encourage frozen biobanking and develop centralised protocols for reproductive tissues (Linder *et al*, 2018), biobanking remains underrepresented due to low funding and increased maintenance (Linder *et al*, 2018). Immediate processing and snap freezing of reproductive samples is not always possible in the clinical or home setting (Srinivasan, Sedmak and Jewell, 2002). Thus, it would be beneficial to utilise the readily available, remnant FFPE samples in clinical research.

The aim of chapter four was to compare the microbiota findings from matched paired FFPE and frozen patient tissues taken from a clinical setting. This to determine if FFPE fetal membrane rolls that are routinely collected and archived are comparable to the current gold standard, and could be applied to microbiota research to produce high quality DNA and outcomes from sequencing methodology.

4.2 Microbiota method recap

Comparison between tissue preparation methods was performed by combining and analysing microbiota data from FFPE and frozen fetal membranes. Only patients with both frozen and corresponding FFPE tissue blocks were included for matched paired analysis to reduce individual variation and bias (n=21). Individual amnion and chorion results from frozen analysis were merged to closer represent the FFPE fetal membrane rolls, which combine the amnion and chorion into one tissue segment.

The frozen sample subset was processed as discussed previously (Chapter two). FFPE samples were processed using comparable protocols. However, a different DNA extraction methodology (BiOstic FFPE tissue DNA isolation kit, MoBio), and one additional method for examining the quality of extracted DNA was applied (Bioanalyzer chip-based gel electrophoresis).

The use of different reagents and manufactured kits may impact microbiota findings (Salter *et al*, 2014), thus respective negative controls taken from the Qiagen kit used for frozen (QIAamp Fast DNA Tissue kit; n=9) or MoBio kit used for FFPE sample DNA extraction (BiOstic FFPE tissue DNA isolation kit; n=18) were compared. For the FFPE subset, additional controls were taken from the surrounding embedded wax adjacent to the tissue to identify the microbiota of infiltrating wax.

Sequencing was performed using MiSeq (Illumina) wet lab SOP, with the universal 16S rRNA gene primer specific to the V4 region (Callahan *et al*, 2016a; Callahan *et al*, 2016b; Kozich *et al*, 2013) by Northumbria University (Newcastle) as described in chapter two. Pre and post-processing data analysis were also comparable to the previous chapter, with FastQ files trimmed, filtered and processed through DADA2 1.4 (Callahan *et al*, 2016b), Bioconductor (Version 2; Callahan *et al*, 2016a), Phyloseq (McMurdie and Holmes, 2013) pipelines and packages in R (R Core Team, 2017), and Microbiome Analyst (Dhariwal *et al*, 2017) under the same criteria and thresholds as previously. Decontam was also integrated into FFPE sample analysis (Davis *et al*, 2018).

4.3 Results

4.3.1 Matched paired patient demographics

Patient demographics (n=21) are listed in Table 4.1, with those available from the preterm and HCA subsets only listed in Table 4.2.

		Patients (n=21)
Condition	HCA	9.0 (42.8)
	PTB	6.0 (28.6)
	Term	6.0 (28.6)
Gestational age (mean (SD))		33.3 (5.2)
Birthweight (mean (SD))		2097.1 (861.3)
Maternal age (mean (SD))		28.3 (6.4)
Maternal BMI (mean (SD))		23.4 (4.1)
Smoker	Yes	5.0 (23.8)
	No	14.0 (66.7)
	NA	2.0 (9.5)
Parity (mean (SD))		1.2 (1.6)
Fetal sex	Male	9.0 (42.9)
	Female	12.0 (57.1)
Apgar (mean (SD))		7.6 (2.2)

Table 4.1 Matched paired patient demographics. Patient characteristic data from all patients providing fetal membrane samples for the study, assessed from matched paired Formalin-Fixed Paraffin-Embedded (FFPE) and frozen fetal membranes. Unless stated data is displayed as n (%).

		HCA and PTB only (n=15)
Mode of delivery	Vaginal	11.0 (73.3)
	Caesarean section	4.0 (26.7)
Type of labour	Spontaneous	5.0 (33.3)
	PPROM	9.0 (60.0)
	NA	1.0 (6.7)
Days to birth (following PPROM) (mean (SD))		4.4 (3.3)
Antibiotics	Yes	8.0 (53.3)
	No	6.0 (40.0)
	NA	1.0 (6.7)
Antenatal corticosteroids	Yes	13.0 (86.7)
	No	2.0 (13.3)
Maternal inflammatory stage (mean (SD))		1.8 (0.7)
Maternal inflammatory grade (mean (SD))		1.4 (0.5)
Number of clinical CA signs (mean (SD))		1.1 (1.0)
C-reactive protein (mean (SD))		38.6 (53.4)
White blood cell count (mean (SD))		17.6 (7.1)
Previous PTB	Yes	5.0 (33.3)
	No	10.0 (66.7)
Previous early PTB	Yes	2.0 (13.3)
	No	13.0 (86.7)

Table 4.2 Matched paired patient demographics from HCA and PTB only. Patient characteristic data from all preterm patients providing fetal membrane samples for the study, with matched paired Formalin-Fixed Paraffin-Embedded (FFPE) and frozen fetal membranes only available from histological chorioamnionitis (HCA) and preterm birth (PTB) patients. Unless stated data is displayed as n (%).

4.3.2 Results of matched paired fetal membranes

4.3.2.1 Sequencing read counts from matched paired patients

Read counts were detected within all FFPE fetal membrane samples (3178 individual ASVs), similar to that from frozen samples (3758 ASVs).

4.3.2.2 Relative and percentage abundance of matched paired patients

Escherichia/Shigella was detected as the most prominent genus, contributing 38% to FFPE and 29% to frozen samples (Figure 4.1). *Ureaplasma* (29%) and *Prevotella* (20%) were also highly abundant genera in frozen tissue preparation, compared to <1% and 6% in FFPE tissues, respectively. In FFPE tissues, *Pasteurella* (5%), *Bacillus* (4%) and *Pseudomonas* (3%) were all greater compared to frozen samples, where these all contributed <1% to relative abundance.

Univariate analysis highlighted 30 genera significantly different between FFPE and frozen samples (Table 4.3). The majority of these (28/30) were significantly higher in FFPE samples, including *Escherichia/Shigella* (p=<0.001, FDR=<0.001). *Pasteurella* was also greater in FFPE samples, due to no detection in frozen tissues (p=<0.001, FDR=<0.001). Only two genera were significantly greater in frozen samples, these were *Flavobacterium* (p=<0.001, FDR=<0.001) and *Collinsella* (p=0.008, FDR=0.014).

At the ASV level, 61 ASVs were significantly different across sample preparation type (Table 4.4). This included three ASVs from *Escherichia/Shigella*, three *Prevotella*, and one *Pasteurella*, *Flavobacterium* and *Collinsella*. The majority of ASVs were of significantly greater abundance in FFPE tissues (56/61), including one ASV assigned to *Prevotella* and *Pasteurella,* plus a *Micrococcus*, only detected in FFPE samples. Those significantly greater in frozen samples were two ASVs assigned to *Faecalibacterium*, plus one *Prevotella*, *Collinsella,* and a *Flavobacterium*, which was only detected in frozen samples.

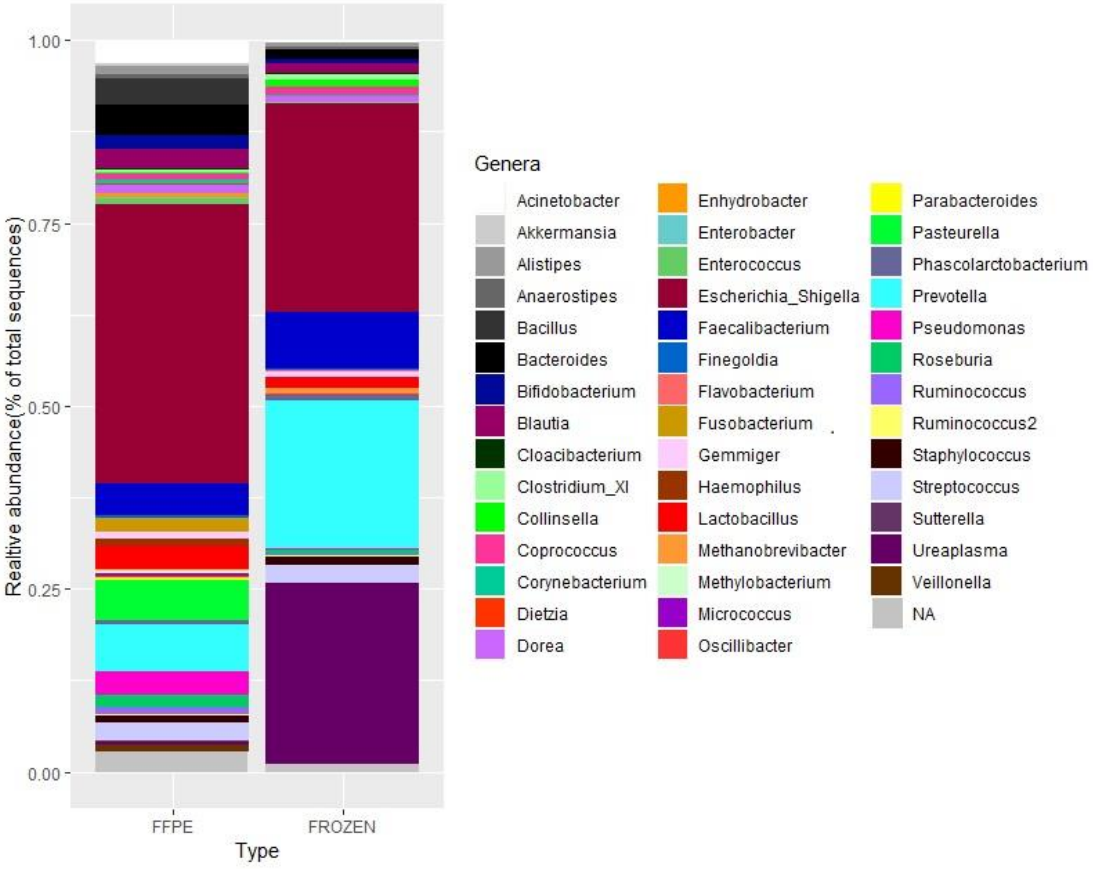

Figure 4.1 Relative abundance of matched paired fetal membranes. Relative abundance plots from V4 16S rRNA amplicon sequencing of extracted DNA from matched paired fetal membrane samples divided by tissue preparation type of Formalin-Fixed Paraffin-Embedded (FFPE) or frozen tissue samples. ASVs were clustered into genera for visual analysis plots created in ggplot2 (R Core Team, 2017).

	Genus	*p.value*	FDR
1	*Escherichia/Shigella*	<0.001	<0.001
2	*Bacillus*	<0.001	<0.001
3	*Pseudomonas*	<0.001	<0.001
4	*Pasteurella*	<0.001	<0.001
5	*Micrococcus*	<0.001	<0.001
6	*Enhydrobacter*	<0.001	<0.001
7	***Flavobacterium***	**<0.001**	**<0.001**
8	*Acinetobacter*	<0.001	<0.001
9	*Fusobacterium*	<0.001	<0.001
10	*Bifidobacterium*	<0.001	<0.001
11	*Blautia*	<0.001	<0.001
12	*Veillonella*	<0.001	<0.001
13	*Streptococcus*	<0.001	<0.001
14	*Methylobacterium*	<0.001	0.001
15	*Corynebacterium*	<0.001	0.001
16	*Alistipes*	<0.001	0.001
17	*Staphylococcus*	0.001	0.001
18	*Enterobacter*	0.001	0.002
19	*Bacteroides*	0.001	0.002
20	*Dietzia*	0.001	0.002
21	*Coprococcus*	0.004	0.007
22	*Haemophilus*	0.004	0.008
23	*Dorea*	0.004	0.008
24	*Parabacteroides*	0.004	0.008
25	*Roseburia*	0.007	0.011
26	***Collinsella***	**0.008**	**0.014**
27	*Ruminococcus*	0.017	0.027
28	*Faecalibacterium*	0.019	0.029
29	*Phascolarctobacterium*	0.021	0.031
30	*Cloacibacterium*	0.033	0.047

Table 4.3 Univariate analysis of matched paired fetal membranes by genera. Comparison of Formalin-Fixed Paraffin-Embedded (FFPE) and frozen fetal membranes by univariate nonparametric Kruskal-Wallis analysis and controlled for false discovery rates (FDR) to a threshold of p=≤0.05. Bacteria in **bold** were significantly greater in frozen samples, with the remaining greater in FFPE samples.

	ASV	Genus	*p.value*	FDR
1	C3	*Bacillus*	<0.001	<0.001
2	C1	*Escherichia/Shigella*	<0.001	<0.001
3	C31	*Pseudomonas*	<0.001	<0.001
4	C9	*Pasteurella*	<0.001	<0.001
5	C231	*Escherichia/Shigella*	<0.001	<0.001
6	C503	*Escherichia/Shigella*	<0.001	<0.001
7	C64	*Enhydrobacter*	<0.001	<0.001
8	C54	*Acinetobacter*	<0.001	<0.001
9	**C361**	***Flavobacterium***	**<0.001**	**<0.001**
10	C244	*Pseudomonas*	<0.001	<0.001
11	C35	*Blautia*	<0.001	<0.001
12	C181	*Micrococcus*	<0.001	<0.001
13	C76	*Acinetobacter*	<0.001	<0.001
14	C39	*Fusobacterium*	<0.001	<0.001
15	C49	*Acinetobacter*	<0.001	<0.001
16	C51	*Streptococcus*	<0.001	<0.001
17	C8	*Streptococcus*	<0.001	<0.001
18	C83	*Pseudomonas*	<0.001	<0.001
19	**C114**	***Faecalibacterium***	**<0.001**	**<0.001**
20	C556	*Micrococcus*	<0.001	<0.001
21	C129	*Methylobacterium*	<0.001	<0.001
22	C146	*Streptophyta**	<0.001	<0.001
23	C10	*Pseudomonas*	<0.001	0.001
24	C13	*Faecalibacterium*	<0.001	0.001
25	C304	*Corynebacterium*	<0.001	0.001
26	C5	*Staphylococcus*	0.001	0.002
27	C109	*Enterobacter*	0.001	0.003
28	C32	*Acinetobacter*	0.001	0.003
29	C20	*Blautia*	0.001	0.003
30	C68	*Streptococcus*	0.001	0.003
31	C150	*Dietzia*	0.001	0.003
32	**C60**	***Faecalibacterium***	**0.001**	**0.003**
33	C174	*Veillonella*	0.001	0.003
34	C44	*Bifidobacterium*	0.002	0.004
35	C184	*Methylobacterium*	0.002	0.005

36	C11	*Bifidobacterium*	0.002	0.005
37	C75	*Veillonella*	0.002	0.006
38	C12	*Bacteroides*	0.003	0.006
39	C86	*Blautia*	0.003	0.006
40	C74	*Faecalibacterium*	0.003	0.007
41	C59	*Alistipes*	0.004	0.008
42	C21	*Bacteroides*	0.004	0.009
43	C79	*Haemophilus*	0.004	0.009
44	C34	*Dorea*	0.004	0.009
45	C80	*Parabacteroides*	0.004	0.009
46	C17	*Roseburia*	0.005	0.010
47	C19	*Coprococcus*	0.005	0.011
48	C155	*Corynebacterium*	0.006	0.012
49	C7	*Faecalibacterium*	0.006	0.013
50	C71	*Lachnospiraceae**	0.007	0.014
51	C30	*Prevotella*	0.008	0.015
52	C139	*Acinetobacter*	0.008	0.015
53	**C36**	***Collinsella***	**0.008**	**0.015**
54	C56	*Alistipes*	0.013	0.024
55	C69	*Bacteroides*	0.016	0.028
56	C37	*Ruminococcus*	0.017	0.029
57	C58	*Faecalibacterium*	0.019	0.031
58	C22	*Prevotella*	0.019	0.031
59	C27	*Phascolarctobacterium*	0.021	0.034
60	**C16**	***Prevotella***	**0.025**	**0.040**
61	C105	*Bifidobacterium*	0.030	0.047

Table 4.4 Univariate analysis of matched paired fetal membranes by ASV. Comparison of Formalin-Fixed Paraffin-Embedded (FFPE) and frozen fetal membranes by nonparametric univariate Kruskal-Wallis analysis and controlled for false discovery rates (FDR) to a threshold of p=≤0.05. Amplicon sequence variants (ASVs) highlighted in **bold** were significantly greater in frozen samples, remaining ASVs were all significantly greater in FFPE tissue preparations. Bacteria are displayed by cluster number (C), ASV and genera, when genus was not assigned, the next highest order was used (*).

4.3.2.3 Bacterial diversity structure of matched paired patients

There was greater alpha diversity from FFPE (2.680) compared to frozen tissue preparation (2.253), yet not significant (p=0.232; Figure 4.2A).

Beta diversity highlighted significance between FFPE and frozen tissues (R^2=0.208, p=<0.001). Distinct clusters were detected for each preparation type, with FFPE samples clustering at a closer distance and frozen with greater beta diversity distances (Figure. 4.2B).

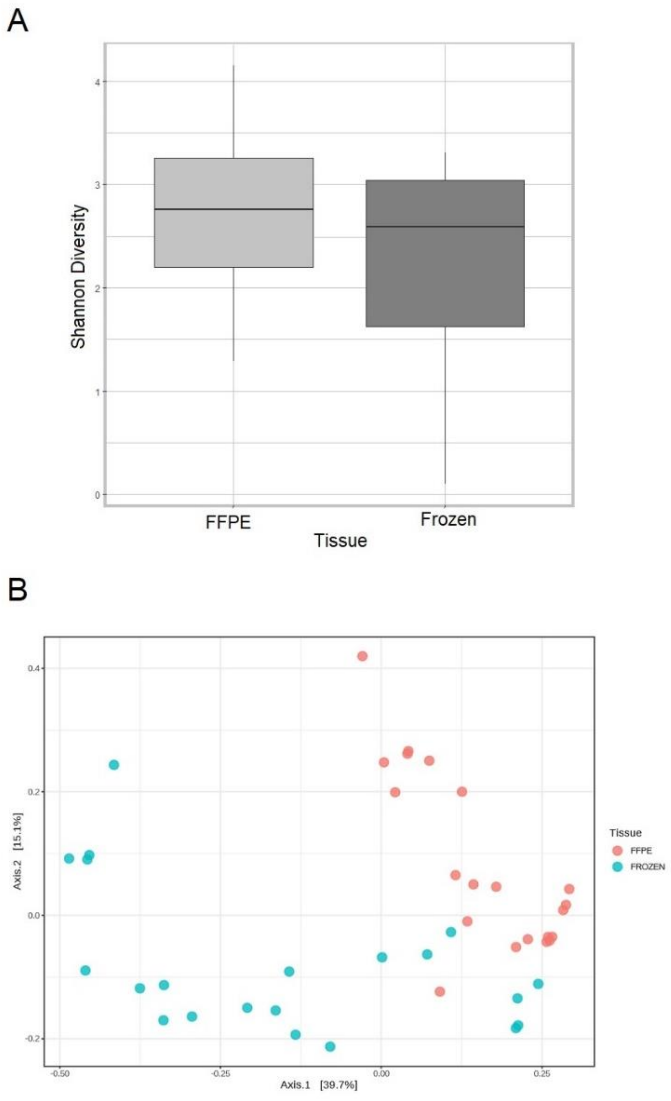

Figure 4.2 Diversity analysis of matched paired fetal membranes. Alpha and beta diversity analysis of ASV data from V4 15S RRNA amplicon sequencing from matched paired fetal membrane samples. Samples were divided into groups of Formalin-Fixed Paraffin-Embedded (FFPE) or frozen sample preparation for Shannon alpha diversity (A), or GUniFrac PERMANOVA beta diversity analysis (B). Significance was analysed via nonparametric Kruskal-Wallis and nonparametric Pairwise Wilcoxon Rank-Sum to a threshold of p=≤0.05.

4.3.3 Quantification of extracted DNA from matched paired patients

Due to differences detected in the microbiota between FFPE and frozen fetal membranes, further investigation was conducted to explore the reason behind this, including DNA quantity and quality analysis, plus the impact of different DNA extraction reagents and manufacturers.

4.3.3.1 NanoDrop spectrophotometer results from matched paired patients

Frozen tissues yielded a significantly higher mean quantity of extracted DNA than FFPE samples (270.5 ng/µl vs 47.6 ng/µl, p=<0.001). With this ranging from 79.5-1375.1 ng/µl in frozen, and 12.6-131.6 ng/µl in FFPE samples. Purity levels were optimum and comparable across preparation types (1.8 vs 1.8, p=0.940).

4.3.3.2 Agarose gel electrophoresis results from matched paired patients

High molecular weight DNA was extracted from frozen fetal membrane samples, with clear comparable molecular weight banding at >10,037 bp from all samples tested (Figure 4.3A). In comparison to highly fragmented, low quality and quantity DNA from FFPE samples, with faint banding detected at 200-400 bp (Figure 4.3B).

A

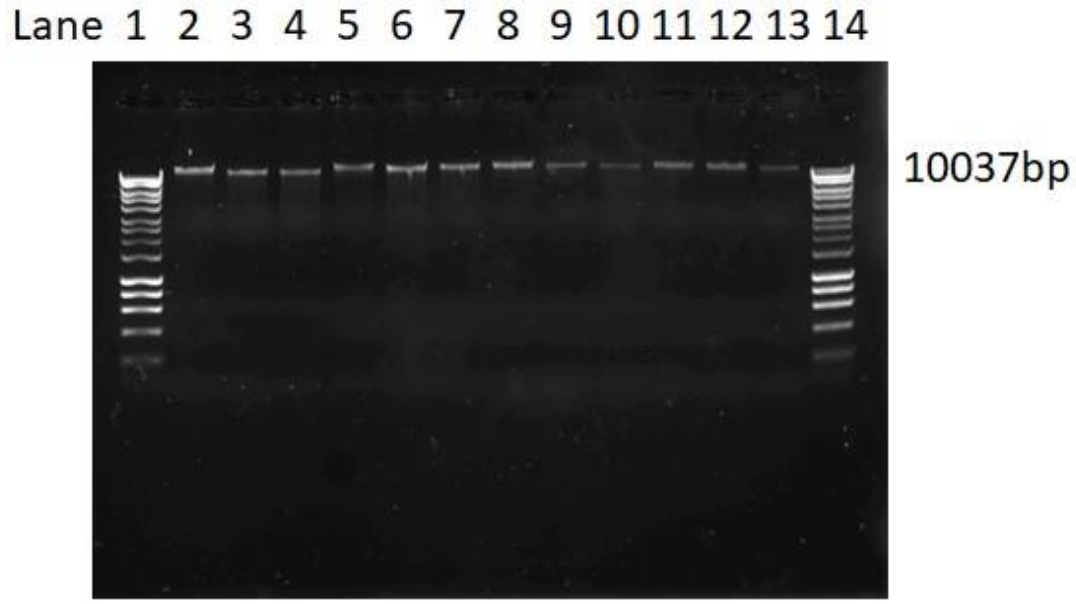

B

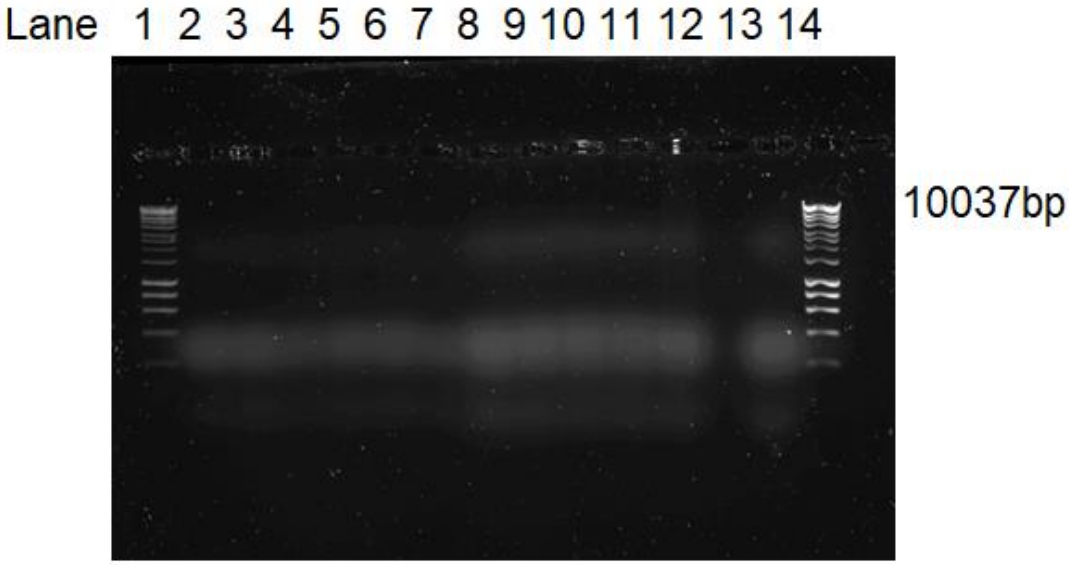

Figure 4.3 Agarose gel electrophoresis from matched paired fetal membranes. Agarose gel electrophoresis image of a subset of DNA extracts from fetal membranes (n=12; histological chorioamnionitis=7, preterm=4, Term=1) from either frozen membrane samples (A), or Formalin-Fixed Paraffin-Embedded (FFPE) samples (B) performed via agarose gel electrophoresis and imaged via GBox SynGene Chemi-XX6. Lane one and lane 14 represent 1KB reference HyperLadder.

4.3.4 FFPE sample comparison to negative controls

4.3.4.1 Sequencing read counts from FFPE samples and negative controls

The FFPE tissue sample microbiota was compared to negative controls of sections of surrounding paraffin wax and DNA extraction kit reagents. Wax negatives displayed the greatest average read counts (21,314.6), followed by samples (11,863.2), with the lowest from kit negative controls (4510.7).

A significantly greater quantity of DNA was extracted from samples (47.6 ng/µl), followed by wax controls (5.9 ng/µl), and the lowest from kit negative controls (2.4 ng/µl, p=<0.001). Specifically, DNA yields were significantly greater from FFPE samples compared to kit negative (p=<0.001) and wax controls independently (p=<0.001), yet wax and kit reagent negative controls were not significantly different (p=1.000).

4.3.4.2 Relative and percentage abundance from FFPE samples and negative controls

Escherichia/Shigella was the most abundant genera in samples and controls, greatest from kit negatives (68%), followed by samples (46%) and wax controls (31%; Figure 4.4). *Prevotella* was the second most abundant genera in wax controls (20%), but this decreased in both samples and kit negatives (<1%).

At the genera level, 32 genera were significantly different between samples and controls (Table 4.5). From this, 14 were significantly greater in samples, 14 significantly greater in wax controls, and four significantly greater in kit negative controls. *Escherichia/Shigella* was significantly greater from kit controls (p=0.002, FDR=0.004), with *Prevotella* significantly greater in wax controls (p=0.004, FDR=0.006). *Enterobacter* (p=<0.001, FDR=<0.001) and *Veillonella* (p=<0.001, FDR=0.002) were both significantly greater in samples compared to controls, with neither detected from kit negative controls.

Within samples, 3178 individual ASVs were detected, with 1682 from wax controls and 452 from kit negative controls. At the ASV level, 56 sequences were significantly different between samples and controls (Table 4.6). This including three ASVs assigned to *Escherichia/Shigella* and three assigned to *Prevotella*, plus one ASV assigned to *Enterobacter* and *Veillonella*.

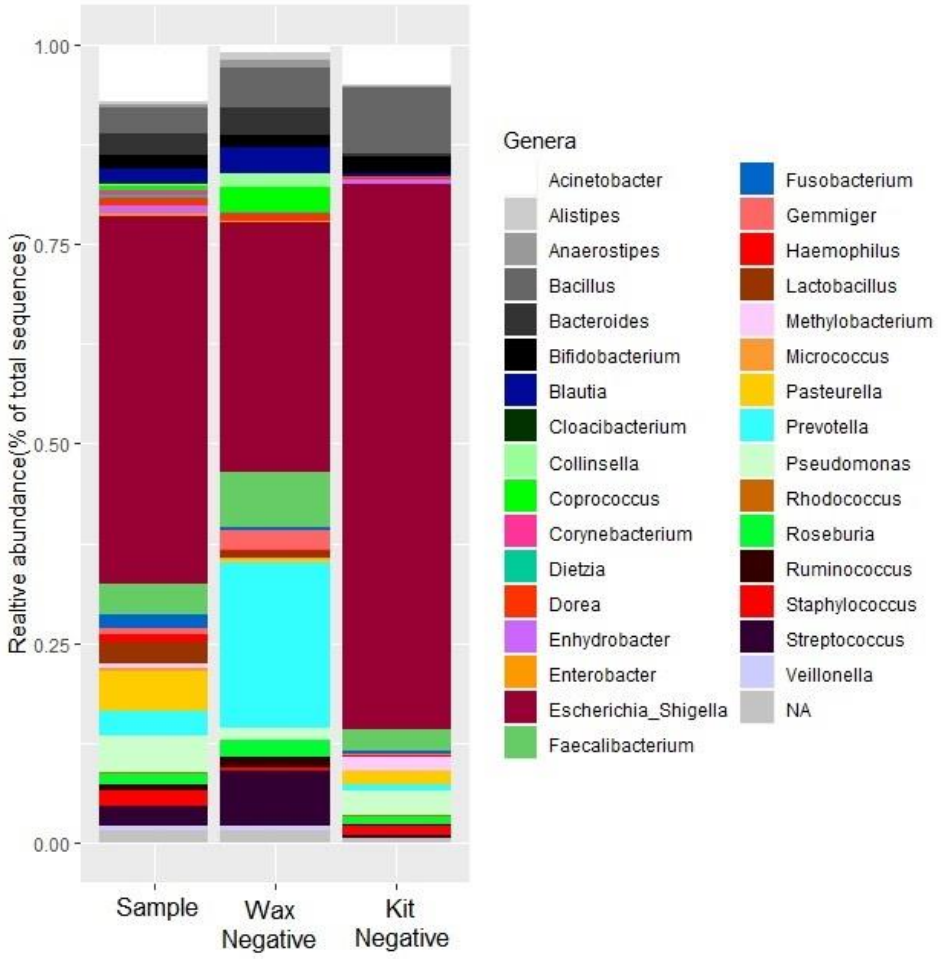

Figure 4.4 Relative abundance of FFPE membrane rolls and negative controls. Relative abundance plots from V4 16S rRNA amplicon sequencing of extracted DNA from Formalin-Fixed Paraffin-Embedded (FFPE) tissue (samples), corresponding wax control and kit negative control, to investigate the bacterial contribution from surrounding wax and DNA extraction kit negatives. ASVs were clustered into genera for visual analysis relative abundance plots created in ggplot2 (R Core Team, 2017).

	Genus	p.value	FDR	Greater in
1	*Micrococcus*	<0.001	<0.001	Sample
2	*Enterobacter*	<0.001	<0.001	Sample
3	*Lactobacillus*	<0.001	<0.001	Sample
4	*Enhydrobacter*	<0.001	<0.001	Sample
5	*Blautia*	<0.001	<0.001	Wax
6	*Corynebacterium*	<0.001	<0.001	Sample
7	*Staphylococcus*	<0.001	<0.001	Sample
8	*Veillonella*	<0.001	0.002	Sample
9	*Bacteroides*	<0.001	0.002	Wax
10	*Dorea*	<0.001	0.002	Wax
11	*Streptococcus*	<0.001	0.002	Wax
12	*Pseudomonas*	<0.001	0.002	Sample
13	*Ruminococcus*	<0.001	0.002	Wax
14	*Roseburia*	0.001	0.002	Wax
15	*Acinetobacter*	0.001	0.002	Sample
16	*Bacillus*	0.001	0.003	Kit
17	*Coprococcus*	0.002	0.004	Wax
18	*Escherichia/Shigella*	0.002	0.004	Kit
19	*Fusobacterium*	0.003	0.005	Sample
20	*Prevotella*	0.004	0.006	Wax
21	*Dietzia*	0.004	0.006	Sample
22	*Alistipes*	0.006	0.008	Wax
23	*Collinsella*	0.007	0.009	Wax
24	*Pasteurella*	0.009	0.011	Sample
25	*Faecalibacterium*	0.009	0.011	Wax
26	*Cloacibacterium*	0.009	0.011	Sample
27	*Rhodococcus*	0.010	0.011	Sample
28	*Anaerostipes*	0.012	0.013	Wax
29	*Methylobacterium*	0.023	0.026	Kit
30	*Gemmiger*	0.027	0.028	Wax
31	*Haemophilus*	0.042	0.044	Wax
32	*Bifidobacterium*	0.050	0.050	Kit

Table 4.5 Univariate analysis of FFPE samples compared to negative controls by genera. Comparison of Formalin-Fixed Paraffin-Embedded (FFPE) fetal membrane samples with negative controls from DNA extraction kit reagents and surrounding wax block controls. Univariate analysis was performed by nonparametric Kruskal-Wallis and controlled for false discovery rate (FDR) to a threshold of p=≤0.05.

	ASV	Genus	p.value	FDR
1	C181	*Micrococcus*	<0.001	<0.001
2	C109	*Enterobacter*	<0.001	<0.001
3	C51	*Streptococcus*	<0.001	<0.001
4	C304	*Corynebacterium*	<0.001	<0.001
5	C244	*Pseudomonas*	<0.001	<0.001
6	C83	*Pseudomonas*	<0.001	<0.001
7	C64	*Enhydrobacter*	<0.001	<0.001
8	C25	*Lactobacillus*	<0.001	<0.001
9	C40	*Lactobacillus*	<0.001	<0.001
10	C146	*Streptophyta**	<0.001	<0.001
11	C35	*Blautia*	<0.001	<0.001
12	C76	*Acinetobacter*	<0.001	<0.001
13	C2	*Prevotella*	<0.001	<0.001
14	C54	*Acinetobacter*	<0.001	<0.001
15	C150	*Dietzia*	<0.001	<0.001
16	C21	*Bacteroides*	<0.001	<0.001
17	C5	*Staphylococcus*	<0.001	<0.001
18	C13	*Faecalibacterium*	<0.001	<0.001
19	C49	*Acinetobacter*	<0.001	0.001
20	C20	*Blautia*	<0.001	0.001
21	C503	*Escherichia/Shigella*	<0.001	0.001
22	C75	*Veillonella*	<0.001	0.001
23	C34	*Dorea*	<0.001	0.001
24	C7	*Faecalibacterium*	<0.001	0.002
25	C231	*Escherichia/Shigella*	0.001	0.002
26	C37	*Ruminococcus*	0.001	0.002
27	C139	*Acinetobacter*	0.001	0.002
28	C17	*Roseburia*	0.001	0.002
29	C3	*Bacillus*	0.001	0.003
30	C31	*Roseburia*	0.002	0.003
31	C58	*Faecalibacterium*	0.002	0.003
32	C11	*Bifidobacterium*	0.002	0.004
33	C12	*Bacteroides*	0.002	0.004
34	C129	*Methylobacterium*	0.002	0.004
35	C19	*Coprococcus*	0.002	0.004

36	C1	*Escherichia/Shigella*	0.003	0.004
37	C4	*Prevotella*	0.003	0.004
38	C30	*Prevotella*	0.003	0.004
39	C155	*Corynebacterium*	0.003	0.004
40	C10	*Pseudomonas*	0.003	0.004
41	C39	*Fusobacterium*	0.003	0.005
42	C68	*Streptococcus*	0.003	0.005
43	C32	*Acinetobacter*	0.003	0.005
44	C59	*Alistipes*	0.006	0.008
45	C36	*Collinsella*	0.007	0.009
46	C8	*Streptococcus*	0.007	0.009
47	C9	*Pasteurella*	0.009	0.011
48	C201	*Cloacibacterium*	0.009	0.011
49	C209	*Rhodococcus*	0.010	0.012
50	C84	*Lachnospiraceae**	0.010	0.012
51	C105	*Bifidobacterium*	0.011	0.012
52	C41	*Anaerostipes*	0.012	0.013
53	C26	*Gemmiger*	0.027	0.030
54	C47	*Lachnospiraceae**	0.027	0.030
55	C74	*Faecalibacterium*	0.036	0.040
56	C79	*Haemophilus*	0.042	0.045

Table 4.6 Univariate analysis of FFPE samples compared to negative controls by ASV. Comparison of Formalin-Fixed Paraffin-Embedded (FFPE) fetal membrane samples with negative controls from DNA extraction kit reagents and surrounding wax block controls. Displayed as amplicon sequence variant (ASV) cluster number (C) and genus. Univariate analysis was performed by nonparametric Kruskal-Wallis and controlled for false discovery rate (FDR) to a threshold of $p=\leq 0.05$.

4.3.4.3 Bacterial diversity structure from FFPE samples and negative controls

There were significant differences in alpha diversity between FFPE samples, kit negative and wax controls (p=<0.001; Figure 4.5A). Samples displayed the greatest alpha diversity score (2.107), significantly greater than wax controls (1.636, p=0.030) and kit negative controls, independently (1.221, p=<0.001). A trend for higher alpha diversity in wax controls compared to kit negative controls was present, but not significant (p=0.051).

A significant difference in beta diversity between samples, wax and kit negative controls was present, with a distinct cluster for samples yet controls displaying greater beta diversity distance (R^2=0.210, p=<0.001 Figure 4.5B).

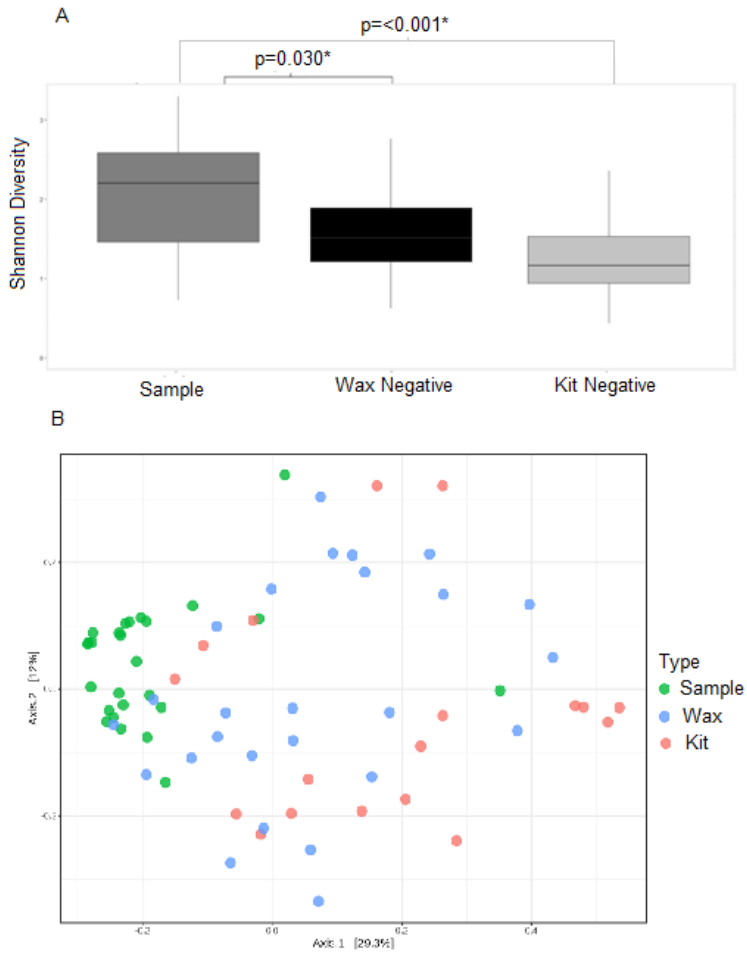

Figure 4.5 Diversity analysis of FFPE tissues and negative controls. Alpha and beta diversity analysis of ASV data from V4 16S rRNA amplicon sequencing from Formalin-Fixed Paraffin-Embedded (FFPE) fetal membrane rolls and negative controls of corresponding wax and kit reagent negative controls. Presented by alpha diversity (A) and beta diversity (B). Significance was analysed via nonparametric Kruskal-Wallis and nonparametric Pairwise Wilcoxon Rank-Sum to a threshold of p=≤0.05.

4.3.5 DNA extraction kit comparison

4.3.5.1 NanoDrop spectrophotometer results from kit comparison

MoBio FFPE kit yielded a significantly greater quantity of detected DNA within blank reagent controls (2.4 ng/µl) compared to Qiagen negative controls (frozen kit; 0.9 ng/µl, p=0.014).

4.3.5.2 Relative and percentage abundance from kit comparison

Different contributing genera were detected from DNA extraction kit manufacturers. *Escherichia/Shigella* was the most abundant genus in MoBio, contributing 66% to overall genera, with this the second most prominent in Qiagen (12%; Figure 4.6). *Bacteroides* were the greatest contributor to Qiagen negative controls (17%) with this reduced in MoBio reagents (<1%). *Prevotella* was of greater relative abundance from Qiagen (10%) compared to MoBio (1%).

Univariate analysis highlighted six genera as significantly different between MoBio and Qiagen kit negative controls. Of which, 5/6 were in greater abundance within the Qiagen frozen kit controls, including; *Enterococcus*, (p=0.002, FDR=0.040), *Chryseobacterium* (p=0.005, FDR=0.040), *Lactobacillus* (p=0.005, FDR=0.040), *Sphingomonas* (p=0.007, FDR=0.040) and *Prevotella* (p=0.008, FDR=0.040). *Bacillus* was the one genus significantly greater in MoBio FFPE kit, as this was not detected in Qiagen frozen kit controls (p=0.008, FDR=0.040).

At the ASV level, 21 ASVs were significantly different between DNA extraction kits, the majority of which were greater in Qiagen frozen kit controls (Table 4.7), including three ASVs for *Prevotella*, plus one *Enterococcus*, *Lactobacillus*, *Sphingomonas* and *Chryseobacterium*. One ASV (*Bacillus*) was significantly greater in MoBio FFPE controls and was not detected in Qiagen kit controls (Table 4.7).

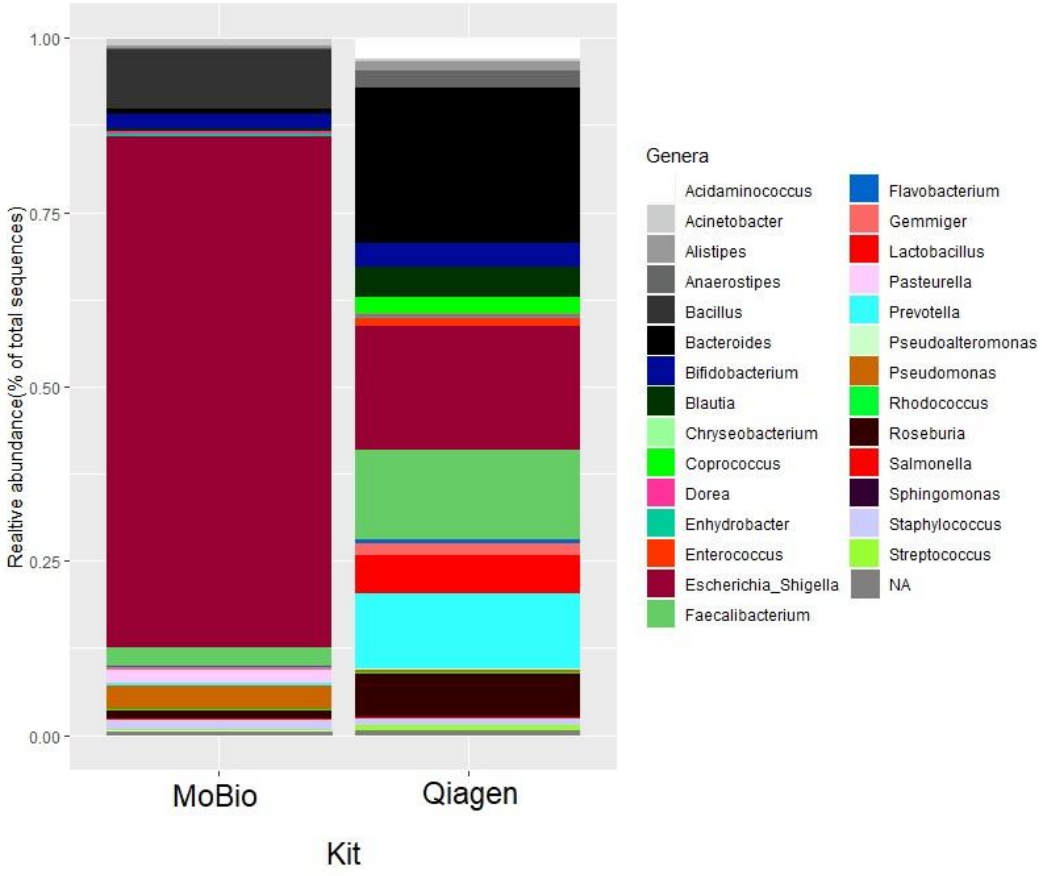

Figure 4.6 Relative abundance of DNA extraction kit controls. Relative abundance plots from V4 16S rRNA amplicon sequencing of extracted DNA from kit negative controls from MoBio (FFPE) and Qiagen (Frozen) DNA extraction kit reagents, to investigate the bacterial contribution from different commercial manufacturers. ASVs were clustered into genera for visual analysis of relative abundance created by ggplot2 (R Core Team, 2017).

	ASV	Genus	*p.value*	FDR
1	C6	*Prevotella*	<0.001	0.013
2	C62	*Bacteroides*	0.001	0.013
3	C60	*Faecalibacterium*	0.001	0.013
4	C180	*Lactobacillus*	0.001	0.013
5	C114	*Faecalibacterium*	0.002	0.013
6	C28	*Enterococcus*	0.002	0.013
7	C990	*Blautia*	0.002	0.013
8	C376	*Alistipes*	0.004	0.023
9	C283	*Bifidobacterium*	0.005	0.023
10	C4	*Prevotella*	0.005	0.023
11	C2002	*Chryseobacterium*	0.005	0.023
12	C1343	*Faecalibacterium*	0.005	0.023
13	C2598	*Sphingomonas*	0.007	0.028
14	C688	*Pseudomonas*	0.007	0.029
15	**C3**	***Bacillus***	**0.008**	**0.030**
16	C21	*Bacteroides*	0.011	0.035
17	C73	*Bacteroides*	0.012	0.039
18	C13	*Faecalibacterium*	0.013	0.039
19	C18	*Salmonella*	0.014	0.039
20	C110	*Roseburia*	0.014	0.039
21	C2	*Prevotella*	0.015	0.039

Table 4.7 Univariate analysis of DNA extraction kit controls by ASV. Comparison of MoBio Formalin-Fixed Paraffin-Embedded (FFPE) and Qiagen frozen kit negative controls by univariate nonparametric Kruskal-Wallis analysis and controlled for false discovery rates (FDR) to a threshold of p=≤0.05. Results displayed by cluster number (C) and genus. Amplicon sequence variants (ASVs) highlighted in **bold** were significantly greater in MoBio FFPE, with the remaining significantly greater in Qiagen frozen kit controls.

4.3.5.3 Bacterial diversity structure from kit comparison

When comparing kit negative controls only the Qiagen kit for frozen tissue DNA extraction displayed significantly higher alpha diversity compared to MoBio kit negative controls (2.778 vs 1.687, p=0.014; Figure 4.7A).

Significant differences in beta diversity were detected between negative controls from MoBio and Qiagen kits, with greater beta diversity distances from MoBio kit controls (R^2=1.357, p=0.012; Figure 4.7B).

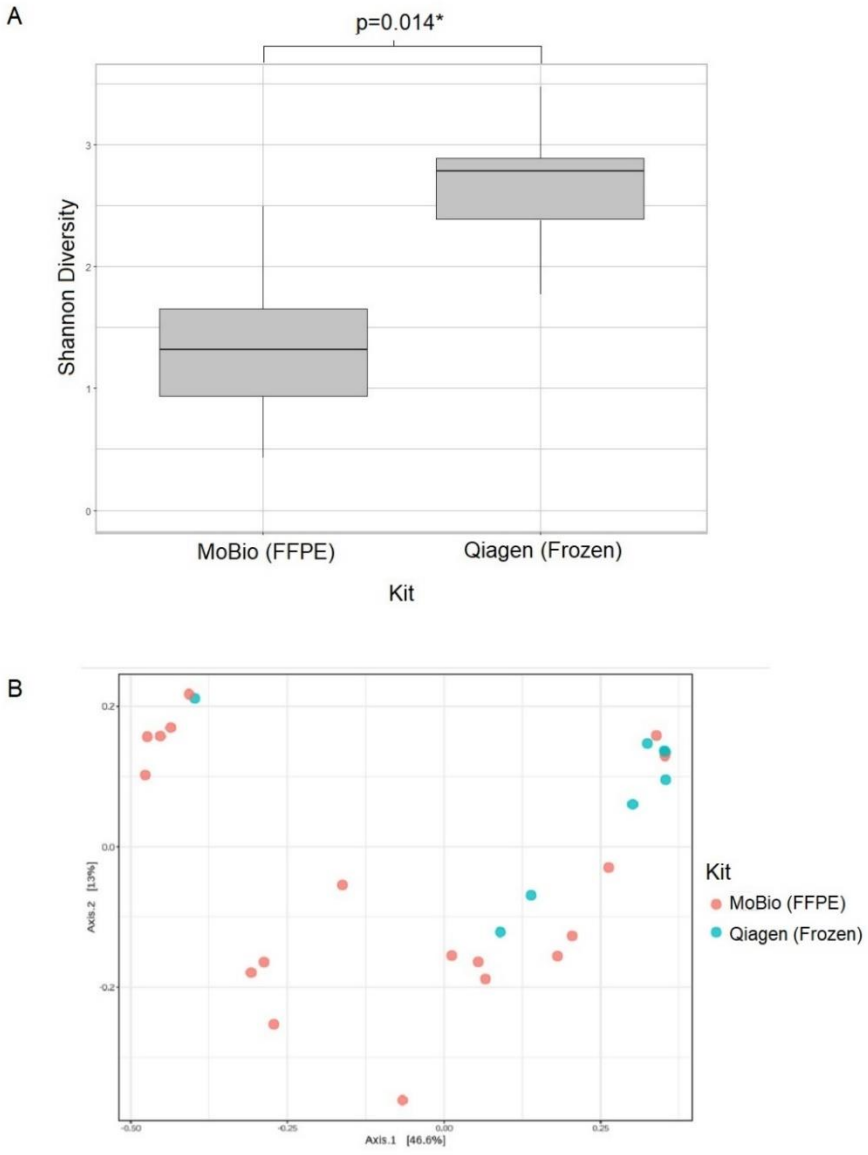

Figure 4.7 Diversity analysis of DNA extraction kit controls. Alpha and beta diversity analysis of ASV data from V4 16S rRNA amplicon sequencing from negative controls only from extraction kit reagents segmented into MoBio (Formalin-Fixed Paraffin-Embedded kit; FFPE) or Qiagen (Frozen kit) for Shannon alpha diversity (A) or GUniFrac PERMANOVA beta diversity analysis (B). Significance was analysed via nonparametric Kruskal-Wallis and nonparametric Pairwise Wilcoxon Rank-Sum to a threshold of p=≤0.05.

4.3.6 Decontam results from FFPE samples

Decontam prevalence filtering was applied to ASVs from FFPE samples and DNA extraction kit negative controls to detect contaminating sequences arising from processing.

Decontam output determined that 52% of ASVs generated in DADA2 were contaminants (FALSE=1690), whereas 48% were genuine signals (TRUE=1560). From the 1560 genuine ASVs, 318 were significantly different between FFPE samples and negative controls. The most prevalent genuine ASVs can be found in Table 4.8. None of the bacteria categorised as contaminants were significantly different between samples and negative controls, with a subset of contaminants displayed in Table 4.9.

The most prevalent ASV detected in both samples and controls was assigned to the *Escherichia/Shigella* genus, which was detected as a genuine signal, and not significantly different between samples and negative controls (p=0.205; Table 4.8). Out of six ASVs assigned to *Escherichia/Shigella*, five were identified as genuine bacteria including the most prevalent, with one low abundant ASV detected as a contaminant.

For *Prevotella*, 34 ASVs were identified as genuine and 25 as contaminating sequences. The genuine bacteria included four common ASVs detected in previous HCA analysis.

	ASV	Genus	Prevalence	p.value	Not. Contaminant
1	C1	*Escherichia/Shigella*	43	0.205	TRUE
2	C10	*Pseudomonas*	30	<0.001	TRUE
3	C11	*Bifidobacterium*	25	<0.001	TRUE
4	C2	*Prevotella*	24	<0.001	TRUE
5	C3498	*Unclassified bacteria**	22	0.030	TRUE
6	C12	*Bacteroides*	22	0.003	TRUE
7	C109	*Enterobacter*	19	<0.001	TRUE
8	C4	*Prevotella*	19	0.002	TRUE
9	C3	*Bacillus*	18	<0.001	TRUE
10	C15	*Bacillus*	18	0.017	TRUE
11	C8	*Streptococcus*	17	<0.001	TRUE
12	C105	*Bifidobacterium*	15	0.009	TRUE
13	C5	*Staphylococcus*	13	<0.001	TRUE
14	C7	*Faecalibacterium*	12	<0.001	TRUE
15	C113	*Roseburia*	12	0.026	TRUE
16	C101	*Bacteroides*	11	<0.001	TRUE
17	C1059	*Prevotella*	11	0.007	TRUE
18	C503	*Escherichia/Shigella*	10	<0.001	TRUE
19	C40	*Lactobacillus*	10	<0.001	TRUE
20	C117	*Anaerostipes*	10	0.001	TRUE

Table 4.8 Genuine bacterial sequences in FFPE samples identified by decontam. Top twenty amplicon sequence variants (ASVs) and genera detected as genuine non-contaminating sequences in decontam when comparing Formalin-Fixed Paraffin-Embedded (FFPE) samples to negative controls. Bacteria displayed as cluster number (C) and genera, ranked by prevalence. If genus was not classified the next highest order is displayed (*).

	ASV	Genus	Prevalence	p.value	Not. Contaminant
1	C2809	*Acetobacteraceae**	11	0.591	FALSE
2	C827	*Clostridia**	10	0.591	FALSE
3	C2745	*Prevotella*	7	0.591	FALSE
4	C629	*Unclassified bacteria**	7	0.591	FALSE
5	C1989	*Facklamia*	4	0.591	FALSE
6	C1303	*Bacteroides*	3	0.591	FALSE
7	C2481	*Leuconostoc*	3	0.591	FALSE
8	C3668	*Deinococcus*	3	0.591	FALSE
9	C4468	*Actinomycetales**	3	0.591	FALSE
10	C1027	*Blautia*	2	0.591	FALSE
11	C1040	*Gammaproteobacteria**	2	0.919	FALSE
12	C1097	*Fusobacterium*	2	0.591	FALSE
13	C1144	*Clostridiales**	2	0.591	FALSE
14	C1177	*Roseburia*	2	0.591	FALSE
15	C1189	*Pasteurella*	2	0.591	FALSE
16	C1455	*Cytophaga*	2	0.591	FALSE
17	C1757	*Streptomycetaceae*	2	0.591	FALSE
18	C1760	*Ruminococcaceae**	2	0.591	FALSE
19	C2113	*Mannheimia*	2	0.591	FALSE
20	C2132	*Pseudomonas*	2	0.591	FALSE

Table 4.9 Contaminating bacterial sequences in FFPE samples identified by decontam. Top twenty amplicon sequence variants (ASVs) and genera detected as contaminating bacteria in decontam from Formalin-Fixed Paraffin-Embedded (FFPE) samples compared to negative controls. Bacteria displayed as cluster number (C) and genera, ranked by prevalence. If genus was not classified the next highest order is displayed (*).

4.4 Discussion

Frozen sample preparation is the current gold standard for microbiota research (Dietrich *et al*, 2013; Roberts *et al*, 2019). However, FFPE samples are routinely collected, processed and stored, for structural preservation with minimal impact on integrity (Ruane and Austin, 2017). If FFPE samples are comparable to frozen tissues, the use of FFPE samples in microbiota research would be possible, which would benefit multiple pathological investigations, including maternal and fetal research. Furthermore, use of FFPE tissues would prevent limitations associated with frozen tissue storage and biobanking, such as space restrictions and funding (Dietrich *et al*, 2013; Linder *et al*, 2018).

The comparison of clinical FFPE and frozen fetal membrane sequencing outcomes have not yet been presented in the literature, with most comparison studies focussing on high biomass samples, or artificial scenarios (Bennike *et al*, 2016; Coudry *et al*, 2007; Mittempergher *et al*, 2011; Wimmer *et al*, 2018). Thus, the aim of this chapter was to compare the DNA quality and bacterial profiles of matched paired FFPE and frozen fetal membrane samples to determine if FFPE membranes can be beneficially used in microbiota research.

Overall, this chapter highlights a difference in bacterial profiles between freezing and fixing identical patient tissues. Decreased DNA quality and quantity were observed from FFPE frozen fetal membrane tissues. Furthermore, over half of bacteria detected in FFPE fetal membrane rolls were classified as contaminants when compared to negative controls using the post-processing decontam package. It was observed that 32 specific genera were significantly different between FFPE samples and DNA extraction kit negative controls. After applying decontam, 318 ASVs identified as genuine were significantly different between samples and negative controls, yet bacteria assigned as contaminants did not significantly differ. Overall, this suggests that FFPE samples are not suitable to replace frozen tissues in fetal membrane microbiota research.

4.4.1 FFPE samples have diminished DNA quantity and quality compared to frozen tissues, which may decrease the success of downstream methodologies. The quality of DNA extracted from FFPE samples was suboptimum, with fragmentation detected at 200-400 bp. Fragmentation of FFPE samples was previously detected in placental tissues, with 500 bp from FFPE and 5 kb from frozen

samples (Dietrich *et al*, 2013), FFPE prostate samples also displayed heavily fragmented DNA at 102, 165, 225 and 300 bp (Patel *et al*, 2017). Fragmentation occurs due to crosslinkage, which increases DNA sensitivity to mechanical stress and decreases enzyme accessibility. These factors reduce the impact of extraction methods and result in short target fragments (Dietrich *et al*, 2013). Fragmentation of DNA has been linked to processing and storage duration (Ruane and Austin, 2017). Samples used in this study were stored for a maximum of three years, within the seven years the limit for optimum results (Nagahashi *et al*, 2017). Age related pH changes may cause oxidation of formalin to formic acid causing further DNA fragmentation and degradation (Imrit *et al*, 2006; Patel *et al*, 2017). But high quality DNA has been extracted from >100year archived specimens (Ruane and Austin, 2017). Immediate analysis of samples would have shown the initial fragmentation and degradation status, with reanalysis in a longitudinal study showing of the impact of storage time on FFPE fetal membranes. Current commercial DNA extraction kits aim to limit the issues of crosslinkage by modified methodology (Senguven *et al*, 2014). However, full eradication of pre-processing fixative effects is difficult. Selecting appropriate measures to monitor the DNA quality and quantity is important, with the combination of multiple methods increasing accuracy.

The short fragment lengths of ~200 bp created by formalin crosslinkage may restrict target primer size in qPCR and sequencing methods (Oh *et al*, 2015; Spencer *et al*, 2013). Thus, modification of protocols may be required to enhance the beneficial use of FFPE samples, including decreasing the target size to 75 bp in Illumina sequencing (Ruane and Austin, 2017), or increasing polymerase and dNTP concentration, plus increased elongation time in PCR amplification to improve results (Dietrich *et al*, 2013).

4.4.2 Decontam identifies over half of bacterial sequences from FFPE membranes as contaminants, questioning the reliability of FFPE samples for microbiota research. However, samples and negative controls did display distinct alpha and beta diversity, plus 318 significantly different genuine bacteria after applying decontam. Decontam has been beneficially applied to placental research previously (Davis *et al*, 2018; Lauder *et al*, 2016), where <1% of ASVs were assigned to the genuine category, compared to 48% within this research. In the Davis *et al* (2018) and Lauder *et al* (2016) study, all samples were taken from term

patients, and as discussed earlier term patients present with reduced bacterial presence.

Escherichia/Shigella displayed the greatest abundance in all samples, conditions and controls, plus was assigned as a genuine bacteria by decontam. However, the high abundance in samples and controls questions the origin of these bacteria. High detection in all patient samples could be due to high genuine levels in fetal membranes, as suggested by Aagaard *et al* (2014). Alternatively, the high abundance in controls could suggest contamination of samples during DNA extraction or sequencing methodology (Laurence, Hatzis and Brash, 2014). Decontam prevalence filtering relies on the assumption that contaminating sequences are greater in negative controls. The opposite was true for *Escherichia/Shigella* here, which was greater in samples, although not significant. One ASV was the main contributor to the high abundance of *Escherichia/Shigella*, which suggests the potential impact of this one ASV, highlighting the importance of ASV or species level analysis.

This research highlights the beneficial use of decontam, but further post-processing may be required. Although beneficial, decontam strictly assigns each ASV to a ‘genuine’ or ‘contaminant’ category, without the option of being both, which may be possible for bacteria of human origin and when studying clinical tissues. A change in just one read count value can impact which classification bracket bacterial sequences are assigned too (Davis *et al*, 2018). Heterogeneous samples make assigning ASVs in decontam difficult (Davis *et al*, 2018), with different primary bacteria detected from HCA, PTB and term here potentially limiting application. Decontam is also unable to reliably distinguish the origin of the bacteria; whether arising from the environment or processing conditions (Davis *et al*, 2018). Only samples and kit negative controls were processed in decontam as the negative control group is limited to one category. Bacteria identified as genuine in samples may have therefore originated from the microbiota of the infiltrating wax, as bacterial contribution from wax controls were not assessed or assigned in decontam. None of the ASVs assigned as contaminants were significantly different between samples and controls, thus the contaminating ASVs may still reside from the FFPE sample microbiota.

Although decontam allows detection of contaminants, the extended time, knowledge, skills, and resources required to process samples limits clinical

application. The SourceTracker QIIME package has been suggested for improved accuracy of classification, with >99.8% of ASVs correctly classified (Karstens *et al*, 2019). This method requires prior knowledge of the microbial composition in samples and controls, also limiting practicality for clinical samples (Karstens *et al*, 2019). Reporting pre and post-processing steps and specific bioinformatic codes used within research would be informative to optimise filtering of contaminants in low biomass microbiota samples and improve methodological comparison.

4.4.3 Biological and methodological variation across FFPE and frozen tissues.

Findings highlight distinctive clustering of FFPE and frozen tissues, with negative controls also clustering by manufacturer. This was supported by Biesbroek *et al* (2012), presenting distinct clustering from MoBio and Qiagen extraction kits, rather than tissue type of saliva, oropharynx and nasopharynx. However, the kits used in the Biesbroek *et al* (2012) study were DNeasy from Qiagen and Powersoil from MoBio, thus target different samples yet apply comparable reagents. Whole genome sequencing research presented contrasting findings, with matched paired patient replicates clustered, rather than clustering by FFPE or frozen preparations (Mittempergher *et al*, 2011).

The prominent bacteria from each manufacturer studied here varied, with *Escherichia/Shigella* being the primary genera from MoBio FFPE kit extracts and *Bacteroides* the most prominent from Qiagen frozen kit extractions. *Bacillus* was detected in greater abundance from FFPE samples, corresponding with a significantly greater detection in the respective MoBio kit negative control. The *Bacillus* genus and specific ASV were not detected in Qiagen frozen kit negative controls. Increased DNA quantity was detected in negative controls from MoBio kit reagents here, with previous research also detecting greater DNA in MoBio (19-25 ng/µl) compared to Qiagen negative controls (<1 ng/µl; Glassing *et al*, 2016). These finding suggest that bacteria originated from kit reagents, specifically MoBio FFPE kits.

Awareness of the bias from different manufacturers is needed when analysing microbiota data, as the significant differences in the microbiota from different manufacturers could impact tissue analysis and lead to incorrect assumptions about the genuine microbiota of tissue samples. Most research comparing FFPE and frozen samples universally apply the FFPE or tissue specific Qiagen kits to respective samples, resulting in concordance across DNA quality and quantity

(Simbolo *et al*, 2013; Spencer *et al*, 2013; Wang *et al*, 2013). Using the same kit manufacturer across FFPE and frozen tissue extraction may limit differences due to comparable reagents (Salter *et al*, 2014), and may have been beneficial within this research. However, respective kits were selected here as they were each respectively applied to identical FFPE and frozen samples in previous research (Waring *et al*, 2015), allowing comparison and expansion of this research project.

4.4.4 Further considerations

The use of different fetal membrane sections were analysed for FFPE and frozen patients. For FFPE samples combined fetal membrane rolls were available, whereas individual amnion and chorion membranes were used in the frozen sample cohort. Computationally combining the amnion and chorion membranes from frozen samples following initial analysis aimed to better reflect the FFPE fetal membrane rolls. However, the amnion and chorion were initially separated, washed in PBS and the chorion scraped upon preparation, resulting in the potential loss of tissue components, which would otherwise be intact within combined membrane rolls. This could contribute to microbiota differences across FFPE and fetal membranes. To be confident with results generated here, tissues and negative controls could be spiked with known concentrations of selected microorganisms before processing through both FFPE and frozen preparation methods.

Analysis included a small patient subset (n=12), as the research criteria ensured that only patients with both FFPE and frozen membrane samples were included. This inclusion criteria aimed to improve sample comparison by reducing the impact of individual variation. Matched paired analysis strengthens findings as identical patient samples should present comparable microbiotas, if pre and post-processing of samples has minimal impact on the tissue microbiota.

The use of FFPE samples in microbiota research faces the same criticisms as frozen tissues (Heydt *et al*, 2014; Senguven *et al*, 2014), but additional steps in FFPE processing increases the possibility of contamination. Instead of immediate freezing for sample preservation, FFPE tissues undergo multiple processing procedures in various locations by different technicians and clinical staff. The differences in preparation time, storage condition (Arreaza *et al*, 2016), storage duration (Carrick *et al*, 2015; Imrit *et al*, 2006) and length of fixation (Nagahashi *et al*, 2017), all impact DNA quality and the microbiota of FFPE samples. Samples were utilised from a

previous study for this research, thus real-time assessment of processing was not possible.

During processing steps the tissue is submerged, embedded and penetrated by the paraffin wax which replaces all water content within tissue samples (Belloni *et al,* 2013; Pikor *et al*, 2011). The comparison of samples to wax controls from corresponding tissues, as performed here is beneficial. However, it is difficult to elucidate the origin of bacteria due to the close interaction between tissues and infiltrating wax. Inclusion of a blank paraffin wax block prepared at the time of the samples and processed following the identical procedure would be beneficial to determine the genuine paraffin wax microbiota. Laser capture dissection to retrieve samples from surrounding wax before processing may increase the accuracy of separation and decrease wax contamination (Liu *et al*, 2013). It would be beneficial to include both amendments to methodology in future research and clinical protocols.

Modifying existing methodology may improve comparison between FFPE and frozen tissue samples. Previous research found that FFPE placental samples failed to amplify using standard qPCR methodology (Dietrich *et al*, 2013), as DNA polymerase may fail to recognise cross linkage leading to errors in qPCR and sequencing (Oh *et al*, 2015). Reduction in the target sequence primer to 50 or 75 bp improved comparison between FFPE and frozen samples (Mittempergher *et al,* 2011; Ruane and Austin, 2017).

An alternative fixative reagent which bridges the gap between FFPE and frozen processing methods may improve clinical comparison and application of microbiota research. PAXgene tissue fixative reagents have been suggested as this intermediate method (Belloni *et al*, 2013). This uses a reduced four-hour fixative time compared to 24 hours in formalin (Belloni *et al*, 2013). The aim of PAXgene is to preserve sample morphology yet decrease fragmentation, leading to increased template size for qPCR and sequencing (Belloni *et al*, 2013). Longitudinal studies are required to understand long term preservation following this method.

The application of FFPE tissues to microbiota research has been beneficial in some tissues, including the ability to distinguish between diseased and healthy FFPE gut samples, with the use of comparable sequencing methodology (Stewart *et al*, 2019). Conversely, reliability of results in low biomass samples is questioned due to externally contributing bacteria concealing genuine signals (Glassing *et al*, 2016).

A universal protocol for FFPE sample preparation is not currently available. Introducing an SOP and universal tissue banking process for clinicians and scientists could widen the use of FFPE samples in clinical diagnostics. This would ensure consistent handling and preparation to remove bias from different methodologies and improve comparison between studies (Rubin *et al*, 2014). The SOP could include suggested optimum procedures including immediate fixation, use of deparaffinisation in extraction protocols and restricting storage time to one year before analysis (von Ahlfen *et al*, 2007).

4.5 Conclusion

The use of FFPE samples in microbiota research would reduce the time, cost, resource requirements, processing steps and storage limitations currently present in fresh/frozen tissue analysis. Findings here show that FFPE and frozen fetal membranes are not of comparable quality, with differences across bacterial profiles from matched paired analysis. This combined with the high level of contamination detected in fetal membrane FFPE tissues, questions the genuine representation of the fetal membrane microbiota once processed through fixative and embedding procedures. Although decontam allows detection of contaminating sequences, the extended time, knowledge, skills and resources required to process samples limits clinical application. Utilisation of FFPE fetal membranes in microbiota research is no more beneficial than the current gold standard of frozen tissues. Thus, FFPE samples should not replace frozen tissues in fetal membrane microbiota research.

Chapter Five: Bacterial load in fetal membranes with and without histological chorioamnionitis.

Abstract

Aim

The aim of this chapter was to investigate the bacterial load of low risk term fetal membranes using quantitative PCR (qPCR), to determine if bacteria can be detected from healthy fetal membranes. Plus to understand bacterial load levels related to the maternal inflammatory condition of histological chorioamnionitis (HCA). In addition, the relationship between bacterial load on the fetal membranes and inflammatory response was investigated.

Methods

Bacterial loads were initially assessed on fetal membrane rolls from low risk term labour (n=58). A further patient cohort of HCA (n=12), preterm (n=6) and term without HCA (n=6) amnion and chorion samples were analysed independently. Bacterial load was measured by BactQuant absolute qPCR targeting the 16S rRNA V3-V4 gene region. Copy number was calculated /µl and /mg of tissue. Comparison across HCA status were analysed via nonparametric Kruskal-Wallis or nonparametric Wilcoxon Rank-Sum. Correlation analysis was performed via nonparametric Spearmans Rank Bonferroni adjustment.

Results

Bacterial signals were detected in 21% of low risk term fetal membranes, increasing to 68% of fetal membranes from samples of HCA amnion (100%) and chorion (82%), compared to PTB amnion (80%) and chorion (33%). Significantly greater bacterial loads were detected from HCA (5013.066 copies/µl) compared to preterm (228.873 copies/µl) and term membranes (254.819 copies/µl), with no difference detected between non-HCA samples; or between non-HCA samples and negative controls (193.601 copies/µl). Bacterial load displayed a significant positive linear relationship to inflammatory response and correlated to five inflammatory factors across the amnion and chorion, these were TLR1, TLR2, IRAK2, LY96 and IL-8.

Conclusion

No support for a distinct bacterial load in low risk and non-HCA fetal membranes is present. Findings support the involvement of bacteria in HCA, with greater bacterial loads correlating to increasing maternal inflammation. Findings suggest activation

of the inflammatory pathway via a dose dependent response following bacterial activation.

5.1 Introduction

Bacterial colonisation of the fetus and fetal membranes *in utero* is questioned in healthy pregnancies (Kuperman *et al*, 2020; Perez-Munoz *et al,* 2017; Theis *et al*, 2019). Current theories suggest that bacteria ascending from the vagina contribute to the healthy fetal membrane microbiota *in utero* (Aagaard *et al*, 2014). Whereas sceptics of this mechanism suggest that organisms are acquired during labour or delivery from the vaginal canal or skin microbiota (Jones *et al*, 2009; Perez-Munoz *et al*, 2017). Further theories suggest that no bacterial colonisation occurs *in utero* but following exposure to environmental sources (Lauder *et al*, 2016; Theis *et al*, 2019). Evidence for bacterial detection in pregnancy related conditions including histological chorioamnionitis (HCA) observed that 94% of HCA cases present with bacterial colonisation, as detected by 16S rRNA gene qPCR (Musilova *et al*, 2015). Bacterial loads up to 5.2 $\log_{10}$ copies/µl have been detected in fetal membranes with HCA (Doyle *et al*, 2017). In contrast, Romero *et al* (2014b) detected bacteria in 11% of amniotic fluid samples from preterm birth (PTB) with culture confirmed intra-amniotic inflammation, compared to 26% with a sterile inflammatory response. It is important to confirm if bacterial load can be detected on healthy fetal membranes prior to investigation of a maternal condition. The majority of research uses sequencing methods; thus the exact bacterial load copy number cannot be accurately determined. The use of qPCR is the optimum methodology for quantifying bacterial load.

Furthermore, understanding if bacterial load is related to the inflammatory response in fetal membranes is important to increase current knowledge of HCA development and progression. Inflammatory biomarkers are routinely investigated for risk of PTB (Menon, Taylor and Fortunato, 2010) and CCA (Dudzik *et al*, 2015), including C-reactive protein (CRP), interleukin-6 (IL-6) and IL-8 (Jung *et al*, 2010, Tita and Andrews, 2010). These biomarkers have been researched in relation to HCA, but not yet integrated into a clinical setting due to reduced specificity to HCA. Previous findings suggest changes in inflammatory receptors and proinflammatory cytokines linked to HCA, including a two-fold increase in Toll-like receptors (TLR1 and TLR2; Waring *et al*, 2015) and IL-8 (Kasper *et al*, 2010). Both suggesting the involvement of bacteria as inflammatory agents, but how these are initiated and linked to the amount of bacteria present is unknown.

The gene expression of TLR signalling pathway components in HCA patients were previously investigated on identical samples used for this thesis and reported in a previous paper (Waring *et al*, 2015). Findings suggested the involvement of TLRs in HCA, with an increased gene expression of TLR1, TLR2 and LY96 in chorion, or increased IL-8, IRAK2 and TLR4 in amnion with HCA. Plus a positive correlation between increased TLR1 and TLR2 gene expression to increased HCA staging in both the amnion and chorion (Waring *et al*, 2015). These findings improved the understanding of the inflammatory pathway response in HCA, but further research confirming the link between bacterial presence and load to initiate the inflammatory response in HCA was required, as performed in this chapter.

The aim of this chapter was to initially investigate if bacteria can be detected in low risk term fetal membranes via TaqMan probe based 16S rRNA gene targeted absolute qPCR. Following this, a further aim was to investigate the bacterial load of the amnion and chorion with and without HCA, via comparable methodology to understand bacterial load levels in an inflammatory condition. Finally, we aimed to investigate the relationship between bacterial load on the fetal membranes and HCA severity, inflammatory response and inflammatory biomarkers.

5.2 qPCR method recap

Absolute qPCR was selected to quantify bacterial load from membrane rolls of low risk term patients, plus amnion and chorion samples from HCA and non-HCA patients. In addition, to understand if bacterial load is related to the inflammatory response in fetal membranes.

5.2.1 Sample processing

qPCR was performed on pre-extracted DNA from two patient subsets. Initially, a low risk term cohort was analysed. Samples were collected as part of a British Maternal and Fetal Medicine Society Research Project Bursary by Dr Inge Christiaens. Samples were collected following written informed consent. Term fetal membrane rolls (n=58) were collected from term spontaneous vaginal delivery (n=21), or term elective caesarean section (ELCS; n=37). Inclusion criteria required gestation between 37-42 weeks and singleton births from low risk patients, defined as the

absence of a known maternal or fetal complication. Exclusion criteria was clinical signs of infection or chorioamnionitis, antibiotic use in labour, preterm premature rupture of membranes (PPROM) >24 hours, fetal growth restriction, pre-eclampsia, placental abruption or manual removal of the placenta after delivery.

Amniochorionic membranes were prepared as per standardised criteria and HCA assessed as described previously (Chapter two). Only patients diagnosed as negative for HCA were processed. A fetal membrane roll was prepared from each patient, ensuring that the amnion and chorion were intact. Fetal membrane rolls were stored at -80 °C before use in this study. Total genomic DNA was extracted from 25 mg frozen membranes via QIAamp Fast DNA Tissue Kit (Qiagen) as described previously (Chapter two). DNA extraction kit negatives (four) were also processed alongside samples using identical methodology.

In addition, the previous patient cohort utilised in chapter three sequencing methods were also analysed to understand bacterial load in fetal membranes when a maternal condition is present. Patients consisted of preterm with HCA (n=12), PTB without HCA (n=6) and term birth without HCA (n=6). Following initial extraction, 25 µl aliquots of DNA were stored for one year at -80 °C prior to qPCR experiments.

5.2.2 BactQuant qPCR method recap

The BactQuant primer and TaqMan probe methodology was modified as described previously (Liu *et al*, 2012; Chapter two), and amplified to target the 16S rRNA gene using a CFX real-time thermal cycler (Bio-Rad). All samples were quantified against an *E. coli* reference standard curve. Findings were calculated to copy number/µl and /mg for clinical relevance, before comparing across HCA status and to controls, plus correlating to HCA severity and inflammatory biomarkers. CQ values of samples were compared to SQ of standard curves to determine copy numbers of 16S rRNA gene within each sample.

The initial output from qPCR is provided as SQ per reaction. As 1 µl of template DNA was added to reactions no conversion was required to determine copy number/µl. For clinical relevance, copy number/mg of tissue was calculated, with

knowledge that 25 mg of tissue was used for the initial extraction of 50 µl eluted DNA, and 1 µl of template DNA was required per qPCR reaction. Thus, the SQ was multiplied by two to generate copy number/mg of tissue. Logarithm of copy numbers (log_{10}) were calculated and used for visual analysis.

The MIQE guidelines were followed throughout qPCR experiments (Bustin *et al*, 2009). Amplification efficiency was monitored based on the slope of the regression line, calculated by 'Efficiency= $10^{-(1/slope)}$ -1' (Svec *et al*, 2015). If theoretical doubling is met then an optimum efficiency score of 100% and R^2 value of 1.000 would be expected (Ruijter *et al*, 2012). However, efficiency of 90-110% or R^2 >0.980 are accepted (Larionov, Krause and Miller, 2005). Efficiency <90% represents low reaction efficiency, with scores >110% suggesting sample inhibition (Thermo Fisher Scientific Inc, 2014). If the R^2 value of standard curves decreased below the threshold (<0.980), the qPCR experiment was rejected and repeated to avoid misinterpretation of results.

Standards and samples were assayed in triplicate (technical replicates), with starting quantity (SQ) copy numbers calculated as the average of the three results. If standard deviation of the replicates was >4.000 then analysis was repeated, as this indicates inaccuracy and unreliable results. However, if the removal of an anomalous replicate decreased the standard deviation to an acceptable level (<4.000), then two replicates were used to calculate the average copy number.

The limit of detection (LOD) for this assay was <100 copies/µl due to sensitivity range of the BactQuant primer and probe (Liu *et al*, 2012), confirmed by standard curve limits. Samples falling below the threshold were stated as out of range (OOR) and not analysed to ensure accuracy of results.

No template controls (NTCs) were processed alongside standards and samples to monitor contamination. NTCs contain all reaction components apart from the sample to act as a background negative control and aid in detecting contamination (Bustin *et al*, 2009). The expected copy number from NTCs is zero, due to the absence of target DNA for the primer sequence to bind and amplify (Thermo Fisher Scientific Inc, 2014). Contamination was suspected if amplification was observed greater than the threshold and/or within ten cycles of the most dilute standard. If detected, the experiment was rejected and repeated with fresh reagents. To further reduce the

possibility of contamination, assays were prepared in a designated restricted access qPCR area. Designated pipettes, reagents and sterile consumables, including filter tips and sterile Eppendorf tubes were also used throughout preparation and experiments.

5.3 Results

5.3.1 PCR optimisation

PCR optimisation was performed to ensure assay conditions would achieve maximum amplification efficiency. Plasmid standards were used as the PCR template. Negative controls did not display amplification of the target sequence throughout optimisation (Figure 5.1).

5.3.1.1 Temperature gradient

A temperature gradient PCR was performed to optimise the primer annealing temperature (45-56 °C, Figure 5.1A; 55-65 °C, Figure 5.1B). The optimum amplification was detected at 55 °C (Lane 9; Figure 5.1B). Amplification did not occur above 63 °C.

5.3.1.2 $MgCl_2$ concentration

The optimum $MgCl_2$ concentration was selected as 4 mM per reaction due to high intensity clear banding and reduced product remaining within the wells (Lane 2; Figure 5.1C), compared to 3 or 5-7 mM.

5.3.1.3 Formamide concentration

Formamide increased amplification efficiency to a maximum concentration of 2%. The optimum percentage was selected as 1% due to improved banding, with no amplification detected at higher concentrations (5-10%; Figure.5.1D).

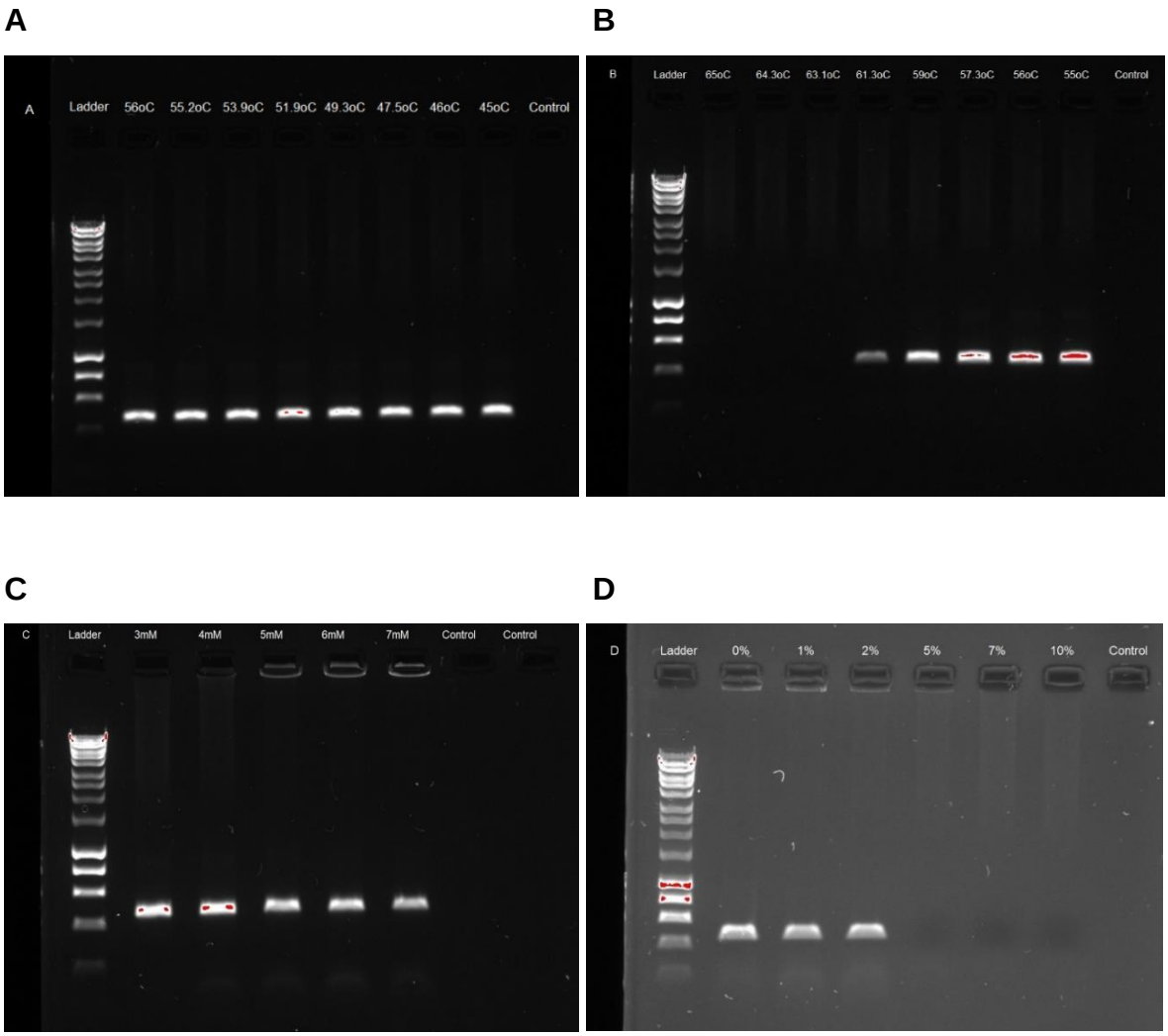

Figure 5.1 PCR optimisation. Agarose gel images of PCR optimisation including temperature gradients of 45-56 °C (A) and 55-65 °C (B), $MgCl_2$ optimisation from 3-7 mM (C), and formamide optimisation from 0-10% (D). Lane one in each image is represented by 1Kb HyperLadder, target band present at 466 bp.

5.3.1.4 Tissue sample inhibition results

Optimised PCR protocols were then applied to qPCR methodology and sample inhibition was investigated across a subset of samples prior to analysis (n=11). This included six HCA, three term and two negative controls. Samples were diluted 1 in 2,1 in 10 and 1 in 20. An inverse relationship between increasing quantification cycle (CQ) values and decreasing SQ values proportional to concentration indicated no inhibition. An example from one inhibition experiment is presented in Table 5.1.

Sample	Dilution	CQ	CQ mean	Cq std. dev	SQ	SQ mean	Within range?	Inhibition?
HCA21	Neat	24.819	24.472	0.351	1181.682	1383.289	Yes	No
		24.481			1258.379			
		24.117			1709.807			
	1 in 2	25.077	25.011	0.361	760.954	830.481	Yes	No
		25.334			612.543			
		24.621			1117.947			
	1 in 10	26.161	26.330	0.151	708.667	620.887	Yes	No
		26.379			593.910			
		26.451			560.085			
	1 in 20	27.842	28.103	0.385	196.663	168.558	Yes	No
		27.922			184.397			
		28.545			124.615			

Table 5.1 qPCR tissue sample inhibition analysis. An example of results to investigate potential inhibition in fetal membrane samples by analysing undiluted samples (neat), plus diluting 1 in 2, 1 in 10 and 1 in 20, amplified by BactQuant V3-V4 16S rRNA gene primers. Presented as quantification cycle (CQ) and starting quantity (SQ).

5.3.2 Standard curve results

Standard curves were used as a reference to determine 16S rRNA gene copy number within samples (10^2-10^8). Standards were assayed in triplicate, with CQ and SQ calculated as the mean of the three values. Example standard curve qPCR results are presented, including amplification plot (Figure 5.2), standard curve copy number results (Table 5.2) and standard curve example (Figure 5.3).

The accuracy of sample results from a qPCR assay is dependent on the accuracy of the standard curve (Thermo Fisher Scientific Inc, 2014). All standards included in analysis presented an acceptable R^2 value, with an average of 0.984 (0.975-0.996). The slope of the standard curves ranged across experiments from -3.287 to -3.931, with an average of -3.474. The optimum slope would be -3.333 to display perfect doubling, with a range from -3.100 to -3.600 accepted (Thermo Fisher Scientific Inc, 2014).

The average amplification efficiency across experiments was 94.02%, with this ranging from 79.63-101.48%. Although two experiments presented below the optimum efficiency, the average was still within the optimum range. Low efficiency is not a criterion to reject an assay but can indicate less than optimum conditions (Thermo Fisher Scientific Inc, 2014).

The LOD of each assay was assessed by monitoring standard curves. Standard 08 was the lowest concentration standard for the assay, with a known concentration of 10^1 and an average CQ of 30.97. However, the LOD was set at 10^2 for this method, as this was the sensitivity limit for the BactQuant primers and probe (Liu *et al*, 2012), with caution required for low biomass samples. The LOD was confirmed, as standard 08 presented with greater standard deviation and less consistency across experiments, compared to standard 07 (10^2; Figure 5.2). If samples fell below the LOD threshold, they were stated as OOR for this specific assay.

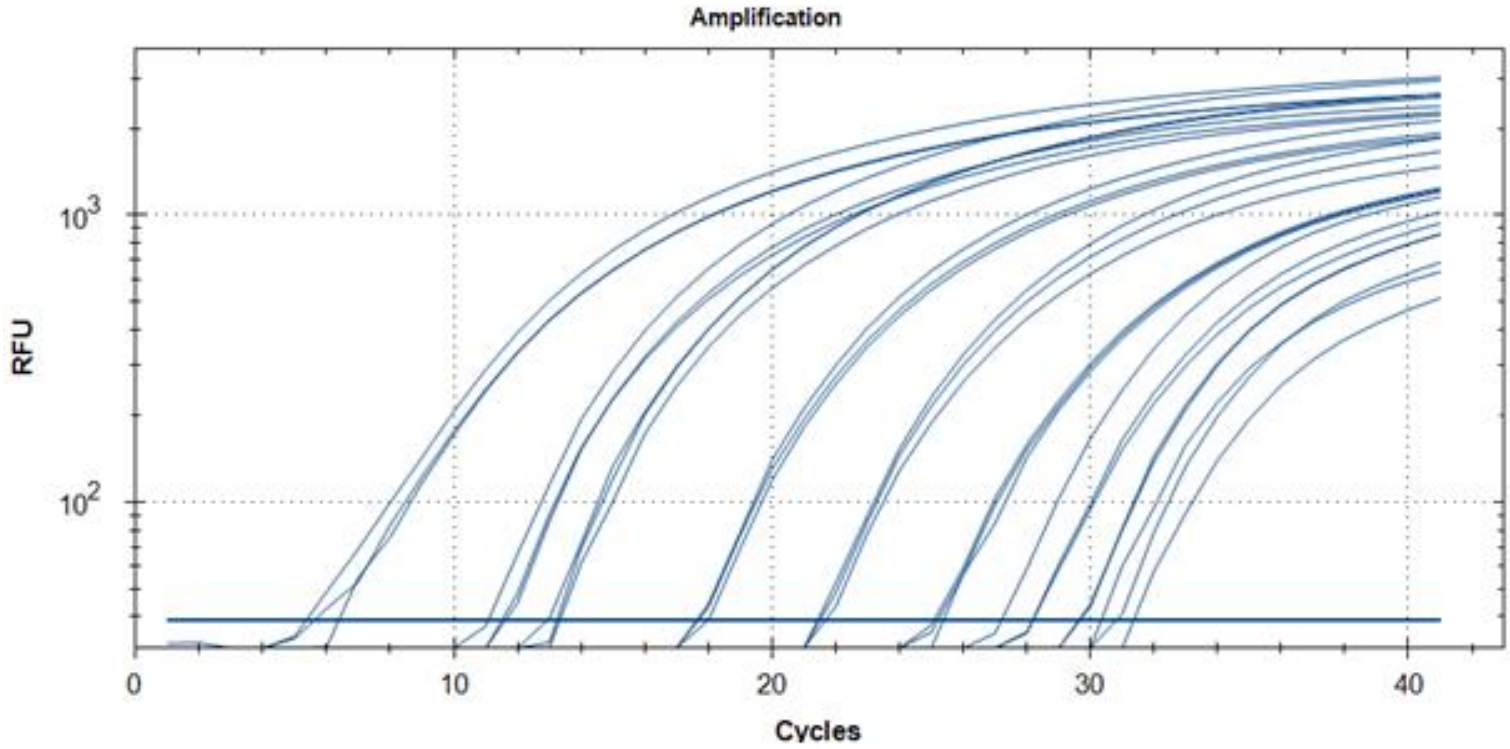

Figure 5.2 qPCR standards amplification plot. An example of the qPCR amplification plot of standard curves created on CFX Manager V3.1. Displayed as cycle number (cycles) compared to relative florescence units (RFU).

Content	CQ	CQ mean	Cq std. dev	SQ	SQ (log_{10})
Standard 01	5.420	5.741	0.354	3.0×10^8	8.477
	5.680				
	6.122				
Standard 02	11.742	11.473	0.362	3.0×10^7	7.477
	11.062				
	11.615				
Standard 03	13.174	13.146	0.158	3.0×10^6	6.477
	12.975				
	13.288				
Standard 04	17.767	17.857	0.126	3.0×10^5	5.477
	17.810				
	17.994				
Standard 05	21.523	21.586	0.136	3.0×10^4	4.477
	20.493				
	21.741				
Standard 06	25.172	25.188	0.124	3.0×10^3	3.477
	25.073				
	25.319				
Standard 07	28.151	27.924	0.397	3.0×10^2	2.477
	27.466				
	28.154				
Standard 08	30.293	30.737	0.385	3.0×10^1	1.477
	30.987				
	30.930				

Table 5.2 qPCR standard curve copy number results. An example of calculated copy numbers from an *Escherichia coli* plasmid standard curve (Standard 01-08) amplified by BactQuant V3-V4 16S rRNA gene primers, presented as quantification cycle (CQ), starting quantity (SQ) and SQ log_{10}.

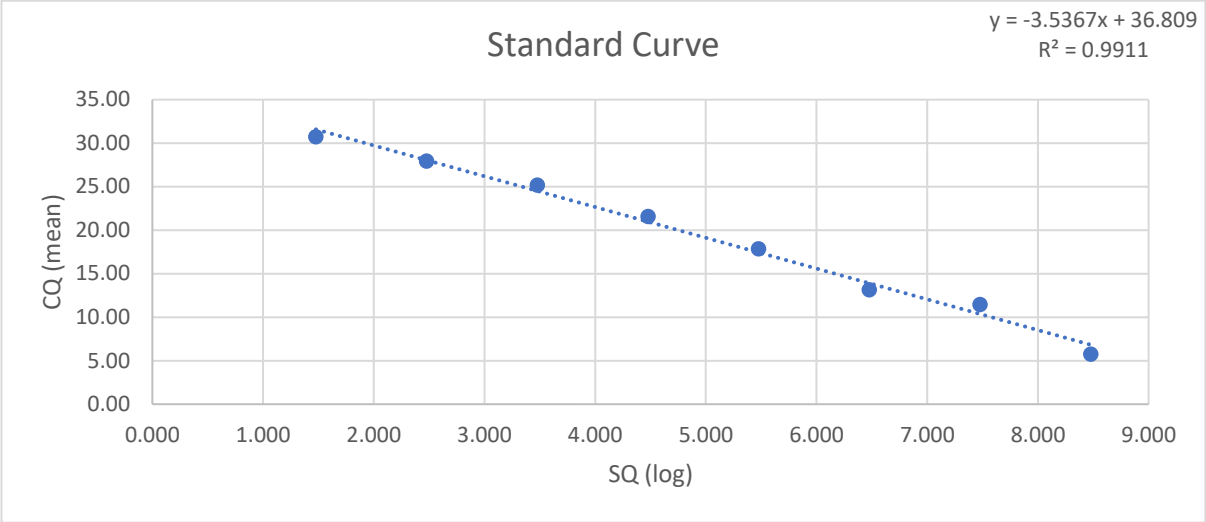

Figure 5.3 qPCR standard curve example. An example qPCR standard curve used for reference, comparing $\log_{10}$ starting quantity (SQ) with mean quantification cycle (CQ). R^2 and slope displayed. Results correlate to Table 5.2.

5.3.3 Low risk patient demographics

For the low risk patient cohort, fetal membrane rolls were collected from 58 patients (Table 5.3). Gestational age was the only patient variable with a significant difference, as this was higher in vaginal delivery (39.966) compared to ELCS (39.235; p=0.005).

	Patients (n=58)	**ELCS (n=37)**	**Vaginal (n=21)**	***p.value***
Gestational age (mean (SD))	39.5 (0.9)	39.2 (0.6)	40.0 (1.1)	***0.005****
Maternal age (mean (SD))	31.4 (5.3)	31.9 (5.1)	30.5 (5.3)	0.353
Maternal BMI (mean (SD))	25.5 (5.3)	24.7 (4.4)	27.3 (6.7)	0.276
Smoker Yes	0.0 (0.0)	0.0 (0.0)	0.0 (0.0)	1.000
No	58.0 (100.0)	37.0 (100.0)	21.0 (100.0)	
Birthweight (mean (SD))	3588.1 (407.2)	3586.8 (420.2)	3590.6 (392.6)	0.973

Table 5.3 Low risk term fetal membrane patient demographics. Patient characteristic from all patients providing fetal membrane rolls, with data assessed from low risk term fetal membranes, including elective caesarean section (ELCS) and vaginal delivery (vaginal). Comparison between groups was performed via parametric two-sample independent T-test or nonparametric Wilcoxon Rank-Sum. Categorical data was assessed using nonparametric Fisher's exact test. Significance threshold was p=≤0.05. Unless stated results are displayed as n (%).

5.3.4 Low risk patient sample qPCR results

Pre-extracted DNA from low risk term fetal membrane rolls (n=58), plus DNA extraction kit negative controls (n=4), NTCs and plasmid standards were assayed in triplicate following identical processing and procedures.

5.3.4.1 The majority of low risk fetal membranes were OOR for the assay.

The majority of low risk term fetal membranes (79%; 46/58) fell below the LOD for this assay (<100 copies/µl). With, 78% of ELCS (29/37) and 81% of vaginal deliveries (17/21) having no detectable bacterial load on the fetal membranes. Thus bacterial load above the predetermined threshold was detected from 21% (12/58) of low risk term patients.

To ensure reliability of results, samples with a copy number below the LOD for the assay were stated as OOR and removed from investigations (<100 copies/µl). This led to the analysis of 12 patients, with eight ELCS and four vaginal deliveries. The mean bacterial load from the new subset of low risk fetal membranes was 213.815 copies/µl, 2.282 $\log_{10}$ (427.631 copies/mg, 2.584 $\log_{10}$) ranging from 110.471-407.758 copies/µl.

5.3.4.2 Mode of delivery does not impact bacterial load of low risk term fetal membranes.

The ability to detect bacteria was not significantly different across mode of delivery, as 22% (8/37) of ELCS and 19% (4/21) of vaginal delivery samples displayed detectable bacterial loads (p=0.827). From the within range subset (n=12) ELCS samples had a greater average copy number of 216.156 copies/µl, 2.284 $\log_{10}$ (432.312 copies/mg, 2.585 $\log_{10}$), compared to vaginally delivered fetal membranes at 209.134 copies/µl, 2.280 $\log_{10}$ (418.267 copies/mg, 2.581 $\log_{10}$), yet not significantly different across mode of delivery (p=0.808; Figure 5.4). No difference in bacterial load was present across other patient demographics including; gestational age (p=0.905), birthweight (p=0.443), or maternal age (p=0.430) and maternal BMI (p=0.416).

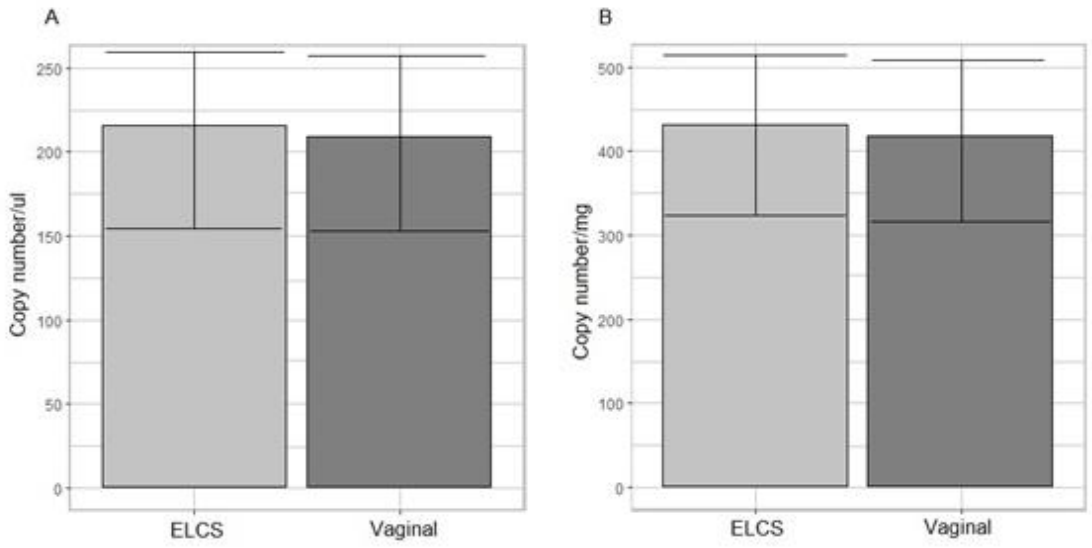

Figure 5.4 qPCR analysis of bacterial load in low risk term fetal membranes by mode of delivery. qPCR data from low risk term fetal membranes with elective caesarean section (ELCS) or vaginal delivery (vaginal) displayed as 16S rRNA gene copy number/µl (A) or 16S rRNA gene copy number/mg (B). Extracted DNA was amplified using BactQuant V3-V4 16S rRNA gene primers.

5.3.4.3 Low risk fetal membrane bacterial load is comparable to negative controls.

To investigate the bacterial signal from DNA extraction kit reagents, negative controls were compared to low risk fetal membranes.

Negative controls yielded detectable bacterial load in 75% (3/4), with detection below the threshold in 25% (1/4). The mean detectable bacterial load from negative controls was 133.387 copies/µl (2.122 $\log_{10}$; Figure 5.5), ranging from 111.928-150.626 copies/µl. The ability to detect bacteria above the threshold was significantly different between samples and negative controls (p=0.016), with greater ability to detect a bacterial load in negative controls (75%) compared to fetal membrane samples (21%). However, when a signal was detected there was no significant difference in copy number between fetal membranes (213.815 copies/µl) and negative controls (113.387 copies/µl, p=0.365; Figure 5.5).

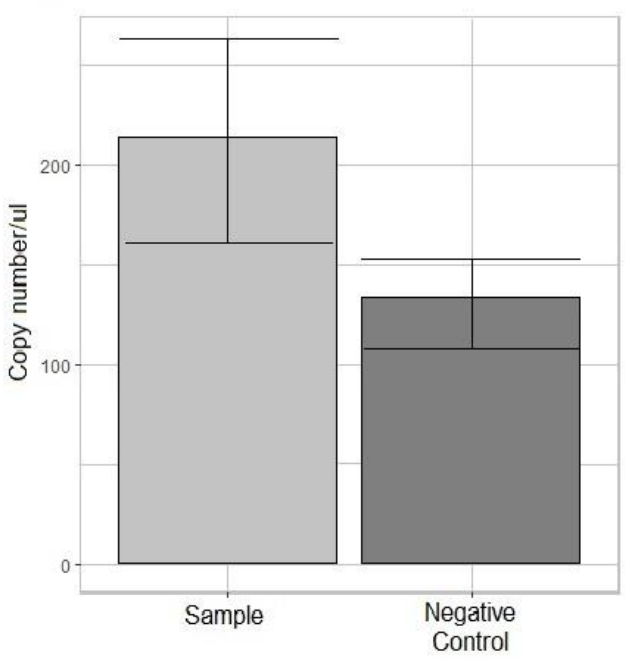

Figure 5.5 qPCR analysis of bacterial loads from low risk term fetal membranes and negative controls. qPCR data of low risk fetal membranes (samples) and negative controls within the range of the assay. Extracted DNA was amplified using BactQuant V3-V4 16S rRNA gene primers and displayed as 16S rRNA copy number/µl.

5.3.5 HCA cohort sample demographics

To investigate bacterial load in high risk or HCA fetal membranes, identical frozen samples to those used in chapter three for sequencing experiments were utilised for this qPCR protocol.

Briefly, patient demographics displaying significant differences between HCA, PTB and term were gestational age and birthweight (p=0.001). This specifically between HCA and term (p=<0.001), or PTB and term (p=<0.001), but gestational age (p=0.799), or birthweight (p=0.291) were not different between HCA and PTB. Significant differences were also detected for fetal sex (p=0.013) and Apgar score (p=0.033). Characteristics monitored only in HCA and PTB patients with significant differences were; maternal inflammatory stage (p=<0.001) and grade (p=0.036), plus CRP level (p=0.006). Detailed patient demographic information can be found in chapter three.

5.3.5.1 Tissue sample qPCR results

Extracted DNA from frozen amnion and chorion (n=37), plus DNA extraction kit negative controls (n=10), NTCs and plasmid standards were assayed in triplicate following identical procedures. qPCR experiments were accepted based on efficiency of the standards, NTC amplification and standard deviation of triplicates, as discussed previously. Sample analysis included 24 patients, with 12 HCA, six PTB and six term. Tissue replicates led to the analysis of 37 samples (20 HCA, 11 PTB and six term). All sample and control results from qPCR assays can be found in the appendix (Table A.4 and A.5).

5.3.5.2 The majority of fetal membrane samples had detectable bacterial loads.

Bacterial load above the predetermined threshold (100 copies/µl) was detected in 68% of fetal membrane samples (25/37). Amnion samples displayed the greatest percentage of detectable bacterial load, in 100% (9/9) of HCA and 80% (4/5) of preterm patients, yet not significant (p=0.233). Within the chorion, 82% (9/11) of HCA patients, but 33.3% (2/6) preterm and 50% (3/6) term chorion tissues generated detectable bacterial loads, this not significant between HCA, PTB and term patients (p=0.132).

Bacterial load levels out of the LOD for this assay (<100 copies/µl) were found in 32% (12/37) samples. PTB chorion had the most OOR samples (4/6), yet, only 1/5 PTB amnion were OOR. Term chorion had 3/6 samples OOR. Two HCA chorion

samples were OOR (2/11), but no OOR samples derived from HCA amnion (0/9). OOR copy numbers did not differ between HCA, PTB or term patients (p=0.632).

Removal of all OOR replicates for this assay led to the analysis of 18 HCA samples (nine amnion, nine chorion), six PTB samples (four amnion, two chorion) and three term samples (three chorion). From these patients an average of 3421.218 copies/µl were detected, with the lowest bacterial load from a preterm amnion sample (115.221 copies/µl) and the highest from an HCA chorion sample (33,851.73 copies/µl).

5.3.5.3 Bacterial load is increased with histological inflammation of the amnion and chorion.

Fetal membranes with HCA displayed a significantly greater mean bacterial load (5013.066 copies/µl, 10,026.132 copies/mg) compared to preterm (228.873 copies/µl, 457.746 copies/mg) and term patients (254.819 copies/µl, 509 copies/mg; p=<0.001). The significance remained when comparing HCA and PTB only (p=<0.001), or HCA and term only (p=0.011), yet not significant when comparing PTB and term (p=0.548). Bacterial loads from HCA ranged from 172.075-33,851.731 copies/µl, from PTB this was 115.222-405.954 copies/µl and 200.692-304.220 copies/µl from term fetal membranes.

No difference in mean bacterial loads were found between amnion and chorion results in HCA (4110.932 copies/µl vs 5915.199 copies/µl, p=0.436) or amnion and chorion from PTB (172.280 copies/µl vs 342.062 copies/µl, p=0.133).

When focussing independently on the amnion, significantly greater bacterial loads were detected in HCA amnion compared to PTB amnion (4110.932 copies/µl (3.614 $\log_{10}$) vs 172.280 copies/µl (2.236 $\log_{10}$); p=0.006; Figure 5.6A). When independently analysing chorion tissues, HCA bacterial loads were also greater than preterm and term, with a significance detected between HCA and PTB chorion (5915.199 copies/µl (3.772 $\log_{10}$) vs 342.062 copies/µl (2.534 $\log_{10}$); p=0.036), plus HCA and term chorion (254.819 copies/µl (2.406 $\log_{10}$); p=0.009). Bacterial loads did not differ between preterm and term chorion (p=0.400, Figure 5.6B).

When presented as copy number/mg of tissue for clinical relevance, bacterial load levels for HCA amnion were 8221.864 copies/mg (3.915 $\log_{10}$), compared to 344.556 copies/mg from PTB amnion (2.537 $\log_{10}$; Figure 5.6C). For HCA chorion

this was 11,830.401 copies/mg (4.073 $\log_{10}$), compared to PTB (684.123 copies/mg (2.835 $\log_{10}$)) and term chorion (509.638 copies/mg (2.707 $\log_{10}$); Figure 5.6D).

The greatest bacterial load on both the amnion and chorion was detected from one patient in the HCA subset (HCA patient 17), with a bacterial load of 28,706.990 copies/µl from the amnion, and 33,851.730 copies/µl from the chorion. For interest, when removed from analysis, the mean bacterial load in HCA reduced but remained significantly greater from amnion compared to preterm and term patients (1729.779 copies/µl (3.238 $\log_{10}$) p=0.008), and chorion when compared to preterm patients (3459.588 copies/ µl (3.539 $\log_{10}$) p=0.012).

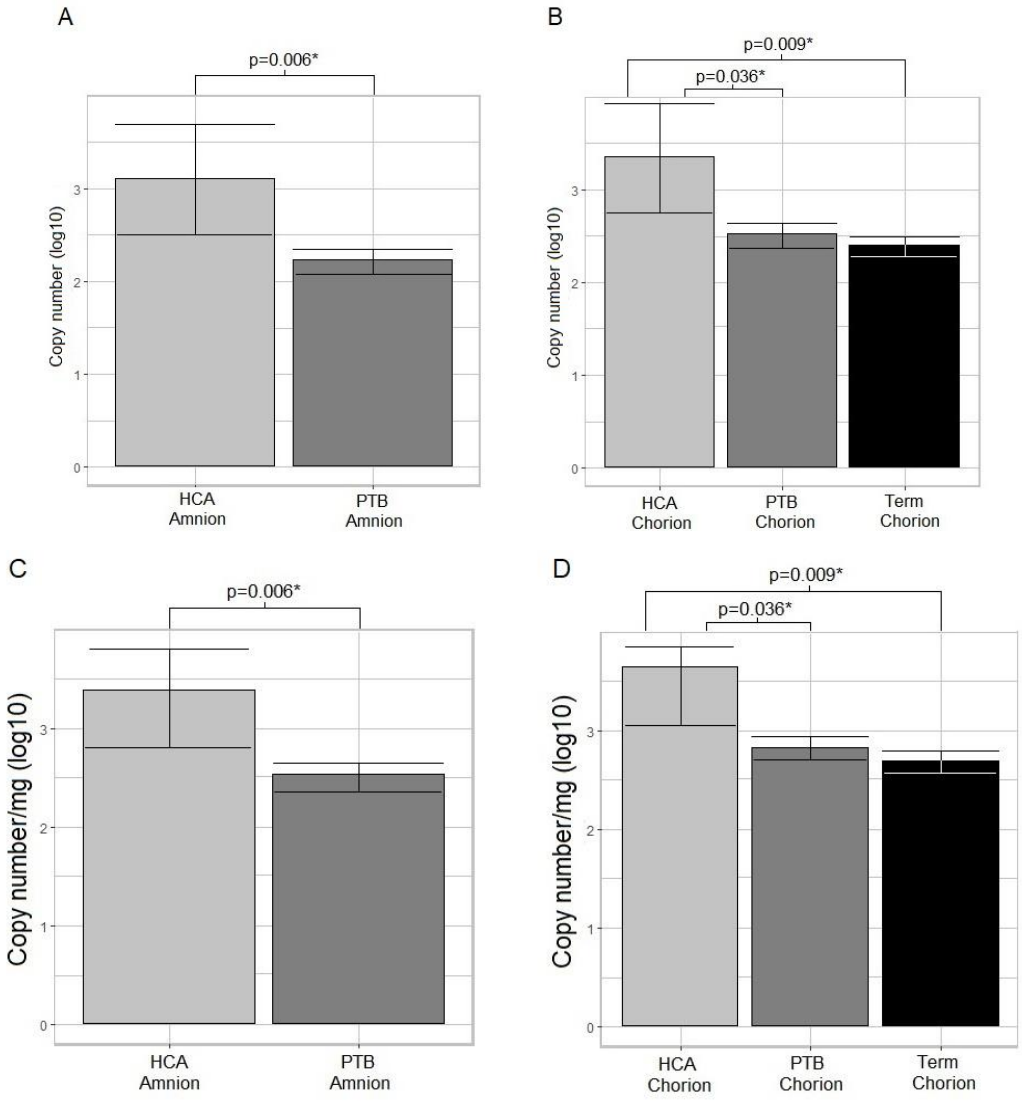

Figure 5.6 qPCR analysis of bacterial load by HCA status in the amnion and chorion. qPCR data displayed by log_{10} copy number/µl from amnion (A) and chorion samples (B) or log_{10} copy number/mg of tissue from amnion (C) and chorion samples (D). Patients were analysed in groups of histological chorioamnionitis (HCA), or preterm (PTB) and term birth without HCA (Term). Extracted DNA was amplified using BactQuant V3-V4 16S rRNA gene primers. Significance was analysed via nonparametric Kruskal-Wallis and nonparametric Pairwise Wilcoxon Rank-Sum to a threshold of p=≤0.05.

5.3.5.4 Non-HCA samples and negative controls have comparable bacterial loads.

Bacterial loads above the threshold were detected in 71% (5/7) of negative controls, with an average of 193.601 copies/µl (147.326-248.612 copies/µl). As previously, OOR values were not included in analysis.

Fetal membrane samples displayed significantly greater bacterial loads (3421.218 copies/µl) compared to negative controls (193.601 copies/µl, p=<0.001; Figure 5.7A). HCA samples were then removed from comparison and only preterm and term patients without HCA (non-HCA) were compared to negative controls to determine if the difference was due to inflammation. There was then no significant difference in bacterial load between non-HCA samples (237.521 copies/µl) and negative controls (193.601 copies/µl, p=0.387; Figure 5.7B).

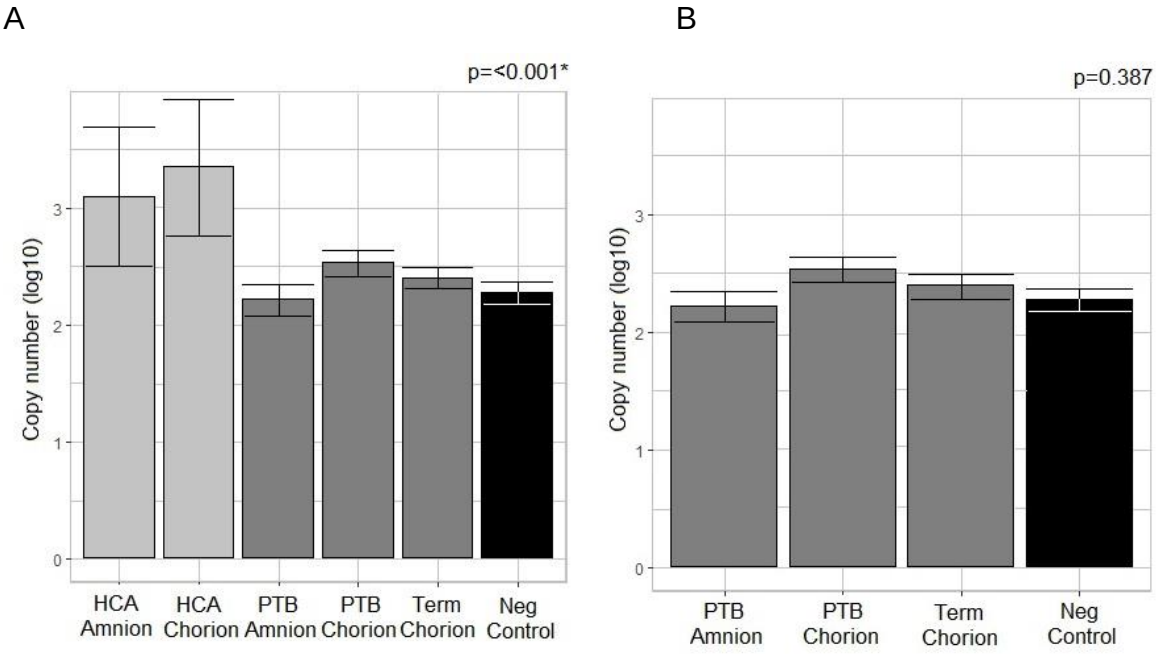

Figure 5.7 qPCR analysis of bacterial load from fetal membranes and negative controls. qPCR data displayed by log_{10} copy number/µl of samples compared to DNA extraction kit negative controls. Samples include histological chorioamnionitis amnion and chorion (HCA Amnion, HCA Chorion) or preterm amnion and chorion (PTB Amnion, PTB Chorion), plus term chorion without HCA (Term Chorion). Samples were compared to negative controls (Neg Control; A). Only non-HCA samples were compared to negative controls (B). Extracted DNA was amplified using BactQuant V3-V4 16S rRNA gene primers. Significance was determined via nonparametric Kruskal-Wallis to a threshold of p=≤0.05.

5.3.6 Increased bacterial load is positively correlated to increased inflammatory stage and grade.

Bacterial load levels were correlated to histologically confirmed inflammatory staging and grading to investigate the link between the amount of bacteria on the fetal membranes and the severity of maternal inflammation.

There was a strong positive significant correlation between bacterial load and inflammatory staging (R^2=0.782, p=0.002; Figure 5.8A) and grading in the amnion (R^2=0.673, p=0.012, Figure 5.8B). In the chorion, a strong positive significant correlation between bacterial load and inflammatory staging (R^2=0.841, p=<0.001; Figure 5.9A) and grading was also present (R^2=0.730, p=0.003; Figure 5.9B).

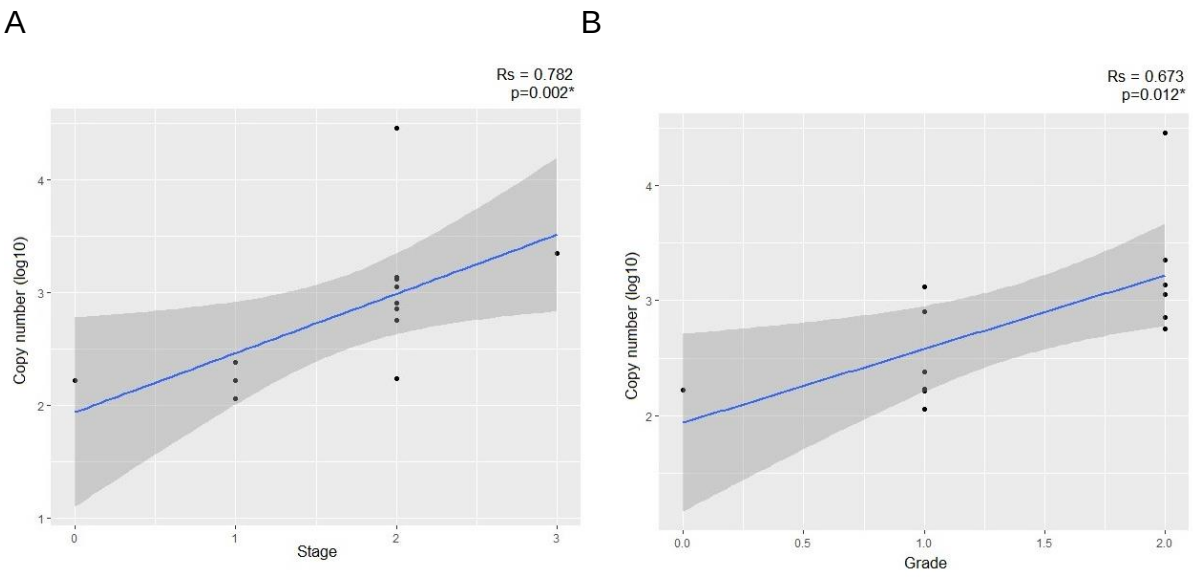

Figure 5.8 Amnion inflammatory stage and grade correlated to bacterial load. Analysis between bacterial load log_{10} copy number/µl and histologically confirmed inflammatory staging (A) and grading score (B) within the amnion via nonparametric Spearman's Rho correlation analysis to a threshold p=≤0.05.

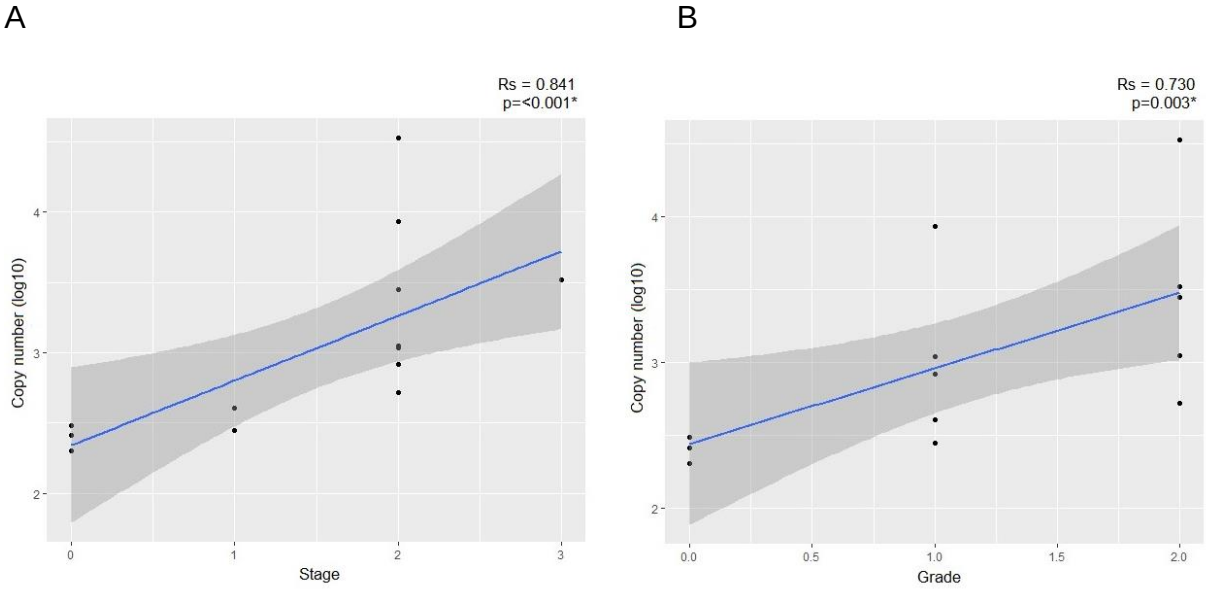

Figure 5.9 Chorion inflammatory stage and grade correlated to bacterial load. Analysis between bacterial load log_{10} copy number/µl and histologically confirmed inflammatory staging (A) and grading score (B) in the chorion via nonparametric Spearman's Rho correlation analysis to a threshold p=≤0.05.

5.3.6.1 Increased bacterial load is positively correlated with inflammatory gene expression.

To further investigate the relationship between bacterial load and the inflammatory response, bacterial load levels detected in this research were compared to inflammatory gene expression levels determined by relative qPCR in a previous paper utilising identical samples (Waring *et al*, 2015). Previous research indicated than an increase in TLR1, TLR2, LY96, IL-8 and IRAK2 genes were linked to inflammation in the fetal membranes (Waring *et al*, 2015).

Bacterial load from amnion and chorion were correlated to the expression of inflammatory mediator genes (Table 5.4). In the amnion, bacterial load was significantly positively correlated to TLR1 (R_s=0.599, p=0.034), TLR2 (R_s=0.626, p=0.025), and IL-8 (R_s=0.560, p=0.050). In the chorion, bacterial load was significantly positively correlated to TLR1 (R_s=0.604, p=0.025), TLR2 (R_s=0.776, p=0.002), LY96 (R_s=0.763, p=0.002), IL-8 (R_s=0.692, p=0.008) and IRAK2 (R_s=0.732, p=0.004). The majority of the remaining inflammatory factors were also positively correlated to bacterial load across amnion and chorion fetal membranes, yet insignificant (Table 5.4). TIRAP, SARM1 and HMGB1 were negatively correlated in the amnion, with TLR6, HMGB1 and SIGIRR negatively correlated in the chorion. All negative findings were weak non-significant correlations (Table 5.4).

Amnion			Chorion		
Inflammatory gene	**Spearman's correlation**	**p.value**	**Inflammatory gene**	**Spearman's correlation**	**p.value**
TLR1	0.599	***0.034***	TLR1	0.604	***0.025***
TLR2	0.626	***0.025***	TLR2	0.776	***0.002***
TLR4	0.489	0.093	TLR4	0.275	0.341
TLR6	0.011	0.978	TLR6	-0.112	0.704
SARM1	-0.214	0.482	SARM1	0.103	0.727
MyD88	0.308	0.366	MyD88	0.125	0.671
LY96	0.364	0.224	LY96	0.763	***0.002***
IL-8	0.560	***0.050***	IL-8	0.692	***0.008***
IRAK2	0.434	0.146	IRAK2	0.732	***0.004***
HMGB1	-0.049	0.878	HMGB1	-0.178	0.542
SIGIRR	0.083	0.843	SIGIRR	-0.173	0.614
TIRAP	-0.044	0.892	TIRAP	0.169	0.563

Table 5.4 Bacterial load correlated to inflammatory gene fold change in the amnion and chorion. Correlation was performed via nonparametric Spearman's Rank Bonferroni adjustment (p=≤0.05, bold and italics) between absolute qPCR bacterial loads from amnion and chorion fetal membranes and inflammatory gene fold change results from relative qPCR from a previous publication (Waring *et al*, 2015) between matched paired samples.

5.4 Discussion

The aim of chapter five was to initially determine if a bacterial signal can be detected in low risk term fetal membranes using 16S rRNA gene BactQuant primer and probe based qPCR. In addition, to then investigate the bacterial load in fetal membranes with the maternal inflammatory condition of HCA, to understand if the amount of bacteria on the fetal membranes impacts development of HCA. Also, the relationship between bacterial load and HCA inflammatory diagnosis criteria or inflammatory marker expression on fetal membranes were investigated.

Overall, this chapter highlights that the majority of low risk term fetal membranes do not have detectable bacterial loads, with only 21% of fetal membranes above the LOD. Yet, bacterial loads were present in the majority of fetal membranes from HCA (90%), PTB (55%) and term patients (50%). The bacterial load of low risk and non-HCA fetal membranes could not be distinguished from DNA extraction kit negative controls, with negative controls more likely to have a detectable signal (75%). HCA fetal membranes had significantly greater bacterial loads (5013.066 copies/µl) than non-HCA samples (237.521 copies/µl), with no impact of gestational age. Findings support that bacterial loads are distinct only when a maternal condition is present. Increased bacterial loads were positively correlated to increased maternal inflammation and five inflammatory factors. All of which confirm the relationship between bacterial infection and higher bacterial load related to inflammatory HCA.

5.4.1 Bacterial load cannot always be detected in low risk term fetal membranes, but are increasingly detected in negative pregnancy outcomes.

When analysed by qPCR the majority of low risk term fetal membranes (79%) did not have a detectable bacterial load above the LOD for the assay, yet were detected from 68% of fetal membranes from the second subset, including HCA (90%), preterm (55%) and term patients (50%). These findings suggest that the majority of low risk term fetal membranes do not have a genuine detectable bacterial load above the LOD for this assay, supporting the sterile placenta theory in low risk patients (de Goffau *et al*, 2019; Kuperman *et al*, 2020; Perez-Munoz *et al,* 2017; Theis *et al*, 2019). However, it is possible that there is a bacterial load below the LOD for this assay. Support for current findings have been observed in comparable qPCR assays, with bacterial loads from healthy term membrane rolls below the LOD of 10^2 copies/µl (Theis *et al*, 2019), with this confirmed by culture negative findings

from 28/29 samples (Theis *et al*, 2019). This is reflected by Doyle *et al* (2017), where 68% of fetal membranes from preterm patients had detectable bacterial loads from 16S rRNA qPCR (Doyle *et al*, 2017). Alternative research has observed bacteria at lower percentages, with only 14% of preterm fetal membranes with microbial invasion (Kim *et al*, 2009), and 11% of late PTB placental tissues presenting with detectable bacterial load (Sweeney *et al*, 2016), both by 16S rRNA PCR and sequencing.

Bacterial loads were more likely to be detected from HCA (90%), with lower detection from PTB (55%) and term (50%), yet still greater than low risk term patients (21%). Findings suggest the potential role of bacteria in HCA, with a greater bacterial signal from HCA. This is supported by Musilova *et al* (2015), finding bacteria in 97% of HCA amnion samples by 16S rRNA PCR, plus from Sweeney *et al* (2016), detecting bacteria in 54% of HCA, compared to 19% in non-HCA membranes, irrespective of gestational age from 16S rRNA PCR and sequencing. Findings from the low risk term group in this research match those detected from non-HCA membranes in the Sweeney *et al* (2016) study. However, the high risk term subset displayed a greater percentage of samples with detectable levels. Patient demographics and inclusion/exclusion criteria differed, with more rigorous criteria applied to the low risk patient group, possibly explaining the difference across low risk term and non-HCA term patients. Multiplex qPCR has previously failed to detect *Ureaplasma* or *Mycoplasma* in term or preterm fetal membranes, yet were detected in 22% of HCA membranes (Kim *et al*, 2009). This suggesting the multifactorial characteristic of this condition where load of species may be important.

Increased bacteria on fetal membranes in pregnancy related conditions is supported by Jones *et al* (2009), detecting bacteria in 70% of PPROM compared to 50% non-PPROM term patients. Alternatively, Kuperman *et al* (2020) failed to amplify or detect the 16S rRNA gene in 27 placentas from healthy or pre-eclampsia patients, also using the BactQuant primer and probe. However, this was amplified by PCR and analysed by agarose gel, rather than the more sensitive qPCR method used here. But these findings were confirmed by negative culture and negative Gram stain results (Kuperman *et al*, 2020).

5.4.2 HCA fetal membranes have significantly greater bacterial load than PTB and term without HCA. Bacterial loads of up to 5.2 log_{10} copies/µl have been detected in HCA fetal membranes previously (Doyle *et al*, 2017), greater than 3.7 log_{10} copies/µl detected here. Conversely, similar bacterial loads from chorioamnionitis, PTB and term have been detected from placental samples by qPCR amplification of the 16S rRNA gene (Leiby *et al*, 2018). However, this research included CCA, without the specificity to HCA as focused on in this project.

Increased bacterial load in reproductive and pregnancy related conditions is supported by research into PPROM, with increased 16S rRNA gene copy number from PPROM (7700 copies/ml) compared to non-ruptured membranes (664 copies/ml; Rehbinder *et al*, 2018). This utilised the BactQuant protocol with modified digital droplet PCR used to increase the sensitivity of the assay (Rehbinder *et al*, 2018). The patient demographics in this research project had 75% of patients with PPROM compared to 25% with spontaneous PTB, thus further investigation into the clinical reason for PTB linked to bacterial load would be of interest. Although bacterial load was significantly different between HCA and non-HCA patients, no difference in the percentage of samples with detectable bacterial loads were evident, suggesting that bacterial load is of greater importance in HCA than bacterial presence.

One HCA patient (patient 17) presented with exceptionally high levels of bacteria, but inclusion had minimal impact on research outcomes. The patient was diagnosed at inflammatory stage two, however was the only patient to also present with clinical signs of chorioamnionitis, including, high temperature indicating maternal fever and vaginal discharge. Not all CCA diagnostic criteria were met, as WBC and heartrate were not elevated, thus CCA was not diagnosed. No impact on results were seen following removal of this patient from analysis. Although the correlation between HCA and CCA is poor (Oh *et al*, 2017), and the findings are from one patient, this does suggest the importance of distinctive HCA and CCA investigation.

5.4.3 Bacterial load is positively correlated to severity of inflammatory response in a dose dependent manner, with greater bacterial loads detected in higher inflammatory staging and grading in the fetal membranes. Increased inflammatory response in relation to increased bacterial load have previously been reported, specifically with higher bacterial loads in amniotic fluid linked to

inflammatory stage two and three in HCA (Kasper *et al*, 2010). This supports the requirement of assigning HCA according to standard criteria, including individual categorisation of stage one as subchorionitis and stage two and above as HCA, as followed in this research project. Previous research supports increased bacterial detection in higher inflammatory staging, as 87% of fetal membranes had detectable bacteria at stage three, compared to 33%, 40% and 60% at stage zero, one and two (Kim *et al*, 2009). However, the range of bacterial load overlapped, with 0-300,000 16S rRNA gene copies/µl from stage three, 0-50,000, 0-200,000 and 0-400,000 copies/µl from stage zero, one and two respectively (Kim *et al*, 2009). No definitive baseline or negative control threshold were stated, thus inclusion of results <10 copies/µl may bias results. Increased bacterial load in higher staging has also been reported in amniotic fluid, with 10^6 16S rRNA gene copy numbers reported in stage three, compared to 10^3 in stage two (Urushiyama *et al*, 2017). However, 10^3 was also reported from stage one and zero (Urushiyama *et al*, 2017), suggesting a definitive threshold level for stage three, but not a linear relationship, as reported here. Although a linear relationship was observed in this research project only one HCA patient was diagnosed as stage three, with the majority of patients diagnosed at stage two inflammatory response. Recruitment of patients representing all staging conditions, plus inclusion of a term HCA subset could improve comparison and provide greater insight.

Inflammatory staging is the main factor monitored for maternal inflammatory research due to a more informative descriptive criteria and greater clinical significance compared to inflammatory grading (Jessop and Sebire, 2011). Staging and grading are routinely combined when assessing HCA (Roberts *et al*, 2012). Findings here support combined analysis due to similar bacterial signal across stage and grade. Yet independent analysis of inflammatory grading may be important when investigating the location of bacteria, as grading reflects infiltration intensity across membranes (Redline *et al*, 2003).

5.4.4 Bacterial load correlates with five inflammatory factors across the amnion and chorion. Increased 16S rRNA gene bacterial load was positively correlated to five inflammatory factors which varied across membranes. A positive correlation between TLR1, TLR2 and IL-8 to bacterial load was observed in both the amnion and chorion, with LY96 and IRAK2 positively correlated to bacterial load in

the chorion only. Findings provide multiple factors involved in the TLR pathway as potential targets for inflammatory detection. An increase of TLR1 and TLR2 in HCA has previously been observed in fetal membranes (Moco *et al*, 2013). Alternatively Rindsjo *et al* (2007) detected less TLR2 in HCA placental samples, compared to healthy patients, but this was related to gestational age, as TLR2 was increased in preterm compared to term patients.

A previous project utilising the same samples also detected increased TLR1, TLR2 and LY96 in the chorion, plus increased IL-8, IRAK2 and TLR4 in the amnion with HCA. TLR1, TLR2, LY96, IL-8 and IRAK2 gene expression was also correlated to increased inflammatory staging in HCA amnion and chorion (Waring *et al*, 2015), supporting the majority of findings here. TLR4 was significantly increased in the amnion with HCA previously, but not significantly correlated to bacterial load here. TLR4 expression and activation may be linked to HCA, but may not be influenced by the amount of bacteria.

The inflammatory mediators significantly correlated to bacterial load here are all components of the NF-κβ pathway. LY96/MD2 is the extracellular gene linking component for lipopolysaccharides (LPS) and TLRs (Kawai and Akira, 2010). IRAK2 and MyD88 are intracellular components of the NF-κβ pathway activated following TLR/IL binding (Kawai and Akira, 2010). IL-8 is a downstream product promoted by the NF-κβ pathway, and has been detected in greater concentrations from fetal membranes with chorioamnionitis via multiplex cytokine assays (Sweeney *et al*, 2016). IL-8 has also been linked to inflammatory grading of the fetal membranes (Kasper *et al*, 2010), and has been investigated for predictive HCA staging in amniotic fluid (Kacerovsky *et al*, 2009). However, IL-8 detection has also been related to membrane weakening and rupture during active labour (Noda-Nicolau *et al*, 2016), thus may not be specific to HCA.

TLR1 and TLR2 gene expression were positively correlated to bacterial loads in both amnion and chorion membranes. These receptors are ligand specific to lipopeptides from Gram-negative triacylated bacteria, for example *Ureaplasma* (Moco *et al*, 2013). This suggests that specific microbial components may activate the inflammatory response in HCA via the TLR1/2 hetero/homodimer to trigger the NF-κβ pathway (Kawai and Akira, 2010). Thus the abundance of Gram-negative bacteria on the fetal membranes may be important to the inflammatory response in HCA, with interest to specifically investigate this theory by species-specific qPCR.

It is possible that activation of the inflammatory response is due to cellular trauma tissue ischemia, hypoxic stress or danger signalling rather than bacterial load (Rock *et al*, 2010). Damage associated molecular patterns (DAMPs), including HMGB1 may activate the MyD88 pathway in the sterile inflammatory response theory (Kawai and Akira, 2010; Romero *et al*, 2014b). However, our work suggests that bacterial load is the key driver to inflammation in the fetal membranes studied here.

Further research investigating the threshold of overall bacterial load or specific bacteria required to generate an inflammatory response should be investigated. *In vitro* bacterial stimulation of primary fetal membrane cell culture with a variety of bacterial components in varying concentrations, over different time periods may aid to detect which bacterial ligand and at what threshold load are required to activate the inflammatory response. Plus, to monitor how the inflammatory response transcends downstream pathway activation and expression of inflammatory mediators in response to bacterial presence. This would also involve monitoring the inducible expression of inflammatory factors following stimulation, as inflammatory factors may be potential biomarkers for HCA. The sensitivity and specificity of one or a combination of inflammatory factors would be required prior to clinical application.

5.4.5 Amnion and chorion display comparable bacterial loads irrespective of HCA. Similar bacterial loads from different fetal environments has been supported by healthy term placental research, with 2.6 x10^2 16S rRNA gene copies/µl detected across maternal and fetal placental surfaces (Lauder *et al*, 2016; Theis *et al*, 2019). Contrastingly, greater bacterial signals have been detected on the chorion than amnion with PPROM (Fortner *et al*, 2014). The reverse has been reported by Kim *et al* (2009), observing more bacteria on the amnion than chorion with microbial invasion of the amniotic cavity (Kim *et al*, 2009). Increased bacteria on the amnion is suggested to reflect increased inflammatory response, as bacteria originating from vaginal or lower female reproductive tract environments would have to transverse the chorion prior to the amnion (Park *et al*, 2009). Further imaging analysis would allow visualisation of bacteria on each membrane to confirm bacterial presence and load. This could be investigated by IHC or Raman microspectroscopy, with the later allowing label free, non-destructive bacterial location analysis with

minimal processing from confounding factors of DNA extraction kits or PCR reagents (Chen *et al*, 2014).

5.4.6 There is no difference in bacterial load between non-HCA fetal membranes irrespective of gestational age or mode of delivery. This strengthens the specificity of linking bacterial load and inflammatory HCA. Similar detection levels across gestational age has also been reported by Sweeney *et al* (2016), as 10% of PTB and 14% of term placenta had detectable bacteria in 16S rRNA sequencing analysis. This was also seen with species-specific qPCR, as 59% and 50% of preterm and term fetal membranes were positive for *U. parvum* (Sweeney *et al*, 2016). Alternatively, Jones *et al* (2009) found differences across gestational age, with bacteria present in 90% PTB, but not within term tissues. However, for the study all PTB were spontaneous vaginal deliveries and all term were ELCS (Jones *et al*, 2009), thus variation in mode of delivery may bias results. Findings here suggest that mode of delivery does not impact bacterial load or bacterial presence in low risk term fetal membranes, with similar signals from ELCS and vaginal deliveries. This suggests minimal bacterial contribution to the fetal membranes during labour or delivery; thus mode of delivery may not be the origin of bacteria on the fetal membranes. However, bacteria were only detected in 21% of low risk term samples using these methods, leading to a small cohort of 12 patients. For the low risk cohort sequencing was not conducted, and bacterial profiles were not analysed. Bacterial profiles could vary between mode of delivery, as previously found by Dominguez-Bello *et al* (2010), with vaginally originating bacteria, including *Lactobacillus* and *Prevotella* colonising the neonate from vaginal deliveries, and skin originating bacteria including *Staphylococcus* on caesarean section neonates. Conversely, a longitudinal study observed no impact on infant microbiota following vaginal or caesarean section delivery, from labour to ten weeks (Stewart *et al*, 2017). Variation in bacterial origin would be expected if mode of delivery contributed to bacterial communities, yet findings here question the confidence in detecting bacteria on low risk term fetal membranes.

5.4.7 The bacterial load of non-HCA fetal membranes cannot be distinguished from negative controls, suggesting no distinct bacterial load levels in PTB and term fetal membranes in absence of a negative maternal condition. This supports

the sterile placenta theory discussed by the majority of research (de Goffau *et al*, 2019; Kuperman *et al*, 2020; Perez-Munoz *et al,* 2017; Theis *et al*, 2019), due to concordance with negative control bacterial loads, plus greater ability to detect bacterial loads in negative controls than non-HCA fetal membranes. However, HCA did display a significantly higher bacterial load compared to negative controls. This supports the theory that the fetal membranes are sterile unless a maternal condition is present, and further indicates the infection related inflammatory response of HCA.

Comparable bacterial loads between healthy placenta and negative controls of PCR grade water has been supported in contamination research studies (Leiby *et al*, 2018; Theis *et al*, 2019), with 10^2 16S rRNA copies/µl detected from healthy placental membranes, plus comparable levels from negative controls of sterile water, extraction blanks and air swabs (Lauder *et al*, 2016). The low levels from samples and controls are similar to signals detected within this research project. Alternatively, negative controls of air swabbed theatre room have shown to have greater bacterial loads than healthy placenta (Theis *et al*, 2019). Bacterial load levels have also shown to be location specific, with a 20-fold increase from placental compared to fetal membrane samples (Parnell *et al*, 2017). In the Theis *et al* (2019) study all bacterial signals were $<10^2$, thus under the LOD and may not be accurate and reliable. Whereas in the Parnell *et al* (2017) study, placenta and fetal membranes had 400 copies/µl compared to 34 copies/µl from negative controls and sterile water (Parnell *et al*, 2017). The LOD was set at $<10^2$ in this research project, thus confidence in bacterial signals is only possible above this limit. Nevertheless, a signal below this LOD may be present but not accurately assessed in this assay.

Inability to distinguish between the non-HCA patients and negative control signals here, indicates the low bacteria present on non-HCA fetal membranes. The low amounts of bacteria in non-HCA samples are likely due to external contribution rather than *in utero* origin; either from sample handling, processing, extraction and sequencing methodology or environmental contamination during labour or delivery (de Goffau *et al*, 2019; Kuperman *et al*, 2020; Perez-Munoz *et al,* 2017; Theis *et al*, 2019). Negative controls in this research consisted of dH_2O and DNA extraction kit negative controls. Further negative controls could have been included to understand the impact of environmental contamination, including air swab or open tubes, beneficial to understand bacterial contribution from theatre suites, hospital wards and qPCR processing locations (Lauder *et al,* 2016; Theis *et al*, 2019). Introducing a positive control of spiked samples or further body site analysis from high bacterial

load locations would increase comparison and ensure accountability of results (Kuperman *et al*, 2020). This including positive control vaginal samples, which display 10^6 16S rRNA gene copies/µl compared to 10^2 from placenta and fetal membranes (Lauder *et al*, 2016).

5.5 Conclusion

Overall findings suggest the involvement of bacterial infection to inflammatory HCA and highlights that greater bacterial load levels are linked to HCA inflammatory severity and specific inflammatory factors in the fetal membranes. No support for a distinct bacterial signal in non-HCA and low risk term fetal membranes was found. In combination, findings support the sterile inflammation theory, with low bacterial involvement unless an inflammatory related condition is confirmed.

Chapter Six: Raman spectroscopy for the detection and distinction of bacteria in mono and polymicrobial culture conditions.

Abstract

Aim

The aim of chapter six was to determine if Raman spectroscopy could identify bacteria based on a spectral fingerprint or distinct spectral peaks. In addition, this chapter aims to investigate the ability to discriminate individual bacteria in polymicrobial cultures. It is hoped that understanding this technology allows for potential application to clinical tissues.

Methods

The spectral fingerprint of bacterial droplets from cultured *Escherichia coli*, *Klebsiella pneumoniae* and *Staphylococcus aureus* were measured using Raman spectroscopy (inVia, Renishaw) at conditions of 532 nm laser, 500-2000 cm^{-1} spectral range, at 80 seconds for four accumulations before processing in WIRE (5.1; Renishaw, 2020b). Bacteria were investigated in multiple concentrations (10^{-1}-10^{-5}), or in mono and polymicrobial combinations.

Results

The Raman spectral peak at 1003 cm^{-1} was consistent across all bacteria, combinations and concentrations but not present in controls, with intensity of this peak significantly correlated to *E. coli* and *K. pneumoniae* concentrations. *E. coli* and *K. pneumoniae* shared three spectral peaks. *S. aureus* had the most distinct Raman peaks (95%) these assigned to Gram-positive cell wall components.

Conclusion

Findings show that bacteria can be identified by one spectral peak, with characteristic Raman peaks relevant to specific bacterial characteristics including Gram status identified. Quantitative analysis and bacterial discrimination in polymicrobial cultures is inconclusive. Additional Raman spectra from a wider variety of bacteria in culture and clinical conditions is required for confidence in species level resolution.

6.1 Introduction

In a clinical setting the requirement for timely bacterial identification is critical for diagnosis and treatment options. Current clinical detection methods include bacterial culture, PCR and sequencing (Lorenz *et al*, 2017; Pahlow *et al*, 2015). Identification is reliable and sensitive, but requires increasing time commitments, with contamination issues from culture media and sequencing reagents (Maquelin *et al*, 2002; Pahlow *et al*, 2015).

A method requiring less time and processing would increase the efficiency, accuracy and confidence in detecting bacterial presence in low biomass clinical tissues. Previously, Fourier-transformed infrared spectroscopy (FTIR) and matrix-assisted laser desorption/ionization (MALDI) spectroscopy techniques have been applied to bacterial culture and clinical samples for timely detection of clinical conditions without excess processing (Bocklitz *et al*, 2015; Pielesz *et al*, 2019). These spectroscopy techniques allow biochemical and molecular profiling (Bocklitz *et al*, 2015), rather than morphological characterisation and sequence detection as per previous culturing and sequencing technologies (Lorenz *et al*, 2017; Pahlow *et al*, 2015). However, these spectroscopy methods are destructive and require high sample volumes, limiting clinical application (Hlaing *et al*, 2013; Maquelin *et al*, 2002).

A novel method for bacterial detection and pathological diagnosis has been applied to bacterial cultures (Almarashi *et al*, 2012; de Siqueira E Oliveria, Giana and Silveira, 2012; Kusters *et al*, 2015), and placental tissues (Chen *et al*, 2014). This method is Raman spectroscopy, which acts to identify the presence and location of specific bacteria or tissue differences based on biochemical information, molecular composition, functional groups and chemical structures displayed as a unique spectral fingerprint (Ashton *et al*, 2011; Mlynarikova *et al*, 2015). Raman spectroscopy is a non-destructive, non-invasive label free spectroscopy method, which is a beneficial choice for bacterial and tissue analysis due to decreased preparation and processing steps (Pahlow *et al*, 2015). This decreases analysis time and improves reliability of results, due to the removal of confounding culture or DNA extraction steps (Mlynarikova *et al*, 2015).

In bacterial detection research, 23 identifying spectral peaks across multiple bacteria have been observed, with the ability to distinguish between Gram-positive and negative bacteria at the 857, 907 and 1382 cm^{-1} peaks with 87-100% specificity (de Siqueira E Oliveria, Giana and Silveira, 2012). Strain specific distinctive peaks

have also been suggested, with differentiation possible between pathogenic O157:H7 and non-pathogenic K-12 *E. coli* strains (Hamasha *et al*, 2013), or based on antibiotic properties (Kusters *et al*, 2015; Li *et al*, 2018). Although spectral fingerprints have been explored for bacterial identification, the current limit of detection (LOD) for microbiological identification using Raman spectroscopy has not yet been determined.

6.1.1 Clinical relevance of Raman spectroscopy

Non-destructive Raman spectroscopy could be beneficial in the clinical setting of pregnancy related conditions, including histological chorioamnionitis (HCA), to improve point of care diagnosis. Current diagnosis methods require fixative and embedding procedures, before applying staining protocols (Holzman *et al*, 2007; Stout *et al*, 2013). All of which require extended preparation steps, which modify the genuine tissue composition and interfere with the microbiota, as shown with the Formalin-Fixed Paraffin-Embedded samples used in chapter four of this thesis. Sequencing or culture methods are then applied for bacterial detection. A non-destructive diagnostic method which would remove staining and labelling, plus combining microbiological analysis with visual detection may improve HCA diagnosis. Previous research has applied Raman spectroscopy to placental and fetal membrane samples (Chen *et al*, 2014; O'Brien *et al*, 2014; Pielesz *et al*, 2019). This includes the detection of spectral peaks distinctive to protein side chains from hypoxic placentas with pre-eclampsia (Chen *et al*, 2014), and decreased lipid content in preterm cervical cells (O'Brien *et al*, 2014). Thus, suggesting a sound rationale for application to HCA fetal membrane samples.

This thesis has found that increased bacterial loads are present on the fetal membranes in the mostly asymptomatic condition of HCA (Chapter five). Bacterial load is therefore a suggested marker for HCA, yet due to the low biomass sample characteristics further confirmation of bacterial load and presence would be beneficial. Raman offers the potential opportunity to determine bacterial presence from biochemical characteristics measured by spectroscopy, as well as visualising the spatial location of bacteria on the fetal membranes by microspectroscopy. Prior to clinical application, confidence in the LOD from low bacterial concentrations is required. Plus, understanding the ability to identify bacteria to species level, and identifying individual microbes in a polymicrobial culture. Confidence is required to

ensure correct identification and assignment, allow targeted analysis, plus generate known reference spectra for comparison when applied to low concentration polymicrobial clinical tissues.

The aim of chapter six was to determine if Raman spectroscopy could detect and differentiate between three bacteria (*E. coli, K. pneumoniae* and *S. aureus*) in a polymicrobial environment, based on a spectral fingerprint or distinct spectral peaks. In addition, to understand the LOD of the instrument for future application to low biomass fetal membrane tissues.

6.2 Theory and review of Raman spectroscopy

6.2.1 Theory of Raman spectroscopy

Raman spectroscopy is used for identifying unique functional groups, molecular composition and chemical structures within a sample. This is based on the vibration of chemical bonds caused by intense laser light scattering creating high resolution narrow bands (Ashton *et al*, 2011; Mlynarikova *et al*, 2015; Movasaghi, Rehman and Rehman, 2007)(Figure 6.1).

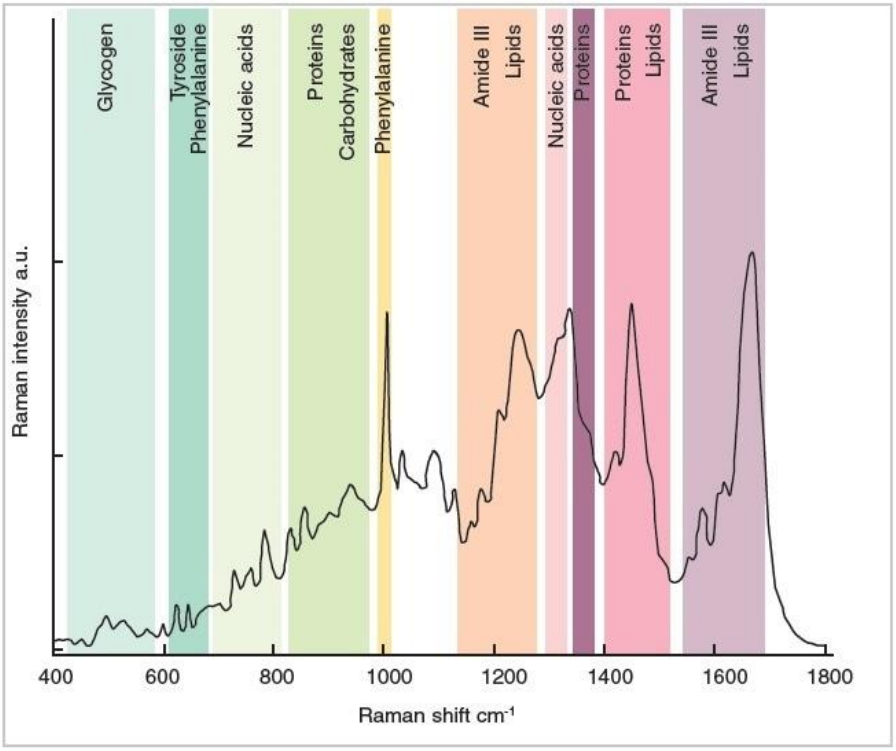

Figure 6.1 Typical Raman biological spectra. Representation of a typical spectra from Raman spectroscopy reflective of relevant biological material peaks and bands, with identifying groups highlighted. Image provided by Renishaw (Renishaw, 2020a).

6.2.2 Raman spectroscopy instrumentation

The Raman instrument consists of a monochromatic light source which emits a laser light onto the sample causing molecule excitation (Lorenz *et al*, 2017; Pahlow *et al*, 2015). The photon molecules are excited from the ground state to a virtual energy state, before returning to a lower vibrational state (Butler *et al*, 2016; Hlaing *et al*, 2013; Larkin, 2011). It is this vibrational energy that is measured in Raman spectroscopy, and is unique to each molecule creating individual spectral fingerprints (Larkin, 2011).

In the specific instrument used here (inVia Raman, Renishaw), the initial laser light travels through a beam expander to direct the light source (Figure 6.2), before passing through a focus mirror via a holographic notch filter. The laser then focuses on the sample positioned on a microscope stage (Smith and Dent, 2005). Following reflection from the sample and microscope slide surface the scattered light travels away from the sample and passes back through the holographic notch filters, through a focus slit and into a diffraction grating device to split the scattered light into a spectrum of wavelengths (Smith and Dent, 2005). The spectra are then detected by a light sensitive device. The charge coupled device detection camera (CCD; Figure 6.3), is a multichannel detector with photosensitive elements, which detects, and stores charged molecular information converted to a numerical value (Hamasha *et al*, 2013; Larkin, 2011). Software then displays results by wave number Raman shifts from incident frequency (cm^{-1}) for spectral intensity measurements (Movasaghi, Rehman and Rehman, 2007).

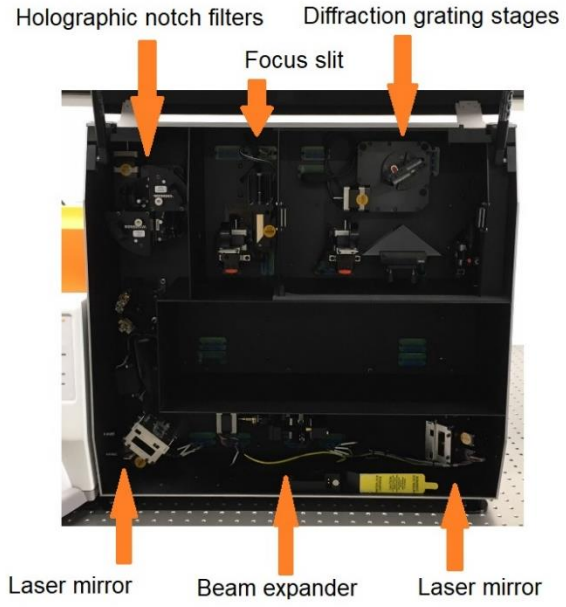

Figure 6.2 Internal view of inVia Raman enclosure. A labelled photograph of the internal instrument of the inVia Raman enclosure used in this research. The laser light initially travels through the beam expander, to the laser mirror, through the holographic notch filter and into the focus slit to be directed onto the microscope slide surface. The light is reflected from the sample and microscope slide surface back through the focus slit and into the diffraction grating device to split the laser into a spectra and direct this to the charge coupled device detection camera to store the measured molecular information.

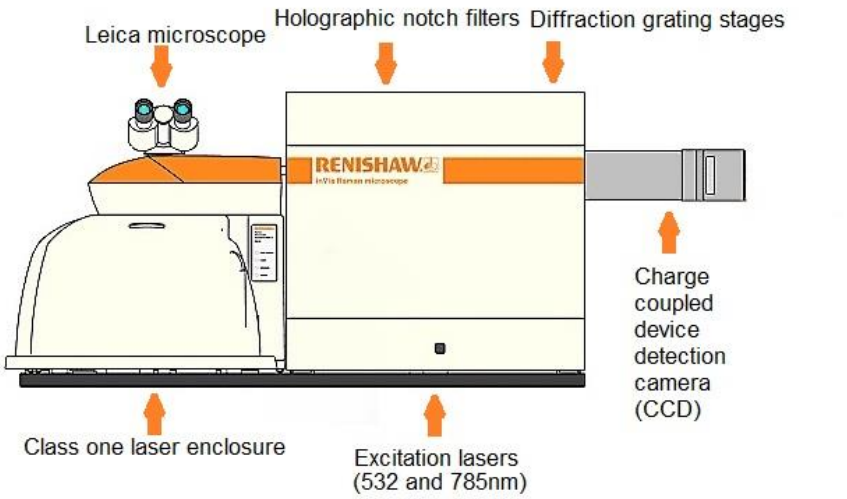

Figure 6.3 External view of inVia Raman enclosure. An external diagrammatic representation of the inVia Raman enclosure (Renishaw). Image provided by Renishaw (Renishaw, 2020a) with additional labelling. The class one laser enclosure contains the microscope and microscope stage. The main enclosure contains the structures depicted in figure 6.2. The charge coupled device detection camera can be viewed to the left of the enclosure.

6.2.3 Raman spectral processing

The output from Raman spectroscopy is a spectral graph comparing Raman shift (cm^{-1}) and intensity (au), plus a numerical intensity information table. Output spectra require post-processing to ensure that only genuine molecular vibrations from laser excitation are processed, and confounding factors are not highlighted as relevant features. Estimated baseline correction can firstly be applied. This to remove sample and background fluorescence, plus thermal fluctuations from the CCD to give a flat baseline for the spectra (Butler *et al*, 2016; Guo, Bocklitz and Popp, 2016). Cosmic ray removal should then be performed to remove any sporadic random narrow band spikes which may be observed on the spectra. These occur when a high energy particle collides with the CCD leading to random disturbance (Butler *et al*, 2016; Hlaing *et al*, 2013). The Raman shift spectra can then be truncated to increase focus to a desired range, in biological research the relevant area is mainly 600-1600 cm^{-1} (Butler *et al*, 2016; Hamasha *et al*, 2013; Smith and Dent, 2005).

Spectral peak tables provide information for peaks to be classified and assigned to a product by supervised or unsupervised methodology (Butler *et al*, 2016). Unsupervised methodology requires no prior knowledge of the sample, with a

pattern recognition approach and comparison to a published reference database, indicating what product each peak represents (Rizkalla *et al*, 2012). Whilst supervised classification compares peak number to a predetermined reference database created on the identical instrument under identical parameters and sample processing (Butler *et al*, 2016).

6.2.4 Sample processing for Raman spectroscopy

Sample processing of biological material must be carefully considered prior to application. For bacterial analysis, the majority of protocols suggest washing and centrifuging the sample, aiming to remove background contribution from the media (Hlaing *et al*, 2013). When media is not removed following *E. coli* culture, peaks have been detected at 886, 1480 and 1620 cm^{-1} from Mueller Hinton media (de Siqueira E Oliveria, Giana and Silveira, 2012). Alternatively 1040, 1360 and 1600 cm^{-1} in RPMI media (Mlynarikova *et al*, 2015), with variance due to different nutritional enrichment products (Mlynarikova *et al*, 2015).

The choice of microscope slide impacts spectral output. Glass and calcium fluoride (CaF2) microscope slides show high background fluorescence (Butler *et al*, 2016), with a key identifiable peak at 321 cm^{-1} from CaF2 slides (Lewis *et al*, 2017). Stainless steel microscope slides show optimal results with low fluorescence and no specific spectral peaks detected (Lewis *et al*, 2017). With the additional benefit of decreased acquisition time and increased intensity due to the double passing of the laser when redirected from the reflective surface (Lewis *et al*, 2017).

6.3 Raman spectroscopy methods

Three different bacterial species (*Escherichia coli*, *Klebsiella pneumoniae* and *Staphylococcus aureus)* were used to evaluate the ability of Raman spectroscopy to differentiate between bacteria at varying concentrations and combinations.

6.3.1 Bacterial culture

Under sterile techniques one colony of *E coli*, *K. pneumoniae* or *S. aureus* was inoculated from a Luria-Bertani (LB) agar plate into 100 ml LB media and incubated at 37 °C for 16 hours. Optical density (OD_{600}) values were measured on a UV spectrophotometer (Jenway 7305), with values of >1.4 biomass processed (OD_{600} x µl of culture). To quantify bacteria, stock solutions and dilutions were then plated on LB agar plates and colony forming units (CFUs) calculated following overnight incubation at 37 °C.

6.3.2 Bacterial preparation for Raman spectroscopy

After incubations, 1 ml of bacterial culture was collected into a microcentrifuge tube. Additional aliquots were collected for serial dilutions and polymicrobial analysis.

To prepare dilutions, 1 ml of overnight culture and 9 ml of fresh LB media were combined, before performing serial dilutions to cover the desired range (10^{-1}-10^{-5}) and aliquoting 1 ml of each dilution into sterile microcentrifuge tubes.

For polymicrobial analysis, 500 µl of two bacterial cultures were collected and combined into microcentrifuge tubes (*E. coli* and *K. pneumoniae*, *E. coli* and *S. aureus* or *K. pneumoniae* and *S. aureus*).

All 1 ml cultures (mono, polymicrobial and dilutions) were then centrifuged at 15,000 xg for four minutes, before discarding the supernatant and repeating the centrifugation step. Supernatants were discarded and pellets were resuspended in 30 µl dH_2O by gentle pipetting. To a stainless steel slide (Renishaw), 10 µl of each culture was added and air dried for two hours before Raman analysis. A control of 10 µl fresh LB media was prepared under identical conditions. This was repeated in triplicate for each mono and polymicrobial culture, concentration and control.

6.3.3 Raman spectroscopy experimental set up

A Raman inVia Qontour system (Renishaw) was used to analyse samples, equipped with a Lecia microscope and Lecia EL600 compact light source. WIRE software (5.1; Renishaw, 2020b) was used to set parameters and analyse output results.

6.3.4 Instrument calibration

Full machine calibration was performed upon installation (May 2019), with monthly calibration performed by technicians. Daily calibrations were performed prior to operation using the quick calibration function in WIRE (5.1; Renishaw, 2020b). This uses an internal silicon reference to monitor accuracy of peak detection, with an expected peak centre of 520.5 cm^{-1} at a constant intensity over time.

6.3.5 Bacterial spectral acquisition

Dried bacterial droplets on stainless steel microscope slides were added onto the Raman microscope stage within the class one enclosure and viewed under 50x magnification using the live video tool. Visible bacterial areas were selected for measurement. Single point scan measurements were performed using the spectral acquisition setup. A 532 nm laser (RL532-08) at 2400 lines/mm grating and 50% laser power (25 mW) was applied and all spectra were initially collected at 200-3200 cm^{-1} at ten seconds exposure time and one accumulation. The spectral range was then reduced to 500-2000 cm^{-1} to increase the focus on biologically relevant material. Samples were measured at 80 seconds for four accumulations to an acquisition time of 320 seconds per spectra.

Bacterial droplets were analysed at four points in the outer perimeter, with replicates merged using the batch measure function. Background spectra were collected from stainless steel slides and fresh LB media under identical parameters.

6.3.6 Raman spectral processing method

Baselines were subtracted from raw spectra using least squared polynomial fit to an order of four (Butler *et al*, 2016; Guo, Bocklitz and Popp, 2016). This removes sample and background fluorescence to an approximate closely related profile without loss of signature peaks (Hamasha *et al*, 2013). Cosmic rays were detected and removed using the nearest neighbour algorithm. Once again ensuring replacement of the cosmic ray to a similar spectral neighbour (Larkin, 2011). Pick peak function was used to automatically assign numerical values to peaks. Information on peak centre, height, width, area, absolute intensity, plus high and low edges were tabulated.

6.3.7 Raman data analysis

Spectra and peak information were exported from WIRE (5.1, Renishaw 2020b). Initial analysis involved comparison of the overall spectral image, bacterial fingerprint and the presence/absence of peaks across mono and polymicrobial cultures. Peak shifts and intensity were also analysed across all concentrations and bacterial combinations. Correlation between peak intensity and bacterial concentration was performed via nonparametric Spearmans Rank Bonferroni adjustment in R (R Core Team, 2017).

Assigning peaks to relevant biomolecular components was conducted by unsupervised methodology, by comparison to published reference databases (de Gelder *et al*, 2007; Maquelin *et al*, 2002; Movasaghi, Rehman and Rehman, 2007; Talari *et al*, 2015), plus from research using comparable systems and protocols (Cheong *et al,* 2016; de Siqueira E Oliveria, Giana and Silveira, 2012; Hamasha *et al*, 2013).

6.4 Results

6.4.1 Calibration and background reference spectra

Positive calibration was confirmed by detection of a high intensity narrow band visible at 520 cm^{-1} relating to the internal silicon chip (Figure 6.4).

Background measurements were taken from stainless steel microscope slides and blank LB culture media. The spectra from the microscope slide returned undistinguishable peaks with counts <70 (Figure 6.5). No detectable spectral peaks and intensity counts <100 were observed from the culture media (Figure 6.6).

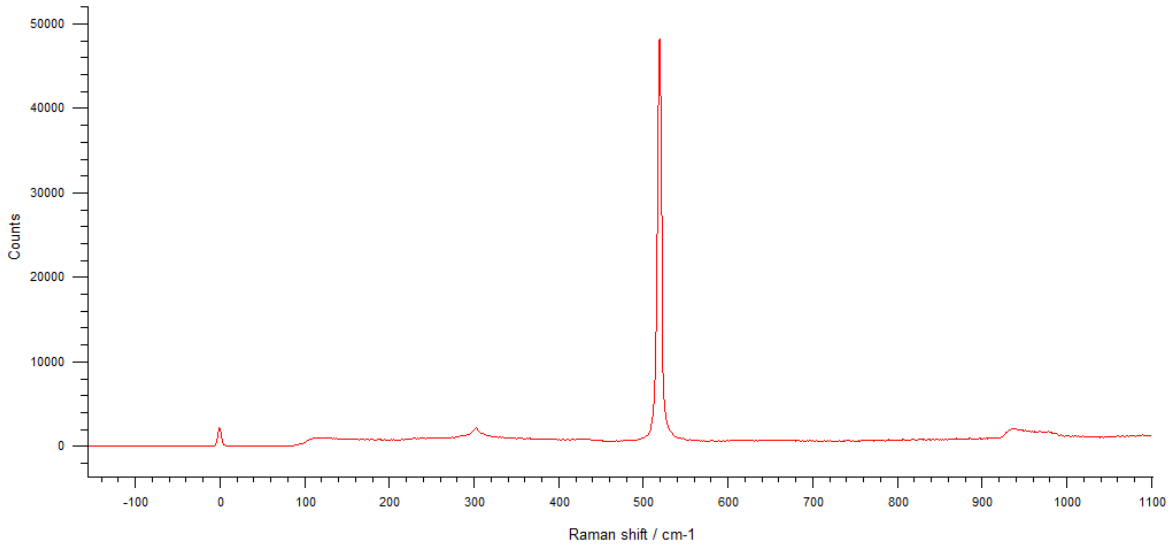

Figure 6.4 Reference calibration spectra of the internal silicon chip. An example of the output spectra for the internal silicon chip within the Raman instrument used for calibration. Figure represents Raman shift cm^{-1} against intensity counts. A defined peak at 520.5 cm^{-1} is expected.

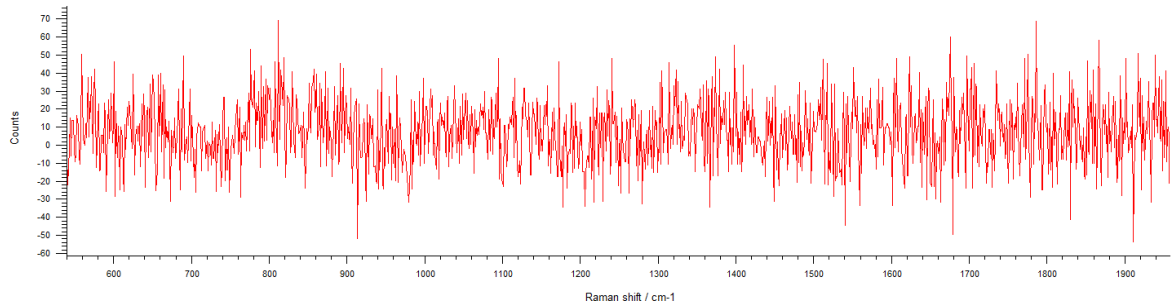

Figure 6.5 Reference background spectra of a stainless steel microscope slide. An example of the reference calibration spectra for the stainless steel microscope slide of which bacterial droplets were mounted. Figure represents Raman shift cm^{-1} against intensity counts.

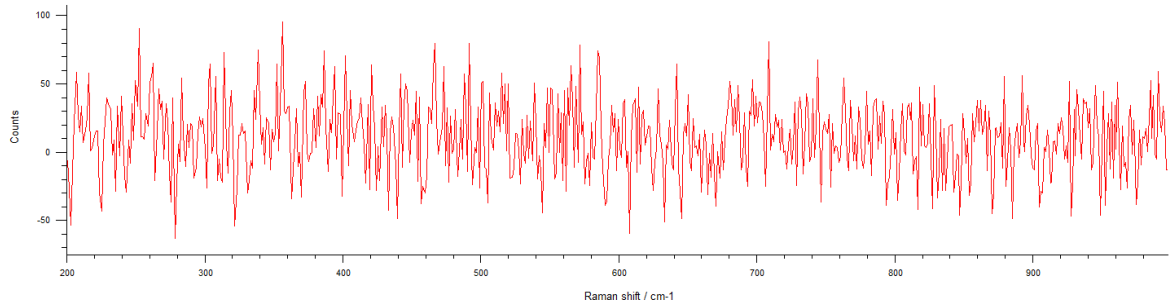

Figure 6.6 Reference background spectra of culture media. An example of the reference calibration spectra for blank Luria-Bertani (LB) culture media of which all bacteria were cultured. Figure represents Raman shift cm^{-1} against intensity counts.

6.4.2 Example spectral processing results

Unprocessed raw Raman spectra from a bacterial sample was collected from WIRE (5.1; Renishaw, 2020b)(Figure 6.7A). Baselines were detected (Figure 6.7B) and subtracted to a least squared polynomial fit (Figure 6.7C). Following cosmic ray analysis on this example, only one cosmic ray was detected and removed (601 cm^{-1}; Table 6.1). Automatic peak assignment was performed to create a final labelled Raman spectra and peak information table (Figure 6.8). Processing was identical across all samples.

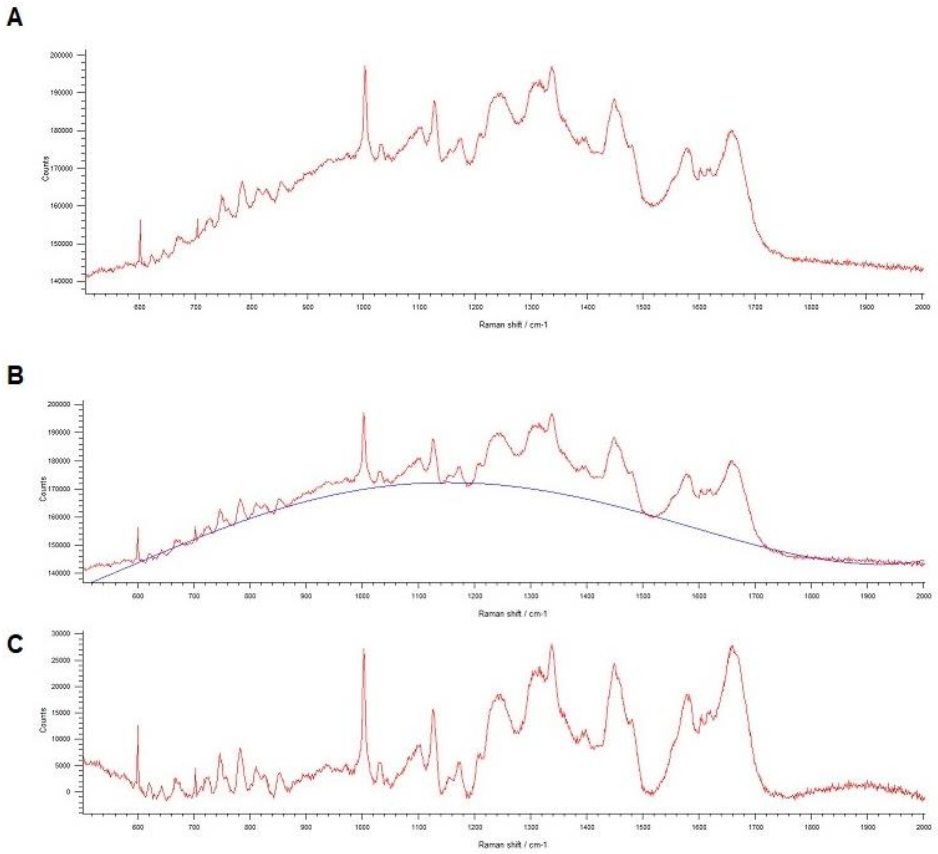

Figure 6.7 Raman baseline subtraction example. An example of a raw Raman bacterial spectra collected at 80 seconds for four accumulations on a 532nm laser, 2400 lines/mm grating, 50% laser power at 500-200cm^{-1} spectral range (A). The baseline detection method was then used to detect baseline levels (B) and subtract baseline signals to remove background and sample autofluorescence (C). Spectra measured and processed in WIRE (5.1; Renishaw, 2020b).

#	Width / pixels	RamanShift	Spectrum	X	Y	Z
1	2	601.0	1			

Table 6.1 Cosmic ray removal table. An example table for the detection and assignment of cosmic rays via WIRE (5.1; Renishaw, 2020b).

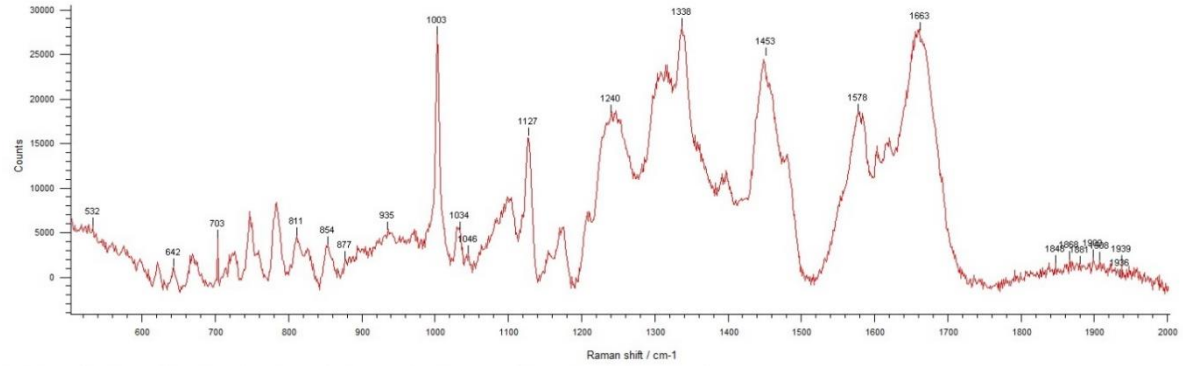

Peak no.	Centre	Height	Width	Area	Absolute intensity	Low edge	High edge
1	532.007	1674.08	2.18385	657627	5870.77	505.422	616.713
2	642.453	1459.95	3.00332	28095.5	1234.79	635.514	672.971
3	702.792	5246.26	1.38276	38419.4	4412.56	696.594	741.141
4	811.2	923.913	1.43985	318881	4774.87	782.959	820.875
5	853.529	902.507	4.0606	145712	3704.17	822.096	856.164
6	877.37	329.365	2.48269	68816.8	2098.13	857.377	879.188
7	935.422	2030.07	14.454	535021	5383.87	881.607	962.176
8	1002.79	2701.05	1.6373	906573	27447.3	963.373	1003.9
9	1033.99	958.674	2.07248	547755	5372.44	1005.09	1039.46
10	1045.52	826.48	1.37527	55819.8	2742.95	1040.65	1056
11	1127.35	11965.7	8.85982	1.02584e+06	16040.4	1057.18	1172.97
12	1240.07	9785.52	35.6516	1.62686e+06	18549.1	1178.76	1271.98

Figure 6.8 Example of pick peak function and final processed spectra. Raman peak assignment was performed automatically following acceptance of cosmic ray removal at 601 cm^{-1} (Table 6.1). Results are displayed as labelled spectral peaks and numerical spectral peak information tabulated in WIRE (5.1; Renishaw, 2020b).

6.4.3 Raman spectra from monomicrobial droplets

Raman spectra in the range of 600-2000 cm^{-1} were collected from four points on each bacterial droplet, repeated in triplicate and merged to present averaged values. Figure 6.9 displays the individual Raman spectra from merged *E. coli* (A), *K. pneumoniae* (B) and *S. aureus* (C).

All bacteria have spectral fingerprints containing defining properties representing biological material. Increased peak intensity, yet decreased resolution was detected between 1200-1700 cm^{-1} (Figure 6.9). Spectra from *E. coli* and *K. pneumoniae* were more similar, with *S. aureus* more different (Figure 6.9).

One Raman peak was consistently detected across all bacteria, combinations and concentrations (Figure 6.9). The peak at 1003 cm^{-1} was assigned to the amino acid phenylalanine (Cheong *et al*, 2017; de Gelder *et al*, 2007; Lorenz *et al*, 2017; Movasaghi, Rehman and Rehman, 2007; Talari *et al*, 2015).

Individual peaks within the 600-1700 cm^{-1} range were assigned to biologically relevant components by comparison to previously generated databases (de Gelder *et al*, 2007; Hlaing *et al*, 2013; Movasaghi, Rehman and Rehman, 2007; Talari *et al*, 2015).

Automatic assignment consistently detected 16 Raman peaks from merged *E. coli* spectra, 12 of which were distinct to *E. coli* (75%). These mainly represent DNA bases, amides, lipids and proteins, yet also specifically assigned to lipopolysaccharides (LPS) and phosphoenolpyruvate (Table 6.2). *K. pneumoniae* had 15 Raman peaks, 11 of which were distinct only to this bacterium (75%). The majority of those specific to *K. pneumoniae* represented universal DNA bases, amides and proteins (Table 6.3). *S. aureus* had the highest number of Raman peaks assigned (19), with 95% (18/19) distinct to *S. aureus*. These covered a greater spectral range and were assigned to a wider variety of categories including, amides, acids, DNA bases and proteins, plus collagen, teichoic acid and myristic acid (Table 6.4).

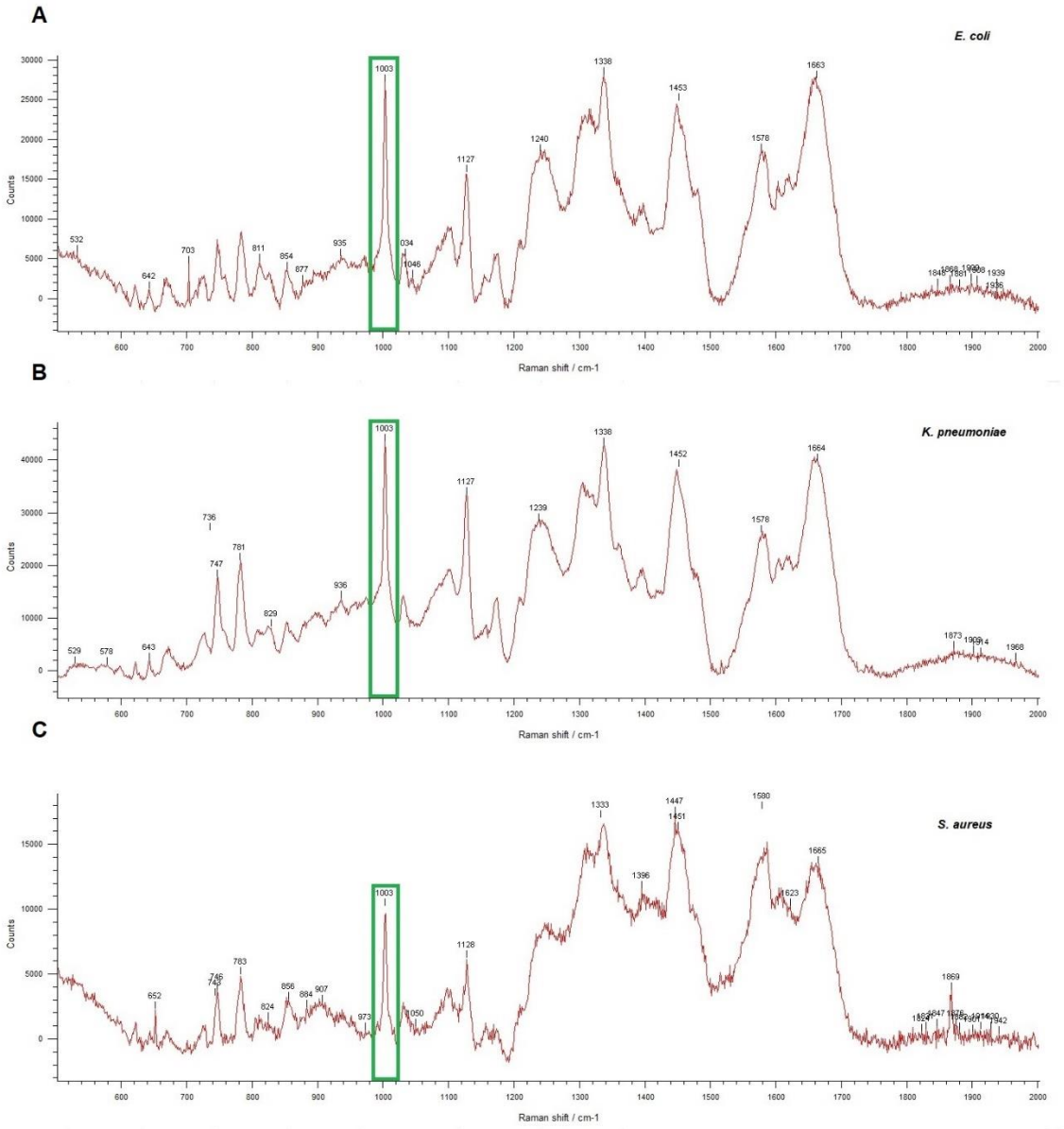

Figure 6.9 Raman spectra from monomicrobial culture droplets. Processed Raman spectra for overnight cultures of bacterial droplets from *Escherichia coli* (A), *Klebsiella pneumoniae* (B) and *Staphylococcus aureus* (C) following background subtraction, cosmic ray removal and automatic peak assignment. Spectra were collected using a 532nm laser at 2400 lines/mm grating, 50% laser power at 80 seconds exposure for four accumulations over a spectral range of 500-2000cm^{-1}. The 1003 cm^{-1} peak consistent across all bacteria is highlighted.

Raman shift (cm^{-1})	**Band assignment**	**Reference**
532	Alanine	de Gelder *et al*, 2007
642	Proline	de Gelder *et al*, 2007
703	DNA/RNA bases	de Gelder *et al*, 2007
811	RNA, riboflavin	de Gelder *et al*, 2007; Hlaing *et al*, 2013; Talari *et al*, 2015
854	Lipopolysaccharides	de Gelder *et al*, 2007
877	Proline	de Gelder *et al*, 2007; Movasaghi, Rehman and Rehman, 2007; Talari *et al*, 2015
935	Proline, valine, glycogen, alpha helix protein backbone	Movasaghi, Rehman and Rehman, 2007; Talari *et al*, 2015
1003	Phenylalanine	Cheong *et al*, 2017; de Gelder *et al*, 2007; Lorenz *et al*, 2017; Movasaghi, Rehman and Rehman, 2007; Talari *et al*, 2015
1034	Phenylalanine, collagen, phosphoenolpyruvate	de Gelder *et al*, 2007; Talari *et al*, 2015
1046	Tryptophan	de Gelder *et al*, 2007
1127	Nucleic acid	Li *et al*, 2018
1240	RNA, amide III, proline	de Gelder *et al*, 2007; Hlaing *et al*, 2013; Talari *et al*, 2015
1338	Cytosine, amide III	Ashton *et al*, 2011; Neugebauer *et al*, 2006
1453	Structural proteins and lipids	de Siqueira E Oliveria, Giana and Silveira, 2012; Movasaghi, Rehman and Rehman, 2007; Talari *et al*, 2015
1578	Adenine, guanine	de Siqueira E Oliveria, Giana and Silveira, 2012; Talari *et al*, 2015
1663	Amide I, DNA, protein	Hlaing *et al*, 2013; Talari *et al*, 2015

Table 6.2 Raman spectral peak assignment for *Escherichia coli*. Raman spectral peaks detected in *E. coli*, with band assignment from pre-established databases and research. Raman peaks highlighted in bold were detected in this bacterium only. Spectral peaks correlate to those detected in figure 6.9A.

Raman shift (cm^{-1})	**Band assignment**	**Reference**
529	Uracil, fructose	de Gelder *et al*, 2007
578	Adenine, guanine	de Gelder *et al*, 2007
643	Tyrosine	Movasaghi, Rehman and Rehman, 2007
736	Adenine	Talari *et al*, 2015
747	Phenylalanine	de Gelder *et al*, 2007
781	Cytosine, uracil	Hlaing *et al*, 2013; Talari *et al*, 2015
829	Tyrosine	de Siqueira E Oliveria, Giana and Silveira, 2012; Maquelin *et al*, 2002
936	Amylose	de Gelder *et al*, 2007
1003	Phenylalanine	Cheong *et al*, 2017; de Gelder *et al*, 2007; Lorenz *et al*, 2017; Movasaghi, Rehman and Rehman, 2007; Talari *et al*, 2015
1127	Nucleic acid	de Gelder *et al*, 2007; Li *et al*, 2018
1239	Amide III, mannose	de Gelder *et al*, 2007; Hlaing *et al*, 2013; Talari *et al*, 2015
1338	Cytosine, amide III	Ashton *et al*, 2011; Neugebauer *et al*, 2006
1452	Amide III, glycine, tryptophan	de Gelder *et al*, 2007; Hlaing *et al*, 2013
1578	Adenine, guanine,	de Siqueira E Oliveria, Giana and Silveira, 2012; Talari *et al*, 2015
1664	Amide I	Talari *et al*, 2015

Table 6.3 Raman spectral peak assignment for *Klebsiella pneumoniae*. Raman spectral peaks detected in *K. pneumoniae*, with band assignment from pre-established databases and research. Raman peaks highlighted in bold were detected in this bacterium only. Spectral peaks correlate to those detected in figure 6.9B.

Raman shift (cm^{-1})	Band assignment	Reference
652	Glucose	de Gelder *et al*, 2007
743	DNA/RNA bases	de Gelder *et al*, 2007
746	DNA/RNA bases	Movasaghi, Rehman and Rehman, 2007; Talari *et al*, 2015
783	DNA/RNA bases	Movasaghi, Rehman and Rehman, 2007; Talari *et al*, 2015
824	Valine, histidine	de Gelder *et al*, 2007
856	Proline	Movasaghi, Rehman and Rehman, 2007; Talari *et al*, 2015
884	Collagen	Movasaghi, Rehman and Rehman, 2007; Talari *et al*, 2015
907	Teichoic acid	de Siqueira E Oliveria, Giana and Silveira, 2012
973	Pyruvate, phosphate	de Gelder *et al*, 2007
1003	Phenylalanine	Cheong *et al*, 2017; de Gelder *et al*, 2007; Lorenz *et al*, 2017; Movasaghi, Rehman and Rehman, 2007; Talari *et al*, 2015
1050	Fatty acids	de Gelder *et al*, 2007
1128	Myristic acid, proteins and carbohydrates	de Gelder *et al*, 2007; Movasaghi, Rehman and Rehman, 2007; Talari *et al*, 2015
1333	Proline, guanine	de Gelder *et al*, 2007; Movasaghi, Rehman and Rehman, 2007; Talari *et al*, 2015
1396	β-carotene	Talari *et al*, 2015
1447	Phenylalanine, proteins	de Gelder *et al*, 2007; Movasaghi, Rehman and Rehman, 2007; Talari *et al*, 2015
1451	Collagen	Movasaghi, Rehman and Rehman, 2007; Talari *et al*, 2015
1580	Phenylalanine	Talari *et al*, 2015
1623	Tryptophan	Talari *et al*, 2015
1665	Amide I, collagen	Movasaghi, Rehman and Rehman, 2007; Talari *et al*, 2015

Table 6.4 Raman spectral peak assignment for *Staphylococcus aureus*. Raman spectral peaks detected in *S. aureus*, with band assignment from pre-established databases and research. Raman peaks highlighted in bold were detected in this bacterium only. Spectral peaks correlate to those detected in figure 6.9C.

6.4.4 Raman spectra from polymicrobial droplets

Spectra from combined polymicrobial bacterial droplets were analysed to determine if previously highlighted distinct peaks from individual bacteria could be detected in a polymicrobial environment.

When monitored independently *E. coli* and *K. pneumoniae* shared similar spectral profiles and four spectral peaks (1003, 1127, 1338 and 1578 cm^{-1}) representing nucleic acid bases and amides, plus the phenylalanine peak detected in all bacteria (Table 6.2 and 6.3).

In combined droplets, the shared 1003 and 1127 cm^{-1} peaks were present, yet 1338 and 1578 cm^{-1} showed a -2 cm^{-1} and +1 cm^{-1} Raman shift to 1336 and 1579 cm^{-1} respectively (Figure 6.10A). The distinct peaks previously detected only in *E. coli* (642 and 1453 cm^{-1}) or *K. pneumoniae* (936 and 1664 cm^{-1}) were also detected in combined droplets (Figure 6.10A). However, 10/12 and 8/11 previously distinct peaks from *E. coli* and *K. pneumoniae* respectively were not detected in combined cultures. Although not detected exactly, slight Raman shifts of +2, -1, +1 and +1 cm^{-1} for peaks of 811, 935, 1578 and 1663 cm^{-1} were detected from *E. coli*, or +2, -1, +1, -1 cm^{-1} for 578, 643, 1452 and 1579 cm^{-1} for *K. pneumoniae*.

E. coli and *S. aureus* shared one specific peak for phenylalanine (1003 cm^{-1}) when analysed independently (Table 6.2 and 6.4), this peak was also observed in the polymicrobial combination (Figure 6.10B). Distinct peaks at 746 and 1451 cm^{-1} previously detected independently from *S. aureus* were present in combined cultures, as was the *E. coli* specific 1663 cm^{-1} peak (Figure 6.10B). Once again 11/12 *E. coli* independent peaks were not detected in combined cultures, neither were 16/19 from *S. aureus*. Closely related peaks were detected in combined cultures with a -1, -2 and +1 cm^{-1} shift for 854, 1453 and 1578 cm^{-1} for *E. coli* and a -2 cm^{-1} shift at 783 cm^{-1} for *S. aureus*.

When compared individually *K. pneumoniae* and *S. aureus* shared the 1003 cm^{-1} spectral peak representing phenylalanine (Table 6.3 and 6.4), also detected in combined cultures (Figure 6.10C). In combined droplets, four peaks previously only detected in *K. pneumoniae* were present (747, 936, 1338 and 1664 cm^{-1}), with two peaks specific to *S. aureus* (973 and 1580 cm^{-1}; Figure 6.10C). Closely related

peaks were detected in combined cultures related to *S. aureus* including a +1, -2, +1 cm^{-1} and +1 cm^{-1} shift for 746, 783, 1447 and 1665 cm^{-1}, or a +2 cm^{-1} shift at 1578 cm^{-1} for *K. pneumoniae*.

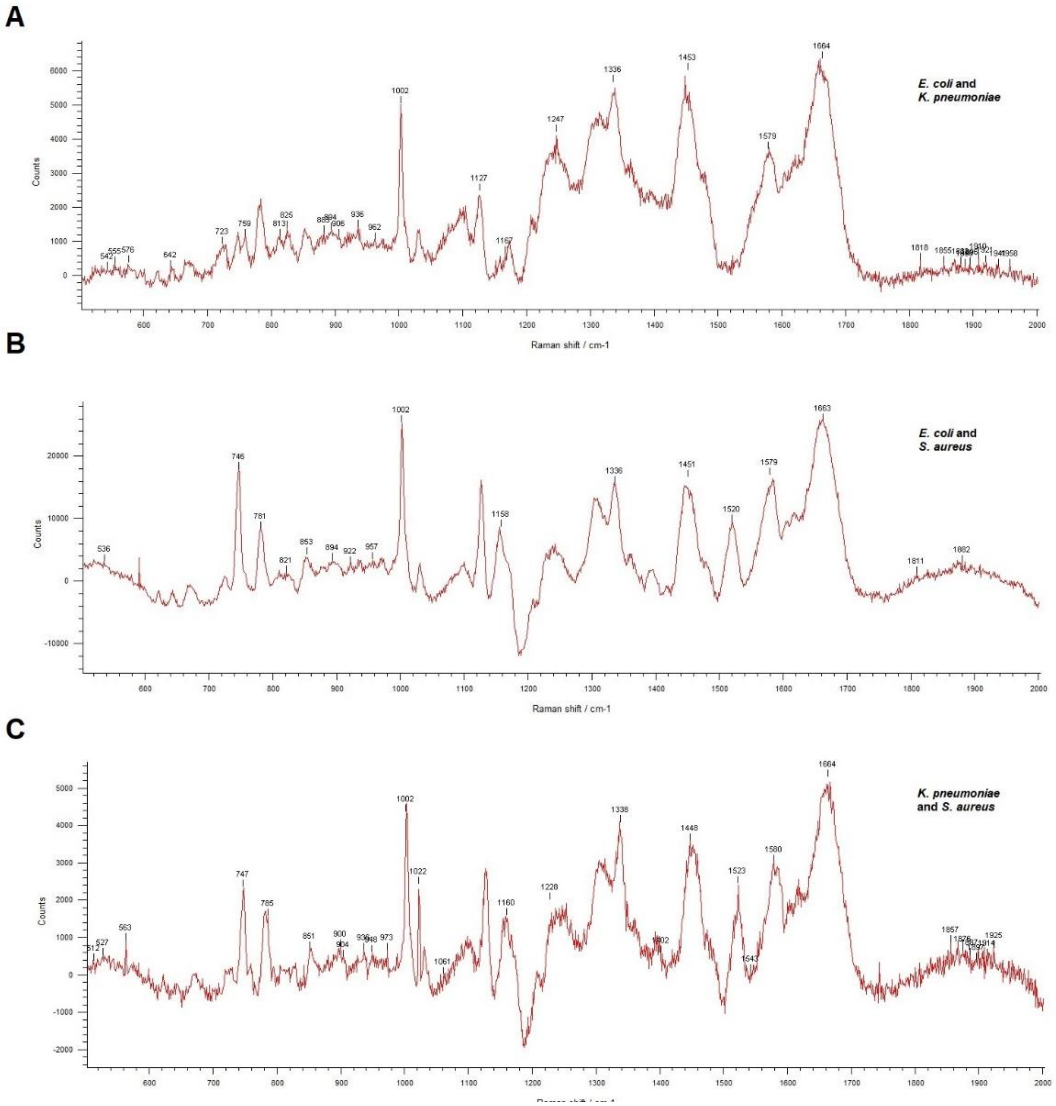

Figure 6.10 Raman spectra from polymicrobial culture droplets. Raman spectra from combined bacterial droplets of overnight washed cultures from *Escherichia coli* and *Klebsiella pneumoniae* (A), *E. coli* and *Staphylococcus aureus* (B), plus *K. pneumoniae* and *S. aureus* (C), following background subtraction, cosmic ray removal and automatic peak assignment in WIRE (5.1; Renishaw, 2020b). Spectra were collected using a 532nm laser at 2400 lines/mm grating, 50% laser power at 80 seconds exposure for four accumulations over a spectral range of 500-2000cm^{-1}.

6.4.5 Raman spectral intensity results

To determine if Raman spectroscopy could be used to quantify bacterial concentration, dilutions of bacterial cultures were analysed (10^{-1}-10^{-5}). Intensity of the 1003 cm^{-1} peak was selected for analysis due to consistent detection throughout all mono and polymicrobial combinations and concentrations.

The intensity of the 1003 cm^{-1} peak varied across undiluted bacteria, with this observed at 27,447, 43,900 and 12,561 counts from *E. coli, K. pneumoniae* and *S. aureus*, respectively. Absolute intensity of the 1003 cm^{-1} peak across dilutions is displayed in Table 6.5 and Figure 6.11. Bacterial concentration was significantly negatively correlated to intensity of the 1003 cm^{-1} spectral peak in *E. coli* (R^2=-0.943, p=0.017) and *K. pneumoniae* (R^2=-1.000, p=0.003), but not for *S. aureus* (R^2=-0.771, p=0.103).

	Undiluted	10^{-1}	10^{-2}	10^{-3}	10^{-4}	10^{-5}
E. coli	27,447	18,451	17,510	13,987	15,973	10,274
K. pneumoniae	43,900	34,336	23,300	18,825	7447	1270
S. aureus	12,561	6231	10,382	11,579	5485	1424

Table 6.5 Table of intensity for the 1003 cm^{-1} spectral peak from serial dilution curves. Intensity of the 1003 cm^{-1} Raman spectral peak from overnight washed cultures of *Escherichia coli*, *Klebsiella pneumoniae* and *Staphylococcus aureus* measured in undiluted bacterial cultures and over a dilution series (10^{-1}-10^{-5}) to determine the quantitative ability of inVia Raman spectroscopy. Spectra were collected using a 532nm laser at 2400 lines/mm grating, 50% laser power at 80 seconds exposure for four accumulations over a spectral range of 500-2000cm^{-1}.

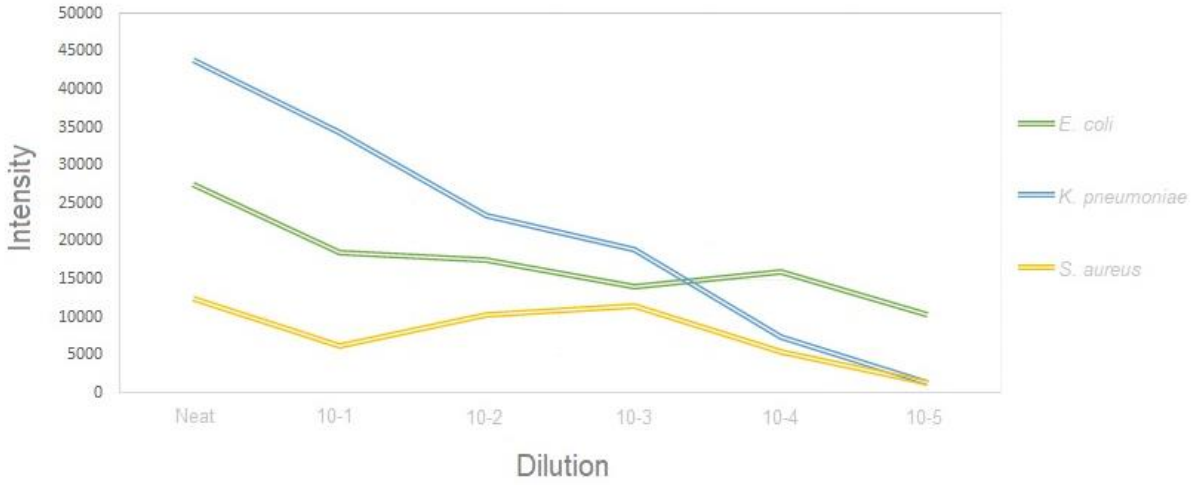

Figure 6.11 Intensity of the 1003 cm^{-1} spectral peak from serial dilution curve. Spectral peak intensity of the 1003 cm^{-1} peak in overnight washed and diluted cultures of *Escherichia coli*, *Klebsiella pneumoniae* and *Staphylococcus aureus* from undiluted bacterial cultures and over a dilution series. Represented as neat or dilutions of 10^{-1}-10^{-5}. Figure correlates to findings from Table 6.5.

6.5 Discussion

Chapter six aimed to determine if Raman spectroscopy could identify bacteria based on a spectral fingerprint or distinct spectral peaks in mono and polymicrobial cultures. In addition, LOD analysis for application to low biomass clinical samples was performed. Overall, findings indicate that the three bacteria studied share one spectral peak (1003 cm^{-1}), with Raman peaks relevant to specific bacterial characteristics including Gram status identified. Raman spectroscopy presents high sensitivity and resolution, yet the ability to confidently discriminate bacteria in polymicrobial cultures was inconclusive, as was the quantitative ability of the instrument. Thus, further optimisation of relevant species in low biomass samples would be required prior to application to clinical conditions.

6.5.1 Bacteria can be detected by a Raman peak at 1003 cm^{-1}. The detection of a sharp high intensity peak at 1003 cm^{-1} was observed across all bacteria regardless of concentration, mono and polymicrobial combination or bacterial status, thus may be a possible characteristic marker to identify bacterial presence in clinical samples. The 1003 cm^{-1} peak represents phenylalanine (de Gelder *et al*, 2007; Movasaghi, Rehman and Rehman, 2007; Talari *et al*, 2015). This essential amino acid has previously been detected in a wide range of bacterium, including confirmation in *E. coli* (Chong *et al*, 2016; Hamasha *et al*, 2013; Hlaing *et al*, 2013; Lorenz *et al*, 2017; Mlynarikova *et al*, 2015), *K. pneumoniae* (Cheong *et al*, 2017) and *S. aureus* (Hamasha *et al*, 2013; Lorenz *et al*, 2017; Mlynarikova *et al*, 2015). Alongside *Staphylococcus epidermidis* (Mlynarikova *et al*, 2015), *Pseudomonas aeruginosa* (Hlaing *et al*, 2013) and *Bacillus subtilis* (Strola *et al*, 2014). The 1003 cm^{-1} peak is ubiquitous across bacteria here, but as an essential amino acid this may also be present in other biological samples and human tissues (Paolini *et al*, 2001). To be confident that this peak is represented universally across bacteria, but specific only to bacteria would require further investigation in a greater range of bacteria, including *Prevotella* and *Ureaplasma* for clinical relevance. Alternatively, it may be intensity of the peak which is distinctive rather than presence. Alternate peaks may be more specific to bacterial detection including bacterial specific LPS detected in *E. coli* at 854 cm^{-1}, or Gram-positive cell wall components detected in *S. aureus*, including teichoic acid at 907 cm^{-1}. Alternatively, the 1453 cm^{-1} peak has been suggested as the spectral peak universal and specific to bacteria, linked to structural lipids and proteins (de Siqueira E Oliveria, Giana and Silveira, 2012). The 1453 cm^{-}

$^{-1}$ peak was detected in *E. coli* within this research project, with a slight shift observed in *K. pneumoniae* (-1 cm^{-1}, 1452 cm^{-1}) and *S. aureus* (-2 cm^{-1}, 1451 cm^{-1}).

6.5.2 *E. coli*, *K. pneumoniae* and *S. aureus* have similar spectral fingerprints, with independent characteristic peaks relevant to each bacteria detected. Biologically relevant band assignments were detected across all bacterial spectra, mainly assigned to DNA bases and amino acids (de Gelder *et al*, 2007). All bacteria displayed similar spectral fingerprints, with increased intensity in the 1200-1700 cm^{-1} range, representing proteins and amides (Butler *et al*, 2016; Talari *et al*, 2015). *E. coli* and *K. pneumoniae* were the only two bacteria to share any identical peaks, other than the universal phenylalanine peak (1003 cm^{-1}), with three additional peaks shared (1127, 1338 and 1578 cm^{-1}). More closely related bacteria may display more similar spectral peaks than distant, due to shared taxonomy to the family level, functional similarities and Gram status (Cheong *et al*, 2017). These peaks represent universal components including amino acids, DNA bases, amides and phenylalanine (de Siqueira E Oliveria, Giana and Silveira, 2012; Li *et al*, 2018), thus potentially non-specific to the investigated bacteria.

Few identified peaks were specific to relevant bacterial properties, including an LPS specific peak observed in *E. coli* (854 cm^{-1}) characteristic to Gram-negative outer membranes (Meredith *et al*, 2016) and phosphoenolpyruvate (1034 cm^{-1}), the primary route for glucose uptake (Long *et al*, 2017). Alternatively, in *K. pneumoniae* the 1239 cm^{-1} peak represents mannose, which is required for glucose uptake in this bacteria (Kostina *et al*, 2005). A peak assigned to teichoic acid (907 cm^{-1}) and peptidoglycan (857 cm^{-1}) was detected in *S. aureus* only. These are main components of Gram-positive bacterial cell walls (Gross *et al*, 2001). The detection of collagen (1451 cm^{-1}) may not be expected in *S. aureus*, but collagen-like proteins, with the same triple helix structure have been previously detected in *Staphylococcus* spp. (Yu *et al*, 2014). These findings support the beneficial use of characteristic bands as biomarkers for individual bacterial species detection or Gram status. The analysis of additional Gram-positive bacteria would be required to confirm findings and ensure detection across species. Previous research has suggested that Raman peaks at 1447 and 1663 cm^{-1} allow resolution between *E. coli* and *S. aureus* (Hlaing *et al*, 2013). This was confirmed here as the 1447 cm^{-1} peak was only detected from *S. aureus*, and 1663 cm^{-1} was only detected from *E. coli* in both mono and polymicrobial cultures. This suggests that specific discrimination between the two

bacteria is possible, however assignment was to generic DNA or proteins, thus may not be specific to each bacteria in a polymicrobial clinical environment. This has been reflected with the inability to resolve *E. coli, K. pneumoniae, S. aureus* and *P. aeruginosa* bacteria due to similarities in cell wall, cell membrane, nucleic acid content and metabolomic processes (Martinez *et al*, 2019). The ability to discriminate between the three species studied has previously been observed, with contrasting findings to this research project. de Siqueira E Oliveria, Giana and Silveira (2012) found peaks of 1382 cm^{-1} specific to *S. aureus*, 1130 cm^{-1} specific to *E. coli* and 1157 cm^{-1} for *K. pneumoniae*.

6.5.3 Bacterial distinction in polymicrobial environments is inconclusive. Only few independent spectral peaks that were detected in monomicrobial cultures were also detected in polymicrobial cultures. This questions the consistency of detecting specific species across changing environments, including in a polymicrobial clinical sample. One *E. coli*, four *K. pneumoniae* and two *S. aureus* specific peaks were identified in polymicrobial cultures, with greater independent peaks detected from monomicrobial analysis. This constraint has been identified previously using surface enhanced Raman spectroscopy (SERS), with peak differences detected from independent culturing of *E. coli*, *K. pneumoniae*, *S. aureus* and *P. aeruginosa* compared to findings from polymicrobial communities of these species (Martinez *et al*, 2019). Low concordance between mono and polymicrobial spectral peaks could be explained by decreased peak resolution and a shift towards the most dominant bacteria (Martinez *et al*, 2019), or may be due to overlapping and accumulation of two closely related Raman peaks following the merging of spectral replicates, creating a non-specific peak to either independent bacteria (Larkin, 2011).

6.5.4 Peak intensity was related to bacterial concentration in *E. coli* and *K. pneumoniae*, suggesting the possibility of bacterial load quantification using Raman spectroscopy. However, this was not linear along dilutions or consistent across all bacteria studied, as dilution and intensity were not significantly correlated in *S. aureus.* Therefore, quantification may not be possible for all bacteria. Peak intensity may be related to other factors rather than bacterial concentration. Bacterial growth phase has previously been shown to impact spectral intensity (Hlaing *et al*, 2013), with choice of location for analysis within the droplet also impacting results due to bacterial heterogeneity (Butler *et al*, 2016; Cheong *et al*,

2017). Such variables remained consistent across analysis, nevertheless, further investigations over a broad range of bacteria and greater dilutions may improve findings. The intensity of only one Raman peak was correlated to dilutions, with investigation of more peaks required, which may include bacterial independent spectral peak analysis. Nevertheless, the ability to detect bacterial concentrations of 10^{-5} is a beneficial application of Raman spectroscopy to low biomass samples. However, only small staggered steps are performed between each laser measurement point (300 nm), so as long as one bacterial cell is present for the laser to focus on the Raman bacterial spectra can be created (Strola *et al*, 2014), thus not producing uniquely quantifiable findings.

6.5.5 Strengths and limitations of Raman spectroscopy

Low background noise was detected from stainless steel slides and LB culture media, indicating minimal external contribution to spectral peaks and increasing confidence that only genuine bacterial signals were measured. Thus, the washing and centrifuging steps performed prior to analysis remain important as previously advised (Hlaing *et al,* 2013). Integration of washing steps will be increasingly important in future investigations when bacteria may require different experimental conditions, as media-specific peaks independent of bacteria have been detected (Chauvet *et al*, 2017; de Siqueira E Oliveria, Giana and Silveira, 2012; Mlynarikova *et al*, 2015). However, only one culture media was used and monitored in this research so conclusions cannot be derived.

Three bacterial species were used in this research, thus universal application is limited. A greater spectral database is required prior to application on clinical samples. It would be beneficial to include multiple species from the same genus to determine species level resolution patterns. The use of Raman spectroscopy to resolve bacteria to strain level has successfully been observed in *E. coli*, yet heterogeneity across individual colonies were detected (Almarashi *et al*, 2012).
Polymicrobial droplets contained equal volumes and ratios of each bacterium, which may not be representative of a clinical environment, where one species may be of higher abundance, as seen from sequencing analysis earlier in this thesis. Thus further research investigating different ratios within polymicrobial combinations would be useful.

A selection of databases and published research were used as references to determine peak assignment, as standard for the majority of Raman spectroscopy studies (Larkin, 2011; Movasaghi, Rehman and Rehman, 2007). Due to the current lack of SOPs and standardised protocols, different methodologies are conducted and may impact comparison between findings.

The sensitivity and specificity of Raman results would need to be analysed further, as peak differences were sometimes only +/- one cm^{-1} shift different between individual bacteria or when moving from mono to polymicrobial cultures. A shift may not impact results if the peak is assigned to the same product, for example if a spectral range covers the same biological structure. Whereas an impact will be seen if the shift causes a change in band assignment product. This raises uncertainty of independent distinction between bacteria when using the unsupervised assignment method. It would have been optimum to compare peaks to a reference database specific to the instrument and protocol used in this research, which would contain all relevant compounds biologically assigned here, to improve accuracy of peak assignment. However, this would require analysis of an infinite number of bacteria, clinical samples and reagents to ensure that all aspects were covered. This exceeds the scope of this thesis, requiring multiple operators, increased cost and extensive application time. Thus only databases presenting protocols with similar instrumentation and processing steps were used for comparison.

6.5.6 Future research and applications of Raman spectroscopy

The rapid, non-destructive, label free mechanism of Raman spectroscopy could be utilised to detect and determine bacterial presence on clinical samples in a quicker and more efficient way than achieved by current methods, which require the application of multiple methodologies to generate comparable results. Clinical material may add additional challenges to Raman spectroscopy due to greater confounding variables impacting signal intensity. Multiple methods have been developed to enhance the Raman signal, including SERS which utilises a metallic nanoparticle covered surface for bacterial adhesion to increase detection, sensitivity and improve band resolution (Chauvet *et al*, 2017; Cheong *et al*, 2017; Li *et al*, 2018). Application would require additional processing steps, resources, time and instrumentation, reducing comparison to current findings but enhancing clinical application.

Investigating the spectral fingerprint of bacteria *in vitro* is important, but culture methodologies offer limited application to the clinical setting due to differing conditions and without the further impact of the biological tissue on spectral output. Protocol optimisation on clinical samples would be required to investigate tissue autofluorescence, which may conceal genuine Raman signals (Butler *et al*, 2016). Before applying Raman spectroscopy to clinical samples, clinically relevant bacteria could be spiked into tissue samples to create a new database for clinical reference. Raman spectroscopy and sequencing technology could be combined to increase the understanding of clinically relevant microorganisms. Previous sequencing results could inform of the highly abundant or clinically relevant bacteria to be targets of interest within Raman protocols. This could include *Prevotella*, *Ureaplasma* or *Escherichia* in HCA research as detected in Chapter three. Combined application could decrease the time and increase the accuracy of bacterial identification and infection diagnosis.

Application to medically relevant conditions including pre-eclampsia (Chen *et al*, 2014), detection of preterm birth (O'Brien *et al*, 2014) and monitoring placental molecular structure throughout pregnancy (Pielesz *et al*, 2019) have previously been researched, presenting a sensible basis for future fetal membrane research. In relation to previous work explored in this thesis, the application of Raman spectroscopy to fetal membranes with HCA may be beneficial to improve point of care diagnosis. This research has detected an increase in bacterial load from patients with HCA (Chapter five), yet confirmation of bacterial presence and identification would be beneficial without the impact of processing contaminants. A database of clinically relevant HCA bacteria, including *Prevotella* and *Ureaplasma* would be required prior to application. A label free non-destructive method for HCA is increasingly important due to the low biomass characteristics of the fetal membranes. The benefit of decreased processing requirements and limited external bacterial contribution in Raman analysis would enhance genuine bacterial detection in fetal membranes.

Raman microspectroscopy combines the use of spectroscopy and confocal microscopy to map bacterial spatial location on the tissue of interest. This novel application could be applied to samples used in this research to understand the spatial location of bacteria on the amnion and chorion in HCA, to increase understanding of the inflammatory response, plus initiation and progression of the

condition. However, findings here suggest extensive additional *in vitro* research is required prior to transferring into a clinical setting.

6.6 Conclusion

Bacterial presence can be detected by a prominent Raman spectral peak at 1003 cm^{-1}. Characteristic Raman peaks relevant to specific bacterial characteristics including Gram status were identified. Raman spectroscopy can identify concentrations of 10^{-5} bacteria. Application to low biomass clinical samples would require further research and optimisation of techniques, as quantitative analysis, and bacterial discrimination in polymicrobial cultures is inconclusive.

Chapter Seven: Discussion and concluding remarks.

7.1 Research project aims

Histological chorioamnionitis (HCA) impacts up to 30% of preterm births (Kim *et al,* 2015), with links to early life complications of morbidity and mortality, including early onset sepsis and necrotising enterocolitis (Strunk *et al*, 2018; Taft *et al*, 2015). Although advances have been made in understanding the fetal membrane microbiota in chorioamnionitis (Prince *et al*, 2016; Sweeney *et al*, 2016), key redundant areas remain to be investigated.

This research project aimed to increase current knowledge and understanding of the fetal membrane microbiota via multiple technologies. With specific aims;

- To investigate the microbiota of the amnion and chorion from HCA patients and compare these to preterm and term birth without HCA, via Illumina amplicon sequencing (Chapter three).
- To determine if bacteria can be detected from low risk term fetal membranes by probe based quantitative polymerase chain reaction (qPCR), plus to clarify and confirm bacterial signals on the fetal membranes with and without HCA (Chapter five).
- To further understand bacterial load levels in an inflammatory condition by investigating the link between bacterial load and HCA severity or inflammatory markers via probe based qPCR (Chapter five).

For clinical optimisation, research aimed;

- To determine if Formalin-Fixed Paraffin-Embedded (FFPE) fetal membrane samples are comparable to frozen membranes in DNA quantity and microbiota. Plus, to determine if these readily available, collected and archived samples could be utilised in microbiota research for reduced cost, storage and processing impact (Chapter four).
- To investigate if Raman spectroscopy can identify individual bacteria in low biomass mono and polymicrobial cultures. Plus, to understand the potential application of this method to clinical samples (Chapter six).

7.2 Summary of key findings

This thesis indicates the involvement of bacterial infection and bacterial load in inflammatory HCA of the fetal membranes.

Findings indicate that greater bacterial load is positively correlated to increased histological inflammation and inflammatory markers, with bacterial activation of the inflammatory pathway via a dose dependent response (Chapter five). Microbiota analysis suggests that HCA samples have a distinct bacterial profile, with a trend for increased *Prevotella* on the fetal membranes in higher grade HCA (Chapter three). Bacterial abundance and load increase on the fetal membranes with increasing HCA inflammation (Chapter three and chapter five). All indicating that HCA is a bacterial related inflammatory condition.

Findings support the theory of low microbial presence in non-complicated fetal membranes due to no distinct bacterial load identified from low risk term or non-HCA preterm or term patients (Chapter five). With increased likelihood of detecting a bacterial signal from negative controls (Chapter five). This supports the sterile placenta theory and suggests that bacteria are not acquired on healthy fetal membranes *in utero* or during labour and delivery, unless an inflammatory related condition is present.

FFPE and frozen fetal membrane samples were not of comparable quality due to high contamination levels and decreased DNA quality and quantity from FFPE samples (Chapter four). FFPE and frozen samples also displayed distinctly different bacterial profiles across matched paired analysis (Chapter four). The high level of contamination, low DNA quality and minimal concordance with frozen tissues questions the genuine representation of the fetal membrane. Thus it is not recommended to replace frozen fetal membrane samples with FFPE samples for microbiota analysis.

The novel Raman spectroscopy technique identified bacteria by one specific Raman peak, with functionally relevant peaks detected in respective bacteria (Chapter six). Further optimisation of bacterial discrimination in polymicrobial conditions and the quantitative ability of Raman spectroscopy is required prior to application on low biomass clinical samples.

7.3 Strengths and limitations

All samples used in this research were collected from one hospital and one delivery unit, with HCA assessed by the same clinicians to reduce variation and increase consistency of sample handling. All samples from the HCA cohort study displayed progressive labour, limiting sample variation. However, external factors such as health status prior to and during pregnancy may impact findings but could not be analysed.

A 24-patient sample set was utilised within this research project. A larger sample cohort would have strengthened findings and cover greater heterogeneity of the maternal and fetal response, though the low incidence of early preterm birth and HCA is a recognised problem in this field of research.

HCA is asymptomatic in two thirds of cases (Redline *et al*, 2003), but clinical signs were variable between HCA and PTB patients here. This included increased white blood cell count (WBC), and C-reactive protein (CRP) levels, all independent of gestational age. These characteristics are linked to inflammation and potential markers for HCA diagnosis. Increased CRP has been detected from chorioamnionitis (Nair, Ramachandran and Joseph, 2018) and microbial invasion of the amniotic cavity (Musilova *et al*, 2015). However, the predictive value of CRP for HCA has been criticised due to low specificity and sensitivity to the condition (Erdemir *et al*, 2013). Spontaneous labour has also been related to an increase in these characteristics, due to active labour as an inflammatory process (Roberts *et al*, 2012). It remains of interest to continue monitoring clinical signs related to HCA, due to the possible link to inflammatory factor gene expression (Waring *et al*, 2015).

Sample collection was established in 2013, yet optimised guidelines for placental sample collection were not published until after collection (Burton *et al*, 2014; Roberts *et al*, 2019). Future research would ensure implementation of suggested guidelines to improve reliability and reproducibility. This could include immediate snap freezing and processing of the samples, or quadrant biopsy sampling to represent multiple membrane locations (Roberts *et al*, 2019). This would avoid multiple freeze-thaw cycles of large tissue segments (Burton *et al*, 2014), which impacts the microbiota following four plus freeze-thaw cycles (Cuthbertson *et al*, 2015). Additional parturition characteristics could also be recorded, including

duration of labour, as this impacts the opportunity for ascending bacteria (Burton *et al*, 2014).

This research analysed bacterial presence within the amnion and chorion individually. The two fused membranes are independently functioning units with diverse cellular characteristics and properties (Park *et al*, 2009), plus demonstrate different inflammatory response patterns (Kallapur *et al*, 2001). Thus, microbiota characteristics and HCA development may differ. Independent membrane results are important to establish a timeline of bacterial location, inflammatory response progression, origin of bacteria and initiation of HCA. Research focusing on the fetal membranes as a combined entity will not capture the complexity of the individual membranes, thus individual study of the amnion and chorion is recommended. Due to clinical limitations this is not always possible, as noted in this research, as for a subset of patients only amnion or chorion were available, which could bias results and is a known limitation of human tissue collection.

The absence of a known healthy fetal membrane microbiota complicates the ability to determine a microbiota linked to HCA, as no baseline is available for comparison. Fetal membranes without HCA from preterm and term labour are required for within study comparisons, as incorporated into this research. A positive control could have strengthened findings, for example comparable tissue samples spiked at known concentrations with a tissue specific microorganism. As the fetal membrane microbiota is not yet determined, it was not possible to confidently select and include a positive spiked control within this research.

The histological threshold for HCA was set at stage two inflammatory response, due to the accepted reproducible diagnostic criteria (Redline *et al*, 2003). However, only one HCA patient was diagnosed at stage three, limiting conclusions at this level. Excluding stage one subchorionitis from the HCA subset ensures specificity to HCA. Other studies may have included stage one leading to different conclusions of infection and inflammation in HCA.

Bacterial origin cannot be determined in this project as only fetal membrane samples were analysed. Bacteria found in the fetal membranes, including *Ureaplasma* and *Prevotella* have previously been detected in the vaginal microbiota (Doyle *et al*, 2017). Ascending bacteria from the vaginal and lower female reproductive tract could be the possible route of transfer (Doyle *et al*, 2017). Also supported by Brown

et al (2018), detecting *Prevotella* in the vagina, prior to delivery, and the placenta postpartum when chorioamnionitis was present. An alternative route of haematogenous translocation from the oral cavity has been suggested (Fardini *et al*, 2010), due to simultaneous detection of *Prevotella* in the oral cavity and placental membranes (McCuaig *et al*, 2018). In contrast, bacterial contamination of low biomass placenta and fetal membrane samples is also a recognised theory (Leiby *et al*, 2018). The inclusion of vaginal, oral, skin and blood samples would allow greater understanding of the source of bacteria in this research and allow further investigation into the link between reproductive, placental and fetal membrane health.

Longitudinal monitoring of the membranes prior to, during and after development of HCA is not possible. This would be beneficial to determine time of onset for the condition and bacterial pathway. However, the study of fetal membranes throughout gestation is invasive and unethical, with potential harm caused to both maternal and fetal health (Monastero and Pentyala, 2017). Amniotic fluid collected during amniocentesis may be the most representative sample (Jung *et al,* 2010), however the specificity and sensitivity to chorioamnionitis is limited (Lee *et al*, 2018; Monastero and Pentyala, 2017).
Bacterial load and presence in the fetal membranes may be transient throughout gestation, as seen with the lower female reproductive tract (MacIntyre *et al*, 2015). When assessed postpartum, the causal microorganisms could have been eradicated or relocated, thus not detected, as the microbiota and health are not static variables (Stinson, Keelan and Payne, 2018a). This problem impacts a wide variety of pregnancy related conditions, including HCA, increasing the importance of rapid and accurate diagnosis postpartum.

The combination of multiple methodologies, including Illumina sequencing and qPCR used in this research creates a broad view of HCA, increasing accuracy and reliability of findings. Complementary primers were applied across methods, with the V4 16S rRNA gene region used in qPCR matching the target for sequencing analysis. Sequencing provides reliable information to distinguish bacterial sequences to the genus level, with qPCR displaying increased accuracy for bacterial load measurements (Kim *et al*, 2017). Recent research has modified the BactQuant primer pair used in qPCR to increase sequence coverage (Rehbinder *et al*, 2018).

As the modified protocol was published after this research was conducted, the improved primers were not applied here but may be beneficial to investigate in future research.

DADA2 post-processing used amplicon sequence variants (ASVs) rather than operational taxonomic units (OTUs; Callahan *et al*, 2016b). OTUs accumulate sequences into distinct groups, as sequences are mapped with 97% similarity to reference sequences (Kozich *et al*, 2013). In comparison, ASVs detect and cluster by one nucleotide variation, increasing sensitivity (Callahan, McMurdie and Holmes, 2017).

Fetal membrane research receives criticism due to low biomass samples and low bacterial abundance (Glassing *et al*, 2016). In low biomass samples external contamination can be increasingly mistaken for a true microbiota (Stinson, Keelan and Payne, 2018a). To minimise this, negative controls from DNA extraction kits, sequencing negatives and qPCR reagents, plus an independent subset of healthy controls were included and compared to samples to determine a baseline. Incorporating decontam into FFPE microbiota analysis was an additional beneficial method to identify contaminating bacterial sequences in fetal membranes relative to negative controls in this research. This allows detection at the data analysis stage, but integration of further pre-processing steps may minimise initial contamination, including PCR decontamination kits (Stinson, Keelan and Payne, 2018a).

7.4 Future research

Although conclusions have been presented and discussed, further research would be required to allow application and integration into clinical settings. Future research would include, but is not limited to the following suggestions.

Further enhancements to research methodology may include combining species-specific targeted primers with universal 16S rRNA gene qPCR (Brukner *et al*, 2015), to measure the bacterial load of target species of interest highlighted in sequencing analysis. The bacterial load threshold required to trigger an inflammatory response also warrants investigation. Cultured primary fetal membrane explants could be stimulated with bacteria across variable doses and time points to assess the inflammatory response. This could also investigate selected inflammatory factors as potential biomarkers for HCA, including Toll-like receptor (TLR) signalling mediators.

A limitation of qPCR is the inability to select for viable metabolically active bacteria, as both viable and non-viable bacteria are amplified. To overcome this limitation PMA qPCR can be performed (Richardson *et al*, 2017). Propidium monoazide (PMA) is an impermeable dye which intercalates and covalently binds genomic DNA to inhibit amplification of non-viable bacteria during PCR (Richardson *et al*, 2017). This only occurs within a compromised cell membrane, and will not penetrate intact cell membranes, thus distinguishing between viable, metabolically active and non-viable, non-metabolically active bacteria (Richardson *et al*, 2017). This method has shown to improve diversity evenness for rare community members (Rogers *et al*, 2013) and remove sequencing bias (Young *et al*, 2017). This would be informative for HCA analysis, but also for investigation between negative controls and non-HCA samples. The bacterial load levels did not differ between non-HCA tissues and negative controls, but the proportion of viable bacteria may differ and be an interesting and valuable insight.

The collection and comparison of multiple body site samples to understand external bacterial contribution and enhance negative control comparison could include vaginal, oral, skin, amniotic fluid and neonatal samples analysed via sequencing to investigate bacterial origin correlating to fetal membranes. Plus, sequencing analysis of environmental samples and swabs taken from clinical locations within the hospital, and also from laboratories used for extraction and experimentation (Leiby *et al*, 2018). Also, additional neonatal samples would allow investigation of the fetal response to HCA, including fetal inflammatory response syndrome (Park *et al*, 2009). This would also provide information of bacterial translocation across the fetal membranes and placenta to the fetus, exploring negative clinical outcomes relative to bacterial load and HCA inflammation.

Potential application of Raman spectroscopy for bacterial detection in clinical tissues has been presented, however further investigation is required prior to integration into the clinical setting. Current questions including the ability to discriminate individual bacteria in a polymicrobial environment, plus the quantitative capability of Raman spectroscopy needs to be addressed. Currently, no standardised protocols or procedures are available for the inVia Raman instrument. Developing a universally applicable protocol for bacterial detection, preparation and processing parameters would be beneficial to ensure standardised use across research, but

also across the clinical setting. Expanding the initial spectroscopy reference dataset created here would be required to cover all clinically relevant bacteria, polymicrobial combinations, ratios and concentrations. This would be important prior to application on clinical samples to ensure relevance, confidence in detection and act as a reference point for diagnosis.

Applying advanced spectral imaging and mapping for visual location of bacteria on the fetal membranes with HCA could further improve diagnosis in a non-destructive manner. Current tissue and placental based research applies pattern recognition and spectral fingerprint analysis (Pielesz *et al*, 2019; Schlabritz-Loutsevitch *et al*, 2017). The future aim here would be to expand on this and investigate individual peaks of interest related to bacterial detection and visually map these onto the fetal membranes via Raman microspectroscopy.

7.5 Research implications and clinical relevance

Current research provides new insights into the contribution of bacterial load to HCA development and severity of maternal inflammation. Findings enhance existing knowledge of the relationship between infection and inflammation in HCA, aid in understanding the complexity of the fetal membrane response to immunological challenge, plus in the future aims to integrate novel diagnostic methods.

Although a linear relationship between bacterial load and HCA was detected here, the clinical threshold required to trigger the inflammatory response warrants investigation. Highlighted inflammatory markers, including TLR signalling mediators have the potential to be used as diagnostic biomarkers for HCA inflammatory response, yet further investigations into the sensitivity and specificity to HCA diagnosis are required prior to clinical application.

It has been historically assumed that the fetal membranes are sterile (Kovalovski *et al*, 1982), yet this research project shows that with an inflammatory condition, this is not the case. As bacterial loads were associated with inflammation levels in HCA, this could be transferred and investigated in other pregnancy related inflammatory conditions, including pre-eclampsia, preterm premature rupture of membranes (PPROM) or miscarriage. This research could also lead to questioning of other clinically relevant inflammatory conditions and locations otherwise assumed sterile, including acute pancreatitis (Hogue *et al*, 2012).

Beyond HCA, this findings suggests that bacteria may not be acquired on the fetal membranes *in utero* or during labour and delivery in low risk or non-HCA patients, indicating that bacteria are not the main initiator of non-inflammatory related parturition. Colonisation of low risk term neonates may be first acquired after labour from environmental sources, rather than *in utero*, unless an inflammatory related condition is present.

The continued collection and storage of placental and fetal membrane samples is imperative for continual research into HCA, fetal membrane microbiota and the inflammatory response. The World Health Organisation (WHO) developmental goals at the outset of this project included increased research to improve maternal health, plus improve pregnancy outcomes and the health of the mother, baby and child throughout life (WHO, 2015). To achieve these goals, further funding and research is required for the biobanking of underrepresented reproductive material.
It would be advised that fresh-frozen tissues are stored and analysed due to limitations from FFPE samples, as displayed in this thesis. Although application of FFPE tissues would benefit time, cost and resources, the extensive post-processing requirements, plus decreased quantity and quality of DNA make these samples unsuitable for microbiota research, but clinical investigations for HCA diagnosis should continue.

7.6 Conclusion

This thesis indicates that inflammation of the fetal membranes in HCA is associated with bacterial infection and increased bacterial load in a dose dependent manner. The severity of inflammation is positively correlated to bacterial load and activation of the TLR signalling pathway, but the threshold for activation is not yet known.
Non-HCA preterm and term, plus low risk term fetal membranes have indistinguishable low bacterial loads, suggesting minimal bacterial presence on healthy fetal membranes without an inflammatory related condition.
Frozen samples remain the current gold standard for microbiota research. Novel application of Raman spectroscopy to improve current detection and diagnosis of bacterial presence linked to HCA may be possible with further research and optimisation.

References

Aagaard, K., Ma, J., Antony, K.M., Ganu, R., Petrosino, J. and Versalovic, J. (2014) 'The placenta harbours a unique microbiome'. *Science Translational Medicine*, 6 (237) pp. 237ra65 DOI: 10.1126/scitranslmed.3008599.

Aagaard-Tillery, K.M., Silver, R. and Dalton, J. (2006) 'Immunology of normal pregnancy'. *Seminars in Fetal and Neonatal Medicine*, 11 (5) pp. 279-295.

Aaltonen, R., Heikkinen, B.J., Vahlberg, T., Jensen, J.S. and Alanen, A. (2007) 'Local inflammatory response in choriodecidua induced by *Ureaplasma urealyticum'. British Journal of Obstetrics and Gynaecology*, 114 (11) pp. 1432-1435.

Agilent Technologies (2014) '*Agilent 2100 Bioanalyzer System: Applications for DNA, RNA, Protein and Cell Analysis*'. [Online] Available at: http://hpst.cz/sites/default/files/attachments/agilent-2200-tapestation-system-application-compendium_1.pdf (Accessed: 22 March 2017).

Al-Attas, A., Assidi, M., Al-Maghrabi, J., Dallol, A., Schulten, H-J., Abu-Elmagd, M., Chaudhary, A., Abuzenadah, A., Budowle, B., Buhmeida, A. and Al-Qahtani, M. (2016) 'Enhancement of pathologist's routine practice: Reuse of DNA extracted from immunostained Formalin-Fixed Paraffin-Embedded (FFPE) slides in downstream molecular analysis of cancer'. *Cancer Genomics & Proteomics*, 13 (5) pp. 399-406.

Almarashi, J.F.M., Kapel, N., Wilkinson, T.S. and Telle, H.H. (2012) 'Raman spectroscopy of bacterial species and strains cultivated under reproducible conditions'. *Journal of Spectroscopy*, 27 (5) pp. 361-365.

Apgar, V. (1953) 'A proposal for a new method of evaluation of the newborn infant'. *Current Researches in Anaesthesia and Analgesia*, 7 (32) pp. 250-259.

Aroutcheva, A., Ling, Z. and Faro, S. (2008) '*Prevotella bivia* as a source of lipopolysaccharide in the vagina'. *Anaerobe*, 14 (5) pp. 256-260.

Arreaza, G., Qiu, P., Pang, L., Albright, A., Hong, L.Z., Marton, M.J. and Levitan, D. (2016) 'Pre-analytical considerations for successful next-generation sequencing (NGS): Challenges and opportunities for Formalin-Fixed and Paraffin-Embedded tumor tissue (FFPE) samples'. *International Journal of Medical Sciences,* 17 (9) DOI: 10.339/ijms17091579.

Ashton, L., Lau, K., Winder, C.L. and Goodacre, R. (2011) 'Raman spectroscopy: Lighting up the future of microbial identification'. *Future Microbiology*, 6 (9) pp. 991-997.

Ategeka, J., Wasswa, R., Olwoch, P., Kakuru, A., Natureeba, P., Muehlenbachs, A., Kamya, M.R., Dorsey, G. and Rizzuto, G. (2019) 'The prevalence of histological acute chorioamnionitis among HIV infected pregnant women in Uganda and its association with adverse birth outcomes'. *PLoS One*, 14 (4) e0215058.

Badri, M., Kurtz, Z., Muller, C. and Bonneau, R. (2018) 'Normalisation methods for microbial abundance data strongly affects correlation estimates'. *bioRxiv* [Preprint] Available at: https://www.biorxiv.org/content/10.1101/406264v1.full (Accessed: 10 January 2019).

Bassols, J., Serino, M., Carreras-Badosa, G., Burcelin, R., Blasco-Baque, V., Lopez-Bermejo, A. and Fernandez-Real, J-M. (2016) 'Gestational diabetes is associated with changes in placental microbiota and microbiome'. *Paediatric Research*, 80 (6) pp. 777-784.

Bearfield, C., Davenport, E.S., Sivapathasundaram, V. and Allaker, R.P. (2002) 'Possible association between amniotic fluid micro-organism infection and microflora in the mouth'. *British Journal of Obstetrics and Gynaecology*, 109 (5) pp. 527-533.

Becroft, D.M.O., Thompson, J.M.D. and Mitchell, E.A. (2012) 'Placental chorioamnionitis at term: Epidemiology and follow-up in childhood'. *Pediatric and Developmental Pathology*, 13 (4) pp. 282-290.

Been, J.V., Lievense, S., Zimmermann, L.J.I., Kramer, B.W. and Wolfs, T.G.A.M. (2013) 'Chorioamnionitis as a risk factor for necrotizing enterocolitis: A systematic review and meta-analysis'. *The Journal of Pediatrics*, 162 (2) pp. 236-242.

Belloni, B., Lambertini, C., Nuciforo, P., Phillips, J., Bruening, E., Wong, S. and Drummer, R. (2013) 'Will PAXgene substitute formalin? A morphological and molecular comparative study using a new fixative system'. *Journal of Clinical Pathology*, 66 (2) pp. 124-135.

Bennike, T.B., Kastaniegaard, K., Padurariu, S., Gaihede, M., Birkelund, S., Andersen, V. and Stensballe, A. (2016) 'Comparing the proteome of snap frozen, RNAlater preserved, and formalin-fixed paraffin-embedded human tissue samples'. *EuPA Open Proteomics*, 10 (3) pp 09-18.

Bentley, D.R., Balasubramanian, S., Swerdlow, H.P., Smith, G.P., Milton, J., Brown, C.G., Hall, K.P., Evers, D.J., Barnes, C.L., Bignell, H.R., Boutell, J.M., Bryant, J., Carter, R.J.,

Cheetham, R.K., Cox, A.J., Ellis, D.J., Flatbush, M.R., Gormley, N.A., Humphray, J., Irving, L.J., Karbelashvili, M.S., Kirk, S.M., Li, H., Liu, S., Maisinger, K.S., Murray, L.J., Obradovic, B., Ost, T., Parkinson, M.L., Pratt, M.R., Rasolonjatovo, I.M.J., Reed, M.T., Rigatti, R., Rodighiero, C., Ross, M.T., Sabot, A., Sankar, S.V., Scally, A., Schroth, G.P., Smith, M.E., Smith, V.P., Spiridou, A., Torrance, P.E., Tzonev, S.S., Vermaas, E.H., Walter, K., Wu, X., Zhang, L., Alam, M.D., Anastasi, C., Aniebo, I.C., Bailey, D.M.D., Bancarz, I.R., Banerjee, S., Barbour, S.G., Baybayan, P.A., Benoit, V.A., Benson, K.F., Bevis, C., Black, P.J., Boodhun, A., Brennan, J.S., Bridgham, J.A., Brown, R.C., Brown, A.A., Buermann, D.H., Bundu, A.A., Burrows, J.C., Carter, N.P., Castillo, N., Catenazzi, M.C.E., Chang, S., Cooley, R.N., Crake, N.R., Dada, O.O., Diakoumakos, K.D., Dominguez-Fernandez, B., Earnshaw, D.J., Egbujor, U.C., Elmore, D.W., Etchin, S.S., Ewan, M.R., Fedurco, M., Fraser, L.J., Fuentes Fajardo, K.V., Scott Furey, W., George, D., Gietzen, K.J., Goddard, C.P., Golda, G.S., Granieri, P.A., Green, D.E., Gustafson, D.L., Hansen, N.F., Harnish, K., Haudenschild, C.D., Heyer, N.I., Hims, M.M., Ho, J.T., Horgan, A.M., Hoschler, K., Hurwitz, S., Ivanov, D.V., Johnson, M.Q., James, T., Huw Jones, T.A., Kang, G-D., Kerelska, T.H., Kersey, A.D., Khrebtukova, I., Kindwall, A.P., Kingsbury, A., Kokko-Gonzales, P.I., Kumar, A., Laurent, M.A., Lawley, C.T., Lee, S.E., Lee, X., Liao, A.K., Loch, J.A., Lok, M., Luo, S., Mammen, R.M., Martin, J.W., McCauley, P.G., McNitt, P., Mehta, P., Moon, K.W., Mullens, J.W., Newington, T., Ning, Z., Ling Ng, B., Novo, S.M., O'Neill, M.J., Osborne, M.A., Osnowski, A., Ostadan, O., Paraschos, L.L., Pickering, L., Pike, A.C., Pike, A.C., Pinkard, D.C., Pliskin, D.P., Podhasky, J., Quijano, V.J., Raczy, C., Rae, V.H., Rawlings, S.R., Rodriguez, A.C., Roe, P.M., Rogers, J., Rogert Bacigalupo, M.C., Romanov, N., Romieu, A., Roth, R.K., Rourke, N.J., Ruediger, S.T., Rusman, E., Sanches-Kuiper, R.M., Schenker, M.R., Seoane, J.M., Shaw, R.J., Shiver, M.K., Short, S.W., Sizto, N.L., Sluis, J.P., Smith, M.A., Sohna, J.E.S., Spence, E.J., Stevens, K., Sutton, N., Szajkowski, L., Tregidgo, K.L., Turcatti, G., vandeVondele, S., Verhovsky, Y., Virk, S.M., Wakelin, S., Walcott, G.C., Wang, J., Worsley, G.J., Yan, J., Yau, L., Zuerlein, M., Rogers, J., Mullikin, J.C., Hurles, M.E., McCooke, N.J., West, J.S., Oaks, F.L., Lundberg, P.L., Klenerman, D., Durbin R. and Smith, A.J. (2008) 'Accurate whole human genome sequencing using reversible terminator chemistry'. *Nature*, 465 (7218) pp. 53-59.

Berg, D., Malinowsky, K., Reischauer, B., Wolff, C. and Becker, K.F. (2011) 'Use of formalin-fixed and paraffin-embedded tissue for diagnosis and therapy in routine clinical settings'. *Methods in Molecular Biology*, 785 pp. 109-122.

Biesbroek, G., Sander, E.A.M., Roeselers, G., Wang, X., Caspers, M.P.M., Tezcinski, K., Bogaert, D. and Keijser, B.J.F. (2012) 'Deep sequencing analyses of low-density microbial communities: Working at the boundary of accurate microbiota detection'. *PLoS One*, 7 (3) e32942 DOI: 10.1371/journal.pone.0032942.

Bilen, M., Dufour, J-C., Lagier, J-C., Cadoret, F., Daoud, Z., Dubourg, G. and Raoult, D. (2018) 'The contribution of culturomics to the repertoire of isolated human bacterial and archaeal species'. *Microbiome*, 6 (94) DOI: 10.1186/s40168-018-0485-5.

Blanc, W.A. (1980) 'Pathology of the placenta and cord in ascending and in haematogenous infection'. *Perinatal infections,* 77 (3) pp. 17-38.

Blencowe, H., Cousens, S., Oestergaard, M.Z., Chou, D., Moller, A-B., Narwal, R., Adler, A., Garcia, C.V., Rohde, S., Say, L. and Lawn, J.E. (2012) 'National, regional, and worldwide estimates of preterm birth rates in the year 2010 with time trends since 1990 for selected countries: A systematic analysis and implications'. *The Lancet*, 379 (9832) pp. 2162-2167.

Bocklitz, T., Brautigam, K., Urbanek, A., Hoffmann, F., von Eggeling, F., Ernst, G., Schmitt, M., Schubert, U., Guntinas-Lichius, O. and Popp, J. (2015) 'Novel workflow for combining Raman spectroscopy and MALDI-MSI for tissue based studies'. *Analytical and Bioanalytical Chemistry*, 407 (26) pp. 7865-7873.

Bokulich, N.A., Subramanian, S., Faith, J.J., Gevers, D., Gordon, J.I., Knight, R., Mills, D.A. and Caporaso, J.G. (2013) 'Quality-filtering vastly improves diversity estimates from Illumina amplicon sequencing'. *Nature Methods,* 10 (1) pp. 57-59.

Bourne, G. (1962) 'The foetal membranes: A review of the anatomy of normal amnion and chorion and some aspects of their function'. *Postgraduate Medical Journal,* 38 (438) pp. 193-201.

Brown, R.G., Marchesi, J.R., Lee, Y.S., Smith, A., Lehne, B., Kindinger, L.M., Terzidou, V., Holmes, E., Nicholson, J.K., Bennet, P.R. and MacIntyre, D.A. (2018) 'Vaginal dysbiosis increases risk of preterm fetal membrane rupture, neonatal sepsis and is exacerbated by erythromycin'. *BMC Medicine*, 16 (1) DOI: 10.1186/s12916-017-0999-x.

Brukner, I., Longtin, Y., Oughton, M., Forgetta, V. and Dascal, A. (2015) 'Assay for estimating total bacterial load: Relative qPCR normalisation of bacterial load with associated clinical implications'. *Diagnostic Microbiology and Infectious Disease*, 83 (1) DOI: 10.1016/j.diagmicrobio.2015.04.005.

Buermans, H.P.J. and den Dunnen, J.T. (2014) 'Next generation sequencing technology: Advances and applications'. *Molecular Basis of Disease*, 1842 (10) pp. 1932-1941.

Burton, G.J., Sebire, N.J., Myatt, L., Tannetta, D., Wang, Y-L., Sadovsky, Y., Staff, A.C. and Redman, C.W. (2014) 'Optimising sample collection for placental research'. *Placenta*, 35 (1) pp. 09-22.

Bustin, S.A. (2010) 'Why the need for qPCR publication guidelines?- The case for MIQE'. *Methods*, 50 (4) pp. 217-226.

Bustin, S.A., Benes, V., Garson, J.A., Hellemans, J., Huggett, J., Kubista, M., Mueller, R., Nolan, T., Pfaffl, M.W., Shipley, G.L., Vandersompele, J. and Wittwer, C.T. (2009) 'The MIQE guidelines: Minimum Information for publication of Quantitative real-time PCR Experiments'. *Clinical Chemistry*, 55 (4) pp. 611-622.

Butler, H.J., Ashton, L., Bird, B., Cinque, G., Curtis, K., Dorney, J., Esomde-White, K., Fullwood, N.J., Gardner, B., Martin-Hirsch, P.L., Walsh, M.J., McAnish, M.R., Stone, N. and Martin, F.L. (2016) 'Using Raman spectroscopy to characterize biological material'. *Nature Protocols*, 11 (4) pp. 664-687.

Callahan, B. (2016). 'The RDP and GreenGenes taxonomic training data formatted for DADA2' [Data set]. *Zenodo* Available at: http://doi.org/10.5281/zenodo.1589554.

Callahan, B.J., Sankaran, K., Fukuyama, J.A., McMurdie, P.J. and Holmes, S.P. (2016a) 'Bioconductor workflow for microbiome data analysis: from raw reads to community analyses [Version 2]'. *F1000Research*, 5 (1492) DOI: 10.12688/F1000research.8986.2.

Callahan, B.J., McMurdie, P.J., Rosen, M.J., Han, A.W., Johnson, A.J.A. and Holmes, S.P. (2016b) 'DADA2: High resolution sample inference from Illumina amplicon data'. *Nature Methods*, 13 (7) pp. 581-583.

Callahan, B.J., McMurdie, P.J. and Holmes, S.P. (2017) 'Exact sequence variants should replace operational taxonomic units in marker-gene data analysis'. *ISME Journal*, 11 (12) pp. 2639-2643.

Canzoneri, B.J., Feng, L., Grotegut, C.A., Bentley, R.C., Heine, R.P. and Murtha, A.P. (2013) 'The chorion layer of fetal membranes is prematurely destroyed in women with preterm premature rupture of the membranes'. *Reproductive sciences*, 20 (10) pp. 1246-1254.

Caporaso, J.G., Lauber, C.L., Walters, W.A., Berg-Lyons, D., Huntley, J., Fierer, N., Owens, S.M., Betley, J., Fraser, L., Bauer, M., Gormlet, N., Gilbert, J.A., Smith, G. and Knight, R.

(2012) ‘Ultra-high-throughput microbial community analysis on the Illumina HiSeq and MiSeq platforms’. *International Society for Microbial Ecology*, 6 (8) pp. 1621-1624.

Carrick, D.M., Mehaffey, M.G., Sachs, M.C., Altekruse, S., Camalier, C., Chuaqui, R., Cozen, W., Das, B., Hernandez, B.Y., Lih, C-J., Lynch, C.F., Makhlouf, H., McGregor, P., McShane, L.M., Rohan, J.P., Walsh, W.D., Williams, P.M., Gillanders, E.M., Mechanic, L.E. and Schully, S.D. (2015) ‘Robustness of Next Generation Sequencing on older Formalin-Fixed Paraffin-Embedded tissue’. *PLoS One*, 10 (7) e0127353 DOI: 10.1371/journal.pone.0127353.

Casey, B.M., McIntire, D.D. and Leveno, K.J. (2001) ‘The continuing value of the Apgar score for the assessment of newborn infants’. *New England Journal of Medicine*, 344 (7) pp. 467-471.

Catano Sabogala, P.C., Fonseca, J. and Garcia-Perdomo, H.A. (2018) ‘Validation of diagnostic tests for histological chorioamnionitis: Systematic review and meta-analysis’. *European Journal of Obstetrics and Gynecology and Reproductive Biology*, 228 (9) pp. 13-26.

Chan, G.J., Silverman, M., Saman, M., Murillo-Chaves, A., Mahmud, A., Baqui, A.H. and Boyd, T.K. (2016) ‘Prevalence and risk factors of chorioamnionitis in Dhaka, Bangladesh’. *Journal of Perinatology*, 36 (9) pp. 1039-1044.

Chauvet, R., Lagarde, F., Charrier, T., Assaf, A., Thouand, G. and Daniel, P. (2017) ‘Microbiological identification by surface-enhanced Raman spectroscopy’. *Applied Spectroscopy Reviews*, 52 (2) DOI: 10.1080/05704928.2016.1209760.

Chen, S-J., Zhang, Y., Ye, Z-P., Hu, K., Zhu, M-F., Hunag, Y-Y., Zhong, M. and Zhuang, Z-F. (2014) ‘Study of the molecular variation in pre-eclampsia placenta based on micro-Raman spectroscopy’. *Archives of Gynecology and Obstetrics*, 290 (5) pp. 943-946.

Cheong, Y., Kim, Y.J., Kang, H., Choi, S. and Lee, H.J. (2016) ‘Label-free identification of antibiotic resistant isolates of living *Escherichia coli*: Pilot study’. *Microscopy Research and Technique*, 8 (2) pp. 177-182.

Cheong, Y., Kim, Y.J., Kang, H., Choi, S. and Lee, H.J. (2017) ‘Rapid label-free identification *of Klebsiella pneumoniae* antibiotic resistant strains by the drop-coating deposition surface-enhanced Raman scattering method’. *Spectrochimica Acta Part A: Molecular and Biomolecular Spectroscopy*, 183 (8) pp. 53-59.

Clooney, A.G., Fouhy, F., Sleator, R.D., O'Driscoll, A., Stanton, C., Cotter, P.D. and Claesson, M.J. (2016) 'Comparing apples and oranges?: Next Generation Sequencing and its impact on microbiome analysis'. *PLoS One*, 11 (2) e0148028 DOI: 10.1371/journal.pone.0148028.

Cobo, T., Kacerovsky, M. and Jacobsson, B. (2017) 'Noninvasive sampling of the intrauterine environment in women with preterm labor and intact membranes'. *Fetal Diagnosis and Therapy*, 43 (4) pp. 241-249.

Coudry, R.A., Meireles, S.I., Stoyanova, R., Cooper, H.S., Carpino, A., Wang, X., Engstrom, P.F. and Clapper, M.L. (2007) 'Successful application of microarray technology to microdissected Formalin-Fixed, Paraffin-Embedded tissue'. *Journal of Molecular Diagnostics*, 9 (1) pp. 70-79.

Cox, C., Saxena, N., Watt, A.P., Gannon, C., McKenna, J.P., Fairlet, D.J., Sweet, D., Shields, M.D., Cosby, S.L. and Coyle, P.V. (2016) 'The common vaginal commensal bacterium *Ureaplasma parvum* is associated with chorioamnionitis in extreme preterm labor'. *The Journal of Maternal-Fetal & Neonatal Medicine'*. 29 (22) pp. 3646-3651.

Cuthbertson, L., Rogers, G.B., Walker, A.W., Oliver, A., Hoffman, L.R., Carroll, M.P., Parkhill, J., Bruce, K.D. and van der Gast, C.J. (2015) 'Implications of multiple freeze-thawing on respiratory samples for culture-independent analyses'. *Journal of Cystic Fibrosis*, 14 (4) pp. 464-467.

Czikk, M.J., McCarthy, F.P. and Murphy, K.E. (2011) 'Chorioamnionitis: From pathogenesis to treatment'. *Clinical Microbiology and Infection*, 17 (9) pp. 1304-1311.

Davis, N.M., Proctor, D., Homles, S.P., Relman, D.A. and Callagan, B.J. (2018) 'Simple statistical identification and removal of contaminant sequences in marker-gene and metagenomics data'. *Microbiome*, 6 (226) DOI: 10.1186/s40168-018-0605-2.

de Gelder, J., de Gussem, K., Vandenabeele, P. and Moens, L. (2007) 'Reference database of Raman spectra of biological molecules'. *Journal of Raman Spectroscopy*, 38 (4) pp. 1133-1147.

de Goffau, M.C., Lager, S., Salter, S.J., Wagner, J., Kronbichler, A., Charnock-Jones, D.S., Peacock, S.J., Smith, G.C.S. and Parkhill, J. (2018) 'Recognising the reagent microbiome'. *Nature Microbiology*, 3 (8) pp. 851-853.

de Goffau, M.C., Lager, S., Sovio, U., Gacciioli, D., Cook, E., Peackock, S.J., Parkhill, J., Charnock-Jones, D.S. and Smith, G.C.S. (2019) 'Human placenta has no microbiome but can contain potential pathogens'. *Nature*, 572 (7769) pp. 329-334.

de Siqueira E Oliveria, F.S., Giana, H.E. and Silveira, L. (2012) 'Discrimination of selected species of pathogenic bacteria using near-infrared Raman spectroscopy and principal component analysis'. *Journal of Biomedical Optics*, 17 (10) e107004 DOI: 10.1117/1.JBO.17.10.107004.

Decembrino, L., Pozzi, M., Falcone, R. and Stronati, M. (2014) 'Chorioamnionitis and neonatal outcome: Early vs late preterm infants'. *Italian Journal of Pediatrics*, 40 (S2) pp. A22 DOI: 10.1186/1824-7288-40-S2-A22.

Demeka, T. and Jenkins, R.G. (2009) 'Influence of DNA extraction methods, PCR inhibitors and quantification methods on real-time PCR assay of biotechnology-derived traits'. *Analytical and Bioanalytical Chemistry*, 369 (6) pp. 1977-1990.

Desjardins, P. and Conklin, D. (2010) 'NanoDrop microvolume quantitation of nucleic acids'. *Journal of Visual Experiments*, 2565 (45) DOI: 10.3791/2565.

Dhariwal, A., Chong, J., Habib, S., King, I.L., Agellon, L.B. and Xia, J. (2017) 'Microbiome Analyst: A web-based tool for comprehensive statistical, visual and meta-analysis of microbiome data'. *Nucleic Acid Research*, 45 (W1) pp. 180-188.

Di Naro, E., Ghezzi, F., Raio, L., Franchi, M. and D'Addario, V. (2001) 'Umbilical cord morphology and pregnancy outcome'. *European Journal of Obstetrics & Gynecology and Reproductive Biology*, 96 (2) pp. 150-157.

Dietrich, D., Uhl, B., Sailer, V., Holmes, E.E., Jung, M., Meller, S. and Kristiansen, G. (2013) 'Improved PCR performance using template DNA from Formalin-Fixed and Paraffin-Embedded tissues by overcoming PCR inhibition'. *PLoS One*, 8 (10) e77771 DOI: 10.1371/journal.pone.0077771.

DiGiulio, D.B., Romero, R., Amogan, H.P., Kusanovic, J.P., Bik, E.M., Gotsch, F., Kim, C.J., Erez, O., Edwin, S. and Relamn, D.A. (2008) 'Microbial prevalence, diversity and abundance in amniotic fluid during preterm labor: A molecular and culture-based investigation'. *PLoS One*, 3 (8) e3056 DOI: 10.1371/journal.pone.0003056.

Dominguez-Bello, M.G., Costello, E.K., Contreras, M., Magris, M., Hidalgo, G., Fierer, N. and Knight, R. (2010) 'Delivery mode shapes the acquisition and structure of the initial microbiota across multiple body habitats in newborns'. *Proceedings of the National Academy of Sciences of the United States of America*, 107 (26) pp. 11971-11975.

Donnelly, L. and Campling, G. (2019) 'Functions of the placenta'. *Anaesthesia and Intensive Care Medicine*, 20 (7) pp. 932-936.

Doyle, R.M., Alber, D.G., Jones, H.E., Harris, K., Fitzgerald, F., Peebles, D. and Klein, N. (2014) 'Term and preterm labour are associated with distinct microbial community structures in placental membranes which are independent of mode of delivery'. *Placenta*, 35 (12) pp. 1099-1101.

Doyle, R.M., Harris, K., Kamiza, S., Hrjunmaa, U., Ashorn, U., Nkhoma, M., Dewey, K.G., Maleta, K., Ashorn, P. and Klein, N. (2017) 'Bacterial communities found in placental tissues are associated with severe chorioamnionitis and adverse birth outcomes'. *PLoS One*, 12 (7) e0180167 DOI: 10.1371/journal.pone.0180167.

Dudzik, D., Revello, R., Barbas, C. and Bartha, J.L. (2015) 'LC-MS based metabolomics identification of novel biomarkers of chorioamnionitis and its associated perinatal neurological damage'. *Journal of Proteome Research*, 14 (3) pp. 1432-1444.

Edmonds, K. (2008) *Dewhurts's textbook of obstetrics and gynaecology*. 8TH edition. Oxford: Wiley-Blackwell.

Eisenhofer, R., Minich, J.J., Marotz, C., Cooper, A., Knight, R. and Weyrich, L.S. (2019) 'Contamination in low microbial biomass microbiome studies: Issues and recommendations'. *Trends in Microbiology*, 27 (2) pp. 105-117.

Elfayomy, A.K. and Almasry, S.M. (2014) 'Expression of tumour necrosis factor-alpha and vascular endothelial growth factor in different zones of fetal membranes: A possible relation to onset of labor'. *Journal of Molecular Histology*, 45 pp. 243-257.

Erdemir, G., Kultursay, N., Calkavur, S., Zekioglu, O., Koroglu, O.A., Cakmak, B., Yalaz, M., Akisu, M. and Sagol, S. (2013) 'Histological chorioamnionitis: Effects on premature delivery and neonatal prognosis'. *Pediatrics and Neonatology*, 54 (4) pp. 267-274.

Ernst, L.M., Rand, C.M., Bao, R., Andrade, J., Linn, R.L., Minturn, L., Zhnag, C., Kang, W. and Weese-Mayer, D.E. (2015) 'Stillbirth: Genome-wide copy number variation profiling in

archived placental umbilical cord samples with pathologic and clinical correlation'. *Placenta*, 36 (8) pp. 783-789.

Fardini, Y., Chung, P., Dumm, R., Joshi, N. and Han, Y.W. (2010) 'Transmission of diverse oral bacteria to murine placenta: Evidence for the oral microbiome as a potential source of intrauterine infection'. *Infection and Immunology*, 78 (4) pp. 1789-1796.

Fichorova, R.N., Onderdonk, A.B., Yamamoto, H., Delaney, M.L., DuBois, A.M., Allred, E. and Leviton, A. (2011) 'Maternal microbe-specific modulation of inflammatory response in extremely low-gestational-age newborns'. *mBio*, 2 (1) e00280-10 DOI: 10.1128/mBio.00280-10.

Forootan, A., Sjoback, R., Bjorkman, J., Sjogreen, B., Linz, L. and Kubista, M. (2017) 'Methods to determine limit of detection and limit of quantification in quantitative real-time PCR (qPCR)'. *Biomolecular Detection and Quantification*, 12 (6) DOI: 10.1016/j.bdq.2017.04.001.

Fortner, K.B., Grotegut, C.A., Ransom, C.E., Bentley, R.C., Feng, L., Lan, L., Heine, R.P., Seed, P.C. and Murtha, A.P. (2014) 'Bacteria localization and chorion thinning among preterm premature rupture of membranes'. *PLoS One*, 9 (1) e83338 DOI: 10.1371/journal.pone.0083338.

Friese, K. (2003) 'The role of infection in preterm labour'. *British Journal of Obstetrics and Gynaecology*, 110 (20) pp. 52-54.

Fuks, G., Elgart, M., Amir, A., Zeisel, A., Turnbaugh, P.J., Soen, Y. and Shental, N. (2018) 'Combining 16S rRNA gene variable regions enables high-resolution microbial community profiling'. *Microbiome*, 6 (17) DOI: 10.1186/s40168-017-0396-x.

Galinsky, R., Polglase, G.R., Hooper, S.B., Black, M.J. and Moss, T.J.M. (2013) 'The consequences of chorioamnionitis: Preterm birth and effects on development'. *Journal of Pregnancy*, 2013 (412831) DOI: 10.1155/2013/412831.

Gallup, J.M. and Ackermann, M.R. (2008) 'The 'PREXCEL-Q method' for qPCR'. *International Journal of Biomedical Science*, 4 (4) pp. 273-293.

Ghyselinck, J., Pdeiffer, S., Heylen, K., Sessitsch, A. and De Vos, P. (2013) 'The effect of primer choice and short read sequences on the outcome of 16S rRNA gene based diversity studies'. *PLoS One*, 8 (8) e71360 DOI: 10.1371/journal.pone.0071360.

Gilbert, M.T.P., Haselkorn, T., Bunce, M., Sanchez, J.J., Lucas, S.B., Jewell, L.D., Marck, E.V. and Worobey, M. (2007) 'The isolation of nucleic acids from fixed, paraffin-embedded tissues - which methods are useful when?' PLoS One, 2 (6) e537 DOI: 10.1371/journal.pone.0000537.

Glassing, A., Dowd, S.E., Galandiuk, S., Davis, B. and Chiodini, R.J. (2016) 'Inherent bacterial DNA contamination of extraction and sequencing reagents may affect interpretation of microbiota in low bacterial biomass samples'. *Gut Pathology*, 8 (24) DOI: 10.1186/s13099-016-0103-7.

Goldenberg, R.L., Culhane, J.F., Iams, J.D. and Romero, R. (2008) 'Epidemiology and causes of preterm birth'. *The Lancet*, 371 (9606) pp. 75-84.

Gomez-Arango, L.F., Barrett, H.L., McIntyre, C.H., Callaway, L.K., Morrison, M. and Nitert, M.D. (2017) 'Contributions of the maternal oral and gut microbiome to placental microbial colonization in overweight and obese pregnant women'. *Nature Scientific Reports*, 7 (2860) DOI: 10.1038/s41598-017-03066-4.

Grahn, N., Olofsson, M., Ellnebo-Svedlund, K., Monstein, H-J. and Jonasson, J. (2003) 'Identification of mixed bacterial DNA contamination in broad-range PCR amplification of 16S rDNA V1 and V3 variable regions by pyrosequencing of cloned amplicons'. *FEMS Microbiology Letters*, 219 (1) pp. 87-91.

Gross, M., Cramton, S.E., Gotz, F. and Peschel, A. (2001) 'Key role of teichoic acid net charge in *Staphylococcus aureus* colonization of artificial surfaces'. *Infection and Immunity*, 69 (5) pp. 3423-3426.

Guo, S., Bocklitz, T. and Popp, J. (2016) 'Optimisation of Raman-spectrum baseline correction in biological application'. *Analyst*, 8 (141) pp. 2396-2404.

Hamasha, K., Mohaidat, Q.I., Putnam, R.A., Woodman, R.C., Palchaudhuri, S. and Rehse, S.J. (2013) 'Sensitive and specific discrimination of pathogenic and nonpathogenic *Escherichia coli* using Raman spectroscopy - a comparison of two multivariate analysis techniques'. *Biomedical Optics Express*, 4 (4) pp. 481-489.

Han, Y.W., Shen, T., Chung, P., Buhimschi, I.A. and Buhimschi, C.S. (2009) 'Uncultivated bacteria as etiologic agents of intra-amniotic inflammation leading to preterm birth'. *Journal of Clinical Microbiology,* 47 (1) pp. 38-47.

Hecht, J.L., Onderdonk, A., Delaney, M., Allred, E.N., Kliman, H.J., Zambrano, E., Pfluger, S.M., Livasy, C.A., Bhan, I. and Leviton, A. (2009) 'Characterization of chorioamnionitis in 2nd-trimester C-section placentas and correlation with microorganism recovery from subamniotic tissues'. *Pediatric and Developmental Pathology,* 11 (10) pp. 15-22.

Heydt, C., Fassunke, J., Künstlinget, H., Ihle, M.A., König, K., Heukamp, L.C., Schildhaus, H-U., Odenthal, M., Büttner, R. and Merkelbach-Bruse, S. (2014) 'Comparison of pre-analytical FFPE sample preparation methods and their impact on massively parallel sequencing in routine diagnostics'. *PLoS One*, 9 (8) e104566 DOI: 10.1371/journal.pone.0104566.

Hickey, N.A., Shalamanova, L., Whitehead, K.A., Dempsey-Hibbert, N., van der Gast, C.J. and Taylor, R.L. (2020) 'Exploring the putative interactions between chronic kidney disease and chronic periodontitis'. *Critical Reviews in Microbiology*, 12 (1) DOI: 10.1080/1040841X.2020.1724872.

Higgins, R.D., Saade, G., Polin, R.A., Grobman, W.A., Buhimschi, I.A., Watterberg, K., Silver, R.M., Raju, T.N. and Chorioamnionitis Workshop Participants. (2016) 'Evaluation and management of women and newborns with a maternal diagnosis of chorioamnionitis: Summary of a workshop'. *Obstetrics and Gynecology*, 127 (3) pp. 426-436.

Hlaing, M.M., Dunn, M., McArthur, S.L. and Stoddart, P.R. (2013) 'Raman spectroscopy for bacterial identification: Effects of sample preparation and storage'. *International Journal of Integrative Biology*, 15 (1) pp. 11-18.

Hogue, R., Malik, A., Gorelick, F. and Mehal, W. (2012) 'The sterile inflammatory response in acute pancreatitis'. *Pancreas*, 41 (3) pp. 353-357.

Holzman, C., Lin, X., Senagore, O. and Chung, G. (2007) 'Histological chorioamnionitis and preterm delivery'. *American Journal of Epidemiology*, 166 (7) pp. 786-794.

Hori, J., Wang, M., Kamiya, K., Takahashi, H. and Sakuragawa, N. (2006) 'Immunological characteristics of amniotic epithelium'. *Cornea*, 25 pp. s53-s58.

Hsu, P. and Nanan, R.K.H. (2014) 'Innate and adaptive immune interactions at the fetal-maternal interface in healthy human pregnancy and pre-eclampsia'. *Frontiers in Immunology*, 5 (125) DOI: 10.3389/fimmu.2014.00125.

Huang, B., Fettweis, J.M., Brooks, J.P., Jefferson, K.K. and Buck, G.A. (2014) 'The changing landscape of the vaginal microbiome'. *Clinics in Laboratory Medicine*, 34 (4) pp. 747-761.

Huddleston, H. and Schust, D.J. (2004) 'Immune interactions at the maternal-fetal interface: A focus on antigen presentation'. *American Journal of Reproductive Immunology*, 51 pp. 283-289.

Hugerth, L.W., Wefer, H.A., Lundin, S., Jakobsson, H.E., Lindberg, M., Rodin, S., Engstrand, L. and Andersson, A.F. (2014) 'DegePrime, a program for degenerate primer design for broad-taxonomic-range PCR in microbial ecology studies'. *Applied and Environmental Microbiology*, 80 (16) pp. 5116-5123.

Huijsmans, C.J.J., Damen, J., van der Linden, J.C., Savelkoul. H.M. and Hermans, M.H.A. (2010) 'Comparative analysis of four methods to extract DNA from paraffin-embedded tissues: Effect on downstream molecular applications'. *BMS Research Notes*, 3 (239) DOI: 10.1186/1756-0500-3-239.

Hyde, K.J. and Schust, D.J. (2016) 'Immunological challenges of human reproduction: An evolving story'. *Fertility and Sterility*, 106 (3) pp. 499-510.

Imrit, K., Goldfischer, M., Wang, J., Green, J., Levine, J., Lombardo, J. and Hong, T. (2006) 'Identification of bacteria in formalin-fixed, paraffin-embedded heart valve tissue via 16S rRNA gene nucleotide sequencing'. *Journal of Clinical Microbiology*, 44 (7) pp. 2609-2611.

Ivarsson, M. and Carlson, J. (2010) 'Extraction, quantitation and evaluation of function DNA from various sample types'. *Methods in Biobanking*, 675 (1) pp. 261-277.

Jackel, D. and Lai, K. (2013) '*Candida glabrata* sepsis associated with chorioamnionitis in an in vitro fertilization pregnancy: Case report and review'. *Clinical Infectious Diseases*, 56 (4) pp. 555-558.

Janecka, A., Adamczyk, A. and Gasinska, A. (2015) 'Comparison of eight commercially available kits for DNA extraction from formalin-fixed paraffin-embedded tissues'. *Analytical Biochemistry*, 476 pp. 08-10.

Jervis-Bardy, J., Leong, L.E.X., Marri, S., Smith, R.J., Choo, J.M., Smith-Vaughan, H.C., Nosworthy, E., Morris, P.S., O'Leay, S., Rogers, G.B. and Marsh, R.L. (2015) 'Deriving accurate microbiota profiles from human samples with low bacterial content through post-

sequencing processing of Illumina MiSeq data'. *Microbiome*, 3 (19) DOI: 10.1186/s40168-026-0083-8.

Jessop, F. and Sebire, N.J. (2011) 'Histological chorioamnionitis: Current concepts of diagnosis, classification and clinical significance'. *Fetal and Maternal Medicine Review*, 22 (1) pp. 25-44.

Johnson, C.T., Adami, R.R. and Farzin, A. (2017) 'Antibiotic therapy for chorioamnionitis to reduce the global burden of associated disease'. *Frontiers in Pharmacology*, 8 (97) DOI: 10.3389/fphar.2017.00097.

Jones, H.N. and Jansson, P.T. (2007) 'Regulation of placental nutrient transport - A review'. *Placenta*, 28 (8) pp. 763-774.

Jones, H.E., Harris, K.A., Azizia, M., Bank, L., Carpenter, B., Hartley, J.C., Klein, N. and Peebles, D. (2009) 'Differing prevalence and diversity of bacterial species in fetal membranes from very preterm and term labor'. *PLoS One*, 4 (12) e8205 DOI: 10.1371/journal.pone.0008205.

Jovel, J., Patterson, J., Wang, W., Hotte, N., O'Keefe, S., Mitchel, T., Perry, T., Kao, D., Mason, A.L., Madsen, K.L. and Wong, G.K.-S. (2016) 'Characterization of the gut microbiome using 16S or shotgun metagenomics'. *Frontiers in Microbiology*, 7 (459) e1002358 DOI: 10.3389/fmicb.2016.0045.

Jung, H.J., Park, K.H., Kim, S.N., Hong, J.S., Oh, K.J., Kim, G. and Kwon, J.Y. (2010) 'Non-invasive prediction of intra-amniotic inflammation in women with preterm labor'. *Ultrasound in Obstetrics and Gynaecology*, 37 (1) pp. 82-87.

Kacerovsky, M., Drahosova, M., Hornychova, H., Pliskova, L., Bolehovska, R., Forstl, M., Tosner, J. and Andrys, C. (2009) 'Value of amniotic fluid interleukin-8 for the prediction of histological chorioamnionitis in preterm premature rupture of membranes'. *Neuroendocrinology Letters*, 30 (6) pp. 733-738.

Kallapur, S.G., Willet, K.E., Jobe, A.H., Ikegami, M. and Bachurski, C.J. (2001) 'Intra-amniotic endotoxin: Chorioamnionitis precedes lung maturation in preterm lambs'. *American Journal of Physiology*, 280 (3) pp. 527-536.

Karstens, L., Asquith, M., Davin, S., Fair, D., Greogory, W.Y., Wolfe, A.K., Braun, J. and McWeeney, S. (2019) 'Controlling for contaminants in low biomass 16S rRNA gene sequencing experiments'. *mSystems*, 4 (4) e00290 DOI: 10.1128/mSystems.00290-19.

Kasper, D.C., Mechtler, T.P., Reischer, G.H., Witt, A., Langgartner, M., Pollak, A., Herkner, K.R. and Berger, A. (2010) 'The bacterial load of *Ureaplasma parvum* in amniotic fluid is correlated with an increased intrauterine inflammatory response'. *Diagnostic Microbiology and Infectious Disease*, 67 (2) pp. 117-121.

Kawai, T. and Akira, S. (2010) 'The role of pattern-recognition receptors in innate immunity: Update on toll-like receptors'. *Nature Immunology*, 11 (5) pp. 373-384.

Kemp, M.W. (2014) 'Preterm birth, intrauterine infection, and fetal inflammation'. *Frontiers in Immunology*, 5 (574) DOI: 10.3389/fimmu.2014.00574.

Kilman, H.J. (2014) 'Comment on "The placenta harbours a unique microbiome"'. *Science Translational Medicine*, 6 (254) DOI: 10.1126/scitranslmed.3009864.

Kim, M.J., Romero, R., Gervasi, M.T., Kin, J-S., Yoo, W., Lee, D-C., Mittal, P., Erez, O., Kisanovic, J.P., Hassan, S.S. and Kim, C.J. (2009) 'Widespread microbial invasion of the chorioamniotic membranes is a consequence and not a cause of intra-amniotic infection'. *Laboratory Investigations*, 89 (8) pp. 924-936.

Kim, C.J., Romero, R., Chaemsaithong, P., Chaiyasit, N., Yoon, B.H. and Kim, Y.M. (2015) 'Acute chorioamnionitis and funisitis: Definition, pathological features, and clinical significance'. *American Journal of Obstetrics and Gynecology*, 213 (4) S29-S52 DOI: 10.1016/j.ajog.2015.08.040.

Kim, D., Hofstaedter, C.E., Zhao, C., Mattei, L., Tanes, C., Clarke, E., Lauder, A., Sherrill-Mix, S., Chehoud, C., Kelsen, J., Conrad, M., Collman, R.G., Baldassano, R., Bushman, F.D. and Bittinger, K. (2017) 'Optimizing methods and dodging pitfalls in microbiome research'. *Microbiome*, 5 (52) DOI: 10.1186/s40168-017-0267-5.

Klindworth, A., Pruesse, E., Schweer, T., Peplies, J., Quast, C., Horn, M. and Glockner, F.O. (2013) 'Evaluation of general 16S ribosomal RNA gene PCR primers for classical and next-generation sequencing-based diversity studies'. *Nucleic Acids Research*, 41 (1) e1 DOI: 10.1093/nar/gks808.

Knight, R., Vrbanac, A., Taylor, B.C., Aksenov, A., Callewaert, C., Debelius, J., Gonzalez, A., Kosciolek, T., McCall, L-I., McDonald, D., Melnik, A.V., Morton, J.T., Navas, J., Quinn, R.A., Sanders, J.G., Swafford, A.D., Thompson, L.R., Tripathi, A., Xu, Z.Z., Zaneveld, J.R., Zhu, Q., Caporaso, J.G. and Dorrestein, P.C. (2018) 'Best practices for analysing microbiomes'. *Nature Reviews Microbiology*, 16 (7) pp. 410-422.

Konwar, C., Price, E.M., Wang, L.Q., Wilson, S.L., Terry, K. and Robinson, W.P. (2018) 'DNA methylation profiling of acute chorioamnionitis-associated placentas and fetal membranes: Insights into epigenetic variation in spontaneous preterm births'. *Epigenetics and Chromatin*, 11 (63) DOI: 10.1186/s13072-018-0234-9.

Konwar, C., Del Gobbo, G.F., Terry, J. and Robinson, W.P. (2019) 'Association of a placental interleukin-8 generic variant (rs1800796) with DNA methylation, gene expression and risk of acute chorioamnionitis'. *BMC Medical Genetics*, 20 (36) DOI: 10.1186/s12881-019-0768-0.

Kostina, E., Ofek, I., Crouch, E., Friedman, R., Sirota, L., Klinger, G., Sahly, H. and Keisari, Y. (2005) 'Noncapsulated *Klebsiella pneumoniae* bearing mannose-containing O antigens is rapidly eradicated from mouse lung and trigger cytokine production by macrophages following opsonisation with surfactant protein D'. *Infection and Immunity*, 73 (12) pp. 8282-8290.

Kota, S.K., Gayatri, K., Jammula, S., Kota, S.K., Krishna, S.V.S., Meher, L.K. and Modi, K.D. (2013) 'Endocrinology of parturition'. *Indian Journal of Endocrinology and Metabolism,* 17 (1) pp. 50-59.

Kovalovski, L., Villanyi, Z., Pataki, I., Veszelowvsky, I. and Nagy, Z.B. (1982) 'Isolation of aerobic bacteria from the placenta'. *Acta Paediatrica Academiae Scientiarum Hungaricae*, 23 (2) pp. 357-360.

Kozich, J.J., Westcott, S.L., Baxter, N.T., Highlander, S.K. and Schloss, P.D. (2013) 'Development of a dual-index sequencing strategy and curation pipeline for analyzing amplicon sequence data on the MiSeq Illumina sequencing platform'. *Applied and Environmental Microbiology*, 79 (17) pp. 5112-5120.

Kralik, P. and Ricchi, M. (2017) 'A basic guide to real time PCR in microbial diagnostics: Definitions, parameters, and everything'. *Frontiers in Microbiology*, 8 (108) DOI: 10.3389/fmicb.2017.00108.

Kulakov, L.A., McAlister, M.B., Ogden, K.L., Larkin, M.J. and O'Hanlon, J.F. (2002) 'Analysis of bacteria contaminating ultrapure water in industrial systems'. *Applied and Environmental Microbiology,* 68 (4) pp. 1548-1555.

Kuperman, A.A., Zimmerman, A., Hamadia, A., Ziv, O., Gurevich, V., Fichtman, B., Gavert, N., Straussman, R., Rechnitzer, H., Barzilay, M., Shavalb, S., Bornstein, J., Ben-Shachar, I., Yagel, S., Haviv, I. and Koren, O. (2020) 'Deep microbial analysis of multiple placentas shows no evidence for a placental microbiome'. *British Journal of Obstetrics and Gynaecology*, 127 (2) pp. 159-169.

Kusters, J.G., van Leeuwen, W.B., Maquelin, K., Blok, H.E.M., Willemse, H.F.M., de Graaf-Miltenburg, L.A.M., Fluit, A.C. and Troelstra, A. (2015) 'Raman spectroscopy-based identification of nosocomial outbreaks of the clonal bacterium *Escherichia coli*'. *European Journal of Clinical Microbiology Infectious Diseases*, 35 (10) pp. 83-87.

Larionov, A., Krause, A. and Miller, W. (2005) 'A standard curve based method for relative real time PCR data processing'. *BMC Bioinformatics*, 6 (62) DOI: 10.1186/1471-2105-6-62.

Larkin, P. (2011) '*Infrared and Raman spectroscopy; Principles and spectral interpretation'*. Netherlands: Elsevier.

Lauder, A.O., Roche, A.M., Sherrill-Mix, S., Bailey, A., Laughlin, A.L., Bittingner, K., Leite, R., Elovitz, M.A., Parry, S. and Bushman, F.D. (2016) 'Comparison of placenta samples with contamination controls does not provide evidence for a distinct placenta microbiota'. *Microbiome*, 4 (29) DOI: 10.1186/s40168-016-0172-3.

Laurence, M., Hatzis, C. and Brash, D.E. (2014) 'Common contaminants in next-generation sequencing that hinder discovery of low-abundance microbes'. *PLoS One*, 9 (5) e97876 DOI: 10.1037/journal.pone.0097876.

Laursen, M.F., Dalgaard, M.D. and Bahl, M.I. (2017) 'Genomic GC-content affects the accuracy of 16S rRNA gene sequencing based microbial profiling due to PCR bias'. *Frontiers in Microbiology*, 8 (1934) DOI: 10.3389/fmicb.2017.01934.

Ledergerber, C. and Dessimoz, C. (2011) 'Base-calling for next-generation sequencing platforms'. *Briefings in Bioinformatics*, 12 (5) pp. 489-497.

Lee, P.Y., Costumbrado, K., Hsu, C.Y. and Kim, Y.H. (2012) 'Agarose gel electrophoresis for the separation of DNA fragments'. *Journal of Visual Experiments*, 20 (62) pp. 3923.

Lee, S.M., Park, K.H., Jung, E.Y., Kook, S.Y., Park, H. and Jeon, S.J. (2018) 'Inflammatory proteins in maternal plasma, cervicovaginal and amniotic fluids as predictors of intra-amniotic infection in preterm premature rupture of membranes'. *PLoS One,* 13 (7) e0200311 DOI: 10.1371/journal.pone.0200311.

Lei, J., Priddy, L., Lim, J. and Koob, T. (2017) 'Dehydrated human amnion/chorion membrane (dHACM) allografts as a therapy for orthopedic tissue repair'. *Techniques in Orthopaedics*, 32 (3) pp. 149-157.

Leiby, J.S., McCormick, K., Sherrile-Mix, S., Clarke, E.L., Kesslet, L.R., Taylor, L.J., Hofstaedter, C.S., Roche, A.M., Mattei, L.M., Bittinger, K., Elovitz, M.A., Leite, R., Parry, S. and Bushman, F.D. (2018) 'Lack of detection of a human placenta microbiome in samples from preterm and term deliveries'. *Microbiome*, 6 (196) DOI: 10.1186/s40168-018-0575-4.

Leon, L.J., Doyle, R., Diez-Benavente, E., Clark, T.G., Klein, N., Stanier, P. and Moore, G.E. (2018) 'Enrichment of clinically relevant organisms in spontaneous preterm-delivered placentas and reagent contamination across all clinical groups in a large pregnancy cohort in the United Kingdom'. *Applied and Environmental Microbiology*, 84 (14) e00483 DOI: 10.1128/AEM.00483-18.

Lewis, A.T., Gaifulina, R., Isabelle, M., Dorney, J., Woods, M.L., Lloyd, G.R., Lau, K., Rodriguez-Justo, M., Kendall, C., Stone, N. and Thomas, G.M. (2017) 'Mirrored stainless steel substrate provides improved signal for Raman spectroscopy of tissue and cells'. *Journal of Raman Spectroscopy*, 48 (1) pp. 119-125.

Li, J., Wang, C., Kang, H., Shao, L., Hu, L., Xiao, R., Wang, S. and Gu, B. (2018) 'Label-free identification carbapenem-resistant *Escherichia coli* based on surface-enhanced resonance Raman scattering'. *Royal Society of Chemistry*, 8 (1) pp. 4761-4765.

Lind, K., Stahlberg, A., Zoric, N. and Kubista, M. (2006) 'Combining sequence-specific probes and DNA binding dyes in real-time PCR for specific nucleic acid quantification and melting curve analysis'. *BioTecniques*, 40 (3) pp. 315-319.

Linder, J.E., Batey, K., Johnston, R., Cohen, E.M., Wang, Y., Wang, X., Zaleski, N.M., Rogers, L.M., McDonald, W.H., Reyzer, M.L., Judd, A., Goldstein, J., Correa, H., Pulley, J. and Aronoff, D.M. (2018) 'The PathLink acquired gestational tissue bank: Feasibility of project PLACENTA'. *Journal of Reproduction, Biotechnology and Fertility,* 7 (4) pp. 14-27.

Ling, Z., Kong, J., Liu, F., Zhu, H., Chen, X., Wang, Y., Li, L., Nelson, K.E., Xia, Y. and Xiang, C. (2010) 'Molecular analysis of the diversity of vaginal microbiota associated with bacterial vaginosis'. *BMC Genomics*, 11 (488) DOI: 10.1186/2582-2164-11-488.

Liu, C. M., Aziz, M., Kachur, S., Hsueh, P-O., Huang, Y-T., Keim, P. and Price, L.B. (2012) 'BactQuant: An enhanced broad-coverage bacterial quantitative real-time PCR assay'. *BMC Microbiology*, 12 (56) pp. 01-13.

Liu, H., McDowell, T.L., Hanson, N.E., Tang, X., Fujimoto, J. and Rodriguez-Canales, J. (2013) 'Laser capture microdissection for the investigative pathologist'. Ve*terinary Pathology*, 51 (1) pp. 257-269.

Lloyd-Price, J., Abu-Ali, G. and Huttenhower, C. (2016) 'The healthy human microbiome'. *Genome Medicine*, 8 (51) DOI: 10.1186/s13073-016-0307.

Londero, A.P., Rossetti, E., Pittini, C., Cagnacci, A. and Driul,, L. (2019) 'Maternal age and the risk of adverse pregnancy outcomes: A retrospective cohort study'. *BMC Pregnancy and Childbirth*, 19 (261) DOI: 10.1186/s12884-019-2400-x.

Long, C.P., Au, J., Sandoval, N.R., Gebreselassie, N.A. and Antoniewicz, M.R. (2017) 'Enzyme I facilitates reverse flux from pyruvate to phosphoenolpyruvate in *Escherichia coli'*. *Nature Communications*, 27 (8) DOI: 10.1038/ncomms14316.

Lorenz, B., Wichmann, C., Stockel, S., Rosch, P. and Popp, J. (2017) 'Cultivation-free Raman spectroscopic investigations of bacteria'. *Trends in Microbiology*, 25 (5) pp. 413-425.

Lu, L. and Claud, E.C. (2018) 'Intrauterine inflammation, epigenetics and microbiome influences on preterm infant health'. *Current Pathobiology Reports*, 6 (1) pp. 15-21.

MacIntyre, D.A., Chandiramani, M., Lee, Y.S., Kindinger, L., Smith, A., Angelopoulos, N., Lehne, B., Arulkumaran, S., Brown, R., Teoh, T.G., Holmes, E., Nichoholson, J.K., Marchesi, J.R. and Bennet, P.R. (2015) 'The vaginal microbiome during pregnancy and the postpartum period in a European population'. *Scientific Reports*, 5 (8988) DOI: 10.1038/srep08988.

Maddipati, K.R., Romero, R., Chaiworapongsa, T., Chaemsaithong, P., Zhou, S-L., Xu, Z., Tarca, A.L., Kusanovic, J.P., Gomez, R., Docheva, N. and Honn, K.V. (2016) 'Clinical

chorioamnionitis at term: The amniotic fluid fatty acyl lipidome'. *Journal of Lipid Research*, 57 (10) pp. 1906-1916.

Malloy, M.H. (2014) 'Chorioamnionitis: Epidemiology of newborn management and outcome United States 2008'. *Journal of Perinatology*, 34 (5) pp. 611-615.

Mamede, A.C., Carvalho, M.J., Abrantes, A.M., Laranjo, M., Maia, C.J. and Botelho, M.F. (2012) 'Amniotic membrane: From structure and functions to clinical applications'. *Cells and Tissue Research*, 349 (2) pp. 447-458.

Maquelin, K., Kirschner, C., Choo-Smith, L.-P., van den Braak, N., Endtz, H. Ph., Naumann, D. and Puppels, C.J. (2002) 'Identification of medically relevant microorganisms by vibrational spectroscopy'. *Journal of Microbiological Methods*, 51 (3) pp. 255-271.

Martinez, L.A., Spano, J., Bird, T.E., Simecek, J.W., Mallory, A. and Stahl, J.M. (2019) 'Detection of mixed bacterial populations by surface enhanced Raman scattering (SERS) spectroscopy'. *Sensing and Bio-Sensing Research*, 24 DOI: 10.1016/j.sbsr.2019.100282.

Mazzarella, G., Bianco, A., Catena, E., de Palma, R. and Abbate, G.F. (2002) 'Th1/Th2 lymphocyte polarization in asthma'. *Allergy*, 55 (61) pp. 06-09.

McCuaig, R., Wong, D., Gardiner, F.W., Rawlinson, W., Dahlstrom, J.E. and Robson, R.S. (2018) 'Periodontal pathogens in the placenta and membranes in term and preterm birth'. *Placenta*, 68 (8) pp. 40-43.

McMurdie, P.J. and Holmes, S. (2013) 'Phyloseq: An R package for reproducible interactive analysis and graphics of microbiome census data'. *PLoS One*, 8 (4) e61217 DOI: 10.1371/journal.pone.0061217.

McMurdie, P.J. and Holmes, S. (2014) 'Waste not, want not: Why rarefying microbiome data is inadmissible'. *PLoS Computational Biology,* 10 (4) e1003531 DOI: 10.1371/journal.pcbi.1003531.

Menon, R., Taylor, R.N. and Fortunato, S.J. (2010) 'Chorioamnionitis- A complex pathophysiological syndrome'. *Placenta*, 31 (2) pp. 113-120.

Menon, R., Richardson, L.S. and Lappas, M. (2018) 'Fetal membrane architecture, aging and inflammation in pregnancy and parturition'. *Placenta*, 79 (5) pp. 40-45.

Meredith, T.C., Aggarwal, P., Mamat, U., Linder, B. and Woodard, R.W. (2016) 'Redefining the requisite lipopolysaccharide structure in *Escherichia coli*'. *ACS Chemical Biology*, 17 (1) pp. 33-42.

Mi, S., David, A.L., Chowdhury, B., Jones, R.R., Hamley, I.W., Squires, A.M. and Connon, C.J. (2012) 'Tissue engineering a fetal membrane'. *Tissue Engineering*, 18 (3) pp. 373-381.

Mittempergher, L., de Ronde, J.J., Nieuwland, M., Kerkhoven, R.M., Simon, I., Rutgers, E.J.T., Wessels, L.F.A. and Van't Veer, L.J. (2011) 'Gene expression profiles from formalin fixed paraffin embedded breast cancer tissue are largely comparable to fresh frozen matched tissue'. *PLoS One*, 6 (2) e17163 DOI: 10.1371/journal.pone.0017163.

Mlynarikova, K., Samek, O., Bernatova, S., Ruzicka, F., Jezek, J., Haronikova, A., Siler, M., Zemanek, P. and Hola, V. (2015) 'Influence of culture media on microbial fingerprints using Raman spectroscopy'. *Sensors*, 15 (11) pp. 29635-29647.

Moco, N.P., Martin, L.F., Pereira, A.C., Polettini, J., Peracoli, J.C., Coelho, K.I.R. and da Silva, M.G. (2013) 'Gene expression and protein localization of TLR-1, -2, -4 and -6 in amniochorion membranes of pregnancies complicated by histological chorioamnionitis'. *European Journal of Obstetrics & Gynecology and Reproductive Biology*, 171 (1) pp. 12-17.

Monastero, R.N. and Pentyala, S. (2017) 'Cytokines as biomarkers and their respective clinical cutoff levels'. *International Journal of Inflammation*, 4 DOI: 10.1155/2017/40309485.

Mor, G., Aldo, P. and Alvero, A.B. (2017) 'The unique immunological and microbial aspects of pregnancy'. *Nature Reviews Immunology*, 17 (8) pp. 469-482.

Morelli, S.S., Mandal, M., Goldsmith, L.T., Kashani, B.N. and Ponzio, N.M. (2015) 'The maternal immune system during pregnancy and its influence on fetal development'. *Research and Reports in Biology*, 6 pp. 171-189.

Morgan, A.S., Marlow, N., Draper, E.S., Alfirevic, Z., Hennessy, E.M. and Costeloe, K. (2016) 'Impact of obstetric interventions on condition at birth in extremely preterm babies: Evidence from a national cohort study'. *BMC Pregnancy and Childbirth*, 16 (390) DOI: 10.1186/s12884-016-1154.

Movasaghi, Z., Rehman, S. and Rehman, I.U. (2007) 'Raman spectroscopy of biological tissues'. *Applied Spectroscopy Reviews*, 42 (5) pp. 493-541.

Muhl, H., Kochem, A-J., Disque, C. and Sakka, S.G. (2010) 'Activity and DNA contamination of commercial polymerase chain reaction reagents for the universal 16S rDNA real-time polymerase chain reaction detection of bacterial pathogens in blood'. *Diagnostic Microbiology and Infectious Disease*, 66 (1) pp. 41-49.

Murphy, S.V., Kidyoor, A., Reid, T., Atala, A., Wallace, E.M. and Lim, R. (2014) 'Isolation, cryopreservation and culture of human amnion epithelial cells for clinical applications'. *Journal of Visualized Experiments,* 94 (1) DOI: 10.3791/52085.

Musilova, I., Kitova, R., Pliskova, L., Stepan, M., Menon, R., Jacobsson, B. and Kacerovsky, M. (2015) 'Intraamniotic inflammation in women with preterm prelabor rupture of membranes'. *PLoS One*, 10 (7) e0133929 DOI: 10.1371/journal.pone.0133929.

Nadkarni, M.A., Martin, F.E., Jacques, N.A. and Hunter, N. (2002) 'Determination of bacterial load by real-time PCR using a broad-range (universal probe and primers)'. *Microbiology*, 148 (1) pp. 257-266.

Nagahashi, M., Shimada, Y., Ichikawa, H., Nakagawa, S., Sato, N., Kaneko, K., Homma, K., Kawasaki, T., Kodama, K., Lyle, S., Takabe, K. and Wakai, T. (2017) 'Formalin-fixed paraffin-embedded sample conditions for deep next generation sequencing'. *Journal of Surgical Research*, 220 pp.125-132.

Nagy, A., Vitaskova, E., Cernikova, L., Krivda, V., Jirincova, H., Sedlak, K., Hornickova, J. and Havlickova, M. (2017) 'Evaluation of TaqMan qPCR system integrating two identically labelled hydrolysis probes in single assay'. *Scientific Reports*, 7 (41392) DOI: 10.1038/srep41392.

Nair, K.D.D., Ramachandran, L. and Joseph, L. (2018) 'Significance of histological subclinical chorioamnionitis (HCA) in spontaneous preterm labour'. *Indian Journal of Research*, 7 (2) pp. 09-11.

National Institute for Healthcare Excellence (2019) '*Preterm labour and birth'. NICE guidelines*'. Available at: https://www.nice.org.uk/guidance/ng25/chapter/Context (Accessed: 16 October 2019).

Neugebauer, U., Rosch, P., Schmitt, M., Popp, J., Julien, C., Rasmussen, A., Budich, C. and Deckert, V. (2006) 'On the way to nanometre-sized information of the bacterial surface by tip-enhanced Raman spectroscopy'. *A European Journal of Chemical Physics and Physical Chemistry*, 7 (7) pp. 1428-1430.

Nguyen, N-P., Warnow, T., Pop, M. and White, B. (2016) ‘A perspective on 16S rRNA operational taxonomic unit clustering using sequence similarity’. *NPJ Biofilms and Microbes*, 2 (16004) DOI: 10.1038/npjbiofilms.2016.4.

Noda-Nicolau, N.M., Polettini, J., Peltier, M.R., Guimaraes de Silva, M. and Menon, R. (2016) ‘Combinations and loads of bacteria affect the cytokine production by fetal membranes: An in vitro study’. *American Journal of Reproductive Immunology*, 76 (6) pp. 504-511.

Noecker, C., McNally, C.P., Eng, A. and Borenstein, E. (2017) ‘High-resolution characterization of the human microbiome’. *Translational Research*, 179 pp. 07-23.

O'Brien, C.M., Vargis, E., Paria, B.C., Bennet, K.A., Mahadevan-Jansen, A. and Reese, J. (2014) ‘Raman spectroscopy provides a non-invasive approach for determining biochemical composition of the pregnant cervix *in vivo’*. *Acta Paediatrician*, 103 (7) pp. 715-721.

O’Callaghan, J.L., Turner, R., Nitert, M.D., Barrett, H.L., Clifton, V. and Pelzer, E.S. (2019) ‘Re-assessing microbiomes in the low-biomass reproductive niche’. *British Journal of Obstetrics and Gynaecology*, 127 (2) pp. 147-158.

Oh, E., Choi, Y-L., Kwon, M.J., Kim, R.N., Kim, Y.J., Song, J-Y., Jung, K.S. and Shin, Y.K. (2015) ‘Comparison of accuracy of whole-exome sequencing with formalin-fixed paraffin-embedded and fresh frozen tissue samples’. *PLoS One*, 10 (12) e01444162 DOI: 10.1371/journal.pone.0144162.

Oh, K.J., Kim, S.M., Hong, J-S., Maymon, E., Erez, O., Panaitescu, B., Gomez-Lopez, N., Romero, R. and Yoon, B.H. (2017) ‘Twenty-four percent of patients with clinical chorioamnionitis in preterm gestations have no evidence of either culture-proven intraamniotic infection or intraamniotic inflammation’. *American Journal of Obstetrics and Gynecology*, 216 (6) e604 DOI: 10.1016/j.ajog.2017.02.035.

Onderdonk, A.B., Delaney, M.L., DuBois, A.M., Allred, E.N., Leviton, A. and Extremely Low Gestational Age Newborns (ELGAN) Study Investigators. (2008a) ‘Detection of bacteria in placental tissues obtained from extremely low gestational age neonates’. *American Journal of Obstetrics and Gynecology*, 198 (1) DOI: 10.1016/j.ajog.2007.5.044.

Onderdonk, A.B., Hecht, J.L., McElrath, T.F., Delaney, M.L., Allred, E.N. and Leviton, A. (2008b) ‘Colonization of second trimester placenta parenchyma’. *American Journal of Obstetrics and Gynecology*, 199 (1) DOI: 10.1016/j.ajog.2007.11.068.

Pahlow, S., Meisel, S., Cialla-May, D., Weber, K., Rosch, P. and Popp, J. (2015) 'Isolation and identification of bacteria by means of Raman spectroscopy'. *Advanced Drug Delivery Reviews*, 89 (7) pp. 105-120.

Pansky, B. (1982) '*Review of medical embryology',* California: Macmillan USA.

Paolini, C.L., Marconi, A.M., Ronzoni, S., Di Noio, M., Fennessey, P.V., Pardi, G. and Battaglia, F.C. (2001) 'Placental transport of leucine, phenylalanine, glycine, and proline in intrauterine growth-restricted pregnancies'. *The Journal of Clinical Endocrinology & Metabolism*, 86 (11) pp. 5427-5432.

Park, C-W., Moon, K.C., Park, J.S., Jun, J.K., Romero, R. and Yoon, B.H. (2009) 'The involvement of human amnion in histologic chorioamnionitis is an indicator that a fetal and an intra-amniotic inflammatory response is more likely and severe: Clinical implications'. *Placenta*, 30 (1) pp. 56-61.

Park, H., Park, K.H., Kime, Y.M., Kook, S.Y., Jeon, S.J. and Yoo, H-N. (2018) 'Plasma inflammatory and immune proteins as predictors of intra-amniotic infection and spontaneous preterm delivery in women with preterm labor: A retrospective study'. *BMC Pregnancy and Childbirth*, 18 (146) DOI: 10.1186/s12884-018-1780-7.

Parnell, L.A., Briggs, C.M., Cao, B., Delannoy-Bruno, O., Schrieffer, A.E. and Mysorekar, I.U. (2017) 'Microbial communities in placentas from term normal pregnancy exhibit spatially variable profiles'. *Scientific Reports*, 7 (1120) DOI: 10.1038/s41598-017-11514-4.

Patel, A., Harris, K.A. and Fitzgerald, F. (2017) 'What is broad-range 16S rDNA PCR?' *Archives of Disease in Childhood Education and Practice*, 102 (5) DOI: 10.1136/archdischild-2016-312049.

Patel, P.G., Selvarajah, S., Guerard, K-P., Bartlett, J.M.S., Lapointe, J., Berman, D.M., Okello, J.B.A. and Park, P.C. (2017) 'Reliability and performance of commercial RNA and DNA extraction kits for FFPE tissue cores'. *PLoS One*, 12 (6) e0179732 DOI: 10.1371/journal.pone.0179732.

Pennington, R. (2014) '*Dealing with amplification inhibitors: Reagent choice matters'*. Available at: https://www.promega.com/-/media/files/promega-worldwide/north-america/promega-us/webinars-and-events/2014/dealing-with-amplification-inhibitors-webinar-feb-2014.pdf?la=en (Accessed: 30 January 2017).

Perez-Munoz, M.E., Arrieta, M-C., Ramer-Taie, A.E. and Walter, J. (2017) ‘A critical assessment of the "sterile womb" and "*in utero* colonization" hypotheses: Implications for research on the pioneer infant microbiome‘. *Microbiome*, 5 (48) DOI: 10.1186/s40168-017-0268-4.

Pielesz, A., Bobinski, R., Binias, D., Gawlowski, A., Waksmanska, W., Ulam-Wlodarz, I. and Ilczak, T. (2019) ‘FT Raman spectroscopy in the evaluation of biomarkers of normal and pathological placenta tissue’. *Molecular and Cellular Biochemistry*, 458 (2) pp. 125-132.

Pikor, L.A., Enfield, K.S.S., Cameron, H. and Lam, W.L. (2011) ‘DNA extraction from paraffin embedded material for genetic and epigenetic analyses’. *Journal of Visual Experiments*, 49 (2763) DOI: 10.3791/2763.

Pollock, J., Glendinning, L., Wisedchanwet, T. and Watson, M. (2018) ‘The madness of microbiome: Attempting to find consensus "best practice" for 16S microbiome studies’. *Applied and Environmental Microbiology*, 84 (7) e02627 DOI: 10.1128/AEM.02627-17.

Prince, A.L., Ma, J., Kannen, P.S., Gisslen, T., Harris, R.A., Sweeney, E.L., Knox, C.L., Lambers, D.S., Jobe, A.H., Chougnet, C.A., Kallapur, S.G. and Aagaard, K.J. (2016) ‘The placental membrane microbiome is altered among subjects with spontaneous preterm birth with and without chorioamnionitis’. *American Journal of Obstetrics and Gynecology,* 214 (5) pp. 627e1-627e16.

Proctor, L.M. (2011) ‘The human microbiome project in 2011 and beyond’. *Cell Host and Microbiome,* 10 (4) pp. 287-291.

Prosser, J.I., Bohannan, B.J.M., Curtis, T.P., Ellis, R.J., Firestone, M.K., Freckleton, R.P., Green, J.L., Green, L.E., Killham, K., Lennon, J.J., Osborn, M., Solan, M., van der Gast, C.J. and Young, J.P.W. (2007) ‘The role of ecological theory in microbiological ecology’. *Nature Reviews Microbiology*, 5 pp. 384-392.

Pruvost, M., Grange, T. and Geigl, E-M. (2018) ‘Minimizing DNA contamination by using UNG-coupled quantitative real-time PCR on degraded DNA samples: Application to ancient DNA studies’. *Biotechniques*, 38 (4) pp. 569-574.

Purcell, P., Jary, H., Perry, A., Perry, J.D., Stewart, C.J., Nelson, A., Lanyon, C., Smith, D.L., Cummings, S.P. and De Soyza, A. (2014) ‘Polymicrobial airway bacterial communities in adult bronchiectasis patients’. *BMC Microbiology*, 14 (130) DOI: 10.1186/1471-2180-14-130.

R Core Team (2017) *R: A language and environment for statistical computing. R foundation for statistical computing*. [Online]. Available at: https://www.R-project.org/. (Accessed: 21 April 2017).

Redline, R.W. (2006) 'Inflammatory responses in the placenta and umbilical cord'. *Seminars in Fetal & Neonatal Medicine*, 11 (1) pp. 296-301.

Redline, R.W., Faye-Petersen, O., Heler, D., Qureshi, F., Savell, V., Vogler, C. and The Society for Paediatric Pathology, Perinatal Section, Amniotic Fluid Infection Nosology Committee. (2003) 'Amniotic infection syndrome: Nosology and reproducibility of placental reaction patterns'. *Paediatric and Developmental Pathology,* 6 (1) pp. 435-448.

Rehbinder, E. M., Carlsen, K.C.L., Staff, A.C., Angell, I.L., Landro, L., Hilde, K., Gaustad, P. and Rudi, K. (2018) 'Is amniotic fluid of women with uncomplicated term pregnancies free of bacteria?' *American Journal of Obstetrics and Gynecology*, 219 (3) pp. 289.e1-289.e12 DOI: 10.1016/j.ajog.2018.05.028.

Renishaw (2020a) '*inVia confocal Raman microscope'*. Available at: https://www.renishaw.com/en/invia-confocal-raman-microscope--6260 (Accessed: 05 January 2020).

Renishaw (2020b) '*WIRE 5.1 Raman Software'*. Available at: https://www.renishaw.com/en/raman-software--9450 (Accessed: 05 January 2020).

Richardson, L.S., Vargas, G., Brown, T., Ochoa, L., Sheller-Miller, S., Saade, G., Taylor, R.N. and Menon, R. (2017) 'Discovery and characterisation of human amniochorion membrane microfractures'. *The American Journal of Pathology*, 187 (12) pp. 2821-2830.

Rindsjo, E., Holmlund, U., Sverremark-Ekstrom, E., Papadoginnakis, N. and Scheynius, A. (2007) 'Toll-like receptor-2 expression in normal and pathologic human placenta'. *Human Pathology*, 38 (3) pp. 468-473.

Rizkalla, M., Ghane, P., Agarwal, M., Shrestha, S. and Varahramyan, K. (2012) 'Raman spectroscopy for human cancer tissue diagnosis: A pattern recognition approach'. *Journal of Biomedical Science and Engineering*, 5 (113) pp. 892-900.

Roberts, D.J., Celi, A.C., Riley, L.E., Onderdonk, A.B., Boyd, T.K., Johnson, L.C. and Lieberman, E. (2012) 'Acute histological chorioamnionitis at term: Nearly always non-infectious'. *PLoS One*, 7 (3) e31819 DOI: 10.1371/journal.pone.0031819.

Roberts, V.H.J., Gaffney, J.E., Lewandowski, K.S., Schabel, M.C., Morgan, T.K. and Frias, A.E. (2019) 'A standardized method for collection of human placenta samples in the age of functional magnetic resonance imaging'. *Biotechniques*, 67 (2) pp. 45-49.

Rock, K.L., Latz, E., Ontiveros, F. and Kono, H. (2010) 'The sterile inflammatory response'. *Annual Review of Immunology*, 28 pp. 321-342.

Rode, M.E., Morgan, M.A., Ruchelli, E. and Forouzan, I. (2000) '*Candida* chorioamnionitis after serial therapeutic amniocenteses: A possible association'. *Journal of Perinatology*, 5 (1) pp. 335-337.

Rogers, G.B., Cuthbertson, L., Hoffman, L.R., Wing, P.A.C., Pope, C., Hooftman, D.A.P., Lilley, A.K., Oliver, A., Carroll, M.P., Bruce, K.D. and van der Gast, C.J. (2013) 'Reducing bias in bacterial community analysis of lower respiratory infections'. *The ISME Journal,* 7 (4) pp. 697-706.

Romero, R., Hassan, S.S., Gajer, P., Tarca, A.L., Fadroch, D.W., Nikita, L., Galuppi, M., Lamont, R.F., Chaemsaithong, P., Miranda, J., Chaiworapongsa, T. and Ravel, J. (2014a) 'The composition and stability of the vaginal microbiota of normal pregnant women is different from that of non-pregnant women'. *Microbiome*, 2 (4) DOI: 10.1186/2049-2618-2-4.

Romero, R., Miranda, J., Chaiworaponsgsa, T., Kozeniewski, S.J., Chaemsaithong, P., Gotsch, F., Dong, Z., Ahmed, A.I., Toon, B.H., Hassan, S.S., Kim, C.J. and Yeo, L. (2014b) 'Prevalence and clinical significance of sterile intra-amniotic inflammation in patients with preterm labor and intact membranes'. *American Journal of Obstetrics and Gynecology*, 72 (5) pp. 458-474.

Ruane, S. and Austin, C.C. (2017) 'Phylogenomics using formalin-fixed and 100+ year old intractable natural history specimens'. *Molecular Ecology Resources*, 17 (5) pp. 1003-1008.

Rubin, B.E.R., Sanders, J.G., Hampton-Marcell, J., Owens, S.M., Gilbery, J.A. and Moreau, C.S. (2014) 'DNA extraction protocols cause differences in 16S rRNA amplicon sequencing efficiency but not in community profile composition or structure'. *Microbiology Open*, 3 (6) pp. 910-921.

Ruijter, J.M., Pfaffl, M.W., Zhao, S., Spiess, A.N., Boggy, G., Blom, J., Rutledge, R.G., Sisti, D., Lievens, A., De Preter, K., Derveaux, S., Hellemans, J. and Vandesompele, J. (2012)

‘Evaluation of qPCR curve analysis methods for reliable biomarker discovery: Bias, resolution, precision, and implications’. *Methods*, 59 (1) pp. 32-46.

Sah, S., Chen, L., Houghton, J., Kemppainen, J., Marko, A.C., Zeigler, R. and Latham, G.J. (2013) ‘Functional DNA quantification guides accurate next-generation sequencing mutation detection in formalin-fixed, paraffin-embedded tumour biopsies’. *Genome Medicine*, 5 (77) DOI: 10.1186/gm481.

Sahni, M., Franco-Fuenmayor, M.E. and Shattuck, K. (2019) ‘Management of late preterm and term neonates exposed to maternal chorioamnionitis’. *BMC Paediatrics*, 19 (282) DOI: 10.1186/s12887-019-1650-0.

Salafia, C.M., Weigl, C. and Silberman, L. (1989) ‘The prevalence and distribution of acute placental inflammation in uncomplicated term pregnancies’. *Journal of Obstetrics and Gynaecology*, 73 (3) pp. 383-389.

Salter, S.J., Cox, M.J., Turek, E.M., Calus, S.T., Cookson, W.O., Moffatt, M.F., Turner, P., Parkhill, J., Loman, N.J. and Walker, A.W. (2014) ‘Reagent and laboratory contamination can critically impact sequence-based microbiome analyses’. *BMC Biology*, 12 (87) DOI: 10.1186/s12915-014-0087-z.

Satorki, R., Gronroos, T., Laitnen, K., Salminen, S. and Isolauri, E. (2010) ‘Vaginal microbiome of reproductive-age women’. *Proceedings of the National Academy of Sciences of the United States of America*, 108 (1) pp. 4680-4687.

Schlabritz-Loutsevitch, N., Gandhi, K., Soydemir, F., Brownbill, P., Sengar, R., Ventolini, G., Bruillard, P. and Gosink, L. (2017) ‘Raman spectroscopy as a novel method in placental research: Recognising the pattern of placental hypoxia’. *Journal of Raman Spectroscopy*, 48 (12) pp. 1896-1899.

Schloss, P.D., Jenior, M.L., Koumpouras, C.C., Westcott, S.L. and Highlander, S.K. (2016) ‘Sequencing 16S rRNA gene fragments using the PacBio SMRT DNA sequencing system’. *PeerJ*, 4 e1869 DOI: 10.7717/peerj.1869.

Schrader, C., Schielke, A., Ellerbroek, L. and Johne, R. (2012) ‘PCR inhibitors - occurrence, properties and removal’. *Journal of Applied Microbiology*, 113 (5) pp. 1014-1026.

Seferovic, M.D., Prince, A.L., Chu, D.M., Sweeney, A.G., Engevik, M.A., Ganesh, P.B., Andrews, N., Cersalovic, J. and Aagaard, K. (2016) ‘Recovery of placental bacteria is

facilitated by periodontitis in orally inoculated germ-free mice'. *American Journal of Obstetrics and Gynecology*, 214 (1) S144 DOI: 10.1016/j.ajog.2015.10.282.

Seiler, C., Sharpe, A., Barret, J.C., Harrington, E.A., Jones, E.V. and Marshall, G.B. (2016) 'Nucleic acid extraction from formalin-fixed paraffin-embedded cancer cell line samples: A trade-off between quantity and quality?'. *BMC Clinical Pathology*, 16 (17) DOI: 10.1186/s12907-016-0039-3.

Senguven, B., Baris, E., Oygur, T. and Berktas, M. (2014) 'Comparison of methods for the extraction of DNA from formalin-fixed, paraffin-embedded archival tissues'. *International Journal of Medical Sciences*, 11 (5) pp. 494-499.

Seong, H.S., Lee, S.E., Kang, J.H., Romero, R. and Yoon, B.H. (2014) 'The frequency of microbial invasion of the amniotic cavity and histologic chorioamnionitis in women at term with intact membranes in the presence or absence of labor'. *American Journal of Obstetrics and Gynecology*, 199 (4) pp. 375e1-375e5 DOI: 10.1016/j.ajog.2008.06.040.

Serrano, M.A., Bayon, J.E., Pascolo, L., Tribella, C., Ostrow, J.D., Gonzalez-Gallego, J. and Marin, J.J.G. (2002) 'Evidence for carrier-mediated transport of unconjugated bilirubin across plasma membrane vesicles from human placental trophoblast'. *Placenta*, 23 (7) pp. 527-535.

Shannon, C.E. (1958) 'A mathematical theory of communication'. *Bell Labs Technical Journal*, 27 (3) pp. 379-423.

Shannon, B., Gajer, P., Yi, T.J., Ma, B., Humphrys, M.S., Thomas-Pavanel, J., Chieza, L., Janakiram, P., Saunders, M., Tharao, W., Huibner, S., Shahabi, K., Ravel, J. and Kaul, R. (2017) 'Distinct effects of the cervicovaginal microbiota and herpes simplex type 2 infection on female genital tract immunology'. *The Journal of Infectious Diseases*, 215 (9) pp. 1366-1375.

Shapiro-Mendoza, C.K. and Lackritz, E.M. (2012) 'Epidemiology of late and moderate preterm birth'. *Seminars in Fetal and Neonatal Medicine*, 17 (3) pp. 120-125.

Shin, H., Pei, Z., Martinez, K.A., Rivera-Vinas, J.I., Mendez, K., Cavallin, H. and Dominguez-Bello, M.G. (2015) 'The first microbial environment of infants born by C-section: The operating room microbes'. *Microbiome*, 3 (59) DOI: 10.1186/s40168-015-0126-1.

Si, J., You, H.J., Yu, J., Sung, J. and, Ko, G.P. (2017) '*Prevotella* as a hub for vaginal microbiota under the influence of host genetics and their association with obesity'. *Cell Host & Microbiome*, 21 (1) pp. 97-150.

Simbolo, M., Gottardi, M., Corbo, V., Fassan, M., Mafficini, A., Malpeli, G., Lawlor, R.T. and Scarpa, A. (2013) 'DNA qualification workflow for next generation sequencing of histopathological samples'. *PLoS One*, 8 (5) e62692 DOI: 10.1371/journal.pone.0062692.

Sinha, R., Abnet, C.C., White, O., Knight, R. and Huttenhower, C. (2015) 'The microbiome quality control project: Baseline study design and future directions'. *Genome Biology*, 16 (276) DOI: 10.1186/s13059-015-0841-8.

Smith, E. and Dent, G. (2005) '*Modern Raman spectroscopy - A practical approach'*. London: John Wiley and Sons.

Smulian, J.C., Shen-Schwarz, S., Vintzileos, A.M., Lake, M.F. and Anantin, C.V. (1999) 'Clinical chorioamnionitis and histological placental inflammation'*. Obstetrics and Gynecology*, 94 (6) pp. 1000-1005.

Sood, R., Zehnder, J.L., Druzin, M.L. and Brown, P.O. (2006) 'Gene expression patterns in human placenta'. *Proceedings of the National Academy of Sciences of the United States of America*, 103 (14) pp. 5478-5483.

Spencer, D.H., Sehn, J.K., Abel, H.J., Watson, M.A., Pfeifer, J.D. and Duncavage, E.J. (2013) 'Comparison of clinical targeted next-generation sequence data from formalin-fixed and fresh-frozen tissue specimens'. *The Journal of Molecular Diagnostics*, 15 (5) pp. 623-633.

Srinivasan, M., Sedmak, D. and Jewell, S. (2002) 'Effect of fixatives and tissue processing on the content and integrity of nucleic acids'. *The American Journal of Pathology*, 161 (6) pp. 1961-1971.

Steel, J.H., Malatos, S., Kennea, N., Edwards, D., Miles, L., Duggan, P., Reynolds, P.R., Feldman, R.G. and Sullivan, M.H. (2005) 'Bacteria and inflammatory cells in fetal membranes do not always cause preterm labor'. *Pediatric Research*, 57 (122) pp. 404-411.

Stewart, C.J., Embleton, N.D., Marrs, E.C., Smith, D.P., Nelson, A., Abdulkadir, B., Skeath, T., Petrosino, J.F., Perry, J.D., Berrington, J.E. and Cummings, S.P. (2016) 'Temporal

bacterial and metabolic development of the preterm gut reveals specific signatures in health and disease'. *Microbiome*, 4 DOI: 10.1186/s40168-016-0216-8.

Stewart, C.J., Embleton, N.D., Clements, E., Luna, P.N., Smith, D.P., Fofanova, T.Y., Nelson, A., Taylor, G., Orr, C.H., Petrosino, J.F., Berrington, J.E. and Cummings, S.P. (2017) 'Cesarean or vaginal birth does not impact the longitudinal development of the gut microbiome in a cohort of exclusively preterm infants'. *Frontiers in Microbiology*, 8 DOI: 10.3389/fmicb.2017.01008.

Stewart, C.J., Fatemizadeh, R., Parsons, P., Lamb, C.A., Shady, D.A., Petrosino, J.F. and Hair, A.B. (2019) 'Using formalin fixed paraffin embedded tissue to characterize the preterm gut microbiota in necrotising enterocolitis and spontaneous isolated perforation using marginal and diseased tissue'. *BMC Microbiology*, 19 (52) DOI: 10.1186/Ss12866-019-1426-6.

Stinson, L.F., Keelan, J.A. and Payne, M.S. (2018a) 'Identification and removal of contaminating microbial DNA from PCR reagents: Impact on low-biomass microbiome analyses'. *Letters in Applied Microbiology*, 68 (1) pp. 02-08.

Stinson, L.F., Keelan, J.A. and Payne, M.S. (2018b) 'Comparison of meconium DNA extraction methods for use in microbiome studies'. *Frontiers in Microbiology*, 9 (270) DOI: 10.3389/fmicb.2018.00270.

Stout, M.J., Conlon, B., Landeau, M., Lee, I., Bower, C., Zhao, Q., Roehl, K.A., Nelson, M., Macones, G.A. and Mysorekar, U. (2013) 'Identification of intracellular bacteria in the basal plate of human placenta in term and preterm gestations'. *American Journal of Obstetrics and Gynecology*, 208 (3) pp. 226e1-226e7.

Strola, S.A., Baritaux, J-C., Schultz, E., Simon, A.C., Allier, C., Espagnon, I., Jary, D. and Dinten, J-M. (2014) 'Single bacteria identification by Raman spectroscopy'. *Journal of Biomedical Optics*, 19 (11) DOI: 10.1117/1.JBO.19.11.111610.

Strombeck, L., Sandros, J., Holst, E., Madianos, P., Nannmark, U., Papapanou, P. and Mattsby-Baltzer, I. (2007) '*Prevotella bivia* can invade human cervix epithelial (HeLa) cells'. *Journal of Pathology, Microbiology and Immunology*, 115 (3) pp. 241-251.

Strong, M.J., Xu, G., Morici, L., Bon-Durant, S.S., Baddoo, M., Lin, Z., Fewell, C., Taylor, C.M. and Flemington, E.K. (2014) 'Microbial contamination in next generation sequencing

implications for sequence-based analysis of clinical samples'. *PLoS Pathology*, 10 (11) e1004437 DOI: 10.1371/journal.ppat.1004437.

Strunk, T., Campbell, C., Burgner, D., Charles, A., French, N., Sharp, M., Simmer, K., Nathan, E. and Doherty, D. (2018) 'Histological chorioamnionitis and developmental outcomes in very preterm infants'. *Journal of Perinatology*, 39 (2) pp. 321-330.

Svec, D., Tichopad, A., Novosadova, V., Pfaffl, M.W. and Kubista, M. (2015) 'How good is a PCR efficiency estimate: Recommendations for precise and robust qPCR efficiency assessments'. *Biomolecular Detection and Quantification,* 3 (3) pp. 09-16.

Sweeney, E.L., Kallapur, S.G., Gisslen, T., Lambers, D.S., Chougnet, C.A., Stephenson, S-A., Jobe, A.H. and Knox, C.L. (2016) 'Placental infection with *Ureaplasma* species is associated with histologic chorioamnionitis and adverse outcomes in moderately preterm and late-preterm infants'. *The Journal of Infectious Diseases*, 213 (8) pp. 1340-1374.

Taft, D.H., Ambalavanan, N., Schibler, K.R., Yu, Z., Newburg, D.S., Deshmukh, H., Ward, D.V. and Morrow, A.L. (2015) 'Centre variation in intestinal microbiota prior to late-onset sepsis in preterm infants'. *PLoS One*, 10 (6) e0130604 DOI: 10.1371/journal.pone.0130604.

Talari, A.C.S., Movasaghi, Z., Rehman, S. and Rehman, I. (2015) 'Raman spectroscopy of biological tissues'. *Applied Spectroscopy Reviews*, 50 (1) DOI: 10.1080/057049282014.923902.

Tambor, V., Vajrychova, M., Kacerovsky, M., Link, M., Domasinska, P., Menon, R. and Lenco, J. (2015) 'Potential peripartum markers of infectious-inflammatory complications in spontaneous preterm birth'. *BioMed Research International*, 3 (343501) DOI: 10.115/2015/343501.

Theis, K.R., Romero, R., Winters, A.D., Greenburg, J.M., Gomex-Lopez, N., Alhousseini, A., Bieda, J., Maymon, E., Pacora, P., Fettweis, J.M., Buck, G.A., Jefferson, K.K., Strauss, J.F., Erez, O. and Hassan, S.S. (2019) 'Does the human placenta delivered at term have a microbiota? Results of cultivation, quantitative real-time PCR, 16S rRNA gene sequencing, and metagenomics'. *American Journal of Obstetrics and Gynecology*, 220 (3) pp. 267.e1-267.e39.

Thermo Fisher Scientific Inc. (2014) '*Real-time PCR handbook'*. Available at: https://www.thermofisher.com/content/dam/LifeTech/global/Forms/PDF/real-time-pcr-handbook.pdf (Accessed: 13 December 2016).

Tita, A.T.N. and Andrews, W.W. (2010) 'Diagnosis and management of clinical chorioamnionitis'. *Clinical Perinatology*, 37 (2) pp. 339-354.

Tomlinson, M.S., Lu, K., Stewart, J.R., Marsit, C.J., O'Shea, M. and Fry, R.C. (2019) 'Microorganism in the placenta: Links to early-life inflammation and neurodevelopment in children'. *Clinical Microbiology Reviews*, 32 (2) DOI: 10.1128/cmr.00103-18.

Trombley Hall, A., McKay Zovanyi, A., Christensen, D.R., Koehler, J.W. and Devins Minogue, T. (2013) 'Evaluation of inhibitor-resistant real-time PCR methods for diagnostics of clinical and environmental samples'. *PLoS One*, 8 (9) e73845 DOI: 10.1371.journal.pone.0073845.

Tucker, J. (2004) 'Epidemiology of preterm birth'. *British Medical Journal*, 329 (7467) pp. 675-678.

Underwood, M.A., Gilbert, W.M. and Sherman, M.P. (2005) 'Amniotic fluid: Not just fetal urine anymore'. *Journal of Perinatology*, 25 (1) pp. 341-348.

United Nations Inter-Agency Group for Child Mortality Estimation (UNIGME) (2017) '*Levels & trends in child mortality: Report 2017. Estimates developed by the UN inter-agency group for child mortality estimation'*, Available at: https://www.unicef.org/publications/files/Child_Mortality_Report_2017.pdf (Accessed: 10 October 2019).

Urszula, K., Joanna, E., Marek, E., Beata, M. and Magdelana, S.B. (2014) 'Colonization of the lower urogenital tract with *Ureaplasma parvum* can cause asymptomatic infection of the upper reproductive system in women: A preliminary study'. *Archives of Gynecology and Obstetrics*, 289 (5) pp. 1129-1134.

Urushiyama, D., Suda, W., Ohnishi, E., Araki, R., Kiyoshima, C., Kurakazu, M., Sanui, A., Yotsumoto, F., Murata, M., Nabeshima, K., Yasunaga, S., Saito, S., Nomiyama, M., Hattori, M., Miyamoto, S. and Hata, K. (2017) 'Microbiome profile of the amniotic fluid as a predictive biomarker of perinatal outcome'. *Scientific Reports*, 7 (12171) DOI: 10.1038/s41598-017-11699-8.

Varga, P., Berecz, B., Gasparics, A., Dombi, Z., Varga, Z., Jeager, J., Magyar, Z., Rigo Jr, J., Joo, J.G. and Kornya, L. (2017) 'Morbidity and mortality trends in very-very low birth weight premature infants in light of recent changes in obstetric care'. *European Journal of Obstetrics & Gynecology and Reproductive Biology,* 211 (4) pp. 134-139.

Verbruggen, S.W., Oyen, M.L., Phillips, A.T.M. and Nowlan, N.C. (2017) 'Function and failure of the fetal membrane: Modelling the mechanisms of the chorion and amnion'. *PLoS One*, 12 (3) e0171588 DOI: 10.1371/journal.pone.0171588.

Vitrenko, Y., Kostenko, I., Kulebyakina, K., Duda, A., Klunnyk, M. and Sorochynska, K. (2017) 'Fetal tissues tested for microbial sterility by culture- and PCR-based methods can be safely used in clinics'. *Cell Transplantation*, 26 (2) pp. 339-350.

Vogel, J.P., Chawanpaiboon, S., Moller, A-B., Watananirun, K., Bonet, M. and Lumbiganon, P. (2018) 'The global epidemiology of preterm birth'. *Best Practice & Research Clinical Obstetrics & Gynaecology*, 52 (10) pp. 03-12.

von Ahlfen, S., Missel, A., Bendrat, K. and Schlumpberger, M. (2007) 'Determinants of RNA quality from FFPE samples'*. PLoS One*, 2 (12) e1261 DOI: 10.1371/journal.pone.0001261.

Wang, Y. and Qian, P-Y. (2009) 'Conservative fragments in bacterial 16S rRNA genes and primer design for 16S ribosomal DNA amplicons in metagenomic studies'. *PLoS One*, 4 (10) e7401 DOI: 10.1371.journal.pone.0007401.

Wang, Y., Hoenig, J.D., Malin, K.J., Qamar, S., Petrof, E.O., Sun, J., Antonopoulos, D.A., Chang, E.B. and Claud, E.C. (2009) '16S rRNA gene-based analysis of faecal microbiota from preterm infants with and without necrotizing enterocolitis'. *The ISME Journal,* 3 (8) pp. 944-954.

Wang, J.H., Gouda-Vossos, A., Dzamko, N., Halliday, G. and Huang, Y. (2013) 'DNA extraction from fresh-frozen and formalin-fixed, paraffin-embedded human brain tissue'. *Neuroscience Bulletin*, 29 (5) pp. 649-654.

Waring, G.J., Robson, S.C., Bulmer, J.N. and Tyson-Capper, A.J. (2015) 'Inflammatory signalling in fetal membranes: Increased expression levels of TLR 1 in the presence of preterm histological chorioamnionitis'. *PLoS One*, 10 (5) e0124298 DOI: 10.1371/journal.pone.0124298.

Weiss, S., Amir, A., Hyde, E.R., Metcalf, J.L., Song, S.J. and Knight, R. (2014) 'Tracking down the sources of experimental contamination in microbiome studies'. *Genome Biology*, 15 (564) DOI: 10.1186/s13059-014-0564-2.

Wimmer, I., Troscher, A.R., Brunner, D., Rubino, S.J., Bien, C.G., Weiner, H.L., Lassmann, H. and Bauer, J. (2018) 'Systematic evaluation of RNA quality, microarray data reliability

and pathway analysis in fresh, fresh frozen and formalin-fixed paraffin-embedded tissue samples'. *Scientific Reports*, 8 (6351) DOI: 10.1038/s41598-018-24781.

Witt, A., Berger, A., Gruber, C.J., Petricevic, L., Apfalter, P., Worda, C. and Husslein, P. (2005) 'Increased intrauterine frequency of *Ureaplasma urealyticum* in women with preterm labor and preterm premature rupture of the membranes and subsequent caesarean delivery'. *American Journal of Obstetrics and Gynecology*, 193 (5) pp. 1663-1669.

World Health Organisation (2015) '*WHO recommendation on interventions to improve preterm birth outcomes'*. Available at: https://apps.who.int/iris/bitstream/handle/10665/183037/9789241508988_eng.pdf;jsessionid=72A19B45CF95CFEBEA469B4013942017?sequence=1 (Accessed: 10 October 2019).

Young, G.R., Smith, D.L., Embleton, N.D., Berrington, J.E., Schwalbe, E.C., Cummings, S.P., van der Gast, C.J. and Lanyon, C. (2017) 'Reducing viability bias in analysis of gut microbiota in preterm infants at risk of NEC and sepsis'. *Frontiers in Cellular and Infection Microbiology*, 7 (237) DOI: 10.3389/fcimb.2017.00237.

Yu, Z., An, B., Ramshaw, J.A.M. and Brodsky, B. (2014) 'Bacterial collagen-like proteins that form triple-helical structures'. *Journal of Structural Biology*, 186 (3) pp. 451-461.

Yuan, J.S., Reed, A., Chen, F. and Neal Stewart Jr, C. (2006) 'Statistical analysis of real-time PCR data'. *BMC Bioinformatics*, 7 (85) DOI: 10.1186/1471-2105-7-85.

Zhao, S., Bellone, S., Lopez, S., Thakrai, D., Schwab, C., English, D.P., Black, J., Cocco, E., Choi, J., Zammataro, L., Predolini, F., Bonazzoli, E., Bi, M., Buza, N., Hui, P., Wong, S., Abu-Khalaf, M., Ravaggi, A., Bignotti, E., Bandiera, E., Romani, C., Todeschini, P., Tassi, R., Zanotti, L., Odicino, F., Pecorelli, S., Donzelli, C., Ardighieri, L., Facchetti, F., Falchetti, M., Silasi, D-A., Ratner, E., Azodi, M., Schwartz, P.E., Mane, S., Angioli, R., Terranova, C., Quick, C.M., Edraki, B., Bilguvar, K., Lee, M., Choi, M., Stigeler, A.L., Boffon, T.J., Schlessinger, J., Lifton, R.P. and Santin, A.D. (2016) 'Mutational landscape of uterine and ovarian carcinosarcomas implicates histone genes in epithelial–mesenchymal transition'. *Proceedings of the National Academy of Sciences of the United States of America*, 113 (43) pp. 12238-12243.

Appendices

A.1. List of reagents, chemicals and commercial kits

Agilent Technologies

- Agilent high sensitivity DNA kit (5067-4626), including high sensitivity DNA chips, electrode cleaner, syringe kit, syringe, spin filters, plus reagents of high sensitivity DNA ladder, high sensitivity DNA marker (35/10380 bp), high sensitivity DNA dye concentrate, high sensitivity DNA gel matrix

Applied Biosystems

- ExoSap-IT PCR product clean up kit (78201.1) including ExoSap-IT reagent
- 2X TaqMan Fast advanced master mix with UNG (4444554)

Bioline

- 5X DNA loading buffer blue (BIO-37045)
- Agarose, molecular grade (BIO-41026)
- HyperLadder 1 KB (BIO-33053)
- SensiFAST SYBR No-Rox kit (BIO-98005)

Fisher Scientific

- HPLC grade methanol (M/4056/17)
- LB broth Miller molecular media (BP1426-500)
- LB agar Miller molecular powder (BP1425-500)
- SequalPrep normalisation plate kit (A1051001)
- Tris-acetate-EDTA (TAE) 25X powder (BP1331-1)
- Tris-borate-EDTA (TBE buffer 10X)(B52)

Gibco

- Ampicillin, sodium salt irradiated (11593-027)

Illumina

- MiSeq reagent kit (MS-102-2002) including reagent cartridge and flow cell, plus hybridisation buffer (HT1) and incorporation buffer (PR2)
- Nextera index kit i7 (N701-N712), i5 (S501-S508; FC-131-1002)
- PhiX control kit V3 (FC-110-3001)

Invitrogen

- AccuPrime Pfx SuperMix (10053322)
- One shot TOP10 competent cell kit (C404003), including One Shot TOP10 chemically competent *E. coli*, pUC19 DNA (10 pg/µl) and S.O.C. medium.
- SYBR Safe DNA gel stain, 10,000X (S33102)
- X-Gal (15520034)

Kapa Biosystems

- KAPA library quantification kit (KK4824)

MoBio

- BiOstic FFPE tissue DNA isolation kit (12250-50) containing FP1, FP2, FP3, FP4, FP5, FP6, FP7, FP8, 2ml collection tubes and spin filters. Lot numbers FP15D24, FP16B25, FP14E15.

New England BioLabs

- Bovine Serum Albumin (BSA) molecular biology grade 20 mg/ml (B9000S)
- *EcoRI* kit (R0101L) including *EcoRI* enzyme (R0101S) and *EcoRI* reaction buffer 10X (B0101S)

Promega

- 2X PCR mastermix (M750B), including *Taq* DNA polymerase and dNTPs
- $MgCl_2$ solution 25mM (A315H)
- Nuclease free H_2O (P119A)
- PGEM-T easy vector system (A1360) including, PGEM-T easy vector (A137A; 50 ng/ul), control insert DNA (A363A; 4 ng/µl) T4 DNA ligase (M180A), 2X rapid ligation buffer (C671A), nuclease free H_2O (P119A).
- PureYield plasmid miniprep system (A1223) containing, cell lysis buffer (A145D), neutralisation solution (A157D), endotoxin removal wash (A158D), column wash solution (A159D), elution buffer (A160D), mini columns (A166B) and collection tubes (A167B).

Qiagen

- QIAamp fast DNA tissue kit (51404) containing Buffer AVE, VXL, MVL, AW1, AW2, ATE, DX reagent, Proteinase K, RNAse A, mini spin columns, tissue disruption tubes and collection tubes. Lot numbers: 154025312, 154025313.
- QIAprep spin miniprep containing, Buffer P1, P2, N3, PB, PE, EB, spin columns and collection tubes (27104).

Sigma Aldrich

- KAPA SYBR FAST qPCR kit (KK4602)
- LookOut DNA Erase (L8917)
- N-N-Dimethylformamide (D4551-250)

A.2. List of equipment

Agarose gel tank, Edvotek Bio-Rad (HU13, 3638)

Bioanalyzer system, Agilent Genomics, 2100 (5067.4628)

Bio-Rad CFX connect real time system (CFX manager V3.1)

Bio-Rad gel doc EZ gel imager (Image lab 3.0)

Centrifuge, Christ RVC2-18 D-37520

EDVOcycler PCR machine (V6.2)

GBox SynGene Chemi-XX6 (DRXV2/2296)

Illumina MiSeq, Northumbria University, Newcastle, UK

Manual rotary microtome, Leica (RM2125)

Microcentrifuge, Sigma D-37520

Raman InVia Qontour (Renishaw) with WIRE 5.1

Spectrophotometer, NanoDrop One, Thermo Fisher Scientific (V1.4 software)

Spectrophotometer, NanoDrop 1000, Thermo Fisher Scientific (V3.8.1 software)

Thermal cycler, Applied Biosystems (2720)

Thermal cycler, C100 touch Bio-Rad

ThermoMixer, Eppendorf

UV spectrophotometer, Jenway (7305)

Vacubrand diaphragm vacuum pump - 27373308-273525

Vortex Genie 2, Jencons, Scientific Industries

Vortex Chip IKA M51 orbital shaker

A.3. Table of primers

Primer	Use	Sequence	Reference
V4F	Illumina sequencing	5'-GTGCCAGCMGCCGCGGTAA-3'	Biesbroek *et al*, 2012
V4R	Illumina sequencing	5'-GGACTACHVGGGTWTCTAAT-3'	Biesbroek *et al*, 2012
27F	PCR	5'-AGAGTTTGATCMTGGCTCAG-3'	Salter *et al*, 2014
1492R	PCR	5'-TACGGYTACCTTGTTACGACTT-3',	Salter *et al*, 2014
BactQuant Forward	qPCR	5'-CCTACGGGDGGCWGCA-3'	Liu *et al,* 2012
BactQuant Reverse	qPCR	5'-GGACTACHVGGGTMTCTAATC-3'	Liu *et al,* 2012
BactQuant probe	qPCR	(6FAM)5'-CAGCAGCCGCGGTA-3' (MGBNFQ)	Liu *et al,* 2012

Table A.1 Primer sequences. Supporting information of primers and sequences used within Illumina sequencing, PCR optimisation and qPCR.

A.4. Serial dilution calculations

		C1	V1		V2	C2
Dilution	**Source of V1**	**Initial g/µl**	**Vol of DNA Required (µl)**	**Vol of Diluent (µl)**	**Final Vol (µl)**	**Final (g/µl)**
1	Stock	2.68×10^{-7}	10	990	1000	2.68×10^{-9}
2	Dilution 1	2.68×10^{-9}	10	90	100	2.68×10^{-10}
3	Dilution 2	2.68×10^{-10}	10	90	100	2.68×10^{-11}
4	Dilution 3	2.68×10^{-11}	5.48	94.52	100	1.468×10^{-12}
5	Dilution 4	1.468×10^{-12}	10	90	100	1.468×10^{-13}
6	Dilution 5	1.468×10^{-13}	10	90	100	1.468×10^{-14}
7	Dilution 6	1.468×10^{-14}	10	90	100	1.468×10^{-15}
8	Dilution 7	1.468×10^{-15}	10	90	100	1.468×10^{-16}

Table A.2 Serial dilution calculations for qPCR standard curves. Volume of DNA (µl) required calculated in relation to final concentration (g/ µl).

A.5. Formalin-Fixed Paraffin-Embedded tissue block images

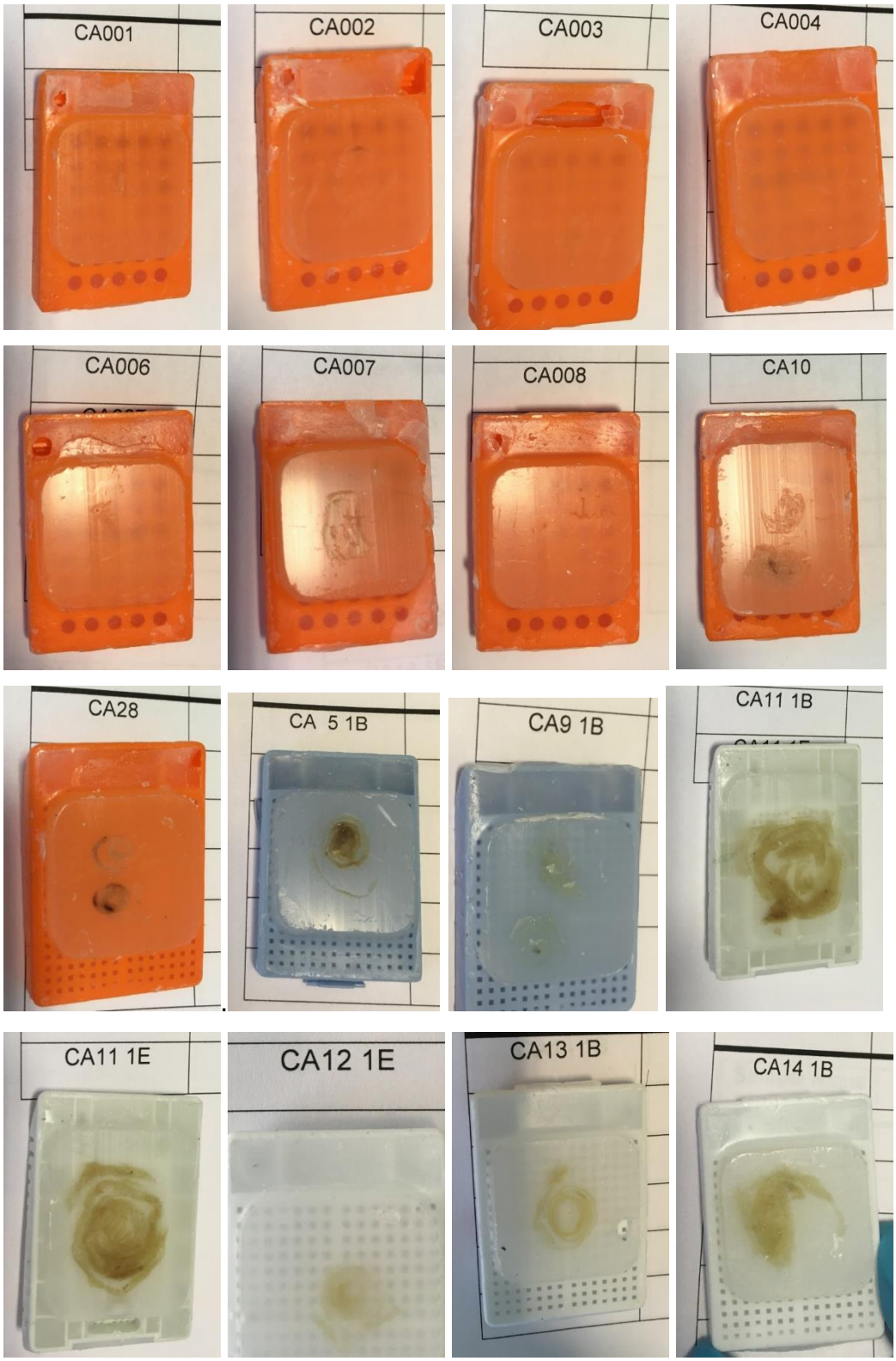

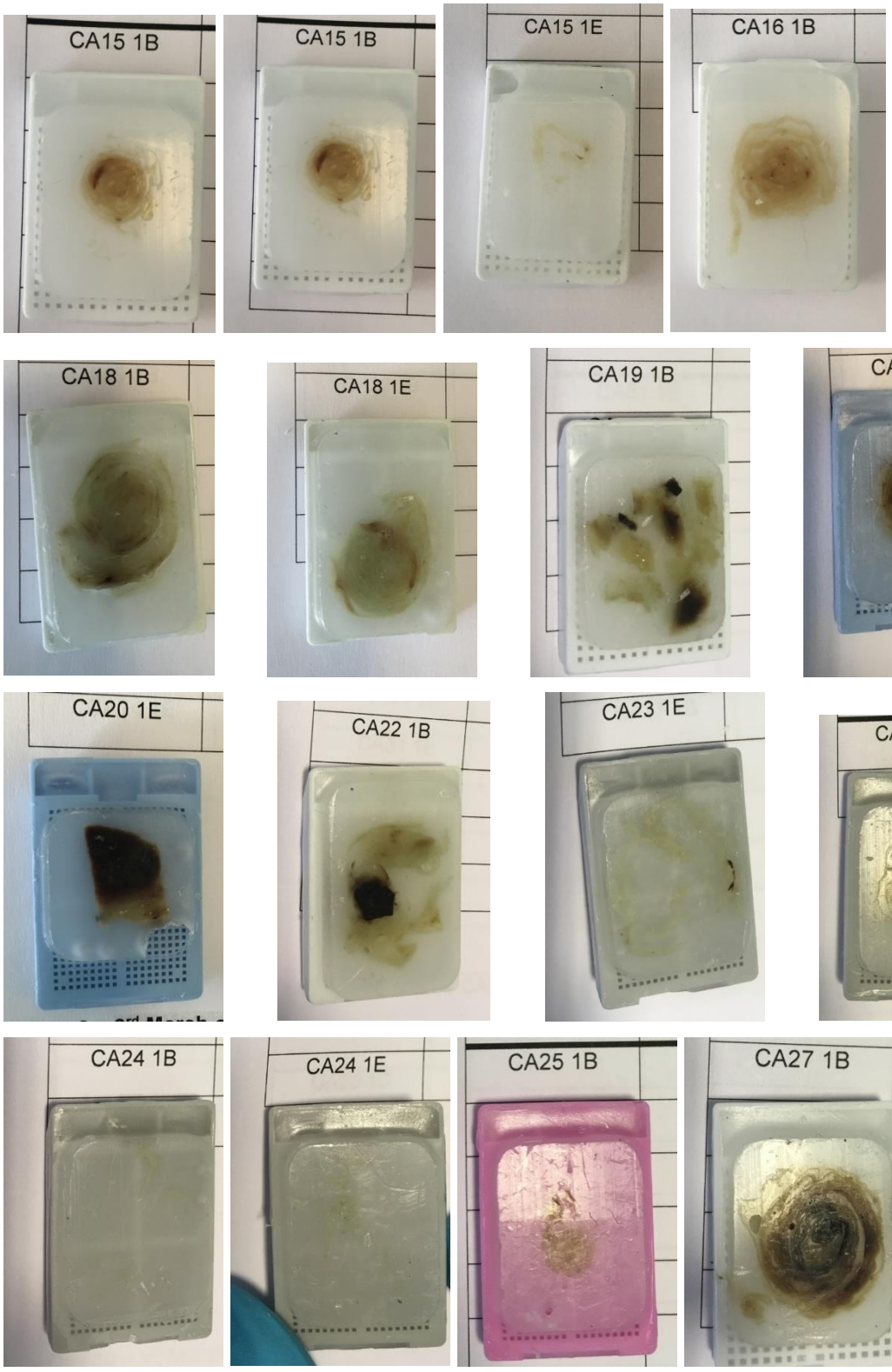
CA15 1B
CA15 1B
CA15 1E
CA16 1B
CA18 1B
CA18 1E
CA19 1B
CA20 1B
CA20 1E
CA22 1B
CA23 1E
CA23 1D
CA24 1B
CA24 1E
CA25 1B
CA27 1B

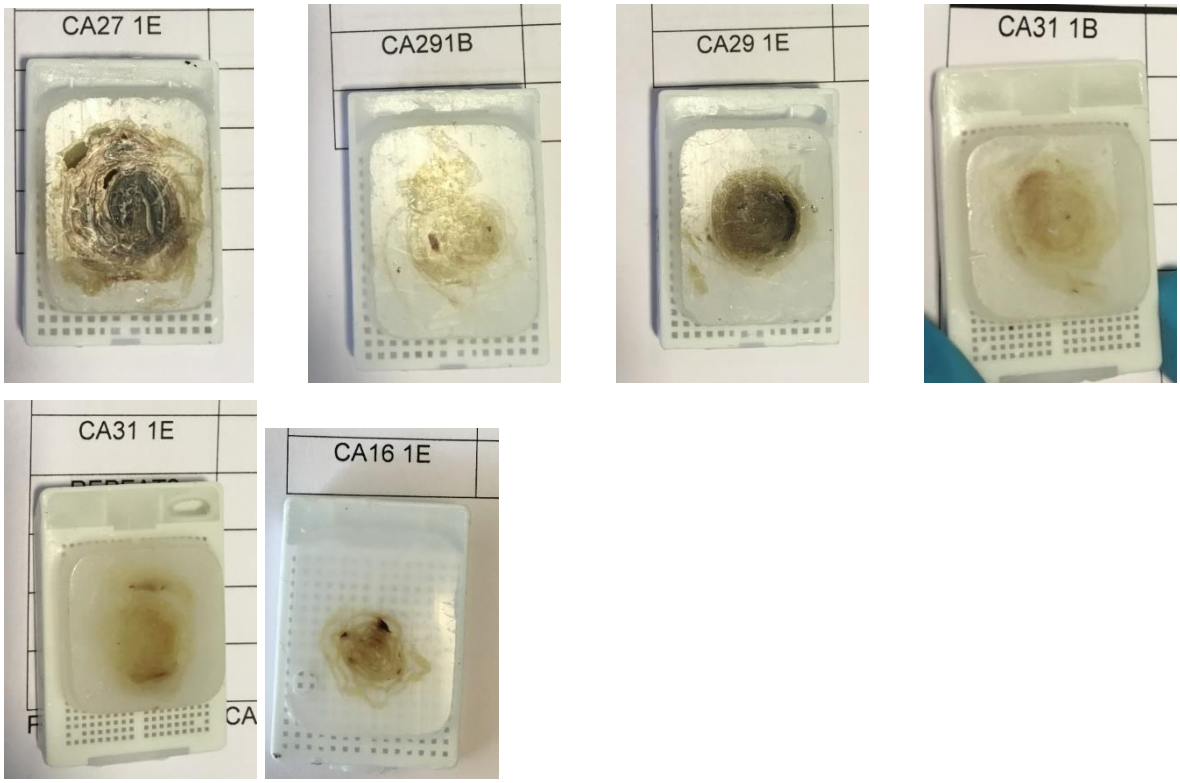

Figure A.1 Formalin-Fixed Paraffin-Embedded tissue block images. Images of wax block FFPE fetal membrane rolls prior to sectioning.

A.6. Additional results

A.6.1 NanoDrop spectrophotometer DNA extraction results example

Sample ID	ng/µl	A260	A280	A260/280	A260/230
A1 04-04 KIT -VE	0.69	0.01	0.01	0.96	0.03
H1 04-04 HCA 19 CH1	532.71	10.65	5.77	1.85	2.36
I1 04-04 HCA 19 CH2	468.31	9.37	5.03	1.86	2.28
J1 04-04 HCA 19 CH3	65.21	1.30	0.70	1.88	1.81
A1 23-02 KIT -VE	2.98	0.06	0.04	1.70	0.32
B1 23-02 CA19 1B WAX -VE	18.99	0.42	0.22	1.83	2.24
K1 23-02 CA19 1B TUBE 1	35.75	0.72	0.35	2.03	2.24
L1 23-02 CA19 1B TUBE 2	46.22	0.92	0.51	1.81	1.38
M1 23-02 CA19 1B TUBE 3	33.19	0.66	0.31	2.11	2.16

Table A.3 Example of NanoDrop spectrophotometer sample results following DNA extractions. Example NanoDrop results from one patient sample in triplicate from the frozen chorion (H1-J1) and the respective FFPE fetal membrane roll (K1-M1). Respective kit negatives are included (A1), plus the wax negative control (B1). DNA concentration (ng/µl), plus purity ratio (A260/280, A260/230) displayed.

A.6.2 Bioanalyzer chip-based electrophoresis results

Due to poor quality results from the agarose gel electrophoresis, chip-based electrophoresis was used on the same subset of Formalin-Fixed Paraffin-Embedded (FFPE) samples for improved detection with this methodology.

Bioanalyzer gel results confirmed previous gel electrophoresis findings that FFPE fetal membranes contain highly fragmented DNA, indicated by multiple bands present, plus low quantity of DNA due to the pale intensity of banding.

A transposed electropherogram is also produced per sample in reference to the gel image (Figure A.2). For the example presented the DNA molecular weight and size is comparable to that viewed on the gel image, with the mean peak at 397 bp and a smaller peak at 132 bp, confirming the multiple and short fragmentation of FFPE samples. Upper and lower reference ladder markers are plotted at 35 bp and 10380 bp. An electropherogram of the whole reference ladder allows comparison to samples (Figure A.2).

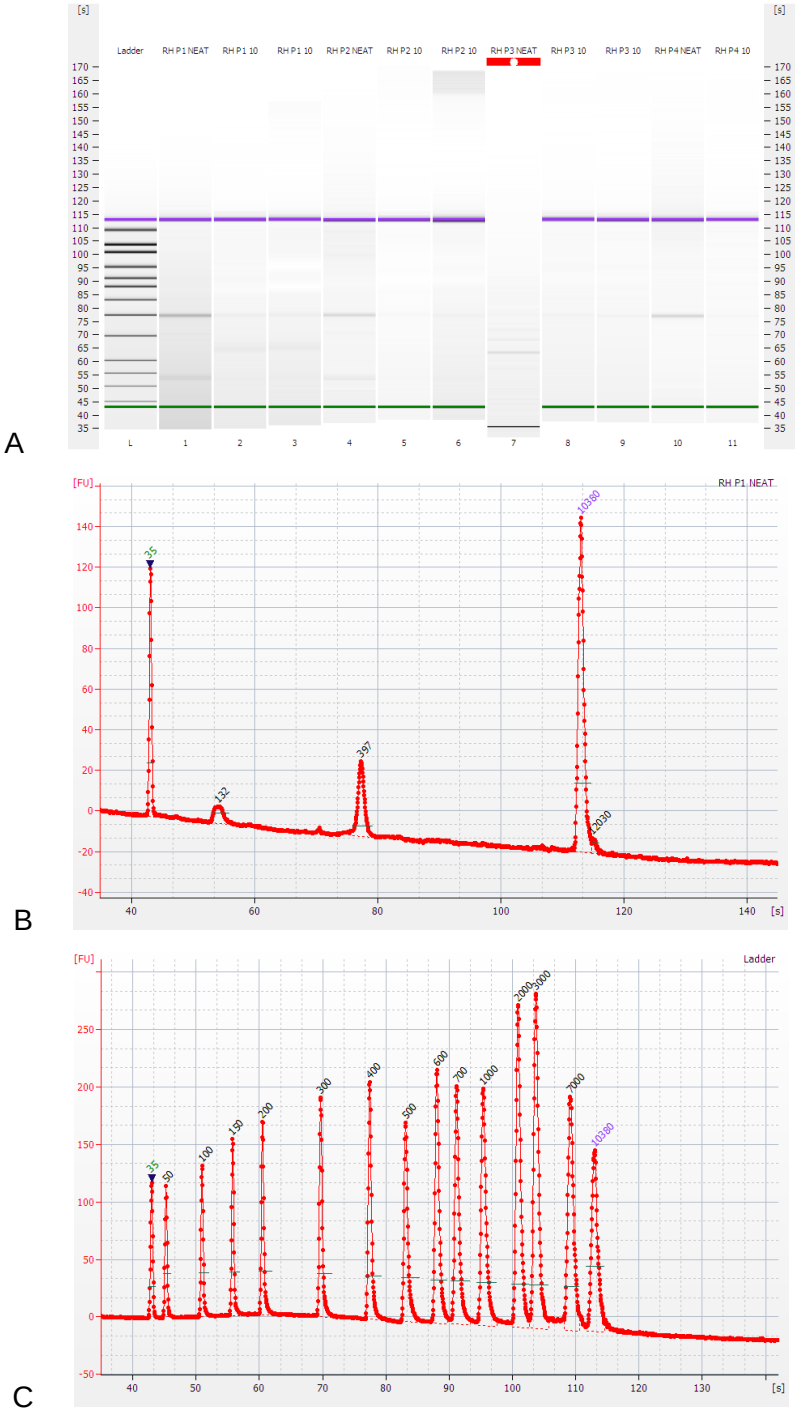

Figure A.2 Bioanalyzer chip-based gel electrophoresis example results Example of a gel electrophoresis image from a subset of Formalin-Fixed Paraffin-Embedded (FFPE) samples (A), plus sample electropherogram (B) and ladder electropherogram (C) from Bioanalyzer Agilent 2100. Ladder is included (L), with upper (purple) and lower (green) markers visible across samples (lane 1-11). Error in lane 7 is visible due to no marker detected (A). Example of an electropherogram from an FFPE sample (B) and gel reference ladder (C) plotted as marker time (s) against fluorescence (FU). Upper and lower marker included for reference (35 bp and 10380 bp).

A.6.3 Additional qPCR sample results

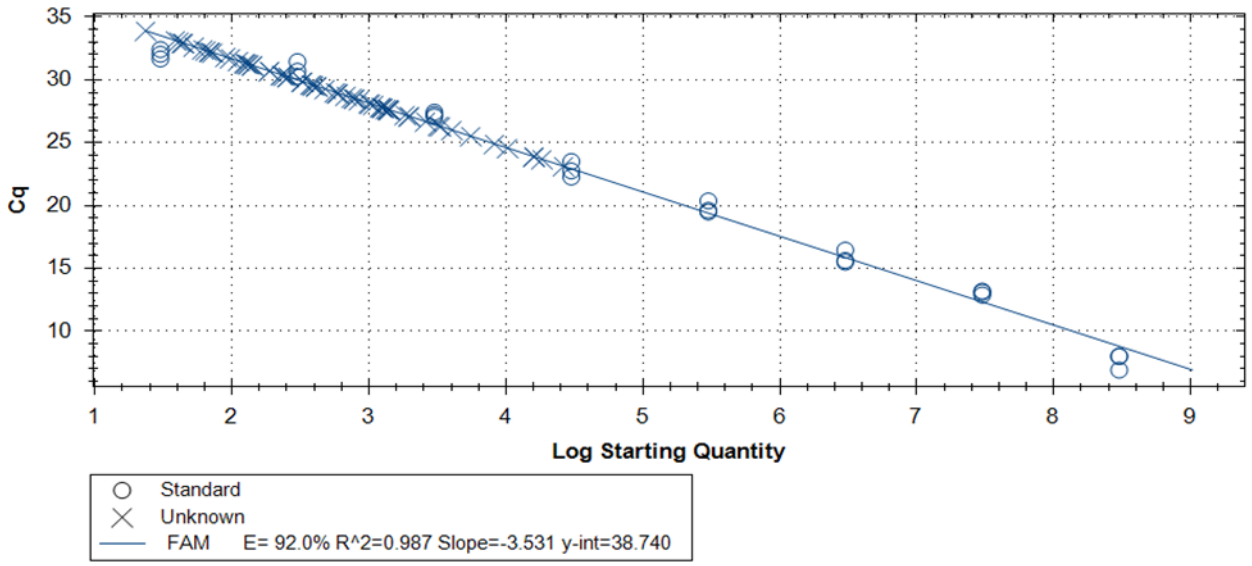

Figure A.3 qPCR samples and standards amplification plot. An example of the qPCR standard curve (O), plus a subset of extracted DNA from frozen amnion and chorion (X) created on CFX Manager V3.1, comparing $\log_{10}$ starting quantity (SQ) with quantification cycle mean (CQ). R^2, slope and efficiency are displayed.

Sample	Tissue section	Copy number/µl	Copy number/mg	Within range?
HCA 09 CH	1	10.380	20.760	No
	2	11.679	23.358	No
	3	33.528	67.055	No
HCA 14 CH	3	48.726	97.452	No
HCA 15 AM	2	322.902	645.805	Yes
	3	21.247	42.494	No
HCA 15 CH	3	8633.842	17267.680	Yes
HCA 16 AM	3	1130.511	2261.021	Yes
HCA 17 AM	1	73441.670	146883.300	Yes
	2	10568.180	21136.370	Yes
	3	2111.117	4222.234	Yes
HCA 17 CH	1	92987.310	185974.600	Yes
	2	4754.246	9508.492	Yes
	3	55484.050	110968.100	Yes
HCA 19 AM	1	224.747	449.495	Yes
	3	1201.345	2402.689	Yes
HCA 19 CH	1	2573.476	5146.952	Yes
	2	293.707	587.415	Yes
	3	475.672	951.344	Yes
HCA 21 AM	1	1484.093	2968.187	Yes
	2	120.325	240.650	Yes
HCA 21 CH	1	2148.411	4296.821	Yes
	2	47.768	95.536	No
HCA 22 AM	1	562.466	1124.933	Yes
	2	422.715	845.430	Yes
	3	720.395	1440.791	Yes
HCA 22 CH	1	231.220	462.441	Yes
	2	338.619	677.239	Yes
	3	1004.616	2009.232	Yes
HCA 24 AM	2	1119.270	2238.540	Yes

	3	1478.768	2957.537	Yes
HCA 24 CH	1	9257.494	18514.990	Yes
	2	148.551	297.102	Yes
	3	490.508	981.015	Yes
HCA 26 AM	1	1688.208	3376.415	Yes
	2	1626.550	3253.100	Yes
	3	769.581	1539.163	Yes
HCA 26 CH	1	4884.652	9769.305	Yes
	3	1208.249	2416.498	Yes
HCA 29 AM	2	1312.972	2625.943	Yes
HCA 29 CH	1	128.211	256.423	Yes
	2	152.892	305.785	Yes
HCA 31 CH	1	1090.911	2181.822	Yes
PTB 05 CH	2	278.150	556.300	Yes
PTB 18 AM	1	398.059	796.118	Yes
	2	61.046	122.092	No
	3	40.938	81.877	No
PTB 18 CH	1	26.696	53.392	No
	2	164.758	329.516	Yes
	3	26.173	52.346	No
PTB 20 AM	1	304.121	608.242	Yes
	2	173.705	347.410	Yes
	3	139.040	278.080	Yes
PTB 20 CH	1	668.226	1336.452	Yes
	2	143.723	287.447	Yes
PTB 23 AM	1	57.537	115.073	No
	2	64.515	129.030	No
	3	41.426	82.852	No
PTB 23 CH	2	90.375	180.750	No
	3	33.927	67.854	No
PTB 25 AM	1	88.432	176.864	No
	3	243.309	486.617	Yes
PTB 25 CH	1	146.773	293.545	Yes

	2	167.800	335.600	Yes
	3	22.770	45.540	No
PTB 27 AM	1	59.218	118.436	No
	2	222.747	445.494	Yes
	3	63.699	127.397	No
PTB 27 CH	2	19.512	39.023	No
	3	36.744	73.488	No
TERM 02 CH	1	304.220	608.439	Yes
TERM 03 CH	1	8.501	17.002	No
TERM 06 CH	1	259.546	519.091	Yes
TERM 07 CH	1	98.175	196.349	No
	2	303.209	606.418	Yes
TERM 08 CH	1	181.213	362.426	Yes
	2	5.309	10.619	No
TERM 28 CH	2	55.469	110.937	No
NEG 01	-	173.358	-	Yes
NEG 02	-	106.293	-	Yes
NEG 03	-	102.989	-	Yes
NEG 04	-	86.741	-	No
NEG 05	-	99.888	-	No
NEG 06	-	252.556	-	Yes
NEG 07	-	105.079	-	Yes
NEG 08	-	134.129	-	Yes
NEG 09	-	83.004	-	No
NEG 10	-	130.437	-	Yes

Table A.4 qPCR fetal membrane sample copy number results. Calculated copy numbers for fetal membrane tissue samples. Values are displayed as starting quantity copy number/µl and copy number/mg and indicated if results were within range for the assay >100 copies/µl. Samples include histological chorioamnionitis (HCA), preterm (PTB) and term without chorioamnionitis (Term), plus kit negative controls (NEG), patient sample number and membrane origin (amnion=AM, chorion=CH). Tissue section represents sample segment utilised.

Sample	Copy number/µl	Copy number/mg	Within range?
1255	114.427	228.855	Yes
1272	186.731	373.461	Yes
1288	171.773	343.546	Yes
1294	319.956	639.916	Yes
1300	407.758	815.516	Yes
1314	116.619	233.237	Yes
1315	301.512	603.023	Yes
1349	110.471	220.942	Yes
1361	86.448	172.895	No
1448	1.802	3.604	No
1567	125.830	251.660	Yes
1568	123.945	247.890	Yes
1258	47.063	94.126	No
1271	38.697	77.393	No
1274	36.772	73.545	No
1283	65.535	131.070	No
1286	37.052	74.104	No
1291	25.401	50.801	No
1297	14.399	28.799	No
1306	0.034	0.068	No
1308	24.060	48.120	No
1313	37.413	74.826	No
1316	25.490	50.979	No
1318	73.131	146.262	No
1328	25.498	50.996	No
1334	14.594	29.188	No
1339	17.490	34.980	No
1340	31.192	62.383	No
1344	27.154	54.308	No
1345	20.798	41.596	No

1362	37.997	75.993	No
1364	66.424	132.847	No
1435	21.777	43.554	No
1437	61.569	123.139	No
1439	80.494	160.989	No
1447	89.888	179.776	No
1449	5.558	11.116	No
1450	50.753	101.505	No
1453	42.043	84.086	No
1354	331.563	663.126	Yes
1383	10.321	20.641	No
1385	74.112	148.223	No
1386	53.612	107.224	No
1408	255.196	510.393	Yes
1426	30.920	61.841	No
1456	39.410	78.820	No
1457	17.075	34.149	No
1463	37.328	74.656	No
1464	13.487	26.974	No
1470	20.510	41.020	No
1471	67.297	134.593	No
1483	20.385	40.771	No
1488	25.710	51.421	No
1495	72.145	144.290	No
1506	38.284	76.567	No
1513	78.455	156.909	No
1523	0.679	1.358	No
1529	1.929	3.858	No
NEG 01	69.332	-	No
NEG 02	150.626	-	Yes
NEG 03	111.928	-	Yes
NEG 04	137.608	-	Yes

Table A.5 qPCR low risk term fetal membrane sample copy number results. Calculated copy numbers for low risk term fetal membrane tissue samples. Values are displayed as starting quantity copy number/µl and copy number/mg and indicated if results were within range for the assay >100 copies/µl. Patient sample number and negative control replicates displayed.

Placenta 91 (2020) 43–51

Contents lists available at ScienceDirect

Placenta

journal homepage: http://www.elsevier.com/locate/placenta

Fetal membrane bacterial load is increased in histologically confirmed inflammatory chorioamnionitis: A retrospective cohort study☆

Rochelle Hockney [a,b], Gareth J. Waring [d], Gillian Taylor [a,b], Stephen P. Cummings [a,b], Stephen C. Robson [d], Caroline H. Orr [a,b,*], Andrew Nelson [c]

[a] School of Health and Life Sciences, Teesside University, Middlesbrough, TS1 3BX, UK
[b] National Horizons Centre, Teesside University, 38 John Dixon Lane, Darlington, DL1 1HG, UK
[c] Faculty of Health and Life Sciences, Northumbria University, Newcastle, NE1 8ST, UK
[d] Institute of Cellular Medicine, Newcastle University, Newcastle, NE2 4HH, UK

ARTICLE INFO

Keywords:
Histological chorioamnionitis
Placenta
Fetal membrane
Microbiome
Inflammation
Bacterial load

ABSTRACT

Introduction: It is widely debated whether fetal membranes possess a genuine microbiome, and if bacterial presence and load is linked to inflammation. Chorioamnionitis is an inflammation of the fetal membranes. This research focussed on inflammatory diagnosed histological chorioamnionitis (HCA) and aimed to determine whether the bacterial load in fetal membranes correlates to inflammatory response, including histological staging and inflammatory markers in HCA.

Methods: Fetal membrane samples were collected from patients with preterm spontaneous labour and histologically phenotyped chorioamnionitis (HCA; n = 12), or preterm (n = 6) and term labour without HCA (n = 6). The bacterial profile of fetal membranes was analysed by sequencing the V4 region of the 16S rRNA gene. Bacterial load was determined using qPCR copy number/mg of tissue. The association between bacterial load and bacterial profile composition was assessed using correlation analysis.

Results: Bacterial load was significantly greater within HCA amnion ($p = 0.002$) and chorion ($p = 0.042$), compared to preterm birth without HCA. Increased bacterial load was positively correlated with increased histological staging ($p = 0.001$) and the expression of five inflammatory markers; IL8, TLR1, TLR2, LY96 and IRAK2 ($p = <0.050$). Bacterial profiles were significantly different between membranes with and without HCA in amnion ($p = 0.012$) and chorion ($p = 0.001$), but no differences between specific genera were detected.

Discussion: Inflammatory HCA is associated with infection and increased bacterial load in a dose response relationship. Bacterial load is positively correlated with HCA severity and the TLR signalling pathway. Further research should investigate the bacterial load threshold required to generate an inflammatory response in HCA.

1. Introduction

Histological chorioamnionitis (HCA) is an inflammation of the fetal membranes [1], linked to adverse maternal and neonatal outcomes, including preterm birth [2], early onset sepsis and necrotising enterocolitis [3,4]. HCA incident rates are higher in preterm (15%) compared to term (5%) infants [5].

The origin of bacteria within the healthy fetal membrane microbiome is widely debated [6]. Conflicting studies have suggested that the placenta and fetal membranes are: (i) sterile [7–9], with any detection of bacteria linked to the mode of delivery [10]; (ii) typically sterile, with any bacteria detected arising due to co-existent maternal conditions, such as periodontal disease [10,11], vaginal infection [12], or gestational diabetes [13]; (iii) universally colonised with low abundant, non-pathogenic bacteria [14]. Although the existence of a unique microbiome in healthy membranes remains debated [6,14], the healthy bacterial profile (composition and proportion of bacteria) is suggested to consist mainly of *Escherichia* spp. [14,15]. Alternatively, HCA

☆ Setting of work reported: National Horizons Centre, School of Health and Life Sciences, Teesside University, United Kingdom and Faculty of Health and Life Sciences, Northumbria University, United Kingdom.

* Corresponding author. School of Health and Life Sciences, Teesside University, Middlesbrough, TS1 3BX, UK.
E-mail addresses: r.hockney@tees.ac.uk (R. Hockney), gareth.waring@newcastle.ac.uk (G.J. Waring), taylor@tees.ac.uk (G. Taylor), s.cummings@tees.ac.uk (S.P. Cummings), s.c.robson@newcastle.ac.uk (S.C. Robson), c.orr@tees.ac.uk (C.H. Orr), andrew3.nelson@northumbria.ac.uk (A. Nelson).

https://doi.org/10.1016/j.placenta.2020.01.006
Received 13 November 2019; Received in revised form 14 January 2020; Accepted 18 January 2020
Available online 21 January 2020

membranes from preterm and term labour have presented with *Ureaplasma* spp. in 59% and 60% of cases respectively [2], suggesting any involvement is independent of gestation. Whilst other studies link HCA and inflammation with increased bacterial load (measurable quantity of bacteria) [16], with a positive correlation between the load of *Prevotella* spp. and HCA severity [17]. Alternatively, lower bacterial diversity has been implicated in preterm HCA membranes compared to controls [15], with monomicrobial characteristics in 83% of HCA cases [2]. In contrast, studies using shotgun and 16S rRNA gene sequencing have reported no distinct bacterial profiles in HCA membranes [6].

Careful consideration is required when elucidating the microbiome of fetal membranes due to low biomass characteristics. It is stated that external bacterial contribution will occur from the use of commercial kits and reagents, especially in low biomass samples [18]. Thus comparison of samples to DNA extraction kit negative controls is required. However, within the placental and fetal membranes this may also originate from contributing vaginal or skin bacteria during delivery or labour [19,20].

Changes in inflammatory receptors and proinflammatory cytokines have been linked to HCA, including a two-fold increase in Toll-like Receptor 2 (TLR2) [21] and Interleukin 8 (IL8) [22], suggesting the involvement of bacteria as pro-inflammatory agents. However, the increase in cytokines may be indicative of active labour rather than being specific to HCA [23]. Inflammatory biomarkers are routinely investigated for risk of preterm birth [24] and clinical chorioamnionitis [25], but not yet applied to monitoring the risk or prediction of HCA.

1.1. Aims and objectives

Given HCA is a leading cause of preterm birth [26], research investigating the aetiology focused specifically on HCA is important. Although HCA and clinical chorioamnionitis overlap, the use of an established reproducible diagnostic criteria as a marker of fetal membrane infection ensures focus on HCA. This study aims to quantify the bacterial load, bacterial profile and diversity in fetal membranes to explore its relationship with the inflammatory response in HCA, including histological staging and inflammatory markers.

2. Methods

2.1. Tissue selection and preparation

Samples of placenta and fetal membranes (amnion and chorion) were collected, stored and phenotyped histologically using the established histological criteria by an independent clinician. Full criteria are described in Waring et al. (2015) [21]. The samples were utilised following informed consent for current research via a transfer agreement, with prior approval from Newcastle and North Tyneside 1 Research Ethics Committee (Ref: 10/H0906/71).

Fetal membrane samples were collected from 24 patients. Following histological diagnosis of HCA, patients were prospectively assigned to spontaneous preterm birth with histological chorioamnionitis (PTB+HCA, n = 12), spontaneous preterm birth without HCA (PTB-HCA, n = 6) and spontaneous term birth without HCA (TB-HCA, n = 6). Amnion and chorion were available for a subset of patients (PTB+HCA = 8, PTB-HCA = 5, TB-HCA = 0). In the remainder, amnion (PTB+HCA = 1, PTB-HCA = 0, TB-HCA = 0), or chorion only were processed (PTB+HCA = 3, PTB-HCA = 1, TB-HCA = 6). Samples were processed in triplicate and prepared with nine DNA extraction kit negative controls. Negative controls were processed identical to samples, with dH_2O replacing tissue samples.

HCA was defined by standardised criteria, at maternal stage two and above [27]. Subchorionitis was defined as inflammatory stage one [27]. Labour was defined as the presence of regular spontaneous uterine contractions with progressive cervical dilation leading to delivery. Term was defined as a gestational age of >37 weeks, term patients were excluded if presenting with histologically indicated chorioamnionitis. Preterm samples were collected from patients delivering with a singleton pregnancy, in spontaneous labour at <34 weeks gestation, due to the inverse relationship between HCA and gestation [5]. Further sampling methods are presented in Waring et al. (2015) [21].

2.2. Genomic DNA extraction

Total genomic DNA was extracted from samples (n = 78) and negative controls (n = 9) using QIAamp Fast DNA Tissue Kit (Qiagen) as per manufacturer protocol. NanoDrop 1000 spectrophotometer (V3.8.1, Thermo Fisher) and agarose gel electrophoresis were used to assess yield, purity and quality of DNA prior to downstream analysis.

2.3. Quantitative PCR

Plasmid standards (16S rRNA gene) were generated using *Escherichia coli* genomic DNA and amplified via 27F (5′-AGAGTTTGATCMTGGCTCAG-3′) and 1492R primers (5′-TACGGYTACCTTGTTACGACTT-3′, Eurofins). PCR amplicons were purified (ExoSap-IT PCR clean up Kit; Thermo Fisher, Cat No:78201.1), before cloning into TOP10 competent *E. coli* cells (Thermo Fisher, Cat No:C404010) using PGEM-T Easy Vector System (Promega, Cat No:A1360). Plasmids were isolated using PureYield Plasmid MiniPrep (Promega, Cat No:A1223). A ten-fold serial dilution of pooled isolated plasmids was performed to create standard curves.

Absolute qPCR aimed to determine bacterial load within fetal membrane samples using BactQuant primers (F = 5′-CCTACGGGDGGCWGCA-3′ *E. coli* 341–356, R = 5′-GGACTACHVGGGTMTCTAATC-3′ *E. coli* 786–806) and probe ((6FAM) 5′-CAGCAGCCGCGGTA-3′ (MGBNFQ) *E. coli* 518–532; Eurofins) [28]. Reactions contained 1 μl sample DNA, 1.8 μm forward and reverse primers, 225 nM probe, 0.05 μg/μl BSA, 4 mM $MgCl_2$, 1% formamide and 1X TaqMan Fast Advanced Master Mix (Thermo Fisher, Cat No:4444557) in a total of 10 μl. Extracted DNA from samples and standards, plus controls of DNA extraction kit negatives and no template controls (NTC) were assayed in triplicate using CFX Connect Real Time System (Biorad, CFX Manager V3.1). BactQuant protocol was used [28], with an optimised annealing temperature of 55 °C.

2.4. Expression of inflammatory markers

The expression of TLR signalling pathway components was undertaken by relative qPCR and has been reported previously [21]. Briefly, genes showing significant change in expression on signalling arrays were individually validated using qPCR. TaqMan GAPDH was selected as an endogenous control due to consistent results as a house-keeping gene in the signalling array study. Each assay was performed in triplicate. Findings indicated the involvement of TLRs in HCA, initiating this research into bacterial involvement in HCA.

2.5. Microbiota analysis

Sequencing of DNA samples and negative controls was performed by NU-OMICs (Northumbria University, UK) as described previously [29], with the universal 16S rRNA gene primer specific to the V4 region [30]. A sequencing negative control and ZymoBIOMICS mock microbial community standard were processed alongside samples.

Package DADA2 1.4 [31] and Bioconductor (Version 2) [32] were used to trim and filter MiSeq data with a q score of <30, to ensure consistent length and high-quality reads [32]. Forward and reverse paired strands were merged and clustered into Amplicon Sequence Variants (ASVs) [33], with clusters differentiated by one nucleotide, for high resolution bacterial detection [33]. Chimeras were removed using remove BimeraDenovo, before assigning taxonomy and constructing a phylogenetic tree using RDP14 reference database [34].

2.6. Statistical analyses

Patient characteristics were analysed using the package TableOne in R [35]. Outcomes were assessed between subgroups using Kruskal Wallis and Wilcoxon Rank-Sum, with categorical data analysed by Pearson's Chi-Squared or Fisher's Exact [35].

For the analysis of bacterial load, copy numbers of 16S rRNA gene/mg of tissue were calculated and $\log_{10}$ transformed. Comparison between conditions were conducted using Kruskal Wallis followed by Pairwise Wilcoxon Rank-Sum and visualised with ggplot2 [35]. The correlation of bacterial load to histological staging or inflammatory marker fold change was performed using linear regression [36] and Spearman's Rho Bonferroni, respectively [35].

For bacterial abundance, PERMANOVA (GUniFrac) and Shannon Alpha diversity were explored using Phyloseq [37]. Shannon Alpha diversity assesses local bacterial composition in a sample, determining variety and number of bacterial genera [38], with this method beneficial for low read count and low abundance samples [38]. Whereas beta diversity matrices (PERMAONVA GUniFrac) compare community level similarity across different samples and subgroups [39]. Further univariate analysis applied false discovery rate corrections (FDR). FDR controls for multiple comparisons and allows understanding of type one errors or false-positive results [39]. Comparison between conditions and the above findings were performed by Kruskal Wallis and Pairwise Wilcoxon Rank-Sum, before visualising with ggplot2 [35].

3. Results

Participant characteristics are shown in Table 1. No differences were identified between participants in the PTB+HCA and PTB-HCA subgroups other than HCA stage (p=<0.001) and grade (p = 0.036). Although the focus of this research was HCA, one patient with inflammatory diagnosed HCA also presented with clinical signs of chorioamnionitis.

3.1. Bacterial load is increased with HCA

Fetal membranes from participants with PTB+HCA displayed a greater mean bacterial load than those with PTB-HCA (3.4 $\log_{10}$/mg vs 2.4 $\log_{10}$/mg, p=<0.001). When investigating individual membranes; significantly greater bacterial load was evident in PTB+HCA amnion tissues compared to PTB-HCA amnion tissues (3.3 $\log_{10}$/mg vs 2.4 $\log_{10}$/mg, p = 0.002; Fig. 1A). In chorion tissues, PTB+HCA bacterial loads were also greater compared with PTB-HCA (3.3 $\log_{10}$/mg vs 2.3 $\log_{10}$/mg, p = 0.042) and TB-HCA (3.3 $\log_{10}$/mg vs 2.3 $\log_{10}$/mg, p = 0.031). No difference was found between PTB-HCA and TB-HCA chorion (p = 0.937, Fig. 1B).

3.2. Bacterial load positively correlates with histological staging in HCA

There was a significantly positive correlation between bacterial load and histological staging of membrane inflammation (p = 0.001; Fig. 2), with higher bacterial load related to higher stage of HCA.

3.3. Bacterial load is positively correlated with inflammatory gene expression

Bacterial loads in amnion and chorion were significantly correlated to the expression of some inflammatory markers (Table 2). In the chorion, bacterial load was positively correlated with IL8 (p = 0.002), LY96 (p = 0.003), IRAK2 (p = 0.004), TLR2 (p = 0.005) and TLR1 (p = 0.013). In the amnion, only IL8 was significantly correlated with bacterial load (p = 0.050).

3.4. There is varied range of bacterial genera present irrespective of histological phenotype

The bacterial profile was significantly different between groups of PTB+HCA, PTB-HCA and TB-HCA in both chorion (R^2 = 0.2, p = 0.010), and amnion (R^2 = 0.2, p = 0.012; Fig. 1C and 1D). However, no specific genera were statistically significantly different when comparing between groups.

3.5. Alpha diversity does not differentiate between conditions

PTB+HCA samples had the higher overall bacterial diversity (0.7), with PTB-HCA (1.0) and TB-HCA lower (1.1), yet no difference between groups (p = 0.220). When analysing by tissue type, although diversity was highest in both PTB+HCA amnion and chorion the differences across conditions were not statistically significant (Fig. 3).

Table 1
Sample characteristic data. Assessed between conditions of histological chorioamnionitis (PTB+HCA), plus preterm (PTB-HCA) and term birth without chorioamnionitis (TB-HCA). Comparison between all three groups was performed using Kruskal-Wallis and Pearson's chi-squared. Characteristics monitored in PTB+HCA and PTB-HCA only using Wilcoxon Rank-Sum and Fisher's exact test. Significance threshold for comparisons was p = ≤0.05 (bold and italics). Results are displayed as n (%) or mean (SD). Data unavailable for term subjects (-).

Characteristic	Preterm birth with HCA (PTB + HCA) (n = 12)	Preterm birth without HCA (PTB-HCA) (n = 6)	Term birth without HCA (TB-HCA) (n = 6)	*p. value* PTB + HCA PTB-HCA TB-HCA	*p. value* PTB + HCA PTB-HCA
Gestational age (mean (SD))	29.6 (2.9)	29.7 (4.0)	40.4 (0.6)	***0.001***	0.779
Birthweight (mean (SD))	1387.0 (504.4)	1736.7 (402.3)	3250.0 (495.6)	***0.001***	0.291
Maternal age (mean (SD))	29.3 (8.0)	27.0 (5.5)	32.2 (6.0)	0.411	0.511
BMI (mean(SD))	22.0 (9.2)	22.5 (4.5)	22.3 (2.1)	0.515	0.580
Smoker	4.0 (33.3)	2.0 (33.3)	0.0	0.329	0.806
Mode of delivery					
Spontaneous vaginal	8.0 (66.7)	5.0 (83.3)	-	-	1.000
Caesarean section	4.0 (33.3)	1.0 (16.7)	-	-	
PPROM	9.0 (75.0)	3.0 (50.0)	-	-	0.330
Interval from PPROM to labour (mean(SD))	7.0 (3.2)	1.7 (0.6)	-	-	0.051
Previous preterm birth	5.0 (41.7)	1.0 (16.7)	-	-	0.600
Antibiotics	7.0 (58.3)	4.0 (66.7)	-	-	0.604
Antenatal corticosteroids	11.0 (91.7)	5.0 (83.3)	-	-	1.000
HCA Stage (mean (SD))	2.2 (0.4)	1.0 (0.0)	-	-	***<0.001***
HCA Grade (mean (SD))	1.6 (0.5)	1.0 (0.0)	-	-	***0.036***
Clinical cases of chorioamnionitis	1.0 (8.3)	0 (0.0)	-	-	0.556

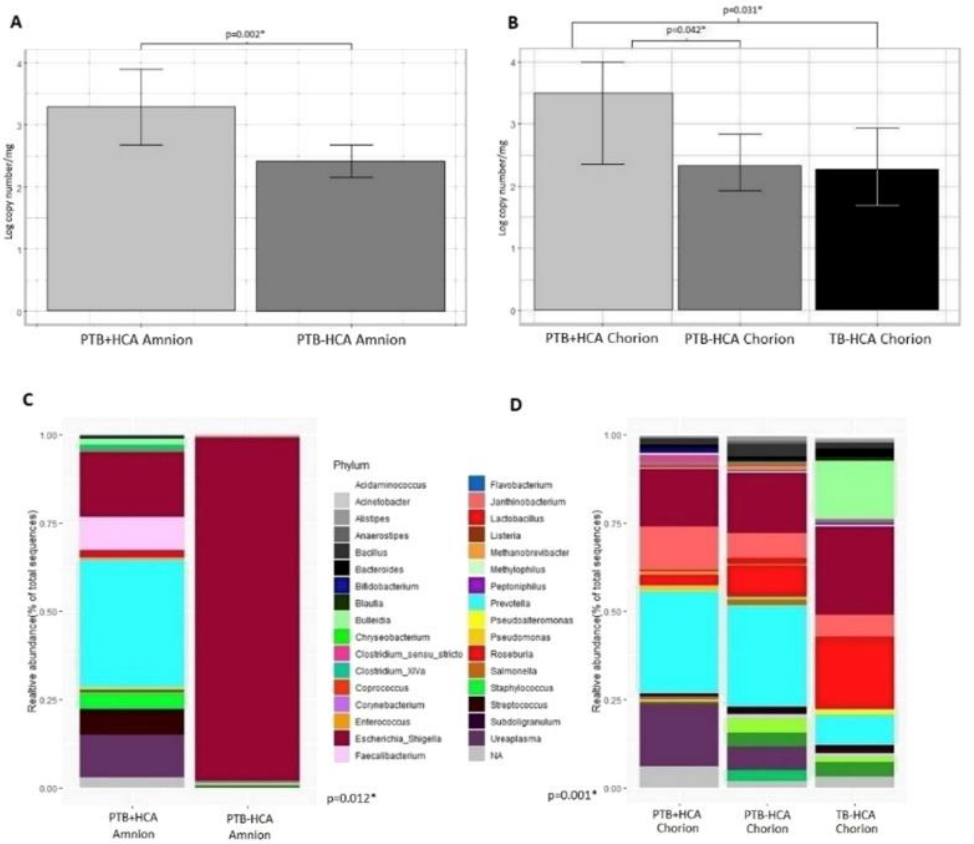

Fig. 1. Quantitative PCR analysis of bacterial load (A + B) and NGS relative abundance (C + D). qPCR data displayed by log copy number/mg of sample from amnion (A) or chorion (B) with histological chorioamnionitis (PTB+HCA), preterm birth without chorioamnionitis (PTB-HCA) and term birth without HCA (TB-HCA). Significance was determined using Kruskal Wallis and Pairwise Wilcoxon Rank-Sum to a threshold of $p = \leq 0.05$. Relative abundance variation was further analysed between PTB+HCA, PTB-HCA and TB-HCA in amnion (C) and chorion (D) using GUniFrac PEMANOVA to a significance of $p = \leq 0.05$. Relative abundance was defined as the abundance of each individual genera relative to total percentage of bacterial genera.

3.6. Non-HCA samples and negative controls differ in bacterial profiles and specific genera, but not bacterial load

Sequencing and qPCR results from preterm and term patients without HCA were compared to negative controls to investigate genuine microbiota detection from non-HCA fetal membranes. The overall bacterial profiles were significantly different between non-HCA samples and negative controls ($r^2 = 0.2$, p=<0.001; Fig. 4A). Further significance was detected between specific genera. *Dorea* was detected in negative controls (average read number = 163.1), but not detected in non-HCA samples ($p = 0.001$, FDR = 0.027). The mean abundance from *Pseudomonas* was significantly greater in negative controls (91.7) compared to PTB-HCA (4.8) and TB-HCA samples (2.8; $p = 0.002$, FDR = 0.030). *Escherichia* was significantly reduced in TB-HCA (45.5), compared to similar levels from PTB-HCA (2295.2) and negative controls (2237.2; p=<0.001, FDR=<0.001). There was no variation in *Lactobacillus* ($p = 0.050$, FDR = 0.303), *Ureaplasma* ($p = 0.073$, FDR = 0.308) or *Prevotella* ($p = 0.608$, FDR = 0.730).

No significant difference was detected when comparing bacterial loads of non-HCA samples to negative controls (2.4 $\log_{10}$, $p = 0.9277$; Fig. 4B). For clarification, no bacterial loads were detected from NTCs for all qPCR experiments.

4. Discussion

4.1. Main findings

Findings indicate that a greater bacterial load is associated with HCA and a greater bacterial load is positively correlated with greater histological staging and inflammatory markers. This supports the suggestion that bacteria act as inflammatory agents in a dose dependent manner in HCA.

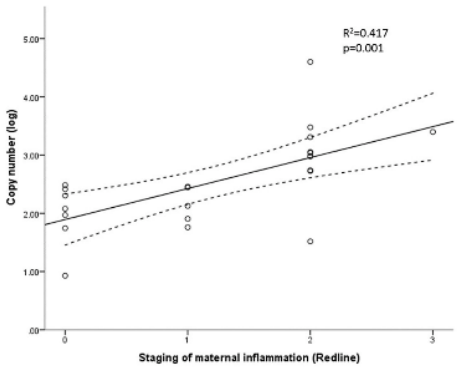

Fig. 2. Linear regression analysis. Analysis between bacterial load (log copy number) and histological staging of membrane inflammation using linear regression to a threshold of p = ≤0.05.

4.2. Interpretation

The key finding of this study is that inflammation in the fetal membranes is associated with presence of bacterial infection and increased bacterial load. Previous research supports the theory that bacterial presence is linked to HCA [19,20], with 97% of HCA cases presenting with bacterial colonisation [40], leading to microbial associated inflammation of the amnion [40]. Bacterial loads of up to 5.2 log_{10} copies/μl have also been detected in fetal membranes with HCA [16], consistent with our findings. In contrast, Romero et al. (2014) [41] detected bacteria in 11% of amniotic fluid samples with PTB and intra-amniotic inflammation, compared to 26% with a sterile inflammatory response [41]. Studies have linked HCA to bacterial loads of specific genera, including *Prevotella* [17] and *Ureaplasma* [40]. The expansion of *Ureaplasma* in HCA was supported here yet did not reach significance. Although inflammation has not been attributed to specific organisms here, investigation of the species-specific bacterial load may play a role in this multifactorial inflammatory condition. As the likely passage of bacteria is ascending, lower bacterial load would be expected in the chorion. Although consistent bacterial load was present across membranes with HCA here, the inflammatory response may differ across membranes impacting clinical relevance and requiring further investigation.

Findings show that bacterial load is positively correlated with HCA severity in a dose dependent manner. This observation is supported across multiple methodologies and tissue types [19,42,43]. Research on chorioamniotic membranes has suggested that as HCA severity increased, so did bacterial load [19]. Bacteria were detected in 87% of membranes with stage three HCA, compared to 33%, 40% and 60% with stage zero, one and two HCA, respectively [19]. In amniotic fluid, bacterial load was 10^6 copies/ml with stage three HCA, compared to 10^3 copies/ml in stages zero, one and two [42]. However, the link between bacterial load and inflammation in HCA has been questioned, with the suggestion that any increase in bacterial load or inflammation is due to active labour rather than specific to HCA [23]. In this study all patients recruited were in spontaneous active labour, limiting variation and controlling for vaginal contamination, and the relationship between histological grading and bacterial load remained consistent. Although the focus here was on preterm patients, studies addressing HCA at term are required.

Data suggests that bacterial load correlates to inflammation via activation of the TLR signalling pathway. We have previously reported an increase in gene expression of TLR1 and TLR2 in HCA in the same samples, with a correlation between the increase in TLR gene expression and HCA stage in both amnion and chorion [21]. Correlation between HCA bacterial load with TLR1/2 suggests that the number of gram-negative bacteria in the fetal membranes may be important in the development of HCA, as the TLR1/2 heterodimer recognises lipopeptides from gram negative bacteria. Although a trend was present, we were unable to identify significant differences in specific genera (including gram-negative bacteria) between groups. IL8 was the only inflammatory marker that correlated with bacterial load in both membranes. The IL8 ligand has been detected in greater concentrations from HCA patients compared to without HCA, as supported by Kacerovsky et al. (2009) [44]. IL8 levels have previously been used to predict HCA staging in amniotic fluid, with high specificity [45]. Alternatively, danger signals including HMGB1 also activate the TLR/MyD88 dependent pathway [46], known as the sterile inflammatory response theory [41]. However, our work suggests that bacterial load is the key driver to inflammation in the fetal membranes studied here.

Findings show that non-HCA samples and negative controls differ in few specific bacterial genera but display no difference in bacterial load. Previous studies have also detected genera originating mainly from negative controls, including *Dorea* and *Pseudomonas* when establishing bacterial profiles of placental samples [18,47]. These genera are suggested to be contaminants in low biomass research [18, 47], thus findings indicating clinical relevance of these bacteria are to be carefully analysed and ensure that correct methodology and negative controls have been included to avoid misinterpretation.

4.3. Research and clinical implications

Conflicting literature highlights the difficulty of reaching a

Table 2
Correlation of bacterial load against inflammatory gene fold change. Significant differences displayed individually by amnion or chorion were determined using Spearman's Rank Bonferroni (p = ≤ 0.05, bold and italics).

Amnion			Chorion		
Inflammatory marker	Spearman's R_s	*p. value*	Inflammatory marker	Spearman's R_s	*p. value*
TLR1	0.346	0.247	***TLR1***	***0.538***	***0.013***
TLR2	0.489	0.093	***TLR2***	***0.600***	***0.005***
TLR4	0.363	0.224	TLR4	0.147	0.524
TLR6	−0.093	0.764	TLR6	0.261	0.252
SARM1	−0.302	0.315	SARM1	0.117	0.613
MyD88	0.346	0.247	MyD88	0.061	0.793
LY96	0.357	0.232	***LY96***	***0.631***	***0.003***
IL8	***0.560***	***0.050***	***IL8***	***0.655***	***0.002***
IRAK2	0.489	0.093	***IRAK2***	***0.612***	***0.004***
HMGB1	0.050	0.878	HMGB1	0.284	0.211
SIGIRR	0.368	0.216	SIGIRR	0.139	0.549
TIRAP	0.088	0.778	TIRAP	0.234	0.306

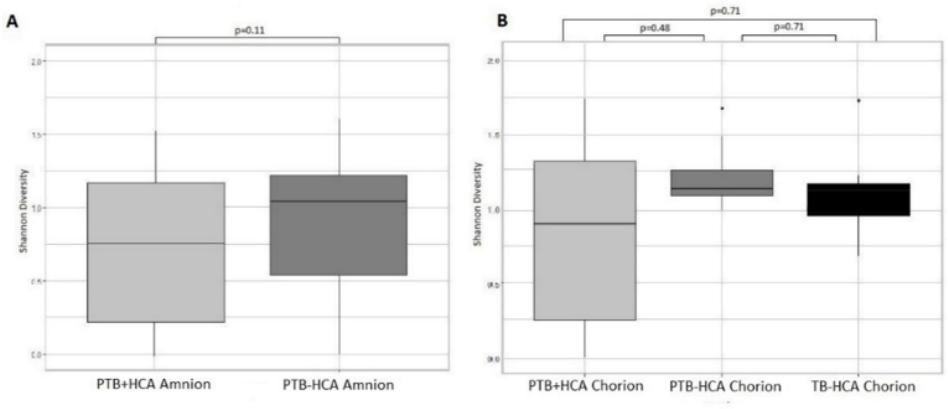

Fig. 3. Alpha diversity analysis. Relative abundance sequencing data analysed by Shannon Alpha diversity between amnion (A) and chorion membranes (B) from preterm birth samples with chorioamnionitis (PTB+HCA), preterm birth without chorioamnionitis (PTB-HCA) and term birth without chorioamnionitis (TB-HCA) to a threshold of $p = \leq 0.05$.

conclusion on the fetal membrane microbiome in HCA [2,16,23,46]. Although a linear relationship between bacterial load and inflammation was detected here, the threshold overall bacterial load required to activate the inflammatory response warrants further study. Investigating selected inflammatory markers as potential biomarkers for HCA, including TLR signalling mediators, may be important, including a focus on LY96 (MD2) which links cell surface TLR to bacterial LPS. PPROM was the most prevalent cause of PTB, occurring in 75% of HCA and 50% of PTB patients, thus it may be of interest to investigate the variation in HCA between PPROM and sPTB. Additional research may also aim to understand the origin of bacteria using multiple body site analysis.

4.4. Strengths and limitations

The absence of a known healthy fetal membrane microbiome complicates the ability to determine a microbiome linked to HCA. Thus, fetal membranes without chorioamnionitis from preterm and term labour are required for within study comparisons, as incorporated into this study. The histological threshold for HCA was set at stage two inflammatory response. However, only one stage three sample was available from the HCA subgroup, limiting conclusions at this level. Excluding stage one subchorionitis ensures specificity to HCA rather than subclinical chorioamnionitis, and is an established reproducible diagnostic criterion for HCA. Other studies may have included stage one, leading to different conclusions as to the role of infection and inflammation in HCA.

The fetal membrane is a low biomass sample [45,47], which increases the risk of contamination [48]. To minimise this, negative controls were included and compared to samples and all samples displayed progressive labour, limiting variation. A 24-patient sample set from one tertiary unit was utilised increasing consistency of sample handling. A larger sample set would have strengthened findings to cover heterogeneity of maternal and fetal response, though the low incidence of early preterm birth and HCA is a recognised challenge in this field of research. For a subset of patients only amnion or chorion were available, which could bias results and is a known limitation of human tissue collection. Bacterial origin cannot be determined as only fetal membrane samples were analysed. The inclusion of vaginal, oral, skin and blood samples would allow greater understanding of the source of bacteria and allow further investigation into the link between reproductive, placental and fetal membrane health [49].

5. Conclusions

The data indicates that inflammation of the fetal membranes is associated with infection and increased bacterial load in a dose dependent relationship, rather than specific bacterial profiles. Bacterial load is positively correlated to HCA severity and activation of the TLR signalling pathway. Further research investigating the bacterial threshold level required to generate an inflammatory response leading to HCA requires attention.

Funding

This work was funded by a grant from the British Maternal and Fetal Medicine Society awarded to Dr Waring and Dr Nelson and supported by the Teesside University Graduate Tutor Scheme with resources provided by the School of Health and Life Sciences.

Details of ethical approval

The samples were utilised for current research via a transfer agreement, with prior approval from Newcastle and North Tyneside 1 Research Ethics Committee (Ref:10/H0906/71).

Contribution to authorship

RH was responsible for qPCR planning, execution, data analysis and interpretation, plus analysis and interpretation of the NGS data, also for drafting the manuscript. GW designed the study, was involved in approval, tissue collection and providing data and analysis for the correlation section. GT and CO were involved in the design, monitoring and support of the study. CO was also involved in qPCR planning. SPC and SCR were responsible for the initial concept and approval for the study. AN was responsible for planning and design of the study, executing the NGS method and support of the study. All authors critically revised the manuscript and gave final approval for publication.

Declaration of competing interest

The Author(s) declare(s) that there is no conflict of interest.

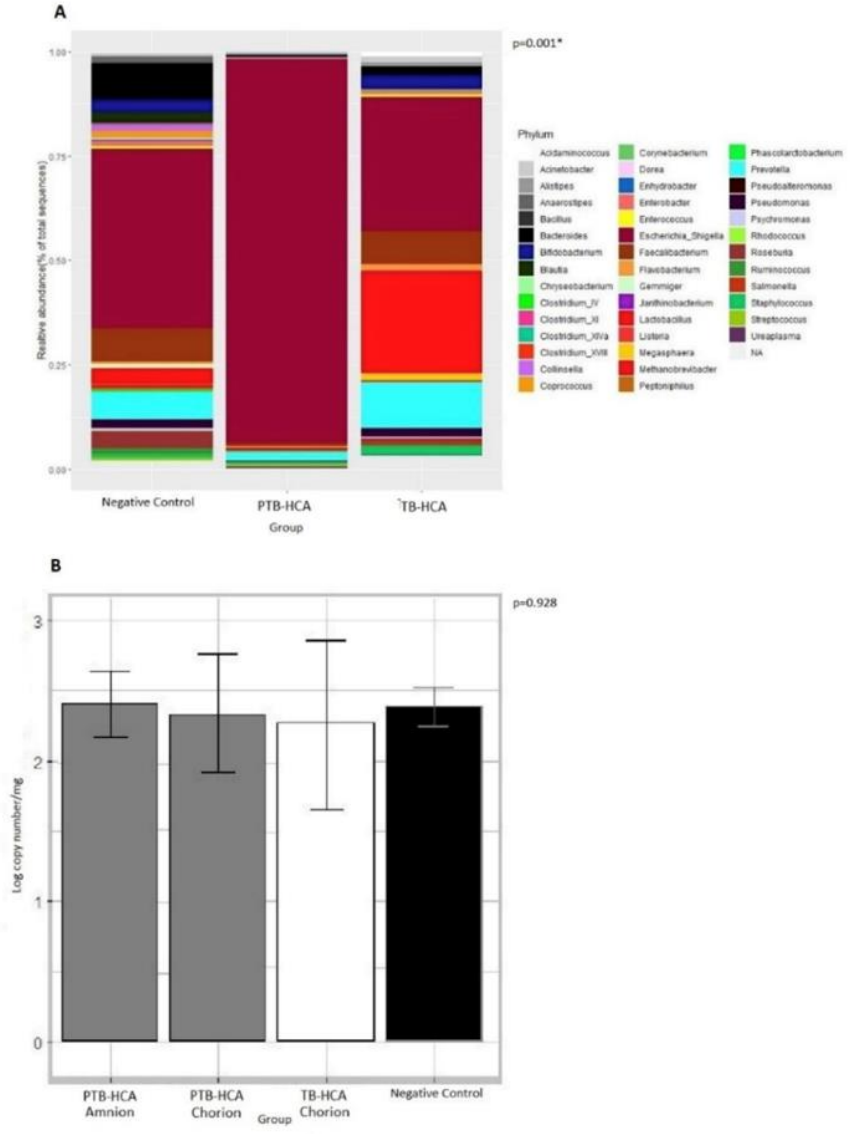

Fig. 4. Negative control comparison; Relative abundance (A) and qPCR bacterial load (B). Analysis between kit negative controls (Negative Control) and non-HCA samples of preterm (PTB-HCA) and term fetal membranes without chorioamnionitis (TB-HCA) were compared. Relative abundance was analysed using GUniFrac PERMANOVA to a significance of $p = \leq 0.05$. qPCR bacterial load (log copy number/mg) results displayed by comparison between PTB-HCA, TB-HCA and Negative Control. Significance was determined using Kruskal Wallis to a threshold of $p = \leq 0.05$.

Acknowledgements

Acknowledgments are made to The Royal Victoria Infirmary (RVI), Newcastle Upon Tyne for allowing collection and access to the tissue samples, also to Dr Judith Bulmer and fellow clinicians at the RVI for collecting and processing samples.

References

[1] A.T.N. Tita, W.W. Andrews, Diagnosis and management of clinical chorioamnionitis, Clin. Perinatol. 37 (2) (2010) 339–354, https://doi.org/10.1016/j.clp.2010.02.003.

[2] E.L. Sweeney, S.G. Kallapur, T. Gisslen, D.S. Lambers, C.A. Chougnet, S. A. Stephenson, A.H. Jobe, C.L. Knox, Placental infection with Ureaplasma species is associated with histologic chorioamnionitis and adverse outcomes in moderately preterm and late-preterm infants, J. Infect. Dis. 213 (8) (2016) 1340–1374, https://doi.org/10.1093/infdis%2Fjiv587.

[3] D.H. Taft, N. Ambalavanan, K.R. Schibler, Z. Yu, D.S. Newburg, H. Deshmukh, D. V. Ward, A.L. Morrow, Centre variation in intestinal microbiota prior to late-onset sepsis in preterm infants, PloS One 10 (6) (2015), e0130604, https://doi.org/10.1371/journal.pone.0130604.

[4] T. Strunk, C. Campbell, D. Burgner, A. Charles, N. French, M. Sharp, K. Simmer, E. Nathan, D. Doherty, Histological chorioamnionitis and developmental outcomes in very preterm infants, J. Perinatol. 39 (2) (2018) 321–330, https://doi.org/10.1038/s41372-018-0288-3.

[5] M.M. Lahra, H.E. Jeffery, A fetal response to chorioamnionitis is associated with early survival after preterm birth, AJOG 190 (1) (2004) 147–151, https://doi.org/10.1016/j.ajog.2003.07.012.

[6] J.S. Leiby, K. McCormick, S. Sherrile-Mix, E.L. Clarke, L.R. Kesslet, L.J. Taylor, C. E. Hofstaedter, A.M. Roche, L.M. Mattei, K. Bittinger, M.A. Elovitz, R. Leite, S. Parry, F.D. Bushman, Lack of detection of a human placenta microbiome in samples from preterm and term deliveries, Microbiome 6 (196) (2015), https://doi.org/10.1186/s40168-018-0575-4.

[7] L.J. Funkhouser, S.R. Bordenstein, Mom knows best: the universality of maternal microbial transmission, PLoS Biol. 11 (8) (2013), e1001631, https://doi.org/10.1371/journal.pbio.1001631.

[8] K.R. Theis, R. Romero, A.D. Winters, J.M. Greenberg, N. Gomez-Lopez, A. Alhousseini, J. Bieda, E. Maymon, P. Pacora, J.M. Fettweis, G.A. Buck, K. K. Jefferson, J.F. Strauss III, O. Erez, S.S. Hassan, Does the human placenta delivered at term have a microbiota? Results of cultivation, quantitative real-time PCR, 16S RRNA gene sequencing, and metagenomics, AJOG 220 (3) (2019), https://doi.org/10.1016/j.ajog.2018.10.018, 267e.1-267.e39.

[9] A.A. Kuperman, A. Zimmerman, A. Hamadia, O. Ziv, V. Gurevich, B. Fichtman, N. Gavert, r. Straussman, H. Rechnitzer, M. Bazilay, S. Shvalb, J. Bornstein, I. Ben-Scachae, S. Yagel, I. Haviv, O. Koren, Deep microbial analysis of multiple placentas shows no evidence for a placental microbiome, BJOG (2019), https://doi.org/10.1111/1471-0528.15896. Epub ahead of print].

[10] R. McCuaig, D. Wong, F.W. Gardiner, W. Rawlinson, J.E. Dahlstrom, R.S. Robson, Periodontal pathogens in the placenta and membranes in term and preterm birth, Placenta 68 (2018) 40–43, https://doi.org/10.1016/j.placenta.2018.06.310.

[11] M.D. Seferovic, A.L. Prince, D.M. Chu, A.G. Sweeney, M.A. Engevik, P.B. Ganesh, N. Andrews, J. Versalovic, K. Aagaard, Recovery of placental bacteria is facilitated by periodontitis in orally inoculated germ-free mice, AJOG 214 (1) (2016) s144, https://doi.org/10.1016/j.ajog.2015.10.282.

[12] R.N. Fichorova, A.B. Onderdonk, H. Yamamoto, M.L. Delaney, A.M. DuBois, E. Allred, A. Leviton for the extremely low gestation age newborns (ELGAN) study investigators, maternal microbe-specific modulation of inflammatory response in extremely low-gestational-age newborns, mBio 2 (1) (2011), https://doi.org/10.1128/mBio.00280-10 e00280-10.

[13] J. Bassols, M. Serino, G. Carreras-Badosa, R. Burcelin, V. Blasco-Baque, A. Lopez-Bermejo, J.-M. Fernandez-Real, Gestational diabetes is associated with changes in placental microbiota and microbiome, Paediatr. Res. 80 (6) (2016) 777–784, https://doi.org/10.1038/pr.2016.155.

[14] K. Aagaard, J. Ma, K.M. Antony, R. Ganu, J. Petrosino, J. Versalovic, The placenta harbours a unique microbiome, Sci. Transl. Med. 6 (237) (2014), https://doi.org/10.1126/scitranslmed.3008599, 127ra65.

[15] A.L. Prince, J. Ma, P.S. Kannen, T. Gisslen, R.A. Harris, E.L. Sweeney, C.L. Knox, D. S. Lambers, A.H. Jobe, C.A. Chougnet, S.G. Kallapur, K.M. Aagaard, The placental membrane microbiome is altered among subjects with spontaneous preterm birth with and without chorioamnionitis, AJOG 214 (627) (2016) e1–627, https://doi.org/10.1016/j.ajog.2016.01.193, e16.

[16] R.M. Doyle, K. Harris, S. Kamiza, U. Hrjunman, U. Ashorn, M. Nkhoma, K. G. Dewey, K. Maleta, P. Ashorn, N. Klein, Bacterial communities found in placental tissues are associated with severe chorioamnionitis and adverse birth outcomes, PloS One 12 (7) (2014), e0180167, https://doi.org/10.1371/journal.pone.0180167.

[17] J.L. Hecht, A. Onderdonk, M. Delaney, E.N. Allred, H.J. Kliman, E. Zambrano, S. M. Pflueger, C.A. Livasy, I. Bhan, A. Lviton, Characterization of chorioamnionitis in 2nd-trimester c-section placentas and correlation with microorganism recovery from subamniotic tissues, Paediatr. Dev. Pathol. 11 (1) (2009) 15–22, https://doi.org/10.2350/07-06-0285.1.

[18] M.C. de Goffau, S. Lager, U. Sovio, F. Gaccioli, E. Cook, S.J. Peacock, J. Parkhill, D. S. Charnock-Jones, G.C.S. Smith, Human placenta has no microbiome but can contain potential pathogens, Nature 572 (7769) (2019) 329–334, https://doi.org/10.1038/s41586-019-1451-5.

[19] M.J. Kim, R. Romero, M.T. Gervasi, J.-S. Kin, W. Yoo, D.-C. Lee, P. Mittal, O. Erez, J.P. Kusanovic, S.S. Hassan, C.J. Kim, Widespread microbial invasion of the chorioamniotic membranes is a consequence and not a cause of intra-amniotic infection, Lab. Invest. 89 (8) (2009) 924–936, https://doi.org/10.1038/labinvest.2009.49.

[20] H.E. Jones, K.A. Harris, M. Azizia, L. Bank, B. Carpenter, J. C Hartley, N. Klein, D. Peebles, Differing prevalence and diversity of bacterial species in fetal membranes from very preterm and term labor, PloS One 4 (12) (2009), e8205, https://doi.org/10.1371/journal.pone.0008205.

[21] G.J. Waring, S.C. Robson, J.N. Bulmer, A.J. Tyson-Capper, Inflammatory signalling in fetal membranes: increased expression levels of TLR 1 in the presence of preterm histological chorioamnionitis, PloS One 10 (5) (2015), e0124298, https://doi.org/10.1371/journal.pone.0124298.

[22] D.C. Kasper, T.P. Mechtler, G.H. Reischer, A. Witt, M. Langgartner, A. Pollak, K. R. Herkner, A. Berger, The bacterial load of Ureaplasma parvum in amniotic fluid is correlated with an increased intrauterine inflammatory response, Diagn. Microbiol. Infect. Dis. 67 (2) (2010) 117–121, https://doi.org/10.1016/j.diagmicrobio.2009.12.023.

[23] D.J. Roberts, A.C. Celi, J.E. Riley, A.B. Onderdonk, T.K. Boyd, L.C. Johnson, E. Lieberman, Acute histological chorioamnionitis at term: nearly always non-infectious, PloS One 7 (3) (2012), e31819, https://doi.org/10.1371/journal.pone.0031819.

[24] R. Menon, R.N. Taylor, S.J. Fortunato, Chorioamnionitis- A complex pathophysiological syndrome, Placenta 31 (2) (2010) 113–120, https://doi.org/10.1016/j.placenta.2009.11.012.

[25] D. Dudzik, R. Revello, C. Barbas, J.L. Bartha, LC-MS based metabolomics identification of novel biomarkers of chorioamnionitis and its associated perinatal neurological damage, J. Proteome Res. 14 (3) (2015) 1432–1444, https://doi.org/10.1021/pr501087x.

[26] V. Tambor, M. Vajrychova, M. Kacerovsky, M. Link, P. Domasinska, R. Menon, J. Lenco, Potential peripartum markers of infectious-inflammatory complications in spontaneous preterm birth, BioMed Res. Int. (2015) 343501, https://doi.org/10.1155/2015/343501.

[27] R.W. Redline, O. Faye-Petersen, D. Heler, F. Qureshi, V. Savell, C. Vogler, The society for pediatric pathology, perinatal section, amniotic fluid infection nosology committee, amniotic infection syndrome: nosology and reproducibility of placental reaction patterns, Paediatr. Dev. Pathol. 6 (5) (2003) 435–448, https://doi.org/10.1007/s10024-003-7070-y.

[28] C.M. Liu, M. Aziz, S. Kachur, P.-O. Hsueh, Y.-T. Huang, P. Keim, L.B. Price, BactQuant: an enhanced broad-coverage bacterial quantitative real-time PCR assay, BMC Microbiol. 12 (56) (2012), https://doi.org/10.1186/1471-2180-12-56.

[29] J.J. Kozich, S.L. Westcott, N.T Baxter, S.K. Highlander, P.D. Schloss, Development of a dual-index sequencing strategy and curation pipeline for analysing amplicon sequence data on the MiSeq Illumina sequencing platform, Appl. Environ. Microbiol. 79 (17) (2013) 5112–5120, https://doi.org/10.1128/AEM.01043-13.

[30] G. Biesbroek, E.A.M. Sanders, G. Roeselers, X. Wang, M.P.M. Caspers, K. Trzcinski, D. Bogaert, B.J.F. Keijser, Deep sequencing analyses of low-density microbial communities: working at the boundary of accurate microbiota detection, PloS One 7 (3) (2012), e32942, https://doi.org/10.1371/journal.pone.0032942.

[31] B.J. Callahan, P.J. McMurdie, M.J. Rosen, A.W. Han, A.J.A. Johnson, S.P. Holmes, DADA2: high resolution sample inference from Illumina amplicon data, Nat. Methods 13 (7) (2016) 581–583, https://doi.org/10.1038/nmeth.3869.

[32] B. Callahan, K. Sankaran, J.A. Fukuyama, P.J. McMurdie, Bioconductor workflow for microbiome data analysis: from to reads to community analyses, F1000 Res. 5 (2016) 1492, https://doi.org/10.12688/f1000research.8986.2.

[33] B.J. Callahan, P.J. McMurdie, S.P. Holmes, Exact sequence variants should replace operational taxonomic units in marker-gene data analysis, ISME J. 11 (12) (2017), https://doi.org/10.1038/ismej.2017.119.

[34] B. Callahan, The RDP and GreenGenes taxonomic training sets formatted for DADA2 [Data set], Zenodo, http://doi.org/10.5281/zenodo.158955, 2016.

[35] R Core Team, R: A Language and Environment for Statistical Computing, R Foundation for Statistical Computing, 2017. Available at: https://www.R-project.org/.

[36] IBM Corp, IBM SPSS Statistics for Windows, IBM Corp, Armonk, NY, 2017. Version 25.0.

[37] P.J. McMurdie, S. Holmes, Phyloseq: an R package for reproducible interactive analysis and graphics of microbiome census data, PloS One 8 (4) (2013), e61217, https://doi.org/10.1371/journal.pone.0061217.

[38] C.E. Shannon, A mathematical theory of communication, Bell Labs Tech. J. 27 (3) (1948) 379–423, https://doi.org/10.1002/j.1538-7305.1948.tb01338.x.

[39] R. Knight, A. Vrbanac, B.C. Taylor, A. Aksenov, C. Callewaert, J. Debelius, A. Gonzalez, T. Kosciolek, L.I. McCall, D. McDonald, A.V. Melnik, J.T. Morton, J. Navas, R.A. Quinn, J.G. Sanders, A.D. Swafford, L.R. Thompson, A. Tripathi, Z. Z. Xu, J.R. Zaneveld, Q. Zhu, J.G. Caporaso, P.C. Dorrestein, Best practice for analysing microbiomes, Nat. Rev. Microbiol. 16 (7) (2015) 410–422, https://doi.org/10.1038/s41579-018-0029-9.

[40] I. Musilova, R. Kitova, L. Pliskova, M. Stepan, R. Menon, B. Jacobsson, M. Kacerovsky, Intraamniotic inflammation in women with preterm prelabor rupture of membranes, PloS One 10 (7) (2015), e0133929, https://doi.org/10.1371/journal.pone.0133929.

[41] R. Romero, J. Miranda, T. Chaiworapongsa, S.J. Korzeniewski, P. Chaemsaithong, F. Gotsch, Z. Dong, A.I. Ahmed, B.H. Yoon, S.S. Hassan, C.J. Kim, L. Yeo, Prevalence and clinical significance of sterile intra-amniotic inflammation in

patients with preterm labor and intact membranes, AJOG 72 (5) (2014) 458–474, https://doi.org/10.1111/aji.12296.
[42] D. Urushiyama, W. Suda, E. Ohnishi, R. Araki, C. Kiyoshima, M. Kurakazu, A. Sanui, F. Yotsumoto, M. Murata, K. Nabeshima, S. Yasunaga, S. Saito, M. Nomiyama, M. Hattori, S. Miyamoto, K. Hata, Microbiome profile of the amniotic fluid as a predictive biomarker of perinatal outcome, Sci. Rep. 7 (12171) (2017), https://doi.org/10.1038/s41598-017-11699-8.
[43] B.W. Kramer, T.J. Moss, K.E. Willet, J.P. Newham, P.D. Sly, S.G. Kallapur, M. Ikegami, A.H. Jobe, Dose and time response after intraamniotic endotoxin in preterm lambs, Am. J. Respir. Crit. Care Med. 164 (3) (2001) 982–988, https://doi.org/10.1164/ajrccm.164.6.2103061.
[44] M. Kacerovsky, M. Drahosova, H. Hornychova, L. Pliskova, R. Bolehovska, M. Forstl, J. Tosner, C. Andrys, Value of amniotic fluid interleukin-8 for the prediction of histological chorioamnionitis in preterm premature rupture of membranes, Neuroendocrinol. Lett. 30 (6) (2009) 733–738.
[45] S. Yoneda, A. Shiozaki, M. Ito, N. Yoneda, K. Inada, R. Yonezawa, M. Kigawa, S. Saito, Accurate prediction of the stage of histological chorioamnionitis before delivery by amniotic fluid IL-8 level, Am. J. Reprod. Immunol. 73 (6) (2015) 568–576, https://doi.org/10.1111/aji.12360.
[46] S.J. Salter, M.J. Cox, E.M. Turek, S.T. Calus, W.O. Cookson, M.F. Moffatt, P. Turner, J. Parkhill, N.J. Loman, A.W. Walker, Reagent and laboratory contamination can critically impact sequence-based microbiome analyses, BMC Biol. 12 (87) (2014), https://doi.org/10.1186/s12915-014-0087-z.
[47] T. Kawai, S. Akira, The role of pattern-recognition receptors of innate immunity: update on Toll-like receptors, Nat. Immunol. 11 (5) (2010) 373–384, https://doi.org/10.1038/ni.1863.
[48] A. Glassing, S.E. Dowd, S. Galandiuk, B. Davis, R.J. Chiodini, Inherent bacterial DNA contamination of extraction and sequencing reagents may affect interpretation of microbiota in low bacterial biomass samples, Gut Pathog. 8 (24) (2016), https://doi.org/10.1186/s13099-016-0103-7.
[49] R. Romero, S.S. Hassan, P. Gajer, A.L. Tarca, D.W. Fadroch, L. Nikita, M. Galuppi, R.F. Lamont, P. Chaemsaithong, J. Miranda, T. Chaiworapongsa, J. Ravel, The composition and stability of the vaginal microbiota of normal pregnant women is different from that of non-pregnant women, Microbiome 2 (4) (2014), https://doi.org/10.1186/2049-2618-2-4.